Master's thesis

NTNU
Norwegian University of Science and Technology
Faculty of Engineering
Department of Structural Engineering

Simen Hølmo
Anton Stubberud

Effects of alkali-silica reactions on the structural behaviour of existing bridges

The slender columns of the Tromsø Bridge

Master's thesis in Bygg- og miljøteknikk
Supervisor: Terje Kanstad
June 2023

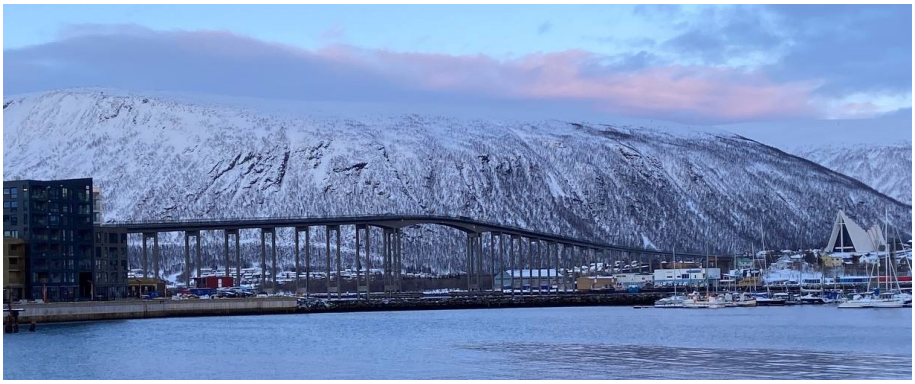

NTNU
Norwegian University of
Science and Technology

Simen Hølmo
Anton Stubberud

Effects of alkali-silica reactions on the structural behaviour of existing bridges

The slender columns of the Tromsø Bridge

Master's thesis in Bygg- og miljøteknikk
Supervisor: Terje Kanstad
June 2023

Norwegian University of Science and Technology
Faculty of Engineering
Department of Structural Engineering

NTNU
Norwegian University of
Science and Technology

Department of Structural Engineering
Faculty of Engineering
NTNU- Norwegian University of Science and Technology

ACCESSIBILITY

Open

MASTER THESIS 2023

SUBJECT AREA:	DATE:	NO. OF PAGES:
Concrete Structures	7. June 2023	95 + 103 Appendix

TITLE:

Effects of alkali-silica reactions on the structural behaviour of existing bridges: The slender columns of the Tromsø Bridge

Effekt av alkalireaksjoner på eksisterende bruers konstruksjonsoppførsel: Tromsøbruas slanke søyler

BY:

Simen Hølmo
Anton Stubberud

Over the last decades, Alkali-silica reactions (ASR) have emerged as a pressing problem for existing concrete structures. This chemical reaction induces internal expansion, resulting in weakened material characteristics of the concrete due to internal stresses. In addition, it imposes additional forces and moments in statically indeterminate structures. There is limited research available on the extent of damage and its effects on structural behaviour, making it difficult to evaluate the ultimate limit state capacity. The Tromsø Bridge, known to have ongoing alkali-silica reactions in large parts of its structure, has been the subject of several studies. However, the slender columns have received little attention. Previous inspections have revealed clear signs of ASR through cracks and expansions that can cause corrosion initiation and column displacement.

To assess the loads and reaction forces, the bridge was modelled in three parts: The west abutment, the main cantilever, and the east abutment. The columns were initially evaluated using interaction diagrams made with the FEM program SAP2000. The most critical columns were further evaluated using a moment-curvature relationship to account for the non-linear behaviour of the reinforced concrete. Finally, some selected columns were subjected to a parametric study, inducing high levels of ASR and corrosion.

The conservative interaction diagrams demonstrate capacity utilization well within limits for the critical load combination, and the more accurate moment-curvature relationships indicate utilization of 79.0% and 78.4% for the most loaded columns. It is evident that ASR expansions significantly affect the capacity. For the most utilized columns, the measured expansion due to ASR gives a moment increase of 12%.

The parametric study shows that full capacity can be reached when the selected columns are subjected to high levels of ASR, loss of concrete cover, and further reinforcement corrosion. The tall columns of the cantilever section will reach a critical situation with a complete loss of concrete cover, combined with significant corrosion. The single columns of the east abutment are sensitive to displacements caused by ASR. They will reach full capacity if the ASR expansion increases, combined with corrosion damage and loss of cover.

There are currently no indications of failure for any of the columns of the Tromsø Bridge. However, it is recommended that the bridge is monitored and inspected more thoroughly, as the parametric study highlights the potential consequences of prolonged propagation of ASR.

RESPONSIBLE TEACHER: Terje Kanstad, NTNU

SUPERVISOR(S): Terje Kanstad, NTNU

CARRIED OUT AT: Department of Structural Engineering, NTNU

NTNU
Kunnskap for en bedre verden

Department of Structural Engineering

Master Thesis

Effects of alkali-silica reactions on the structural behaviour of existing bridges: The slender columns of the Tromsø Bridge

Authors:
Simen Hølmo & Anton Stubberud

7. June 2023

Abstract

Over the last decades, alkali-silica reactions (ASR) have emerged as a pressing problem for existing concrete structures. This chemical reaction induces internal expansion, resulting in weakened material characteristics of the concrete due to internal stresses. In addition, it imposes additional forces and moments in statically indeterminate structures. There is limited research available on the extent of damage and its effects on structural behaviour, making it difficult to evaluate the ultimate limit state capacity. The Tromsø Bridge, known to have ongoing alkali-silica reactions in large parts of its structure, has been the subject of several studies. However, the slender columns have received little attention. Previous inspections have revealed clear signs of ASR through cracks and expansions that can cause corrosion initiation and column displacement.

To assess the loads and reaction forces, the bridge was modelled in three parts: The west abutment, the main cantilever, and the east abutment. The columns were initially evaluated using interaction diagrams made with the FEM program SAP2000. The most critical columns were further evaluated using a moment-curvature relationship to account for the non-linear behaviour of the reinforced concrete. Finally, some selected columns were subjected to a parametric study, inducing high levels of ASR and corrosion.

The conservative interaction diagrams demonstrate capacity utilization well within limits for the critical load combination, and the more accurate moment-curvature relationships indicate utilization of 79.0% and 78.4% for the most loaded columns. It is evident that ASR expansions significantly affect the capacity. For the most utilized columns, the measured expansion due to ASR gives a moment increase of 12%.

The parametric study shows that full capacity can be reached when the selected columns are subjected to high levels of ASR, loss of concrete cover, and further reinforcement corrosion. The tall columns of the cantilever section will reach a critical situation with a complete loss of concrete cover, combined with significant corrosion. The single columns of the east abutment are sensitive to displacements caused by ASR. They will reach full capacity if the ASR expansion increases from 0.55‰ to 1.5‰, combined with corrosion damage and loss of cover.

There are currently no indications of failure for any of the columns of the Tromsø Bridge. However, it is recommended that the bridge is monitored and inspected more thoroughly, as the parametric study highlights the potential consequences of prolonged propagation of ASR.

Sammendrag

I løpet av de siste tiårene har alkalireaksjoner (ASR) blitt et økende problem for eksisterende betongkonstruksjoner. Denne kjemiske reaksjonen fører til en intern ekspansjon, som resulterer i svekkede materialegenskaper i betongen på grunn av indre spenninger. Den påfører også ekstra krefter og momenter i statisk ubestemte konstruksjoner. Imidlertid er det begrenset forskning tilgjengelig på omfanget av skaden og dens effekter på konstruksjoners virkemåte, noe som gjør det vanskelig å vurdere skadens innvirkning på konstruksjoner i bruddgrensetilstand. Tromsøbrua, som er kjent for å ha pågående alkalireaksjoner i store deler av konstruksjonen, har vært gjenstand for flere studier. Imidlertid har de slanke søylene fått lite oppmerksomhet. Tidligere inspeksjoner har avdekket tydelige tegn på ASR i form av sprekker og ekspansjonsmålinger som kan føre til korrosjonsinitiering og forskyvning av søylene.

For å vurdere lastene og reaksjonskreftene ble brua modellert i tre deler: Vestre viadukt, fritt-frem-byggdel og østre viadukt. Søylene ble først evaluert ved hjelp av interaksjonsdiagrammer (MN) laget med FEM-programmet SAP2000. De mest kritiske søylene ble videre evaluert ved hjelp av en moment-kurvatur-relasjon for å ta hensyn til den ikke-lineære oppførselen til betongen. Til slutt ble noen utvalgte søyler underlagt et parameterstudie der søylene ble utsatt for høye nivåer av ASR og korrosjon.

De konservative interaksjonsdiagrammene viser kapasitetsutnyttelse godt innenfor grensene for den kritiske lastkombinasjonen, mens de mer nøyaktige moment-kurvatur-relasjonene indikerer en utnyttelse på 79,0% og 78,4% for de mest belastede søylene. Det er imidlertid tydelig at ASR-ekspansjoner har en betydelig innvirkning på kapasiteten. For søylene med høyest kapasitetsutnyttelse økte momentet grunnet den målte ekspansjonen som følge av ASR med 12%.

Den parametriske studien viser at full kapasitet blir nådd når de valgte søylene utsettes for høye nivåer av ASR, tap av betongoverdekning og ytterligere korrosjon i armeringen. De høye søylene i fritt-frem-byggdelen vil nå en kritisk situasjon med fullstendig tap av betongoverdekning kombinert med betydelig korrosjon. De enslige søylene i østre viadukt er sensitive for forskyvninger forårsaket av ASR. De vil nå full kapasitet hvis ASR-ekspansjonen øker fra $0,55‰$ til $1,5‰$, kombinert med korrosjon og tap av overdekning.

Det er for øyeblikket ingen tegn til svikt i noen av søylene på Tromsøbrua. Imidlertid anbefales det at broen overvåkes og inspiseres mer grundig, da den parametriske studien fremhever de potensielle konsekvensene av ytterligere skade grunnet ASR.

Preface

This master's thesis marks the end of our master's degree program Civil and Environmental Engineering at NTNU, Trondheim. The thesis is written for the Department of Structural Engineering during the spring semester of 2023 and counts for 30 credits.

The desire to apply the theoretical knowledge acquired over five years of studying to a practical and real problem paved the way for the choice of the thesis project. Investigating a relevant subject is motivational, and examining an existing structure facing an emerging problem would serve a significant purpose. A large part of the motivation was to hopefully provide new insight into the current state of the columns and highlight potential challenges arising from further ASR in the coming years. We also see the consequences of ASR propagating throughout the country and hope to contribute in the right direction to gain further knowledge on this sparsely researched topic.

We want to thank our primary supervisor Professor Terje Kanstad at the Department for Structural Engineering, for his great support throughout the semester. A special thanks to Marcin Luczkowski, who has been very helpful in setting up the model and discussing plausible simplifications in the early phases of the thesis. We would also like to extend our gratitude to Rune Lunde Nysted and Tor Erlend Pedersen at Troms og Finnmark Fylkeskommune for welcoming us to Tromsø and facilitating an inspection of selected columns of interest in April 2023.

Table of Contents

1 Introduction **1**

2 Regulations **2**

2.1 Eurocodes 2

2.2 Handbooks 3

3 Tromsø Bridge **4**

3.1 History 4

3.2 Geometry 5

3.3 Materials 8

4 Alkali-reactions **10**

4.1 Alkali-silica reactions (ASR) 10

4.2 Verification and testing of ASR in structures 11

4.3 Effects and consequences of ASR 13

4.4 Prevention of ASR 15

4.5 Propagation of ASR 15

5 Current state - Tromsø Bridge **16**

5.1 Visual inspection 16

5.2 Material tests and determination of expansion 19

6 Loads **20**

6.1 Acting loads 20

6.2 Deformation loads 27

6.3 ASR loads 31

6.4 Load combinations 34

7 Modelling **35**

7.1 Defining geometry - Dynamo Sandbox 35

7.2 Structural system 37

7.3 Mesh and FEM analysis 40

7.4 Application of loads 41

8 Selected columns **43**

8.1 Column 30/31 and 38 43

8.2 Column 32 and 37 43

8.3 Column 33 to 36 . . . 43
8.4 Column 44 to 49 . . . 43
8.5 Variables in cross-section . . . 44

9 Theory **46**
9.1 Buckling and slenderness . . . 46
9.2 Compression field theory . . . 48
9.3 Interaction diagram . . . 49
9.4 Moment-Curvature relationship . . . 51

10 Results **56**
10.1 Buckling and slenderness - columns . . . 56
10.2 Compression field theory - crossbars . . . 57
10.3 Loads and load actions . . . 57
10.4 Shear capacity - columns . . . 70
10.5 Interaction diagram . . . 71
10.6 Moment-curvature relationship . . . 75
10.7 Special ASR effects . . . 76

11 Parametric study **81**
11.1 High temperature and increased ASR expansion . . . 81
11.2 Reduction of concrete cover . . . 84
11.3 Corrosion of reinforcement . . . 86
11.4 Combined situations . . . 87

12 Discussion **90**
12.1 ASR effects . . . 91
12.2 Parametric study . . . 92

13 Conclusion **93**

Bibliography **94**

Appendix **96**
A Technical drawings . . . 97
B Column reinforcement . . . 117
C Loads . . . 119
D Buckling and slenderness . . . 151

E Capacity Shear and crossbars 154
F ASR 168
G Interaction diagrams 193
H Scanning of columns 31 and 34 198

1 Introduction

Over the last decade, the appearance of micro crack patterns on several concrete structures in Norway has emerged. The phenomenon is known as alkali-silica reactions and is an increasing issue in bridges and other structures built from 1950 to 1990. It is estimated that about 1000 bridges are affected today, with the numbers continuing to grow [1]. The effect weakens the material characteristics of the concrete, but the extent of the damage and corresponding effects on the structural behaviour and capacity are complicated to estimate.

Alkali-silica reactions (ASR) were not fully understood until the late 1990s. The main reason is that the reaction propagates slowly over a long time span and is not visual for the first few decades. Alkali-silica reactions are caused by the combination of a moist environment, sufficient alkali in the cement, and reactive silica in the aggregate. This starts a chemical reaction that creates an alkali-silica gel that expands and introduces internal stresses causing the concrete to expand. As a result, reactive aggregate is no longer used in concrete structures. However, many structures in Norway will suffer from ASR in the coming years due to the very slow initiation and propagation of the reaction. As such, the problems and the structural consequences are expected to increase. As the phenomenon is relatively new, there is little research on the structural implications of the reaction. In addition, the best estimates of the future propagation of ASR are from limited, sped-up experiments. As a consequence, future predictions are highly uncertain. One of many bridges with extensive damage due to ASR is the Tromsø Bridge. This is a famous landmark and is part of a heritage program. Therefore, rehabilitation should be prioritized to extend the lifetime of the bridge.

This master thesis aims to investigate the effects of alkali-silica reactions on the structural behaviour of existing bridges, explicitly focusing on the columns of the Tromsø Bridge. The motivation for the thesis is to contribute to a relatively new research topic by applying theoretical knowledge acquired over five years of studying on a specific structure and problem. In addition, while the bridge as a whole and the bridge deck have been previously studied, the columns have been given little attention. Hopefully, this thesis will contribute to the basis for decision-making regarding future inspections and maintenance for *Troms og Finnmark Fylkeskommune*.

The thesis is split into four main parts. The first entails a description of the Tromsø Bridge, its current state, and past inspections. In addition, the theory behind ASR is presented. In part two, the loads are defined, and the entire bridge is modelled. Considerations and simplifications of the model are explained, and columns of particular interest are defined. Part three describes the theory and presents the calculations and results for the current state of the columns of the Tromsø Bridge. Finally, the last part of the thesis is a parametric study where the potential consequences of further ASR propagation are investigated. Some hypothetical cases are modelled to highlight future problems concerning capacity. This part also includes a discussion and conclusions of the thesis.

2 Regulations

2.1 Eurocodes

Laws and regulations heavily govern construction in Norway. This thesis will refer to recent and previous versions of Eurocodes and handbooks published by Statens Vegvesen (The Norwegian Public Roads Administration).

Previously, regulations were based on national standards. However, after the turn of the millennium, the Eurocodes (EC) were introduced to establish a unified European framework for the design of structures. Initially, the bridge was designed according to NS 427 and the load regulations 1/1947. As this was before the partial factor method's introduction, the standard implemented in 1973 (NS 3473) is utilized [2]. The standard NS 3473 was used from 1973 to 2010 before the current Eurocode completely replaced it. This study focuses on an existing bridge and therefore relies on the regulations applicable at the time of its construction, supplemented by current design rules in the Eurocode series. In addition, handbooks published by Statens Vegvesen handling existing bridges will be used. The Eurocodes used are the following:

- Eurocode 0, *NS-EN 1990, Basis of structural design* [3]
- Eurocode 1, *NS-EN 1991, Actions on structures* [4]
  - *NS-EN 1991-2, Traffic loads on bridges* [5]
  - *NS-EN 1991-4, Wind actions* [6]
  - *NS-EN 1991-5, Thermal actions* [7]
- Eurocode 2, *NS-EN 1992, Design of concrete structures* [8]
- NS 3473:1998, *Prosjektering av betongkonstruksjoner* (Concrete structures - Design rules) [9]

While the Tromsø Bridge was constructed using a previous version of the Eurocode known as NS 3473:1998. This paper will handle necessary calculations based on the most recent version, NS-EN 1992. Where necessary, the outdated Eurocode will be used as a compliment to account for the fact that the bridge is much older than the updated regulations and for the materials used.

Eurocode 0 (EC0) describes how load combinations of permanent and variable loads should be handled. It also explains how to treat dominant loads and how favourable and unfavourable loads should be accounted for. This must be handled in the serviceability (SLS) and the ultimate (ULS) limit state.

Eurocode 1 (EC1) describes handling loads such as snow, wind, and traffic loads on a given structure. This is necessary to determine before combining the loads using Eurocode 0.

Eurocode 2 (EC2) outlines the regulations and requirements for concrete design. Ways of handling buckling and slenderness are outlined in this Eurocode. This will partly be the basis for calculations and capacity checks throughout the project thesis. The older version of EC2, NS3473, will be used occasionally.

2.2 Handbooks

Statens Vegvesen published a set of handbooks to be used as a complement, in addition to the Eurocodes. The ones used and referred to in this project thesis are the following:

- N400, *Bruprosjektering* - Bridge design [10]
- V412, *Bæreevneklassifisering av bruer, laster* - Strength classification of bridges, loads [11]
- V413, *Bæreevneklassifisering av bruer, materialer* - Strength classification, materials [12]
- V441, *Bruinspeksjon* - Bridge inspection [13]

N400 is a supplement to the Eurocodes for the design of bridges, harbours, and other supporting structures. This is the most general handbook within the 400-family. The V412 and V413 replace the R412 handbook. These handbooks define loads and material strength accounting for the bridge's construction period. Finally, V441 describes bridge inspection and assessment of damages.

3 Tromsø Bridge

The Tromsø Bridge in Norway connects Tromsøya with the mainland and is a vital part of the infrastructure in northern Norway. Since its opening, it has played a significant role in the development of Tromsø and has become a well-recognized and famous landmark. Recently the bridge was listed as part of the heritage of Tromsø and is thus protected [14].

Figure 3.1: Tromsø Bridge [15]

3.1 History

The idea of a bridge connecting Tromsøya with the mainland was first proposed in the 1870s, but detailed planning didn't begin until the late 1950s. Before the cantilever design was ultimately chosen, several designs were considered, including a suspension bridge and a tunnel. The bridge was designed by Aas-Jacobsen and built by the construction firm Nils Meland A/S and Jernbotn A/S [16].

After several years of planning, the Tromsø Bridge was built between 1958 and 1960 to replace the car ferries that crossed the Tromsø Sound in the 1950s. To tackle the growing lines of cars, consulting firm Dr. Ing. Aas-Jakobsen was engaged to design the bridge. The architect Erling Viksjo led the design of the bridge using the free-cantilever method, making it the first of its kind in Norway. Construction began in December 1957 and was completed in December 1959. The bridge's slim and elegant design won Viksjo the "Betongtavlen" award in 1963. The bridge has become a famous landmark, connecting Tromsøya with the mainland Tromsdalen, and has played a significant role in the development of Tromsø as the capital of northern Norway. In 2008, the Norwegian Directorate for Cultural Heritage declared the bridge a national monument to preserve its primary structure and details. As a result, rehabilitation must be prioritized to preserve the heritage and maintain the bridge in good condition to avoid demolition.

The bridge has undergone several modifications over the years, including adding a steel pedestrian and bicycle lane in 1982 and increasing the safety railing's height in 2005. In the years after the completion of the bridge, Tromsø City was further expanded with an airport, hospital, and a university. Tromsø is now the capital of northern Norway, and the bridge undeniably played an essential part in the city's transformation.

3.2 Geometry

The geometry described below is based on blueprints provided by Dr. Ing. Aas-Jakobsen [17]. The Tromsø Bridge is 1016 meters long, with a main span of 80 meters and a maximum clearance of 38 meters [18].

The bridge is divided into five main sections, A to E. Each bridge superstructure section has a different load-bearing system than its neighbouring section. There are three expansion joints along the length of the bridge, as seen in Figure 3.2. The original axis distribution will be used, starting with 0 at the west end (Tromsøya) and ending at 57 at the east end (Tromsdalen). The axis division is governed by the placement of the columns, meaning that the axis number will be the same as the column number. Each axis has a south and north end referred to as S and N. The global axis definition used in this thesis is also given in Figure 3.2.

- Section A - axis 0 to axis 16
- Section B - axis 17 to axis 31
- Section C - axis 32 to axis 37
- Section D - axis 38 to axis 43
- Section E - axis 44 to axis 60

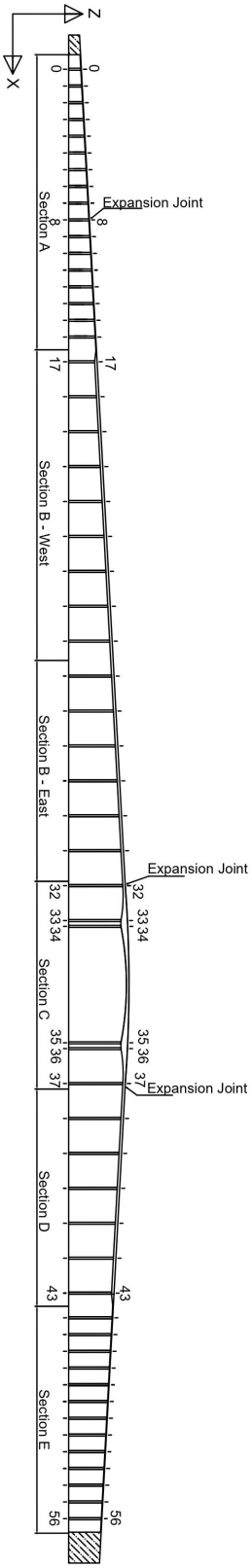

Figure 3.2: Outline of the Tromsø Bridge [17]

The depth of the columns was evaluated based on maps from *Kartverket* [19] and the drawings from *Aas Jakobsen* [17]. All the columns in Section C are assumed to start at 10 m below sea level. The columns in parts A and B are considered equal in depth, as seen in Figure 3.4 at 6 m below sea level. The depth of the columns in parts D and E starts at 8.33 m above sea level and vary linearly (according to Figure 3.4) to ground level at 0 m, between axis 43-44. On the mainland, the columns follow the ground height. For the columns in parts B, C, and D, there are two transverse stiffening beams (referred to as crossbars onwards) placed at 5.50 m above sea level and just below the bridge deck respectively.

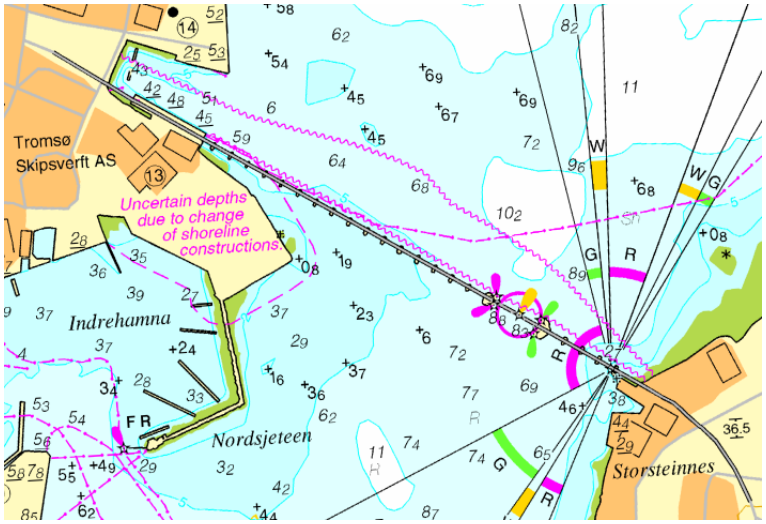

Figure 3.3: Map of water depth [19]

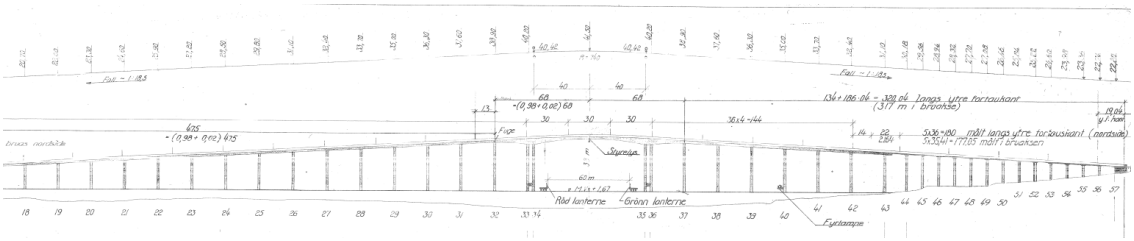

Figure 3.4: Profile of Tromsø Bridge with water depths [17]

Sections A and E have a continuous solid plate cross-section spanning between single hollow columns. The columns are symmetrically reinforced and have an outer diameter of 1400 mm and a wall thickness of 200 mm.

Sections B and D have a continuous double-T cross-section spanning between pairs of hollow columns. The columns are symmetrically reinforced and have an outer diameter of 1400 mm. Two transverse crossbars connect and stiffen each pair.

Section C is the cantilever part. It consists of two short and one main span, all with a varying box-girder cross-section. The columns are massive and have an outer diameter of 1400 mm. The columns are placed in a configuration of two pairs connected with crossbars. Between the columns in axis 33-34 and 35-36, there is an additional crossbar in the longitudinal direction.

The bridge deck is 8.3 m wide, consisting of two traffic lanes and a sidewalk. Pedestrian and bicycle sidewalks (2 m) were added later, widening the bridge. The total width of the bridge deck and sidewalks is 11.1 m. The cross-section and measurements of the bridge deck is found in Figure 3.5

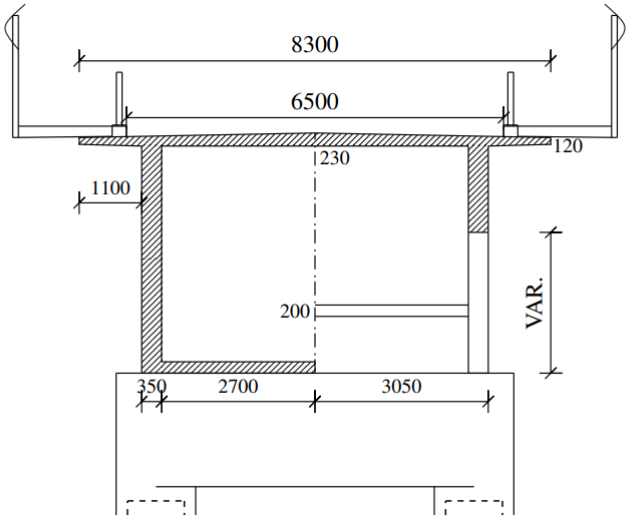

Figure 3.5: Cross-section - section C [2]

The columns are assumed fixed to the foundation and are also assumed fixed to the crossbars. There is a vast difference in stiffness between the bridge deck and the columns, $EI_{bridgedeck} >> EI_{columns}$. Therefore, a small portion of the moment is transferred to the columns through its connections. It is also reasonable to assume that the columns are fixed to the bridge deck beams.

3.3 Materials

3.3.1 Concrete

The bridge deck in the cantilever part (section C) is constructed with B440 concrete, whereas the rest of the deck and the columns are made of A-concrete. The material factors will be modified accordingly based on V413 to account for the old material types [12]. For concrete, the material factor, γ_c, is 1.5.

Using Table 2.2.1 in V413, the old material classes can be converted to be compatible with the most recent Eurocode:

Byggeår	NS 427 (av 1939)	NS 427A (av 1962)	NS 3473 (1973-2003)	NS 3473 (2003-2010)		NS-EN 1992-1-1 (NA 3.1.2)	
	Betong-kvalitet	Betong-kvalitet	Fasthets-klasse	Fasthets-klasse	f_{cn} (N/mm²)	Fasthets-klasse	f_{ck} (N/mm²)
Før 1920	C-betong	B 200	C 15	B 10	11,2	B 12	12
1920-1945	B-betong	B 250	C 20	B 16	14,0	B 16	16
Etter 1945	A-betong	B 300 B 350 B 400 B 450 B 600	C 25 C 30 C 35 C 40 C 45 C 55	B 20 B 25 B 28 B 32 B 35 B 45	16,8 20,3 22,4 25,2 27,3 34,3	B 20 B 25 B 28 B 32 B 35 B 45	20 25 28 32 35 45

Figure 3.6: Concrete strength classes [12]

B440 concrete is equivalent to C32 ($f_{ck} = 32$ MPa), and A-concrete is equivalent to C20 ($f_{ck} = 20$ Mpa). The Young's modulus was calculated based on the past version of the Eurocode, NS 3473:1998, to ensure accuracy and estimate the material strength conservatively [9]. The concrete characteristics are given in Table 3.1.

Table 3.1: Concrete characteristics

Concrete quality		**B440**	**A-Concrete**
Concrete quality after NS 3473		C40	C25
Characteristic compressive cylinder strength	f_{ck}	32 MPa	20 MPa
Design value of compressive strength	f_{cd}	18 MPa	12 MPa
Characteristic modulus of elasticity	E_c	26870 MPa	23336 MPa
Design value of tensile strength	f_{ctd}	1.32 MPa	1.0 MPa

3.3.2 Steel reinforcement

The steel reinforcement used in the bridge deck is of class CFS50, equivalent to Ks50. This is also used for the additional reinforcement in the columns. The longitudinal reinforcement in the columns is of class CFS40, equivalent to Ks40; see Appendix A.

Armeringstype	Armeringskvalitet	Diameter (mm)	f_{yk} (N/mm²)
Glattstål	St. 37	8-32	230
Kamstål	Ks 40 og Ks 40 S	8-20 25-32	400 380
	Ks 50 og Ks 50 S	8-16 20-32	500 480
	Ks 60 og Ks 60 S	8-16	600
	K 400 S og K400 TS	8-32	400
	K500 S og K500 TS	8-32	500
	K500 TE	8-32	500
	B500C	8-32	500

Figure 3.7: Reinforcement strength classes [12]

From Figure 3.7, the characteristic strength of CFS50 is 480 MPa, and the characteristic strength of CFS40 is 380 MPa. The shear reinforcement is smooth steel bars with a diameter $d = 10$ mm. Further, from Table 2.1.1 in V413, the material factor for steel reinforcement is set to $\gamma_s = 1.25$. The Young's modulus for the reinforcement steel is set to $E_s = 200$ GPa [8]. The characteristics are given in Table 3.2.

Table 3.2: Steel characteristics

Steel quality		**CFS50**	**CFS40**	**St.37**
steel quality - NS 3473		Ks50	Ks40	St. 37
Characteristic strength	f_{yk}	480 MPa	380 MPa	230 MPa
Design value of tensile strength	f_{yd}	384 MPa	304 MPa	184 MPa
Characteristic modulus of elasticity	E_s	200 GPa	200 GPa	200 GPa

4 Alkali-reactions

Alkali-related problems in Norwegian concrete structures are a constantly expanding problem. There are two main types of alkali reactions, alkali-carbonate reactions (ACR) and Alkali-silica reactions (ASR) with the latter being assessed in this master thesis. Alkali-Silica Reactions were discovered in the 1990s, and an estimated 1000 bridges are affected throughout the country today [1].

4.1 Alkali-silica reactions (ASR)

ASR is a complex reaction that involves the dissolution of silica in the aggregate, followed by the reaction of the dissolved silica with the alkalies in the pore solution to form a gel-like substance. Several factors, including the type and amount of silica in the aggregate, the alkali content of the cement, the presence of other minerals in the aggregate, and the temperature and moisture conditions in the concrete influence the reaction. As a result, the gel formed will take up more volume than the original products, mainly when it absorbs water and thus cause an expansion in the concrete.

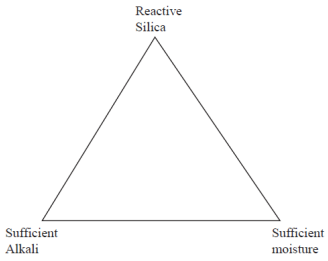

Figure 4.1: Necessary prerequisite for ASR [1]

As shown in Figure 4.1, three things are necessary for alkali-silica reactions to take place. Firstly, there must be reactive silica present in the aggregate. In Figure 4.2, the types of reactive bedrock in Norway can be seen. The aggregate in Norway reacts slowly compared to other countries, and it usually takes 10-15 years before the effects of ASR can be seen. Secondly, there must be sufficient alkali concentrations in the cement. This is the case for Portland cement commonly used [20]. Finally, there must be a moist environment. This is almost always the case for outdoor structures in Norway. For the reaction to start, a relative humidity of $80 - 90\%$ is required [21]. In addition, high temperatures will speed up the naturally slow reaction.

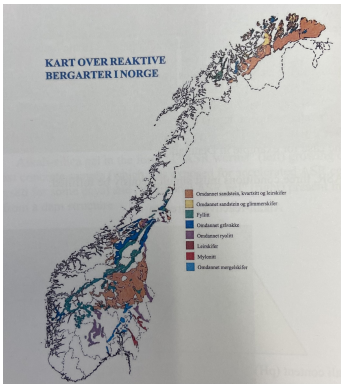

Figure 4.2: Reactive aggregates in Norway [21]

4.2 Verification and testing of ASR in structures

Apart from visual inspections (uncovering cracks, displacement, and deformations), several tests and measurements can be carried out to verify the presence of ASR, investigate the propagation, and assess the current material characteristics of the concrete. The most important ones will be explained in the following subchapter.

4.2.1 Visual measurements

Measuring the sum of crack widths over a fixed length in a vertical surface of the structure provides a clear assessment of the expansion created by ASR [22]. For bridges, this can be done both on the sides of the bridge deck and around the circumference of a circular column. The method gives a crack index, RI (Riss Index [mm/m]), and the rate of damage is categorized within four damage levels as per Figure 4.3.

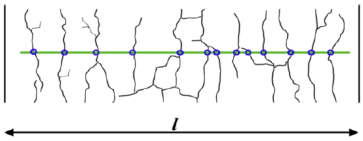

$$RI = \frac{\Sigma rissvidder}{l}$$

[mm/m = ‰]

Fra V441 Bruinspeksjon:

Skadegrad 1	Riss/sprekk < 0,3 mm
Skadegrad 2	Riss/sprekk 0,3 – 1,0 mm
Skadegrad 3	Riss/sprekk 1,0 – 2,0 mm
Skadegrad 4	Riss/sprekk > 2,0 mm

Skadegrad 1	Rissindeks < 0,5 ‰
Skadegrad 2	Rissindeks 0,5-1,0 ‰
Skadegrad 3	Rissindeks 1,0-2,0 ‰
Skadegrad 4	Rissindeks > 2,0 ‰

Figure 4.3: Crack index, RI, and associated degree of damage [22] [13]

A large structure damaged by ASR will show clear signs on a global scale. For example, a bridge may experience the closing of expansion joints, deformation of supports, displacement of column tops, and crushing of concrete. By measuring the displacement on a global scale, an assessment of the expansion due to ASR can be made.

4.2.2 Structural analyses

The expansion can also be measured on a micro-structural level by slicing core samples into fine discs and investigating micro-cracks and reaction products from ASR in a laboratory [23]. This test results in a Damage Rating Index (DRI). DRI and RI correlate well, as shown in Figure 4.4.

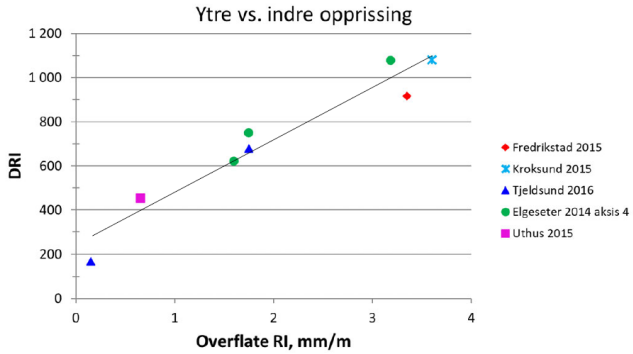

Figure 4.4: Damage Rating Index (DRI) vs. crack index (RI) [22]

An alternative method to assess the expansion and investigate the change in stiffness is by conducting a Stiffness Damage Test (SDT). This mechanical stress-strain test involves subjecting a concrete sample to five load cycles up to a specific load level, as depicted in Figure 4.5. For existing structures, core samples are extracted and used. The original concept of the test was based on the notion that a damaged sample would exhibit a significantly lower initial loading modulus compared to the first part of the unloading modulus, which represents the stiffness of uncracked concrete. The discrepancy between the loading and unloading modulus results in energy dissipation (hysteresis) directly associated with the micro-crack activity. In contrast, an undamaged sample would exhibit a similar loading and unloading modulus [24].

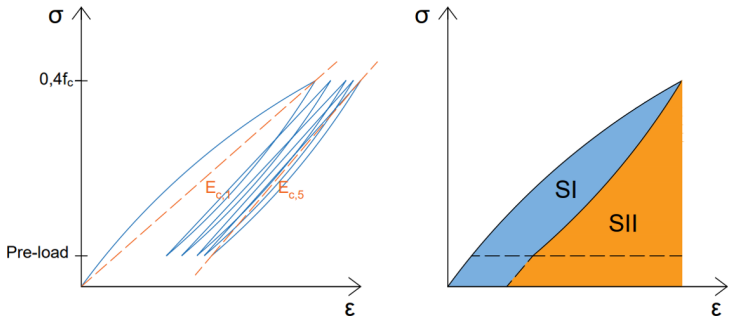

Figure 4.5: Stiffness Damage Test. $E_{c,1}$ and $E_{c,5}$ represent the Young's modulus for the first and fifth load cycles. Areas represent the dissipated energy (SI) and the total applied energy (SII)[24]

By comparing the SI and SII regions, a Stiffness Damage Index can be calculated using Equation 4.1.

$$SDI = \frac{\sum_{i=1}^{5} SI_i}{\sum_{i=1}^{5} (SI_i + SII_i)} \tag{4.1}$$

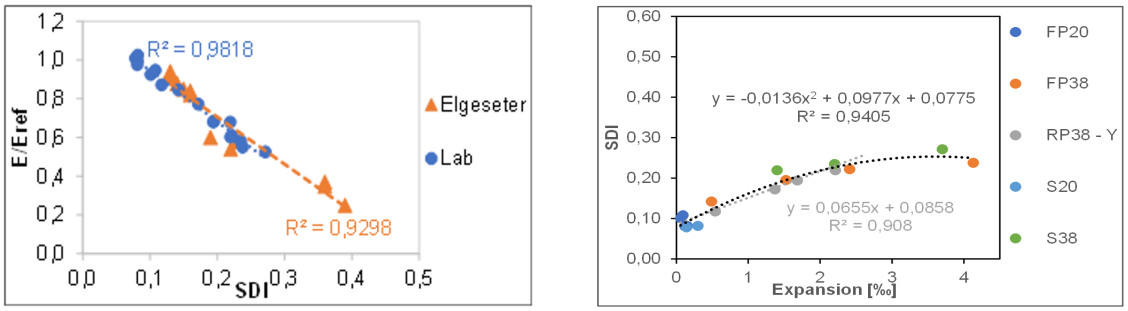

(a) SDI vs. E/Eref

(b) SDI vs Expansion ‰

Figure 4.6: Correlation between SDI and change in Young's modulus, and between SDI and expansion up to 2‰ in the concrete [24]

The SDI correlates linearly with changes in the Young's modulus (Figure 4.6 (a)) and for expansion up to 2‰ (Figure 4.6 (b)) [24]. These correlations are used in Chapter 5 to assess the stiffness and expansion of both the bridge deck and the columns on the Tromsø Bridge.

4.3 Effects and consequences of ASR

The effects of ASR on concrete can vary from minor cracking to complete disintegration of the structure, depending on the severity and duration of the reaction. In non-reinforced concrete, the structure will expand uniformly. In reinforced concrete, it will cause the reinforcement to obtain tensile forces, and the concrete will be subjected to compressive forces. If the surface of the concrete is free to expand, a characteristic crack pattern will occur (Figure 4.7). In structures that are heavily loaded by axial compression like columns, the expansion in the longitudinal direction will be greatly reduced [1]. In columns, the crack pattern will usually appear as crack lines parallel to the load direction because of the relative free expansion in the radial direction for the concrete cover.

Figure 4.7: Typical crack pattern in column and foundation due to ASR [21]

4.3.1 Reduced mechanical characteristics

The mechanical consequences of ASR are mainly reduced Young's modulus and reduced concrete capacity in tension. There might also be a significant reduction in the bond between the reinforcement bars and the concrete. The compression capacity is also affected, but mainly at higher strains ($2-3‰$) [25]. The reduced Young's modulus must be accounted for to evaluate the reduced overall capacity of the columns [26]. The relative change in the Young's modulus can be estimated by Equation 4.2. The reduction in stiffness due to ASR will also shift the stress-strain curve for the concrete, as shown in Figure 4.8. The consequences of this are further explained in Subchapter 10.7.

$$\frac{E}{E_{ref}} = 1 - \frac{\epsilon^{ASR}}{\epsilon^{ASR} + \beta} \tag{4.2}$$

E = Young's modulus concrete with ASR
E_{ref} = Reference Young's modulus
ϵ^{ASR} = Concrete strain due to ASR
β = Coefficient of regression

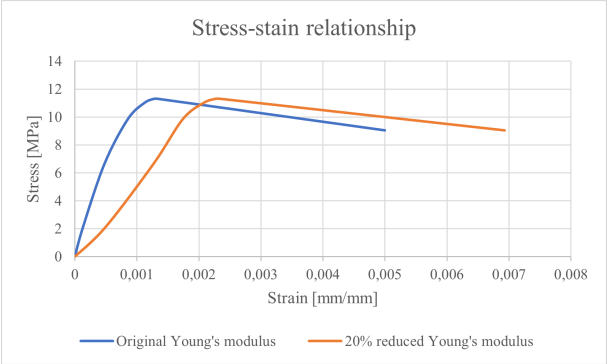

Figure 4.8: Change in the stress-strain curve due to reduced Young's modulus

There is still limited research on the consequences, implications, and propagation of ASR expansions. This makes accurate estimation of the magnitude of expansion, reduction in strength, and future propagation difficult. Furthermore, the relationship between ASR expansions and the reduction in Young's modulus varies depending on the study, aggregate used, and environmental assumptions. For this thesis, the coefficient of regression is extracted from the article *Experimental investigation of ASR-affected concrete*, where $\beta = 0.0035$ was assessed as an accurate estimate for bridges in Norway constructed in the 1950-1960s [26]. Further research, however, might prove a more accurate coefficient of regression depending on the given situation and aggregate used.

The Young's modulus is exponentially decaying with increased expansion. Therefore, a potential expansion due to ASR might further decrease the concrete stiffness, as shown in Figure 4.9. The reduction in tensile strength will not be discussed further in this thesis as all calculations are conducted assuming no tensile strength in the concrete.

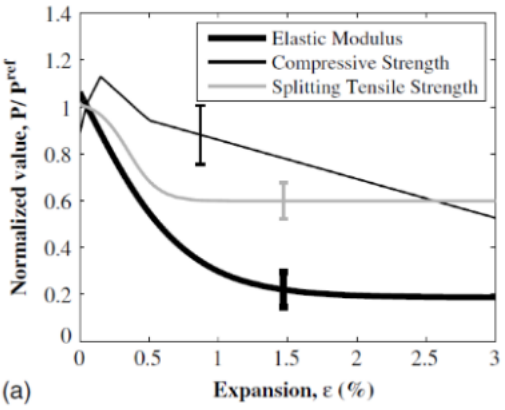

Figure 4.9: Reduction of Young's modulus, tensile strength and compressive strength due to ASR [1]

4.3.2 Frost damage and corrosion due to excessive cracking

The micro-cracking caused by ASR can be expanded by water penetrating and instigating frost expansion cycles. This can lead to weakening the concrete and in turn, facilitate an environment for reinforcement corrosion. For a circular column with a thick concrete cover where the expansion propagates freely in the radial direction, this effect can lead to vast amounts of degradation, causing the capacity contribution of the cover to be critically weakened [1].

4.3.3 Expansion in a global scale

In small structures, an expansion due to ASR is most critical on a material level, but for long constructions like bridges, it can lead to large eccentricities for the columns, restraint forces internally in the bridge, and closing of gaps at the expansion joints [1].

4.4 Prevention of ASR

ASR can be controlled or prevented through a variety of means. One approach is to use low-alkali cement, which contains reduced amounts of alkalies that can react with the silica in the aggregate. Another method is to use non-reactive aggregates, such as limestone or dolomite, which do not contain significant amounts of reactive silica. A third approach is to use pozzolanic materials, such as fly ash or slag, which can help to reduce the alkali content of the cement pore solution and thus reduce the potential for ASR to occur [27].

In the parts of Norway where all or most of the available aggregate will cause ASR (Figure 4.2), the solution is to keep the alkali levels in the concrete below the reference levels given in "NB 21", a publication from Norsk Betongforening about the structural consequences of ASR in concrete structures. This can be done by adding sufficient supplementary cementitious materials (SCMs) like silica fume or fly ash or using a low alkali cement such as CEM 1 [21].

4.5 Propagation of ASR

There is limited research on how alkali-silica reactions propagate and how the expansion varies over time. This has been roughly tested in sped-up experiments as an attempt to understand what to expect in the years to come [24]. However, there is little knowledge regarding the time frame of the reaction. It is assumed that it will level out, reaching an asymptote after the faster, exponential propagation. The main reason for this is that ASR in Norway is a new phenomenon where the full consequences have not yet been seen.

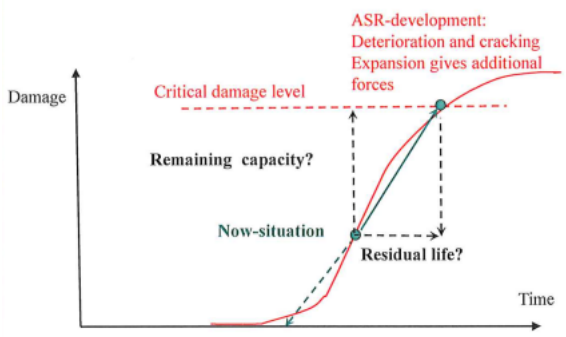

Figure 4.10: ASR propagation [1]

5 Current state - Tromsø Bridge

The assessment of the current state of the Tromsø Bridge is mainly based on previous inspections. The most significant inspections performed in recent years are [28];

- 2010 - General inspection and crack and structure analysis, Multiconsult and NBTL
- 2014 - Test of samples and testing of cracks, expansion, and moisture, SINTEF
- 2016 - General inspection, Multiconsult
- 2021 - Extensive documentation. Core samples for SDT and structure analysis, NTNU, SINTEF, TFFK
- 2022 - Core samples for SDT and structure analysis, NTNU, SINTEF, TFFK

The authors performed an additional inspection in April 2023, mainly focusing on the columns on the east abutment, presented in Subchapter 5.1.1. This chapter will discuss the various damages in Tromsø Bridge, focusing on ASR.

5.1 Visual inspection

Most of the columns of the Tromsø Bridge exhibit significant cracking, especially those placed in seawater. The cracking is most visible on the north-facing side. This is because the south side is more exposed to rain which washes away the alkaline pore water on the concrete surface and higher temperatures due to the sun. However, this does not necessarily mean a higher degree of expansion on the north side. On the contrary, the extra rain on the south side can lead to increased ASR expansion due to higher relative humidity.

Figure 5.1: Difference between ASR on the south and north side of the column of the Tromsø Bridge

Moisture is observed in the overhanging bridge plate with a suspended walkway on top, particularly near the curbstone, indicating limited drainage from the roadway and a lack of drip edge. The columns show signs that the cracking is most pronounced in the massive part below the lower crossbars, with dark spots from moisture due to the drainage hole for the hollow part of the column. Moisture measurements inside selected columns in sections D and E performed by Troms og Finnmark Fylkeskommune show a relative humidity of 100% at most times [29]. Signs of corrosion at the water level are also visible [30].

The findings during the most recent inspection of the bridge can be summarized as follows: All beams have varying degrees of cracking pattern from axis 17 to axis 43. The same applies to pillars from axis 5 to axis 55. The most serious damage/deviation is in expansion joints at axis 32 and axis 37. These joints are closed, removing the bridge's expansion potential in the longitudinal direction.

Based on inspections performed by Multiconsult in 2022, it is clear that corrosion has been initiated. The full corrosion effect has not yet been seen. The degree of corrosion is difficult to estimate without further inspection. However, on some columns, there are visual indications of corrosion on the columns in height with the water surface. Several core samples were also collected, where it was documented "harmful and crack-forming alkali reaction in all samples (visual structural analysis) caused by the rocks quartzite, sandstone, siltstone, shale, mylonite, cataclasite, and quartz-rich rock." [30].

In 2014, the crack index, RI, was measured on columns 16 and 51. The expansion was calculated to 0.7‰ for column 16 and 0.6‰ for column 51. As explained in Chapter 4, this is the expansion in the free direction, and due to the axial forces in the columns, the expansion in the longitudinal direction is likely smaller.

As a result of the use of different aggregates during the construction of Tromsø Bridge, there is a varying degree of ASR expansion for similar structural components. In the slab bridge near the shores on both sides and specific columns in these parts of the bridge, less reactive aggregate has been found, which reduces the expansion and thereby the damage [22].

5.1.1 Inspection April 2023 - East abutment

The bridge was inspected on a sunny and cold day. The temperature was approximately 5 degrees and although the expansion joints were not closely inspected, they all appeared open.

The main scope of the inspection was to assess if the single columns in axis 44-47 are inclined due to ASR expansions. These columns are of particular interest for two main reasons. Firstly, there is little information from previous inspections, as the cantilever part and west abutment have been prioritized. The current state of axis 44-47 should therefore be given more attention. Secondly, the east part of the superstructure is curved, implying a different behaviour as the bridge deck expands. It is expected that the curved part of the bridge will exhibit large displacements normal to the notional lanes, potentially causing a critical situation. This is further discussed in Chapter 8. It is reasonable to assume little to no expansion due to temperature on the day of inspection, hence, the observed displacements are caused by ASR expansions.

The measurements were done using a rotary laser (HILTI - PR 30-HVS 02), with an accuracy of $\pm$ 0.5 mm/10 m. The laser was placed on the ground next to the column of interest, creating a laser-plane parallel to the column. The distance from the laser plane to the column was measured at the base and at 2/3 height. Supported by Troms og Finnmark Fylkeskommune, a portable crane was used to access the top of the columns for measurements, see Figure 5.2.

Figure 5.2: Inspection and measurements from portable lift

The measurement was extrapolated linearly to the top of the column. The displacement was measured in the global X and Y direction. The results are presented in Figure 5.3. The figure clearly shows a pattern of displacements out of the curve, with only one column tilting inwards. All the single columns, apart from one, are also leaning in the positive x-direction. The cause of the displacements is most likely due to combined high-temperature cycles and closed expansion joints due to ASR. If the problem propagates, the additional, second-order moments resulting from the displacements might be critical.

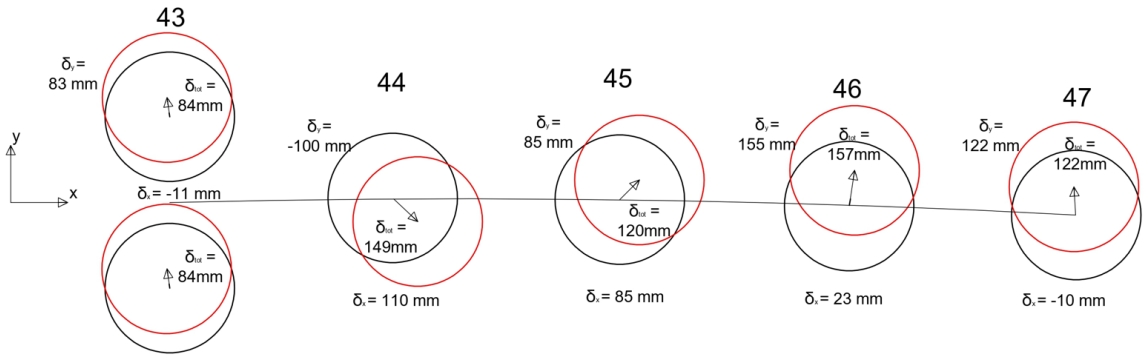

Figure 5.3: Permanent displacement of columns 43-47

Further, the columns were visually inspected. There are clear signs of uniform ASR on the columns, with more visual ASR-product on the north-facing side. Using a drone, the connection at the top of the columns of section E was investigated. Cracks due to bending in the top of the columns are a potential concern due to ASR expansions shifting the curved bridge deck outwards. There were little to no signs of cracks throughout section E caused by bending in the column tops as seen in Figure 5.4.

(a) Column 45 (b) Column 46

Figure 5.4: Visual inspection of column tops in section E

5.2 Material tests and determination of expansion

In 2021 and 2022, 20 core samples from the bridge deck and columns were extracted and tested [31]. ASR reactive aggregates were identified in these tests, and ASR expansion was proven. The test samples were tested with SDT (Stiffness Damage Tests) to assess the material characteristics of the concrete. Based on these tests, an SDI (Stiffness Damage Index) was calculated as explained in Chapter 4. The SDI varied in the core samples examined by SINTEF from 0.135 to 0.245, with the two columns in axis 20 obtaining an SDI of 0.158 on average. The loss in Young's modulus for the test samples was calculated between 10% and 22%, with the columns showing a loss of 11%. The compressive strength was not reduced significantly.

In 2016 Multiconsult carried out an extensive scanning of all columns from axis 1 to 34. The results showed a clear tendency of displacement of the column tops towards the expansion joints. These scans correlate well with the RI and SDI measurements, and based on this, it is determined that the mean ASR expansion in the bridge deck is at 0.55‰ [32].

At the MESLA-seminar (Management and extension of service of life of infrastructure affected by Alkali-silica reaction) held on the 20th of November 2022, it was presented that the expansion joints on the bridge close at 17 °C based on measurements carried out by *Troms og Finnmark Fylkeskommune* and students from *NTNU* [23].

The exact ASR expansion in the columns is not known. The core samples drilled out have been tested with SDTs in the radial direction of the column. In this direction, ASR expansion is considered to be more free than in the axial direction of the column and, therefore of a higher degree. There have also been fewer tests collected from the columns compared to the bridge deck, and thus, the uncertainty of the expansion in the columns is higher. In this study, an investigation of the structural consequences of the ASR expansion in the columns approaching zero, an expansion equal to the bridge deck (0.55‰), and a varying expansion throughout the column ($0 - 0.55$‰) in the radial direction is conducted.

6 Loads

The different types of loads are divided into classes based on their type and the probability of occurrence:

- Permanent loads (self-weight, superimposed dead load, and railing load)
- Variable loads (traffic load, wind load, and temperature load)
- Deformation loads (loss of prestressing force, shrinkage, creep, relaxation, temperature load, and alkali-silica reactions)
- Accidental loads (loads caused by collision, explosion, fire, and avalanche)

The Handbook V412 determines traffic loads based on the bridge usage class, which assumes design control using the partial factor method. The method involves increasing the theoretical load and reducing the theoretical material capacity of the construction elements by multiplying the load effects and capacity with unfavourable load factors. The construction is considered to maintain sufficient capacity if the design capacity is greater than the design load effect.

In this thesis, the following loads are neglected:

- Relaxation and pre-stress - due to symmetry with respect to the columns
- Snow load - this can be neglected on bridges [11]
- Dynamic wind load - this thesis will investigate the bridge in finished condition, thus dynamic wind loads can be neglected [11]
- Wave loads
- Ground pressure and seismic loads

6.1 Acting loads

6.1.1 Self-weight

Permanent loads are based on EC1, Table A.1. The weight of reinforced concrete is based on N400 [10]: $\gamma_{\text{reinforced concrete}} = 25 \text{ kN/m}^3$

The super self-weight is defined as the self-weight of all permanent parts of the bridge except the reinforced concrete. This is the weight of pedestrian walkways, bicycle lanes, asphalt, membrane, and tear-off-layer. From N400, the super self-weight is set to 2.5 kN/m^2 for cantilever bridges with spans between 50 and 200 meters and an annual average daily traffic of over 2000 vehicles. The minimum value for sidewalks and bicycle lanes is set to 1.5 kN/m^2. The steel railing and the crash barrier load are set to 0.5 kN/m line load based on V412 [11].

6.1.2 Traffic loads

The defined traffic loads are based on V412 [11] and EC1-2 [5], describing how traffic loads should be handled for existing bridge structures. The current classification of the bridge is Bk 10/50, allowing a total weight of 500 kN and an axial load of 115 kN for a given vehicle.

The total width of the traffic lanes is $w = 6.5$ m, meaning that heavy traffic can pass on the bridge. Therefore, accounting for heavy traffic gives a width of the notional lane of $w_n = 3 \text{ m} \cdot (2.6 \text{ m} \pm 0.2 \text{ m})$, giving $n = 2$ notional lanes on the bridge.

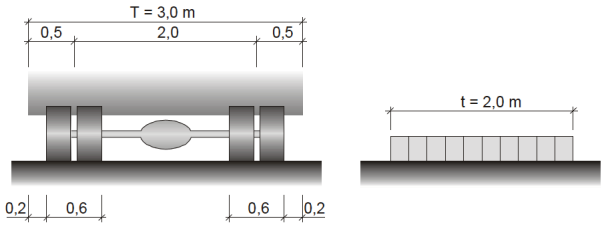

Figure 6.1: Notional lane-, and heavy traffic [11]

The vertical loads consist of heavy and light traffic. The main traffic (referred to as light traffic) has a defined load $p = 6$ kN/m across a width of 2.0m, $p = 3$ kN/m^2. This load must be applied over the entire length of the notional lane. Further, the weight of heavy traffic can be approximated as shown in Figure 6.2. The model simplifies the weight of heavy vehicles to eight-point loads separated by a distance $a = 2.0$ m. This can be further simplified to an evenly distributed load over the length of 14m, $q = 34.29$ kN/m, $q = 17.14$ kN/m^2. This load can be applied up to two times simultaneously on the bridge. It will always appear together with the light traffic load. In addition, the weight of pedestrians and cyclists is approximated to 1 kN/m^2 when applied simultaneously with traffic loads.

Lasttype	Lastfordeling		Ordinære bruksklasser				
			Bk 10/50	Bk T8/50	Bk T8/40	Bk 8/32	Bk 6/28
Boggilast	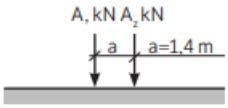	A1	165	125	125	125	100
		A2	120	90	90	55	35
Kjøretøy-last	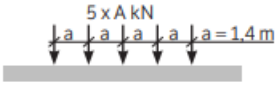	A	80	68	68	58	45
Vogntog-last	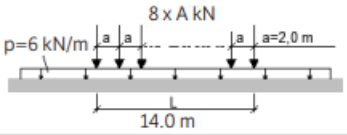	A	60	55	47	38	30

Figure 6.2: Load distribution heavy vehicles [11]

The main horizontal loads are braking loads and sideload due to traffic. They will appear together with the vertical loads. For the classification and length of the Tromsø Bridge, the breaking load is 300 kN. The load appears parallel with the longitudinal direction and is evenly distributed over the width of the notional lane. Therefore, uneven braking must be expected. To account for this, the sideload (S) is set to 25% of breaking load, $S = 75$ kN. The sideload appears in the transversal direction simultaneously with vertical traffic loads and breaking loads.

For the horizontal curvature of the bridge at the east abutment, a centrifugal load S_c should be considered.

$$S_c = v^2 * \frac{V}{127 * R} = 70^2 * \frac{500}{127 * 250} = 77.2 \text{ kN/m} \tag{6.1}$$

v = speed
V = vehicle load
R = Radius of curvature

The centrifugal load, however, does not appear simultaneously with the breaking and sideload. Therefore, this will be neglected as the breaking loads are more decisive [11].

6.1.3 Wind loads

The handbook N400 [6] and the EN-NS 1991-1-4 [10] regulations form the basis for calculating the wind loads affecting the bridge. The handbook N400 categorizes bridges into three classes based on their exposure to dynamic effects. All cantilever bridges are categorized into class 1 as soon as they are completed. As explained previously, this thesis will not examine the bridge during construction, and dynamic wind load can therefore be neglected [10].

The following chapter calculates the wind loads on the bridge in vertical and horizontal directions and the wind loads on the columns. All values used are found in EN-NS 1991-1-4 unless otherwise stated. The basic wind velocity at the location is calculated with Equation 6.2. See Appendix C for the complete calculations.

$$v_b = v_{b,0} \cdot c_{dir} \cdot c_{season} \cdot c_{alt} \cdot c_{prob} \tag{6.2}$$

The fundamental value for the wind velocity, $v_{b,0}$, is obtained from EC 1-4 Table NA.4(901.1) and the value for Tromsø is $v_{b,0} = 27$ m/s. Since $v_{b,0} = 27$ m/s $< v_0 = 30$m/s, the value for c_{alt} is defined by equation 6.3

$$c_{alt} = 1.0 + \frac{(v_0 - v_{b,0}) \cdot (H - H_0)}{v_{b,0} \cdot (H_{topp} - H_0)} \tag{6.3}$$

H = The height above sea level for the structure
$H_0 = 700$ m
$H_{topp} = 1300$ m

This gives $c_{alt} = 0.87$ since the height, H, at the construction site is 0 meters. c_{alt} is set to 1 if the value obtained is lower than 1. The values for c_{dir}, c_{dir}, c_{season} and c_{prob} are also set to 1 according to EC 1-4 NA.4.2(2)P. The mean wind velocity at the location is calculated with Equation 6.4.

$$v_m = v_b \cdot c_0 \cdot c_r \tag{6.4}$$

$c_0 = 1$
The roughness factor, c_r, is given by Equation 6.5

$$c_r = k_r \cdot ln\frac{z}{z_0} \tag{6.5}$$

$k_r = 0.17$
$z_0 = 0.01$ m

According to report 668, section 1.9.3 by the Norwegian Public Roads Administration, the height z is to be equal to an average height for the construction [33]. The wind pressure is calculated separately for the bridge deck and columns. For the bridge deck, the z-value is set to the average deck height in the corresponding section. Section B is split in two to account for the large difference in height over the length of the viaduct. The eastern part of section B is set at the same length as section D. The western part of section B is set at an equal height as section E (see Figure 3.2). This is a slightly conservative simplification. For the columns, the value of the highest column is chosen because the longest and most slender columns are of interest. The different sections are defined in Figure 3.2, and the corresponding heights are found in Table 6.1 below.

Table 6.1: Heights for the different sections of the bridge deck and columns

Section name	**Height above ground** z [m]
C	40.2
C_{colums}	37.2
$D = B_{east}$	35.0
$D_{columns} = B_east, columns$	35.9
$E = B_{west}$	26.7
$E_{columns} = B_{west,columns}$	29.3

This gives a mean wind velocity as presented in table 6.2.

Table 6.2: Mean wind velocity for the different sections of the bridge deck and columns

Section name	**Mean wind velocity** $v_m(z)$ [m/s]
C	38.1
C_{colums}	37.7
$D = B_{east}$	37.5
$D_{columns} = B_{east,columns}$	37.6
$E = B_{west}$	36.2
$E_{columns} = B_{west,columns}$	36.6

The wind gust velocity is calculated with Equation 6.6.

$$v_p(z) = (1 + 2 \cdot k_p \cdot I_v(z))^(\frac{1}{2}) \cdot v_s(z) \tag{6.6}$$

$I_v = \frac{k_I}{c_0 \cdot ln(\frac{z}{z_0})}$
$k_p = 3.5$
$v_s(z) = v_m(z)$
$k_I = 1$

Ultimately, Equation 6.7 is used to calculate the peak velocity pressure on the surface.

$$q_p = 0.5 \cdot \rho \cdot v_p(z)^2 \tag{6.7}$$

ρ = Density of air at ground level at 1.25 N/m^3

All wind loads are calculated with and without traffic. If $v_p(z) > 35$ m/s, then the peak velocity pressure is calculated with $v_p(z) = 35$ m/s when there is simultaneous traffic on the bridge. This gives the following results in Table 6.3.

Table 6.3: Wind gust velocity and peak velocity pressure for the different sections of the bridge deck and columns

Section name	**Wind gust velocity** v_p **[m/s]**	**Peak velocity pressure** q_p [kN/m^2]
C	51.7	1.67
C_{colums}	51.3	1.65
$D = B_{east}$	51.1	1.63
$D_{columns} = B_{east,columns}$	51.2	1.64
$E = B_{west}$	49.7	1.55
$E_{columns} = B_{west,columns}$	50.2	1.57
Without traffic	35	0.77

Loads on bridge deck

The bridge deck has an open parapet with a height of 2.5 meters. According to EC-1-4 Table 8.1, with open parapets and open safety barriers on both sides, the depth to be used in the wind calculations is set to the height of the bridge deck + 1.2 m. The height above the bridge deck with traffic load is 2 m, according to N400 [10].

The bridge deck height is set to 0.93 m for the plate part (section E), 1.5 m for the double T cross-section (sections B and D), and for the cantilever part, a middle height is calculated to 3.11 m. The depth, d, according to EC1-1-4, is calculated as the sum of the height and the parapet/traffic height. The width, b, is set to 10.1 m according to Figure 3.5. Finally, the force coefficient, c_{fx}, is calculated based on the difference between the width and depth of the bridge deck according to Figure 6.3.

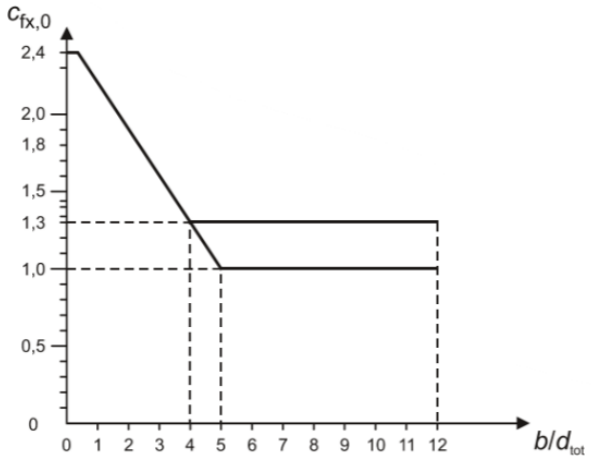

Figure 6.3: Calculation of force coefficient, c_{fx} [6]

The distributed horizontal wind load in the transversal direction, $f_{wind.x}$, is given in Equation 6.8.

$$f_{wind.x} = c_{fx} \cdot c_e \cdot d \cdot q_p \tag{6.8}$$

$c_e(z) = \frac{q_p(z)}{p_b}$
$q_b = 0.5 \cdot \rho \cdot v_b^2$

The distributed horizontal wind load in the longitudinal direction, $f_{wind.y}$, can be neglected, but if accounted for, it has the value of 25% of $f_{wind.x}$. The distributed vertical wind load is calculated in Equation 6.9

$$f_z = c_{fz} \cdot b \cdot q_p \text{ [kN/m]} \tag{6.9}$$

$c_{fz} = 0.9$

Because of load situations with and without traffic, separate values for the three load directions must be calculated. The final loads on the bridge deck are given in Table 6.4.

Table 6.4: Wind loads for the different sections of the bridge deck

Section name	**B-west**	**B-east**	**C**	**D**	**E**
Horizontal transversal w.o. traffic $f_{wind.x}$ [kN/m]	6.6	7.0	12.9	7.0	3.5
Horizontal longitudinal w.o. traffic $f_{wind.y}$ [kN/m]	1.7	1.7	3.2	1.7	0.9
Vertical w.o. traffic f_z [kN/m]	14.1	14.8	15.2	14.8	14.1
Horizontal transversal w. traffic $f_{wind.x.tr}$ [kN/m]	4.8	4.8	7.4	4.8	3.3
Horizontal longitudinal w. traffic $f_{wind.y.tr}$ [kN/m]	1.2	1.2	1.9	1.2	0.8
Vertical w. traffic $f_{z.tr}$ [kN/m]	7.0	7.0	7.0	7.0	7.0

To account for the torsional moment due to the eccentricity of the load vector, the line load is placed at a distance of $\frac{b}{4}$ from the neutral axis.

Loads on columns

The linear pressure on the columns due to the wind is given in Equation 6.10.

$$f_c = c_s c_d \cdot c_f \cdot q_p \cdot d \tag{6.10}$$

$d =$ Column diameter
$c_s c_d = 1$
$\frac{k_{ru}}{D} = 1.43 * 10^{-4}$
$D = 1.4$ m
$c_f = c_{f.0} \cdot \psi_\lambda \cdot \kappa$
$\psi_\lambda = 0.925$

$c_{f.0}$ is given in Figure 6.4 where the roughness, k_{ru}, is set to 1 mm due to the rough concrete on the south side of the bridge, as can be seen in Chapter 5. κ is calculated with EC1-4, Table 7.1. This factor considers the increased wind gust velocity when the wind passes between two columns. The nearer the columns are placed, the larger the increase of the wind. The Reynolds number is given in Equation 6.11.

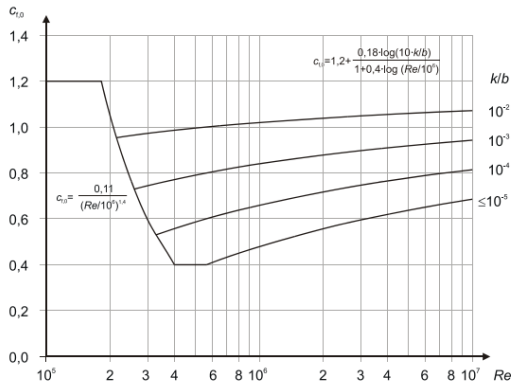

Figure 6.4: Calculation of $c_{f.0}$ [6]

$$Re_c = \frac{D \cdot v_m}{\nu_{air}} \tag{6.11}$$

$\nu_{air} = 15 \cdot 10^{-6} \ \frac{\mathrm{m}^2}{\mathrm{s}}$

Finally, the values of the distributed wind loads on the columns are given in Table 6.5.

Table 6.5: Wind loads for the different sections of columns

Section	**Column nu.**	**Load dir.**	**Load w. traffic [kN/m]**	**Load w.o. traffic [kN/m]**
B west	17 - 25	Longitudinal	1.00	2.02
B west	17 - 25	Transversal	0.94	1.89
B east	26 - 31	Longitudinal	1.00	2.13
B east	26 - 31	Transversal	0.94	2.00
C	32 - 37	Longitudinal	1.00	2.13
C	32, 37	Transversal	0.94	2.00
C	33 - 36	Transversal	0.01	2.14
D	38 - 43	Longitudinal	1.00	2.13
D	38 - 43	Transversal	0.94	2.00
E	44 - 56	Longitudinal	0.87	1.86
E	44 - 56	Transversal	0.87	1.86

The loads on the crossbars 6 m above ground are 1.629 kN/m^2 without traffic load and 0.766 kN/m^2 with traffic load. For the crossbars at the top, the loads are equal to the distributed wind loads divided by 4.2 m.

6.2 Deformation loads

6.2.1 Shrinkage

Shrinkage is the effect of size reduction in concrete due to drying and autogenous processes in the concrete [20]. Shrinkage strains are not affected by the load level. The total shrinkage strain is the sum of the strain due to drying and autogenous shrinkage. Drying shrinkage develops slowly and is influenced by moisture transport through the hardened concrete, while autogenous shrinkage is dependent on the concrete's strength development. As a result, most of the autogenous shrinkage occurs early after the concrete is cast. The total effect of the shrinkage strain on the stress-strain curve can be seen in Figure 6.5.

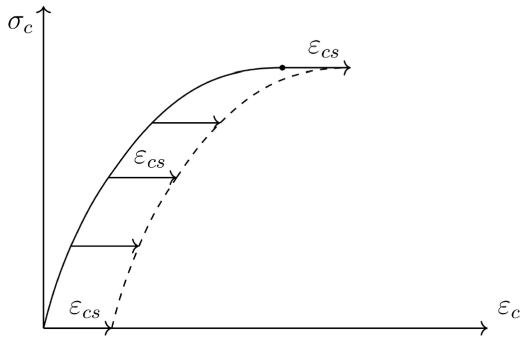

Figure 6.5: The effects on the stress-strain curve due to shrinkage [2]

Shrinkage is calculated for the three different cross-sections of the bridge (plate, double-T, and cantilever) in addition to the columns. For the cantilever, an average value for the cross-section was chosen.

The value for relative humidity in the air is set to 80% for the bridge deck and columns above water and 100% for the columns below water. It can be argued that the relative humidity on the inside of the hollow columns is closer to 100%, as shown in the humidity measurements made by Troms og Finnmark Fylkeskommune, but this has little effect [29]. The cement class is assumed to be of quality N. The general method for shrinkage calculation is based on NS-EN 1992-1-1, 3.1.4, and Annex B and is presented in this subchapter. The complete shrinkage calculations can be found in Appendix C.

The basic drying shrinkage strain is calculated in equation 6.12.

$$\epsilon_{cd,0} = 0.85 \cdot ((220 + 110 \cdot \alpha_{ds1}) \cdot e^{(-\alpha_{ds2} \cdot \frac{f_{cm}}{f_{cmo}}))} \cdot 10^{-6} \cdot \beta_{RH} \tag{6.12}$$

$\beta_{RH} = 1.55 \cdot (-(\frac{RH}{100})^3)$
RH - Relative humidity in %
$\alpha_{ds1} = 4$, for cement class N
$\alpha_{ds2} = 0.12$, for cement class N
f_{cm} = Mean value of concrete cylinder compressive strength
$f_{cmo} = 10$ MPa

The following four equations are found in EC-2 3.1.4:

$$\beta_{ds} = \frac{(t - t_s)}{(t - t_s) + 0.04 \cdot \sqrt{h_0^3}} \tag{6.13}$$

t = Time where drying started in days. Set to 4 days
t_s = Age of concrete in days. Set to $2.3 \cdot 10^4$ days
$h_0 = 2 \cdot \frac{A_c}{U}$ - A_c is area of cross-section and U is circumference.

The total drying shrinkage is given by Equation 6.14.

$$\epsilon_{cd} = \beta_{ds} \cdot k_h \cdot \epsilon_{cd,0} \tag{6.14}$$

k_h is a value between 0.8 and 0.7 for the different cross-sections.

Next, the autogenous shrinkage strain is calculated using Equation 6.15.

$$\epsilon_{ca} = \beta_{as} \cdot \epsilon_{ca,\infty} \tag{6.15}$$

$\beta_{as} = 1 - e^{(-0.2 \cdot t^{0.5})}$
$\epsilon_{ca,\infty} = 2.5 \cdot (f_{ck} - 10) \cdot 10^{-6}$
f_{ck} = Characteristic compressive cylinder strength of concrete at 28 days

Finally, the total shrinkage strain is given in Equation 6.16.

$$\epsilon_{cs} = \epsilon_{ca} + \epsilon_{cd} \tag{6.16}$$

Shrinkage is calculated for each of the three bridge deck types, the massive columns above and below water, and the hollow columns above and below water. The results are shown below in Table 6.6.

Table 6.6: Shrinkage value for the different parts of the bridge

Section	**Shrinkage [‰]**
Plate bridge	0.247
Beam bridge	0.266
Box bridge	0.264
Hollow columns above water	0.240
Hollow columns below water	0.025
Massive columns above water	0.231
Massive columns below water	0.025

6.2.2 Creep

Creep is an additional deformation that is a result of long-term loading. When concrete is subjected to loads over a long period of time, it will continue to be compressed beyond the initial compression that occurs when the load is applied. Creep propagates differently for various strengths and when the concrete is first loaded. For the Tromsø Bridge, the initial load occurrence is set at 28 days. In reality, this is not totally accurate, given the self-weight is probably applied around day 3-5 and the various live loads are applied at a time after 28 days. Because of very little information about the exact load time, the assumption is taken that all loads are applied at 28 days. Since the bridge has two different concrete qualities as per Table 3.6, two creep coefficients are calculated. Creep calculations follow the procedure described in EC2 Annex B.1 [8]. This procedure is presented here and the complete calculations can be found in Appendix C. Coefficients to consider the influence of the concrete strength are calculated using Equations 6.17 to 6.19.

$$\alpha_1 = (\frac{35}{f_{cm}})^{0.7} \tag{6.17}$$

$$\alpha_2 = (\frac{35}{f_{cm}})^{0.2} \tag{6.18}$$

$$\alpha_3 = (\frac{35}{f_{cm}})^{0.5} \tag{6.19}$$

Next, the factor describing the creep development in terms of time after loading is calculated:

$$\beta_c(t, t_0) = \frac{(t - t_0)}{\beta_H - (t - t_0)} \tag{6.20}$$

$\beta_H = 1.5(1 + (0.012RH)^{18}h_0 + 250 < 1500$ for $f_{cm} < 35$ MPa
$\beta_H = 1.5(1 + (0.012RH)^{18}h_0 + 250\alpha_3 < 1500\alpha_3$ for $f_{cm} > 35$ MPa

The factor that takes into account the effect of the standard creep rate at the age of the concrete when loaded is calculated using Equation 6.21.

$$\beta(t_0) = \frac{1}{(0.1 + t_0^{0.2})} \tag{6.21}$$

The factor that takes into account the effect of the concrete strength on the normed creep rate is found with Equation 6.22.

$$\beta(f_{cm}) = \frac{16.8}{\sqrt{f_{cm}}} \tag{6.22}$$

The factor that takes into account the effect of relative humidity on the normalized creep rate is calculated based on the value of f_{cm}. For section C, Equation 6.23 is used and for the rest of the bridge, Equation 6.24 is used.

$$\varphi_{RH} = 1 + \frac{1 - RH/100}{0.1 \cdot h_0^{1/3}} \tag{6.23}$$

$$\varphi_{RH} = (1 + \frac{1 - RH/100}{0.1 \cdot h_0^{1/3}} \cdot \alpha_1) \cdot \alpha_2 \tag{6.24}$$

Finally, the creep coefficient is calculated with Equation 6.25.

$$\varphi(t, t_0) = \varphi_0 \cdot \beta_c(t, t_0) \tag{6.25}$$

$\varphi_0 = \varphi_{RH} \cdot \beta(f_{cm}) \cdot \beta(t_0)$

To calculate the long time Young's modulus of the concrete due to creep, Equation 6.26 is used.

$$E_{cm.c} = \frac{E_{cm}}{1 + \varphi(t, t_0)} \tag{6.26}$$

E_{cm} is the secant modulus of elasticity of concrete after 28 days.

The value for the creep coefficient, $\varphi(t, t_0)$, and long time Young's modulus, $E_{cm.c}$, is calculated for the three cross-sections of the bridge deck and for the columns and presented in Table 6.7.

Table 6.7: Creep coefficients and long time Young's modulus

Section	$\varphi(t, t_0)$	$E_{cm.c}$ **[MPa]**
Plate	1.619	8912
Beam	2.034	7735
Box	1.985	10261
Massive columns above water	1.869	8134
Massive columns below water	1.525	9241
Hollow columns above water	1.947	7918
Hollow columns below water	1.534	9210

6.2.3 Thermal loads

Thermal loads give internal forces caused by the expansion of the bridge due to increased temperature. This happens because the Tromsø Bridge is a multiple-time statically indeterminate structure. The calculations are based on EC5 and handbook N400 [7] [10].

Evenly distributed temperature contribution

The maximum and minimum air temperature in Tromsø with a 50-year return period, based on Figure NA.A1 and NA.A2 in EC1-5 is $T_{max} = 34\ ^\circ C$ and $T_{min} = -25\ ^\circ C$. The max and min evenly distributed temperature in the bridge based on type 3 bridge (concrete), using Figure NA 6.1 is then:

$$\begin{aligned} T_{e,max} &= 34 - 3 = 31\ ^\circ C \\ T_{e,min} &= -25 + 8 = -17\ ^\circ C \end{aligned} \tag{6.27}$$

According to EC1-5 NA.A.1(3), the initial temperature for the expansion and contraction interval can be set to $T_0 = 10\ ^\circ C$. This gives a contraction-expansion interval of $\Delta T_{N,exp} = T_{e,max} - T_0 = 21\ ^\circ C$ and $\Delta T_{N,con} = T_0 - T_{e,min} = 27\ ^\circ C$. As explained in Chapter 5, the expansion joints in the bridge close at $17\ ^\circ C$. The initial temperature for the expansion and contraction interval is therefore set to $17^\circ C$, and the expansion interval is: $\Delta T_{N,exp} = 14\ ^\circ C$.

Vertically varying temperature

The vertically varying temperature is found based on Eurocode 5, NA Table 6.1: where $\Delta T_{M,heat}$ describes the difference in temperature where the top is warmer than the bottom, and $\Delta T_{M,cool}$ describes the opposite. For the box girder part of the bridge (parts of section C):

$$\begin{aligned} \Delta T_{M,heat} &= 10\ ^\circ C \\ \Delta T_{M,cool} &= 5\ ^\circ C \end{aligned} \tag{6.28}$$

For a plate cross-section of the bridge:

$$\begin{aligned} \Delta T_{M,heat} &= 15\ ^\circ C \\ \Delta T_{M,cool} &= 8\ ^\circ C \end{aligned} \tag{6.29}$$

6.3 ASR loads

The expansions associated with ASR provoke internal load effects by imposing strains upon the cross-section. Figure 6.6 provides a visual representation of the expansion that occurs in an under-reinforced beam cross-section, featuring both top and bottom reinforcement.

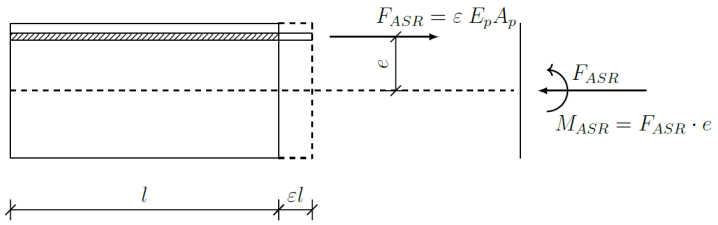

Figure 6.6: Expansion of reinforced concrete beam due to ASR [2]

To accurately determine the stresses occurring within the concrete, it is assumed full bond between reinforcement and concrete is established. Consequently, this expansion causes a fictitious strain, which, in turn, induces additional forces within the reinforcing steel. The forces observed within the concrete are tied to the forces experienced by the reinforcing steel, albeit with opposing signs. Accordingly, this gives rise to a resultant force and a related moment due to the eccentricity between the reinforcement and the neutral axis (NA) of the cross-section. The moment resulting from the ASR-induced expansion can be accurately determined by using Equation 6.30. This equation takes into account reinforcement layers on both sides of the neutral axis.

$$M_{ASR} = F_{ASR,uk} \cdot e_{uk} - F_{ASR,ok} \cdot e_{ok} \tag{6.30}$$

$F_{ASR,x} = \epsilon_c \cdot E_s \cdot A_s$
e = Distance from the neutral axis to the reinforcement bar

In more general terms, it is essential to acknowledge the potential presence of multiple layers of reinforcement located both above and below the neutral axis of the cross-section. In such scenarios, to calculate the corresponding moment, the force in each bar multiplied by the distance from the NA is summed together.

The resulting state of stress within the concrete cross-section is depending on the current condition of the structure. For beam structures in stage I, the neutral axis closely approximates the centroid axis. However, as the structure advances into stage II, deviations between these axes become apparent, primarily because of the propagation of cracks extending toward the neutral axis. Due to the relatively low permanent loads on the bridge and the results from the permanent moments from the master thesis of Sandnes, E. and Skaug, L, the ASR loads are considered to occur in or close to stage I for all the cross-sections and are therefore this method used in this thesis [2].

6.3.1 ASR loads in bridge deck

In order to find the loads from ASR in the bridge deck, the geometry for the three parts of the bridge (plate, beam, and box) must be examined, since ASR expansion gives different internal moments and axial forces depending on the geometry of the cross-section. To accurately represent the ASR load, 12 sections were calculated: 6 in section C due to the varying cross-section, and 6 in the rest of the bridge: Over the supports and in the field of sections B/D and A/E and above support 32/37 and in the field between 31-32/37-38, since these are reinforced differently than sections B/D. The method used for calculating the moments and axial forces is described in this subchapter. The complete calculations are found in Appendix F. The following assumptions are made:

- Concrete in compression and steel are linearly elastic as per Hooke's law.
- The tensile strength of concrete is neglected.
- Euler/Bernoulli's hypothesis regarding plane cross-sections remaining plane and normal to the axis during bending is valid.
- The cross-section is in stage II.

Firstly the equations to work with transformed cross-sections are established in Equation 6.31 to 6.33. This is an example of the calculations for a cross-section between two columns at midspan.

$$\eta = \frac{E_s}{E_{cL}} \tag{6.31}$$

E_s - Young's modulus for steel
E_{cL} - Long time Young's modulus for concrete

$$A_t = A_c + (\eta - 1) \cdot A_s u \tag{6.32}$$

A_c - Area of concrete
A_s - Area of reinforcement

$$I_t = I_c + A_c \cdot y_t^2 + (\eta - 1) A_{su} \cdot e_s^2 \tag{6.33}$$

I_c - Second moment of area for the concrete cross-section
y_t - Difference in the centre line of gravity from the original cross-section due to the transformed cross-section
e_s - Distance from the new centre line of gravity to reinforcement

Based on a uniform ASR expansion of 0.55‰ as per Chapter 5, the final strain $\epsilon_{def} = \epsilon_{ASR} - \epsilon_{shrinkage}$ is calculated for each cross-section. This strain gives a curvature to the member based on the reinforcement placement as calculated in Equation 6.34.

$$\kappa = \frac{M_{ASR}}{E_{cL} I_t} \tag{6.34}$$

$M_{ASR} = N_{ASR} \cdot e_s$
$N_{ASR} = \epsilon_{ASR} \cdot E_s \cdot A_s$

The final curvature, κ, in the cross-sections, is found in Table 6.8.

Table 6.8: Curvature and temperature gradient due to ASR

Section	κ **[1/m]**
B,D - field	$5.7 \cdot 10^{-5}$
A,E - field	$3.8 \cdot 10^{-5}$
31 to 32 and 37 to 38 - field	$7.3 \cdot 10^{-5}$
B,D - support	$-2.6 \cdot 10^{-5}$
A,E - support	$-1.1 \cdot 10^{-5}$
31 and 38 - support	$-3.4 \cdot 10^{-5}$
C - center of cantilever	$7.0 \cdot 10^{-5}$
C - section 4	$-2.0 \cdot 10^{-5}$
C - section 7	$-1.1 \cdot 10^{-5}$
C - section 10	$2.4 \cdot 10^{-5}$
C - section 14	$-2.5 \cdot 10^{-5}$
C - section 20	$-3.2 \cdot 10^{-5}$

6.3.2 ASR loads in columns

The propagation of the ASR expansion in the columns is believed to be quite small in the longitudinal direction as presented in Chapter 5. This is because concrete members loaded in permanent compression will have a reduced expansion. From experiments, it has been found that compression stress of 3 $\frac{\text{N}}{\text{mm}^2}$ is enough to reduce the expansion with as much as 50% [1]. Based on this, the assumption is made that the total ASR expansion is in the same range as the shrinkage and is, therefore, close to 0‰. The only internal effect in the columns which can give moments due to ASR, is if one side of the cross-section experiences larger expansion than the other. This ASR gradient can then give a curvature in the columns. This effect is described in Chapter 10. If the expansion in the columns is equal throughout the cross-section, the double symmetrical reinforcement layout will prevent any curvature of the member.

6.4 Load combinations

For loads that are most likely to occur simultaneously, a combination with combination factors should be calculated. In defined limit states, it must be demonstrated that the load effect does not exceed the resistance. Depending on the usage classification, it may be relevant to perform checks in the following limit states: ultimate limit state (ULS), serviceability limit state (SLS), accidental limit state (ALS), and in some cases also in the fatigue limit state. The minimum requirement is to check in the ultimate limit state, while the other limit states are checked if they are considered relevant.

Collapse or various forms of structural failure are related to the ultimate limit state (ULS). Relevant topics include loss of equilibrium, overturning, sliding, cross-sectional failure, extensive displacements, or fatigue failure. In the ultimate limit state, two critical situations should be considered for each load case, and the most unfavourable of the combination situations is selected for further checks. Table 6.9 provides an overview of the load factors in the ultimate limit state.

Table 6.9: Load-factors for Ultimate Limit State

Loadgroup	**Permanent Loads**		**Deformation**	**Variable**
Combination	**Ground pressure**	**Self-weight**	**loads, D**	**loads Q**
a	$1,0$	$1,15$	γ_D	$\gamma_1 \cdot Q_1$
b	$1,0$	$1,0$	$1,0$	$\gamma_2 \cdot Q_1 + 0,8 \cdot \sum Q_n$

The values for the specific load factors are given on in V412 [11]. The load factors are also specified in Handbook R412 with additional values for special transports, mobile cranes, and one-time transports. Q_1 is the characteristic value for the variable load that is most unfavourable for the load effect being considered, and Q_n is the characteristic value for other variable loads that are unfavourable for the load effect.

In the serviceability limit state (SLS), the focus is on the structure in the usage phase and functionality. This may involve deformations and deflections, vibrations, oscillations, and crack widths. This thesis will not consider SLS or fatigue limit state.

7 Modelling

The bridge was modelled in its entirety using Dynamo Sandbox [34] to define the geometry. Further, a plugin was used to convert the model to Robot Structural Analysis [35]. This approach allowed for a high level of flexibility in defining the geometry of the bridge and making necessary simplifications.

The purpose of modelling the full bridge was to establish the forces in the columns of interest for further investigation. As the bridge deck is much stiffer than the columns, and the acting forces on the columns are the desired output of the analysis, all columns have been designed massive, without reinforcement, but for all columns cast hollow, the second area of moment has been reduced to represent them correctly.

As shown in Figure 3.2 the bridge is split into sections A, B, C, D, and E. There are expansion joints at both ends of the cantilever part (section C). This allows for a natural division of the model at these joints. Figure 7.6 exhibits this division. The cantilever part can be seen as a separate, independent, structural component. All columns are assumed fixed to the foundations, although a small rotation in the cast concrete supports should be expected. The columns are also assumed to be fixed to the main beams at the top. This is reasonable as the main beams and the bridge deck is much stiffer than the columns $EI_{deck} > EI_{columns}$. The support of the bridge deck is further discussed in the following subchapters.

7.1 Defining geometry - Dynamo Sandbox

Dynamo Sandbox is a visual programming tool for parametric modelling, data processing, and geometry manipulation. By using a parametric programming tool, refining the division of members and modifying the geometry becomes much simpler.

By defining the geometry in Dynamo, emphasis could be placed on ensuring a neat, simple, yet effective mesh for analysis. The parametric features were utilized to refine the model, finding an effective synergy between accuracy and runtime. The cross-sections, materials, chosen mesh, and loads were applied in Robot to decrease runtime and make the model easier to process.

Using the add-in feature *Structural Analysis*, the model was automatically converted to Robot and updated simultaneously with the Dynamo model. The geometry was defined by connecting lines between points of intersections or supports. The bridge deck and beams were defined by lofting a surface between lines at the top and bottom of the desired section. The columns were defined by assigning the lines a geometry, thickness, and material previously added to the Robot database. Likewise, the surfaces were given similar attributes making them appear as solid beams or plates in the model.

The "skeleton" models produced in Dynamo for the three different parts of the bridge are shown below in Figures 7.1, 7.2 and 7.3:

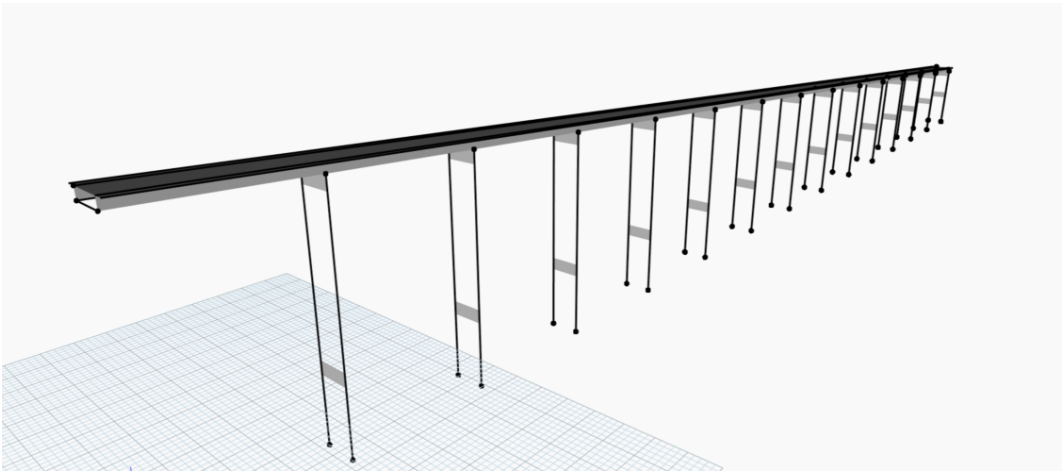

Figure 7.1: Dynamo-model section A,B

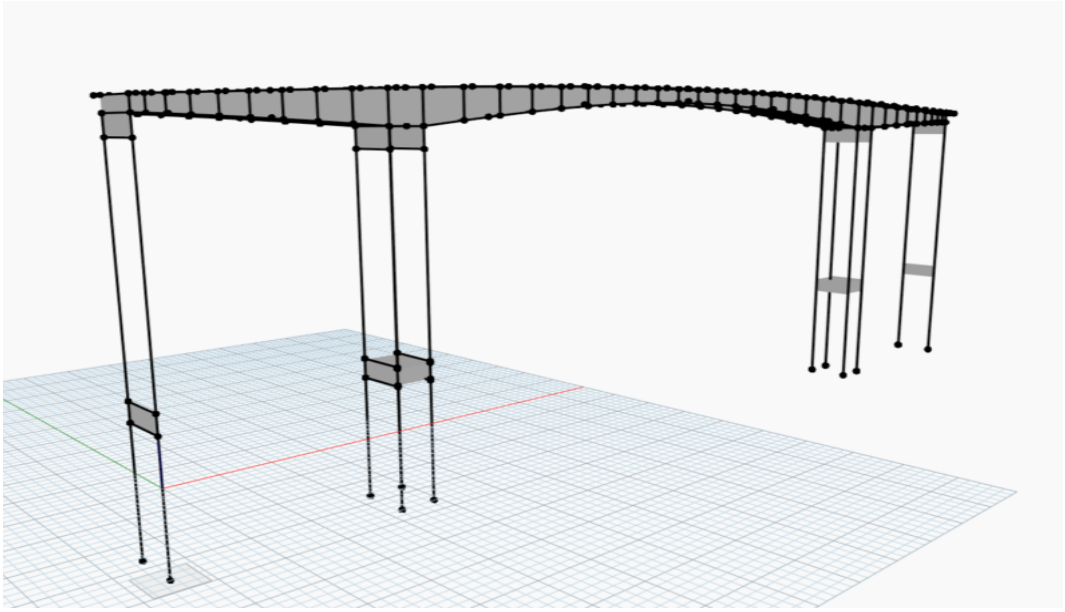

Figure 7.2: Dynamo-model section C

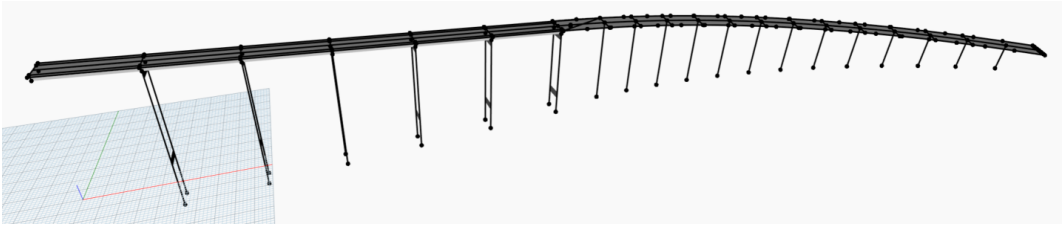

Figure 7.3: Dynamo-model section D,E

Utilizing the parametric features of Dynamo, the complicated shape of the main beams in section C could be split into smaller elements, as shown in Figure 7.4. The simplified connection of the crossbars in the column group axis 33-34 is also shown in the figure.

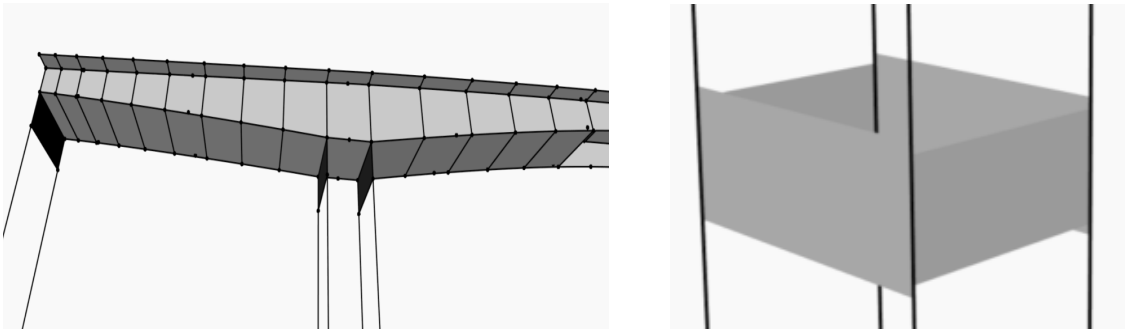

(a) Detail - Main beams (b) Detail - Crossbar connection

Figure 7.4: Details section C

The transition between sections D and E, from a beam section to a plate cross-section, has also been simplified slightly, as shown in Figure 7.5.

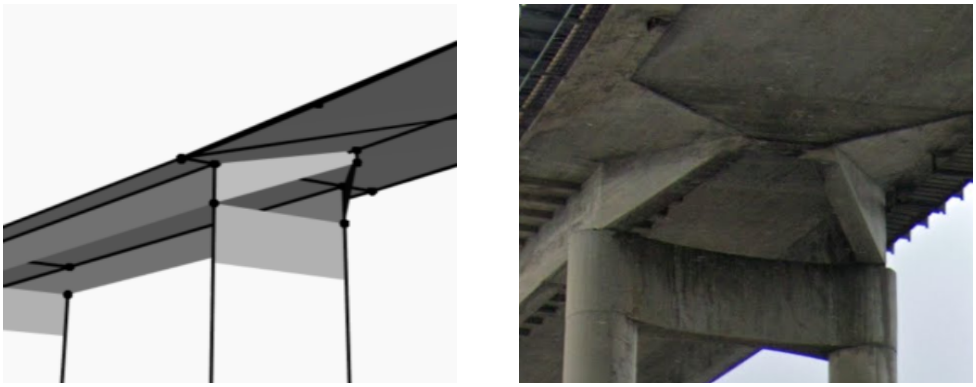

(a) Detail - Robot (b) Detail - Google maps [36]

Figure 7.5: Detail section D,E

7.2 Structural system

As the characteristics of the sections vary, three separate models were designed. This was useful to maintain the models' low run-time and simplicity. Each model and its characteristics are briefly described below.

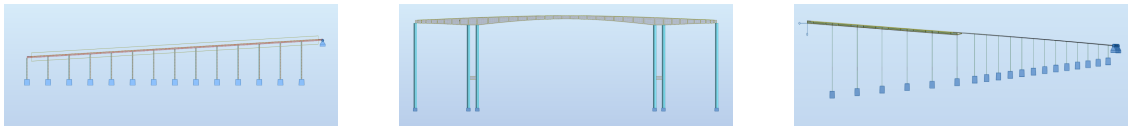

(a) Section A,B (b) Section C (c) Section D,E

Figure 7.6: Overview model section A, B, C, D, and E

7.2.1 Section A, B

Section A, B consist of the viaduct connecting Tromsøya with the cantilever part of the bridge (section C). This part was only modelled from axis 18 to 31 as the columns from axis 0 to 17 are of less interest and will not contribute to the forces in the columns closer to section C, which is more critical in sections A and B. The expansion joint is placed in axis 32, where section A and B ends. The joint is modelled using simple supports simulating a closed joint, free to rotate. The forces in

the most extreme load combination are transferred as point loads to section C. The height of the columns is discussed in Subchapter 3.2. The bridge deck and crossbars are assumed squared. The characteristics of the beams, deck, and columns are shown in Table 7.1. The model in Robot can be seen in figure 7.7.

Table 7.1: Modelled components section A,B

Part	**Material**	**Thickness [mm]**
Beams	A-concrete (C20)	500
Deck	A-concrete (C20)	186
Crossbars	A-concrete (C20)	600
Columns	A-concrete (C20)	Ø1400 - hollow

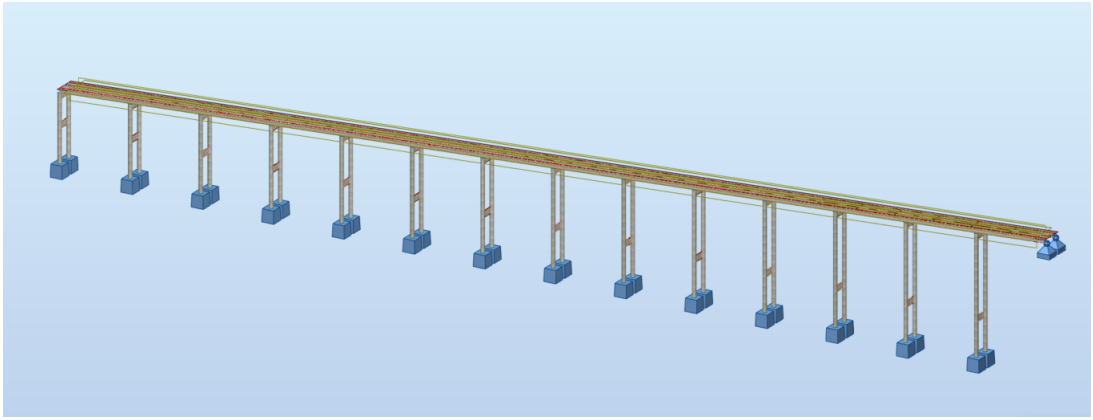

Figure 7.7: Model section A, B

7.2.2 Section C-cantilever

Section C is the cantilever part of the bridge. This part can easily be isolated from the rest of the bridge due to the expansion joints. The columns in axis 32 and 37 are included in section C. The box-girder cross-section is slightly simplified compared to the drawings. The bottom plate providing additional stiffness over the columns has been shifted down slightly to follow the bottom of the main beams. This was done to avoid a complex mesh and singular points in the sharp corners that appeared by following the exact geometry. The simplification will have a very small impact on the results obtained. Further, the crossbars were also assumed square in the model, while they have a concave shape in reality. The columns start at 10 m below sea level as discussed in Subchapter 3.2.

The forces due to the closed expansion joint from sections C to AB and DE are modelled as point loads taken from the most extreme load combination. To allow a difference in these forces, but at the same time avoid displacement in the x-direction due to the continuous bridge deck with closed expansion joints, a support with restricted movement in the x-directions is placed in the bridge deck on the eastern side of model C. The east side is chosen since the AB side is expected to have larger compression forces on the C section due to the possibility of section DE bending out of the bridge deck direction at the curvature on the Tromsdalen side. The model in Robot can be seen in figure 7.8.

The characteristics of the modelled components of section C are shown in Table 7.2.

Table 7.2: Modelled components section C - cantilever

Part	**Material**	**Thickness [mm]**
Beams	B440 concrete (C32)	350
Deck	B440 concrete (C32)	230
Stiffening plates	B440 concrete (C32)	200
Crossbars parallel	A-concrete (C20)	400
Crossbars perpendicular	A-concrete (C20)	600
Columns	A-concrete (C20)	Ø1400 - massive

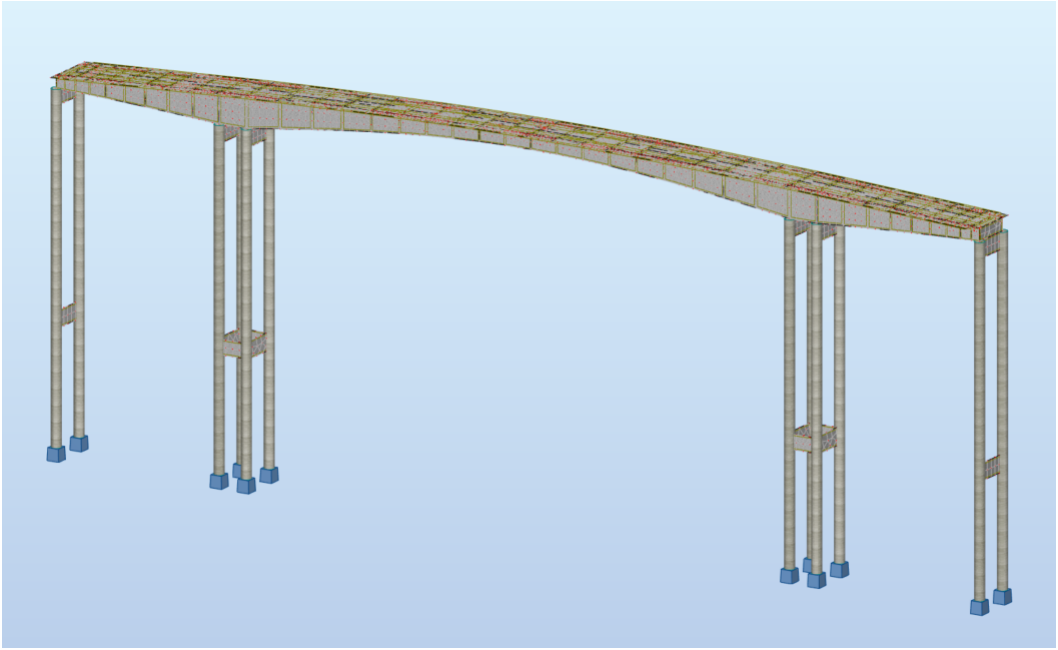

Figure 7.8: Model section D,E

7.2.3 Section D, E

Section D, E was modelled in its entirety, ending in axis 56 where the mainland starts. The connection to the mainland is modelled using simple supports. In the other end, connecting section D to section C, the solution is similar to section B where simple supports are used to replace the columns and to ensure that no moment is transferred to section C. The forces in the most extreme load combination are transferred as point loads where the columns are in section C. The foundation of the columns in section E is set to the inclination of the ground, whereas the foundation of the columns in section D varies from 8.33 m below to 0 m above sea level, see Subchapter 3.2. The model in Robot can be seen in figure 7.3.

The bridge deck and crossbars are assumed squared. The characteristics of the beams, deck, and columns are shown in Table 7.9.

Table 7.3: Modelled components section D,E

Part	Material	Thickness [mm]
Beams	A-concrete (C20)	500
Deck	A-concrete (C20)	186
Crossbars	A-concrete (C20)	600
Columns	A-concrete (C20)	Ø1400 - massive
Deck - curved section	A-concrete (C20)	336
Columns - curved section	A-concrete (C20)	Ø1400 - hollow

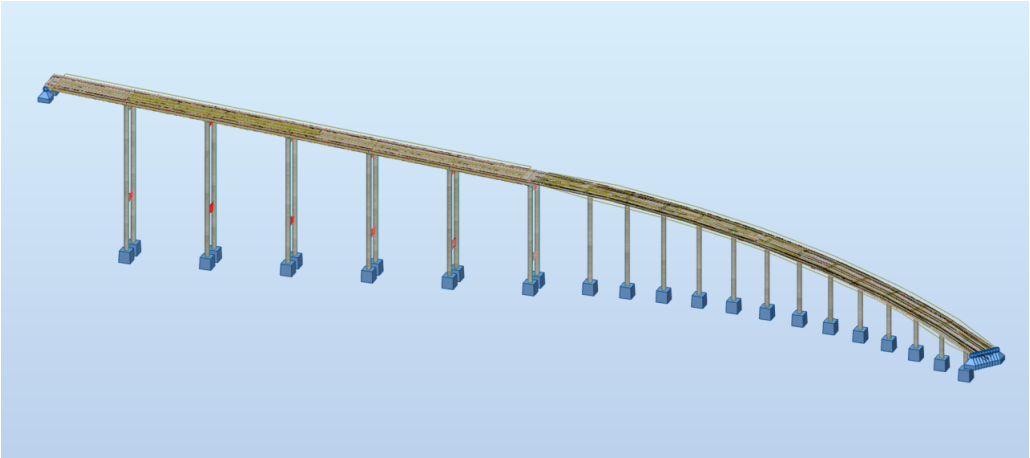

Figure 7.9: Model section D, E

7.3 Mesh and FEM analysis

Robot Structural Analysis [35] is a finite-element analysis program used for static analysis in this thesis. The mesh is made up of 3-node triangular (CST) and 4-node quadrilateral (Q4) elements. 3-node and 4-node elements are sufficient, as opposed to 6 or 8 nodes, for the purposes of this analysis, as the model is made of simple beam and plate elements. The size of the elements was set to 1 m. It was seen that a further decrease in the element size increased the run-time significantly, while the results remained very similar.

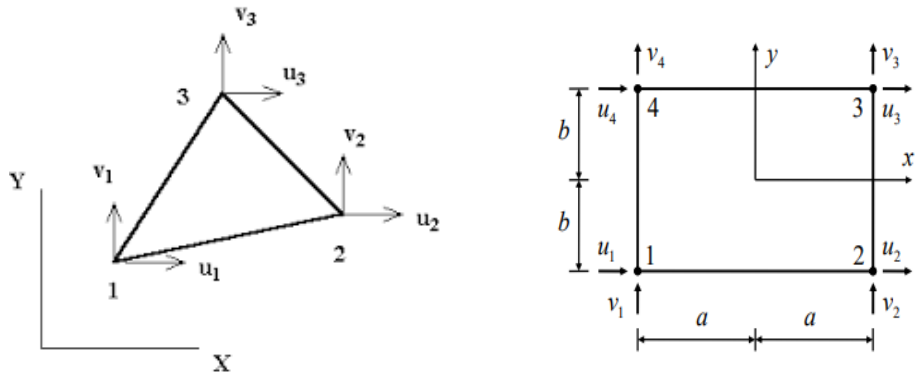

(a) Element - CST (b) Element - Q4

Figure 7.10: Finite elements used in the Robot model [37]

Initially, the stiffening plates connecting the beams underneath the bridge deck were modelled with the exact geometry. This caused several problems with regard to the mesh generated in

Robot, provoking convergence errors and unsustainable run times. Therefore, the geometry of these stiffening plates was modified slightly as described in Subchapter 7.2.2.

The elements have six degrees of freedom per node, including translation and rotation along three axes. The technical beam theory assumes that shear deformations are neglected for the elements and that Navier's hypothesis, stating that plane cross-sections remain plane holds true. The idealized model is based on assumptions of homogeneous elastic material and linear behaviour [37].

All edges of the model have been kept as square-shaped as possible to ensure a neat mesh. This proved to be highly important in obtaining reliable and predictable results. This also eliminated singular points that would have appeared and disturbed the model otherwise.

7.4 Application of loads

7.4.1 Permanent loads

The self-weight of the bridge is taken into account by Robot. The thickness of all elements is defined, as well as the material. Hence this is automatically included as a dead load in the structure.

Super self-weight and traffic loads were applied using the feature referred to as *cladding* in Robot. This defines an area on a given geometry without weight or stiffness. By implementing claddings, notional lanes can be defined, and loads can be applied over specific areas to create special load cases.

7.4.2 Traffic loads

Light traffic was applied over the entire length of the notional lanes, while shorter claddings were defined for heavy traffic. By defining separate claddings for each vehicle and applying the heavy traffic loads separately, finding the desired load combination becomes less challenging. In addition, this allows for combinations where two heavy vehicles are in the same lane next to each other.

The live loads from the pedestrian/bicycle lanes were added as a line load to each end of the bridge deck. This was also done for the safety barriers and the parapet.

7.4.3 Wind loads

The wind loads have two different directions, in the longitudinal and transversal directions of the bridge. These two directions also have five loads each: Loads on columns, crossbars, vertical loads on the bridge deck, moment due to this vertical load eccentricity, and finally, the horizontal load on the bridge deck itself. The loads on the columns and crossbars were applied as line loads and surface loads. This could not be done on the bridge deck as the load was to include the wind load on the parapet as well. To combat this, a beam with no weight and very low stiffness was placed at the height of the neutral axis on the side of the entire bridge deck. The transversal, horizontal load was then applied as a line load. Finally, the horizontal load in the longitudinal direction was applied as a surface load in the x- direction on the bridge deck itself. At the bridge deck surface, the no-weight, low-stiffness beam was placed at a distance $\frac{b}{4}$ from the centre so that the vertical load also gave a moment due to eccentricity. In Section D, where the bridge is curved, this was difficult to offset, so here, the beam was placed at the centre, and a line moment was added.

7.4.4 ASR loads

The curvature due to the combined effects of shrinkage and ASR is converted into a thermal load gradient using Equation 7.1.

$$\Delta_T = \kappa \cdot \frac{h}{\alpha_T} \tag{7.1}$$

h - Height of cross-section
$\alpha_T = 9.8 \cdot 10^{-6} \cdot K^{-1}$

This gives a value for each of the six cross-sections of the plate/beam bridge and the six sections chosen from the cantilever part. The values from the cantilever part were interpolated to fit with the element length for the Robot model, and the rest of the bridge was divided into sections of mid-span and support based on the assumption of where the reinforcement layout changed. The thermal gradients were then applied as thermal loads to the concrete sections.
A temperature gradient was used to calculate the loads due to the curvature of the columns from a possible different ASR expansion on the north vs. south side. This was modelled to represent $2,7‰$ expansion on the south side and $0‰$ on the north side. This is explained further in Chapter 10.

7.4.5 Creep and thermal loads

The creep effect on the structure is automatically accounted for in Robot by defining a creep coefficient. The elements' final creep coefficient was assigned based on the concrete quality.

As explained in Subchapter 6.2.3, the thermal load state was examined at closed expansion joints (temperature $> 17\ ^\circ C$) and at open expansion joints (temperature $< 17\ ^\circ C$). To model this, at closed joints, displacement in the x- direction was prohibited. Two load cases were run, one at low and one at high temperatures. Even though the temperature span was smaller with the expansion joints closed, this gave the columns a more unfavourable load situation. Therefore, this was the effect used for the final model.

8 Selected columns

In the Tromsø Bride, different columns have a different reinforcement layouts. This is because of the variances in lengths and forces due to the variable loads. The reinforcement layout drawings from Aas-Jacobsen are found in Appendix A. This means a shorter column with smaller forces can be closer to failure than a longer column with higher forces. Based on this, this chapter aims to identify the most loaded columns and, based on the reinforcement layout, investigate these more thoroughly. This selection process is done by looking at the bridge's structural system, the attack points of the most critical loads, damage explored in previous inspections, support conditions, ASR damage, and properties of the cross-sections. From this, four regions were chosen to be investigated. These regions and the corresponding columns are described in the next subchapters.

8.1 Column 30/31 and 38

The columns on both sides of the cantilever part are interesting for multiple reasons. They are the tallest, hollow columns on the bridge and are thus the most slender. The expansion joints at axis 32 and 37 are also considered simply supported towards the viaduct, thus allowing rotation of the bridge deck. This means that the moment about the y-axis is assumed greater in columns 31 and 38 than any other in the viaduct.

8.2 Column 32 and 37

The columns in axis 32 and 37 are believed to be less critical than the ones in 33 to 36, but they are still worth investigating for several reasons. Firstly, they are connected to the rest of the cantilever part, which experiences the largest forces of the bridge. Secondly, they are also subjected to point loads from the viaduct due to the expansion joints. They are, however, cast with massive cross-sections [38], but have a higher axial force due to the larger cross-section of the box bridge deck.

8.3 Column 33 to 36

The columns in the centre of the cantilever part are believed to be the most critical. This is mainly because of the load situation. Even though they are cast massive and connected with crossbars in both directions, they are believed to be subjected to the highest stress due to the massive weight of the cantilever part and the added forces from, i.e., wind on the bridge deck.

8.4 Column 44 to 49

The columns in Section E are cast as hollow, single columns. They are shorter than the ones in the viaduct but are also less reinforced. However, the most interesting aspect is the curvature of this section. A high expansion value due to ASR combined with high temperature is shown to push the columns in the transversal direction of the bridge. This causes increased second-order moments. These columns are believed to be cast with a less reactive aggregate, but tests taken in 2022 have proven ASR-reactive aggregates in the concrete [39]. The columns on either side of Tromsøysundvegen E8 (axis 47 and 48 in Figure 8.1) are cast massive for the first few meters and are less critical as the large moments are believed to appear at the bottom.

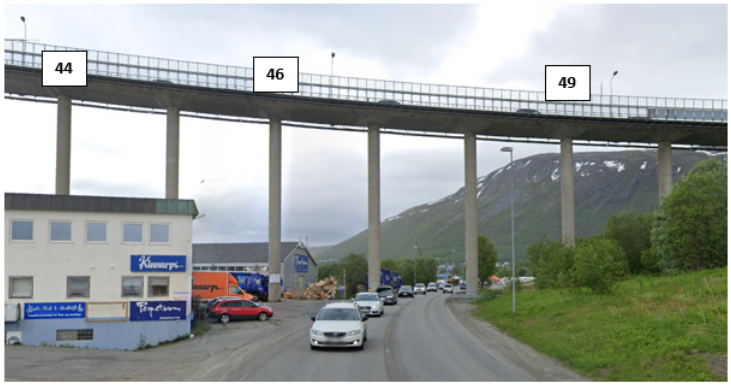

Figure 8.1: Columns in section E [36]

8.5 Variables in cross-section

From the original drawings of the columns found in Appendix A, the amount and length of the reinforcement are given. However, the reinforcement layout in the cross-section is unclear for all columns. The only drawing of a column cross-section where the reinforcement layout is evident is in the drawing of columns 33 to 36 in Figure 8.3 (a) below. Here the filled-in black circles are the reinforcement that runs the entire column length, while the white, non-filled circles are the extra reinforcement around the crossbars and at the supports. As can be seen in the foundation drawing of the same columns (Figure 8.3 (b)) the same reinforcement layout is also found here. Meanwhile, in the foundation drawing of columns 30-31 and 38-39 in Figure 8.2, the continuous and extra reinforcement found here is placed symmetrically. The only other drawing showing asymmetrical reinforcement is the foundation drawing of column 42 (Appendix A), but due to the low moments, this column will not be investigated in this thesis. Based on this, the assumption was taken that only the columns around the mid-span have asymmetrical reinforcement layouts in part of the span. This is based on the high extra moments in the transverse direction due to the wind. For all other columns, the extra reinforcement around the supports and crossbars was placed symmetrically in the columns. Based on the drawings in Appendix A, the concrete cover is assumed to be 70 mm below +5.5 m above sea level and 50 mm above +5.5 m. This is the height to where the bottom crossbars start.

In Figure 8.3 (b), all reinforcement in the inside layer is drawn as an extra line in the section drawing to the right. Based on this, the different reinforcement amounts and layers are shown in Table 8.1 below. The layers are separated by a "+" sign, apart from column 34, where the middle number is used to mark the eight extra bars in the outer layer. See Appendix B for all reinforced cross-sections. In Figure 8.4, the different sections of the five reinforcement "regions" are shown.

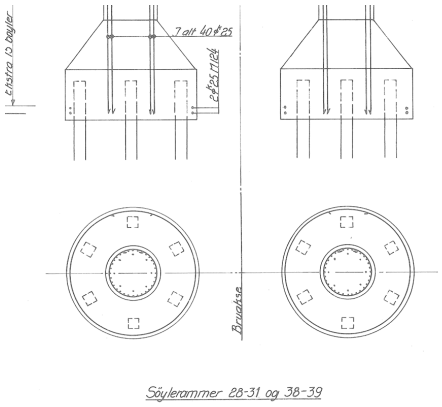

Figure 8.2: Reinforcement of column 31 at foundation

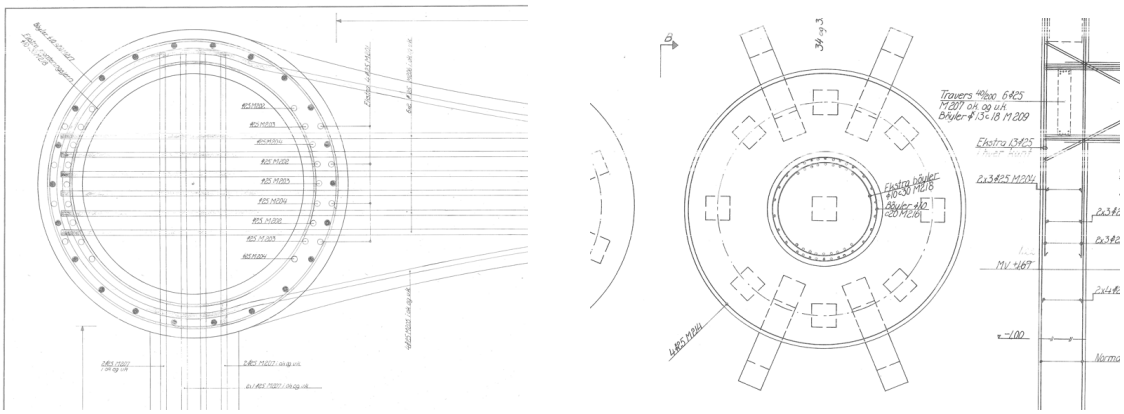

(a) cross-section near crossbar (b) Foundation

Figure 8.3: cross-section of columns 33-37 at crossbar and foundation

Table 8.1: Overview reinforcement selected columns [36]

Cross-section	**30, 31 [index]**	**32 massive [index]**	**34 massive [index]**	**38 [index]**	**44, 46, 49 [index]**
Crossbar top [XX.1]	24+16Ø25 [30.1]	24+24Ø25 [32.1]	22+8+18Ø25 [34.1]	24+8Ø25 [38.1]	16Ø25 [44.1]
Middle upper part [XX.2]	16Ø25 [30.2]	16Ø25 [32.2]	22Ø25 [34.2]	16Ø25 [38.2]	-
Crossbar bottom [XX.3]	24+4Ø25 [30.3]	24+4Ø25 [32.3]	22+8+18Ø25 [34.3]	24+4Ø25 [38.3]	16Ø25 [44.3]
Middle bottom part [XX.4]	16Ø25 [30.4]	16Ø25 [32.4]	22Ø25 [34.4]	16Ø25 [38.4]	-
Bottom [XX.5]	32+8Ø25 [30.5]	32+8Ø25 [32.5]	22+8+18Ø25 [34.5]	32+8Ø25 [38.5]	16Ø25 [44.5]

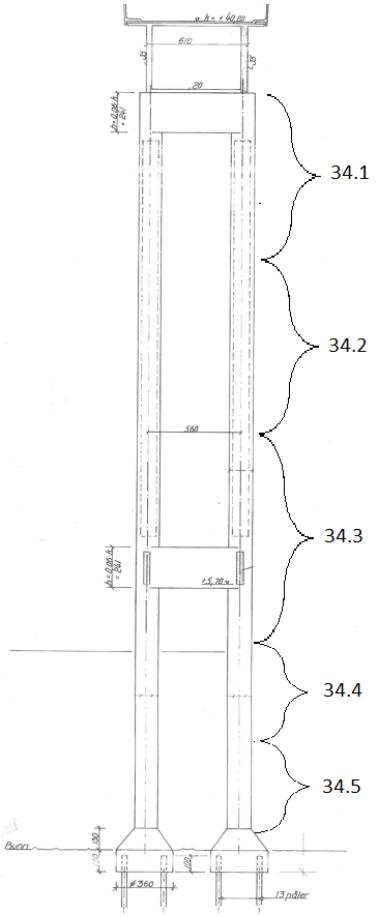

Figure 8.4: Different sections of reinforcement in column 34 as an example

9 Theory

The theory chapter describes the purpose, theory, and method behind the main calculations performed to evaluate the columns. This entails buckling, slenderness, compression field theory, interaction diagrams, and moment-curvature relationships. In addition, it verifies the diagrams produced by the FEM program SAP2000.

9.1 Buckling and slenderness

A simplified method to determine the buckling length can be found in *Systemdefinisjon av elastisk innspente staver*, Table 4.1 in *Profiler og Formler (P&F)* [40]. For the tall columns in section C of the bridge, the buckling length factor can be assessed by looking at one independent column. The system can be compared to case II in Figure 9.1. As discussed in Subchapter 7.2, the bridge deck is much stiffer than the columns. Hence, assuming a fixed connection between the column and the bridge deck is reasonable.

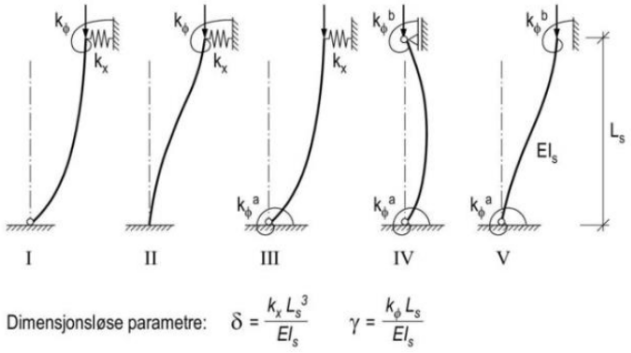

Figure 9.1: General buckling shapes [40]

Assuming the lower crossbar provides infinite stiffness, the rotational stiffness is infinite, $k_\phi = \infty$. The dimensionless stiffness parameter is also infinite, $\gamma = \infty$, and δ is found as shown in Figure 9.1.

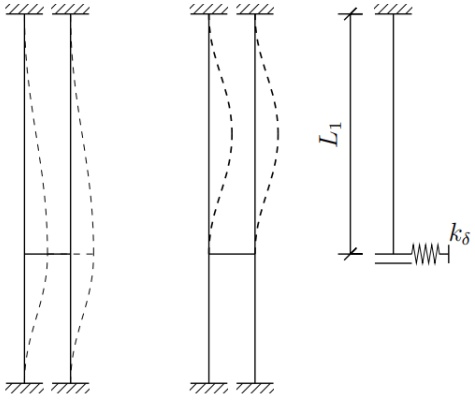

Figure 9.2: Simplified buckling cases for paired columns on the Tromsø Bridge [2]

Further, k_x is approximated based on the system in Figure 9.3.

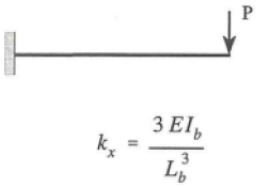

Figure 9.3: Cantilever with point-load [40]

Utilizing Table 4.3 in *(P&F)* and the values described above, the buckling length factor (β) for the given column can be found and used in Equation 9.1 to obtain the final buckling length.

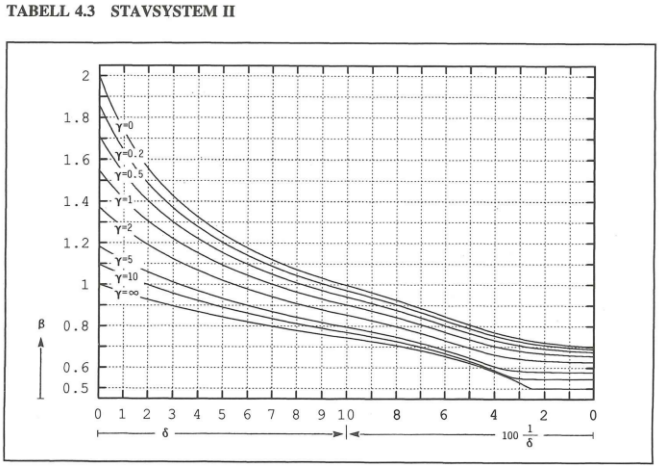

Figure 9.4: Buckling system II [40]

$$l_0 = \beta * L \tag{9.1}$$

The normalized slenderness must be found to evaluate the slenderness of the columns. The slenderness calculations are based on Chapter NA 5.8.3 in EC2 and calculated using Equation 9.2 [8].

$$\lambda_n = \lambda * \sqrt{\frac{n}{1 + 2 * k_a * \omega}} \tag{9.2}$$

λ = Slenderness ratio
n = Relative axial force
k_a = Gyration ratio ($i_{reinforcement}/i_{concrete}$)
ω = Reinforcement ratio

The creep coefficient is calculated in Subchapter 6.2.2 and is used for the slenderness criteria:

$$\begin{aligned} &\text{If} : \lambda_{n,lim,max} = 45 > \lambda_n \Rightarrow \text{Material failure} \\ &\text{If:} \lambda_{n,lim,min} = 13 * A_\phi > \lambda_n \Rightarrow \text{Not slender} \\ &A_\phi = min(\frac{1.25}{1 + 0.2 * \phi_{ef}}, 1.0) \end{aligned} \tag{9.3}$$

Second-order effects should be accounted for if the column is stable and will experience material failure. The moment-curvature relationship will account for the slenderness of the columns.

9.2 Compression field theory

Compression field theory is used for the crossbar capacity calculation, as described in Sørensen's textbook [20]. The method is based on the known forces at each point in the two principal directions and the shear direction of the crossbar. The stresses at each point may lead to cracks with a crack angle θ, oriented with respect to the reinforcement direction (compression or tension) and their relative magnitudes. Equation 9.4 is used, as it accounts for stage II condition, where the concrete cannot transfer tension [20].

$$\tan^4\phi + \frac{N_x}{N_{xy}}\tan^3\phi - \frac{N_y}{N_{xy}}\tan\phi - \frac{A_{sx}}{A_{sy}} = 0 \tag{9.4}$$

$\frac{A_{sx}}{A_{sy}}$ = The relation between the reinforcement in the two directions x and y
ϕ = Crack angle
N_x = Forces in the x-direction
N_y = Forces in the y-direction
N_{xy} = Shear forces

Based on the crack angle and the equilibrium equation of an infinitesimal plate element, the forces acting in the plate's two reinforcement directions, as well as the pressure F_c, can be calculated using equations 9.5, 9.6 and 9.7.

$$F_{sx} = N_x + N_{xy}\tan\phi \tag{9.5}$$

$$F_{sy} = N_y + N_{xy}\cot\phi \tag{9.6}$$

$$F_c = \frac{N_{xy}}{\sin\phi * \cos\phi} \tag{9.7}$$

The resulting stress in the reinforcement at the considered point is obtained by dividing the force F_{sx} and F_{sy} (Equations 9.5 and 9.6) by the cross-sectional area of reinforcement in the corresponding direction. The resulting stress in the concrete at the calculated point is obtained by dividing the force F_c (Equation 9.7) over the unit length and height used. These values are checked against the reinforcement's yield strength and the concrete's compressive strength to determine the degree of utilization.

9.3 Interaction diagram

Interaction diagrams (also referred to as moment-axial force diagrams) are graphical representations of the interaction between axial force capacity and moment capacity in a concrete cross-section. These diagrams are important tools for analyzing and designing reinforced concrete structures, as they allow engineers to evaluate the capacity of a section to resist combined loading.

The shape of the interaction diagram is influenced by several factors, including the shape and size of the section, the strength of the concrete and reinforcing steel, and the reinforcing steel configuration. Generally, a section with a larger cross-sectional area and more reinforcing steel will have a greater capacity to resist loading.

To calculate the interaction diagrams, the equation for the following two states of forces must be derived:

- Failure due to compression across the whole cross-section.
- Failure due to compression with varying degrees of tension due to moment in part of the cross-section.

9.3.1 Pure compression

When there is compression in the whole cross-section, the strain state ϵ_{c0} is equal to 2‰ [8]. In this state, there is no moment capacity, and the total axial capacity for a circular, massive concrete cross-section with uniformly distributed reinforcement is as follows in Equation 9.8.

$$N_{Rd} = 2 \cdot f_{cd} \cdot \int_{-r}^{r} \sqrt{r^2 - x^2} dx + f_{sd} \cdot A_s \cdot n \tag{9.8}$$

f_{cd} = Design value of concrete compressive strength
r = Radius
f_{sd} = Design value of steel reinforcement yield strength
A_s = Area of reinforcement
n = Number of reinforcement bars

9.3.2 Compression and bending

The axial and moment capacity can be found by choosing a strain state in the reinforcement furthest away from the edge of the concrete loaded in compression to crushing. The ultimate strain state in concrete is used, $\epsilon_{cu} = 3.5$‰ [8]. The effective pressure zone height is simplified to $h_e = 0.8 \cdot \alpha \cdot d_r$, where α is the ratio of how much of the cross-section is in pressure and d_r the distance from the edge to concrete to the reinforcement furthest away.

The force in each reinforcement bar is given as:

$$F_s = A_s \cdot \frac{E_s}{\gamma_s} \cdot (-\epsilon_{cu} + \frac{\epsilon_{cu} + \epsilon_{sy}}{d_r} \cdot (r + d_x)) \tag{9.9}$$

E_s = Design value of modulus of elasticity of reinforcing steel
γ_s = Partial factor for reinforcing steel
ϵ_{sy} = Chosen strain in outermost reinforcement bar
d_x = Distance to reinforcement bar from the neutral axis

The pressure force resultant and pressure zone's moment capacity of the concrete cross-section are calculated in Equations 9.10 and 9.11.

$$T_c = 2 \cdot f_{cd} \cdot \int_{r-h_e}^{r} \sqrt{r^2 - x^2} dx \tag{9.10}$$

$$T_{c.m} = 2 \cdot f_{cd} \cdot \int_{r-h_e}^{r} x \cdot \sqrt{r^2 - x^2} dx \tag{9.11}$$

The distance from the neutral axis to the pressure resultant point is given as $y_c = \frac{T_{c.m}}{T_c}$. To calculate the total axial and moment capacity of the cross-section for the given strain state, Equations 9.12 and 9.13 are used.

$$N = T_c + \sum_{i=1}^{n} A_s \cdot f_{sd} \cdot n_s + \sum_{i=1}^{n} A_s \cdot \epsilon_x \cdot \frac{E_c}{\gamma_c} \cdot A_s \cdot n_x \tag{9.12}$$

$$M = T_c \cdot y_c + \sum_{i=1}^{n} A_s \cdot f_{sd} \cdot n_s \cdot y + \sum_{i=1}^{n} A_s \cdot \epsilon_x \cdot \frac{E_c}{\gamma_c} \cdot A_s \cdot n_x \cdot y \tag{9.13}$$

n_s = Number of bars where the strain is greater than f_{sd}
n_x = Number of bars where the strain is lower than f_{sd}
y = Distance from the actual reinforcement bar to the neutral axis

Each strain state gives a new point on the interaction diagram. This gives a curve that represents the combination of axial force and moment that the cross-section can be subjected to before failure. This can be seen in Figure 9.5.

9.3.3 Interaction diagrams using SAP2000

The interaction diagrams for the various columns and the different hollow and massive cross-sections were produced using SAP2000 [41]. This was done to calculate and check all the various cross-sections effectively. To verify the results, the cross-section capacity of column 34 near the crossbars was calculated using Excel [42]. SAP2000 does account for reinforcement bars loaded in compression in its calculations of axial and moment capacity. This gives an interaction diagram that is slightly conservative compared to the Excel calculations, except for a region with low axial forces and high moments. This can be seen in Figure 9.5, where the gap in axial capacity at 0 moment capacity is 6900 kN for column 34 subjected to a moment about its weak axis. The extra capacity due to all reinforcement bars loaded in compression equals $48 \cdot 2‰ \cdot E_s = 7100$ kN. This is in good agreement with the curves in Figure 9.5.

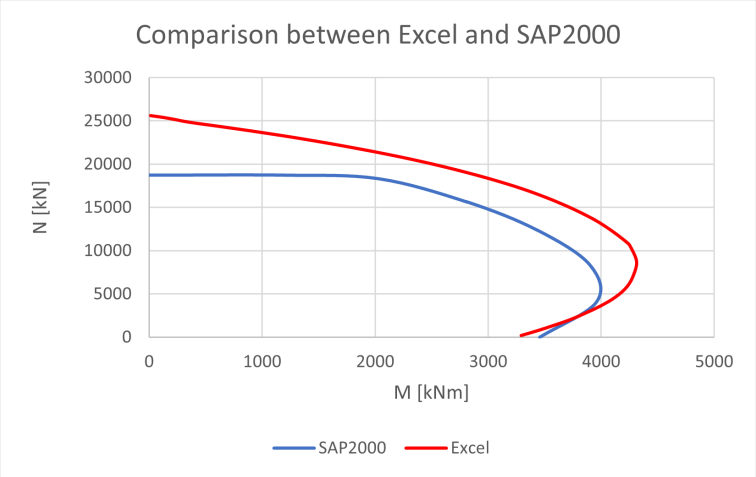

Figure 9.5: Comparison of interaction diagram created in Excel and SAP2000

In all the reinforcement drawings, it is stated that the extra reinforcement in addition to the ones that run the whole span of the columns, have a higher yield strength. They are of quality CSF50, while the rest are of class CFS40 S [17]. The Excel sheet calculated that in column 33, at the point where the higher yield strength would contribute the most, the added effect of changing the strength class would increase the capacity with $1,7\%$. Therefore, the decision was made to model all the cross-sections using CSF40 S to ensure a conservative result and to avoid any confusion in the interpretation of the reinforcement drawings.

9.4 Moment-Curvature relationship

In order to accurately calculate the capacity of the columns, second-order effects must be accounted for. The stiffness of the column varies as the applied moment increases and the height of the compression zone decreases. Due to the nonlinear behaviour of the stress-strain relationship of the concrete, the relationship between the moment and curvature will also be nonlinear [43]. Robot Structural Analysis does not automatically account for this loss in bending stiffness. Therefore, a more accurate, updated stiffness has been evaluated using a moment-curvature relationship curve. The FEM program SAP2000 was used to establish the relationship for the columns of interest in this thesis.

The theory for the moment-curvature relationship is mainly based on the publication of Hellesland discussing second-order principles for reinforced concrete columns. Euler-Bernoulli hypothesis and a perfect bond between the concrete and the reinforcement is assumed [43]. The bending stiffness of a cross-section is defined by the relationship between the moment and the curvature ($\kappa = 1/r$, r= curvature radius) as described by Equation 9.14.

$$EI = \frac{M}{(1/r)} \tag{9.14}$$

The moment-curvature relationship is calculated for the decisive section at the top of the crossbar, where the highest moment is expected. Then, the axial force in the given column is extracted from Robot and kept constant at the given height. The calculation process is based on a constant variation of the compressive strain of the concrete (ϵ_1) and the equilibrium of the axial force in Equation 9.15.

$$N_i = \int \sigma_c dA_c - \sigma_s' A_s' - \sigma_s A_s \tag{9.15}$$

The tensile strain (ϵ_2) must be determined to make the resultant equilibrium force equal to the experienced outer constant axial force. Based on this, the resultant moment can be calculated:

$$M_i = -\int \sigma_c z dA_c - \sigma_s' A_s' z_s' - \sigma_s A_s z_s \tag{9.16}$$

The corresponding curvature is defined as:

$$\kappa = \frac{1}{r} = \frac{\epsilon_2 - \epsilon_1}{h} \tag{9.17}$$

The known moment and curvature for the given strain provide one point of the moment-curvature curve. By iteration through an even distribution of the strain ϵ_1 a complete curve is obtained. It should be noted that the moment is limited by the maximum allowed strain in the concrete at $3.5‰$. The curve will slowly reach its peak, where failure is expected, and the failure curvature and moment are obtained to be used in Equation 9.18. Accounting for the nonlinear behaviour of the reinforced concrete, a more accurate bending stiffness EI_2 is obtained.

$$EI_2 = \frac{M_{failure}}{\kappa_{failure}} \tag{9.18}$$

Since the columns are experiencing a moment and axial force below their estimated maximum capacity, the true stiffness (EI_3) of the columns is expected to lay in between EI_1 and EI_2, ($EI_1 > EI_3 < EI_2$). Therefore, Equation 9.19 determines the columns' true stiffness. Where M_3 and κ_3 are the moment and corresponding curvature experienced by the column, obtained from the Robot model.

$$EI_3 = \frac{M_3}{\kappa_3} \tag{9.19}$$

Figure 9.6 visualises the stiffness values:

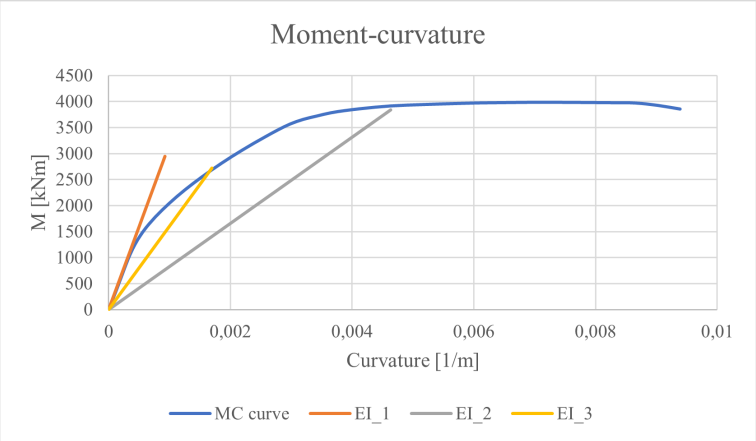

Figure 9.6: Stiffness EI_1, EI_2, EI_3 in moment-curvature diagram

Finally, the obtained nonlinear bending stiffness (EI_3) is compared to the bending stiffness originally used in the Robot model to obtain the axial forces on the columns. In the likely case that the obtained nonlinear bending stiffness, EI_3, differs from the original stiffness, this must be adjusted in the model. Through an iterative process, the stiffness is adjusted in Robot, the axial forces and moments are calculated, the moment-curvature relationship is established, and an updated EI_3 is calculated. The correct stiffness for the reinforced columns is found when the stiffness used in the Robot model matches the stiffness from the moment-curvature graph for the given load case EI_3, with a defined tolerance.

9.4.1 Verification of moment-curvature relationship

As for the interaction diagrams, SAP2000 was also used to produce moment-curvature relationships for the columns. This method proved to be highly effective and accurate. The results from the previously verified interaction diagrams were used to verify that the moment-curvature relationships comply with the theory described above.

The stress-strain relationship for the material is decisive for the moment-curvature diagram. The default stress-strain relationship used in SAP2000 is shown in Figure 9.7. The stress varies nonlinearly for a strain up to $-1.2‰$ and then falls linearly.

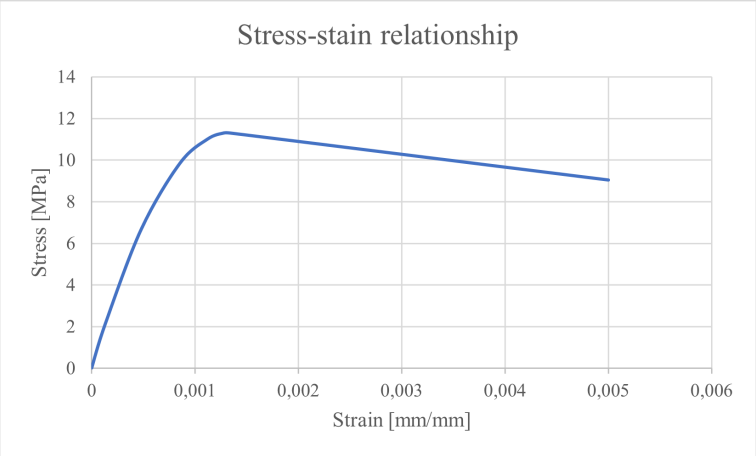

Figure 9.7: Stress-strain relationship for C20/25 concrete

The moment-curvature diagram is based on a calculation model where the stress relationship is approximated as shown in Figure 9.8, combining nonlinear and linear variation. On the other hand, the interaction diagram is based on constant stress in the concrete, with a height of $0.8 \cdot$ of compressive zone as can be seen in the same figure. This causes a small difference between the two methods.

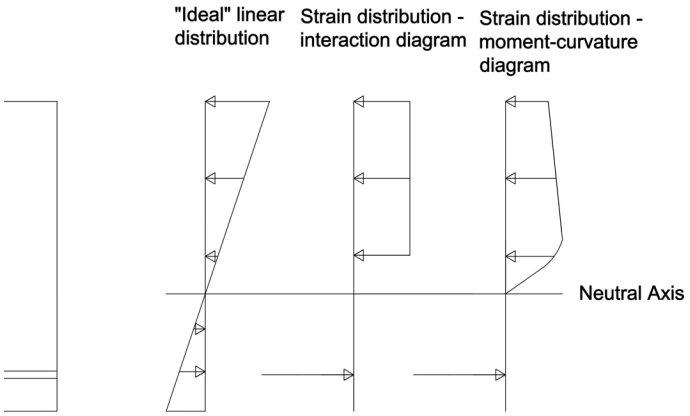

Figure 9.8: Difference in stress distribution within the compression zone for the interaction diagram and the moment-curvature calculation

As the moment-curvature relationship is defined for a given axial load, this load acts as the basis for the verification. The strains for this given axial force and any moment value along the curve can be extracted and found by establishing an equilibrium state.

To verify the accuracy of the moment-curvature relationship, column 30 is used. Firstly it can be shown that at small moments and curvatures, the stiffness is equal to the original stiffness corresponding to $E = 23336.3$ MPa as shown in Figure 9.9.

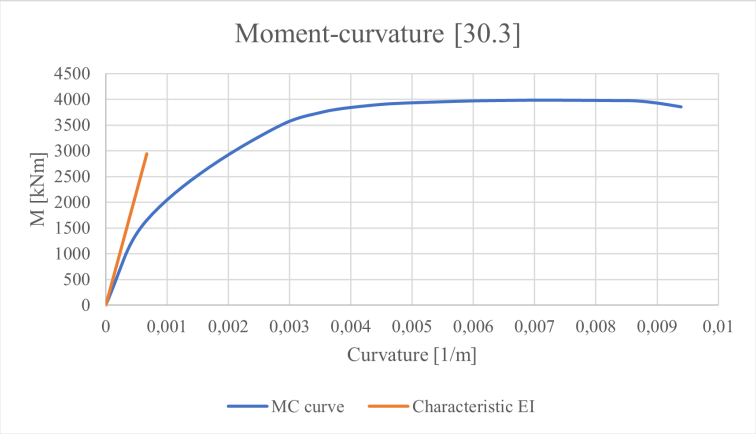

Figure 9.9: Moment-curvature relation column 30.3

To verify the peak value in the moment-curvature diagram, the strain state is extracted as shown in Figure 9.10. The diagram is based on an axial force $N = 4652$ kN and the peak moment is found to be $M = 3842$ kNm.

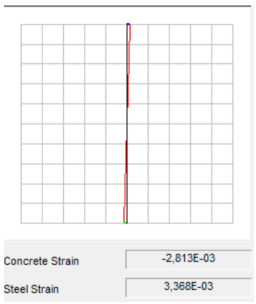

Figure 9.10: Strains at max moment

The calculated moment and the axial force should correspond to a point on the capacity curve of the interaction diagram to verify the accuracy of the moment-curvature diagram. This is shown in Figure 9.11.

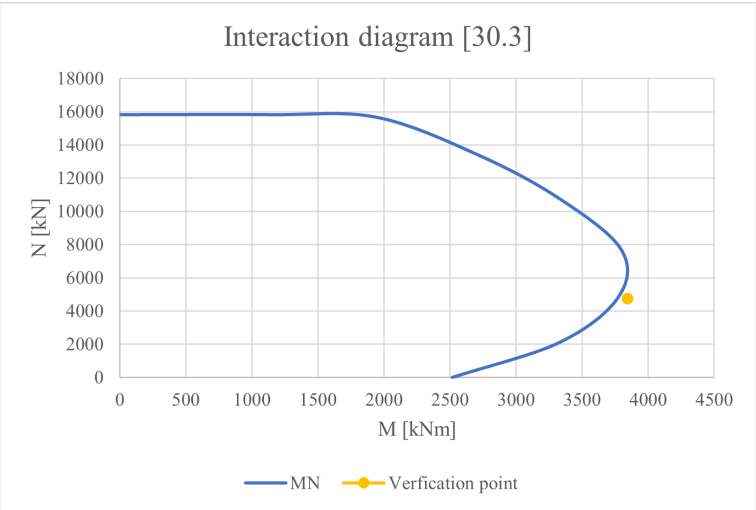

Figure 9.11: Verification point plotted in interaction diagram

The deviation between the methods can be found by evaluating the distance from the verification point to the curve, indicating the maximum capacity for the same axial capacity on the interaction diagram.

$$Deviation = \frac{3841 - 3775.5}{3842} * 100\% = 1.73\% \tag{9.20}$$

The small deviation can be explained by the different strain theories used to produce the interaction diagram and the moment-curvature diagram, respectively. This verifies the accuracy and effectiveness of the diagrams produced in SAP2000.

10 Results

In this chapter, the results from the model and calculations will be presented. In short, the checks for buckling and slenderness, forming the basis for the analysis types in Robot, will be presented. The results from the compression field theory for the crossbars will be presented, and the results from the various loads will be shown as displacement and axial force and/or interaction diagrams. The chosen load combinations and results will be displayed for the three models, and the column forces and moments will be plotted in interaction diagrams. The results for the iteration process of the moment-curvature for the critical points on the most loaded columns will be presented, and ultimately, various ASR effects on the columns will be considered.

10.1 Buckling and slenderness - columns

The buckling factor for column 34 based on hand calculations is $\beta = 0.55$ (see Figure 10.1). The full calculation is presented in Appendix D.

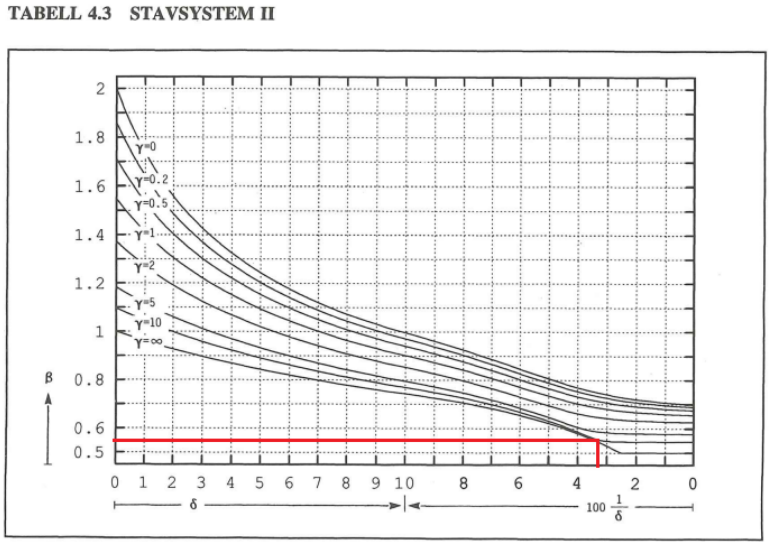

Figure 10.1: Buckling factor based on hand calculations [40]

Further, the slenderness of the column is checked. The normalized slenderness used for the stability and slenderness check is $\lambda_n = 23.6$ (see Appendix D). The check for stability indicates if the column will experience material failure, meaning that the column is stable and that the full strength of the material can be utilized. The slenderness check determines if it is necessary to account for second-order effects when assessing the columns.

$$\begin{aligned} &\text{If:} \lambda_{n,lim,max} = 45 > \lambda_n = 23.6 \Rightarrow \text{Material failure} \\ &\text{If:} \lambda_{n,lim,max} = 13 * A_\phi = 11.8 < \lambda_n = 23.6 \Rightarrow \text{Slender} \end{aligned} \tag{10.1}$$

The Eurocode checks indicate that the column is stable and will experience material failure. In addition, the column is slender and second-order moments must be accounted for. Calculations in Robot were performed accounting for second-order effects.

10.2 Compression field theory - crossbars

The most heavily loaded crossbars are the ones between the north and south column pairs in axis 34 and 35. The critical load combination was combination a3 - wind. One of these crossbars was chosen for further investigation. The mesh was locally refined to obtain more accurate values. Six points were investigated to cover the stress distribution, as shown in Figure 10.2.

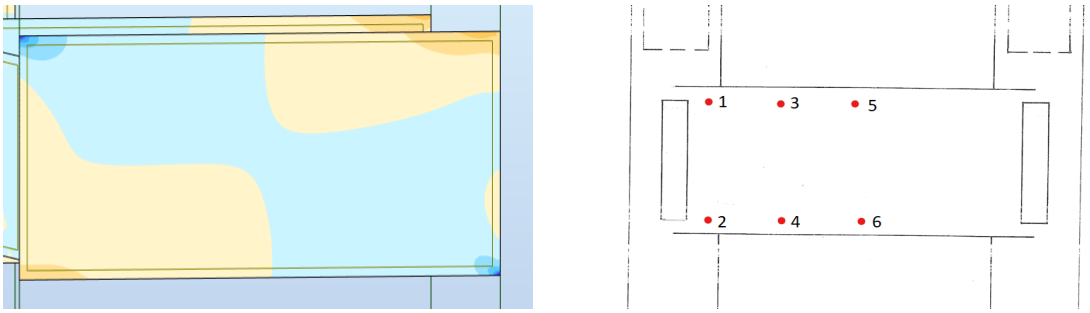

(a) Stresses on crossbar

(b) Investigated points

Figure 10.2: Stresses and selected points for control of the crossbar

The force distribution and utilization of the six points were calculated using the equations presented in Subchapter 9.2 and are shown in Figure 10.1.

Table 10.1: Stresses and utilization of crossbar

Point	σ_{sx} [Mpa]	σ_{sy} [Mpa]	σ_c [Mpa]	η_{sx} [%]	η_{sy} [%]	η_c [%]
1	105	154	1.4	27	40	12
2	151	117	1.2	39	30	11
3	330	297	1.8	86	77	16
4	154	147	0.4	40	38	3
5	15	12	0.4	4	3	3
6	225	167	0.8	58	44	7

10.3 Loads and load actions

In this subchapter, the displacement, moments and/or axial forces from the various loads are presented. This is done to verify the model works as intended and to present which loads have the largest effect on the columns. The figures presented are results from the models in Robot, where the largest effects for the selected loads are visualized. After the individual loads, the various load combinations are presented for the model of section C, and the critical load combination for the two other models is presented. The models presented with moments are either about the global x-axis, M_x (bending of the columns in the transversal direction), or about the global y-axis, M_y (bending in the longitudinal direction).

10.3.1 Permanent loads

Permanent loads include the self-weight and the super self-weight as presented in Chapter 9. This load acts over the entire bridge and mainly contributes to axial force in the columns. Figures 10.3 to 10.5 display the effect on the three models.

Section A, B:

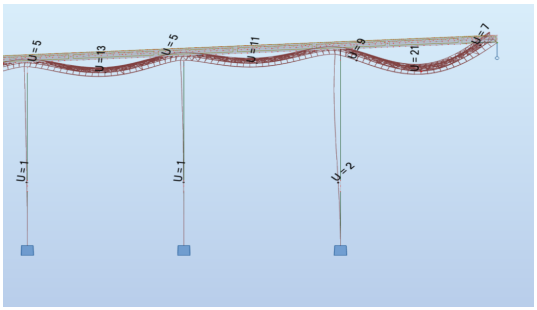

(a) Displacement, U. $U_{max} = 21$ mm

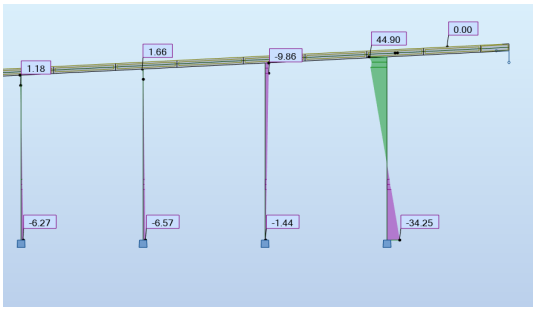

(b) Moment, M_y. $M_y.max = 45$ kNm

Figure 10.3: Permanent-loads on section A,B. The permanent load gives small deformations and moments in the columns. The largest moments are found in column 31 (right) due to the support condition allowing rotation near section C

Section C:

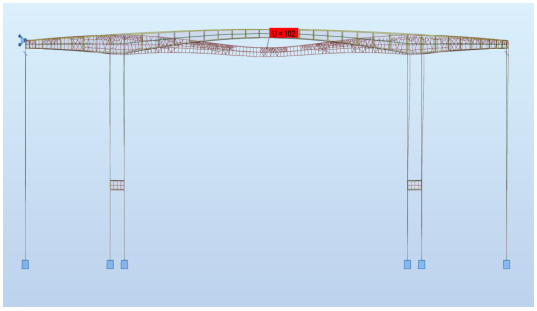

(a) Displacement, U. $U_{max} = 102$ mm

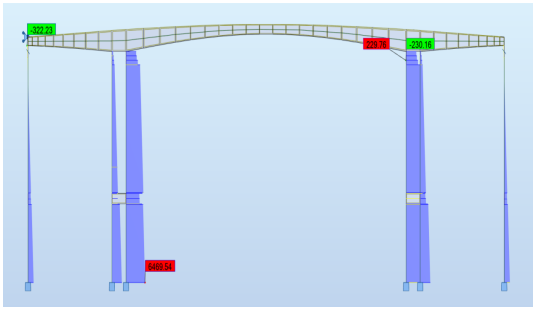

(b) Axial forces, N. $N_{max} = 6469$ kN

Figure 10.4: Permanent-loads on section C. The permanent load gives small deformations but large axial forces in the most loaded columns near the cantilever part

Section D, E:

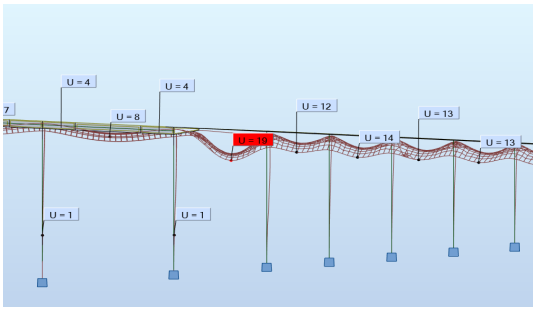

(a) Displacement, U. $U_{max} = 19$ mm

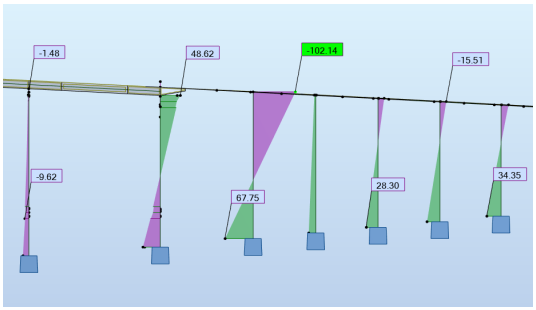

(b) Moment, M_y. $M_y.max = 102$ kNm

Figure 10.5: Permanent-loads on section D,E. The permanent load gives small deformations and moments in the columns. The largest moments are found in column 44 (centre of figure) due to the large span between sections D and E

10.3.2 Additional loads due to ASR

The ASR load, modelled in Robot, includes the effect of shrinkage. The calculations are presented in Appendix F and explained in Subchapter 6.3. ASR expansions mostly affect the moments in the bridge superstructure, and any forces of significance in the columns are found due to asymmetrical support conditions or different bridge-deck cross-sections on each side of the column top. The resulting displacements and axial forces or moments are found in Figures 10.6 to 10.8.

Section A, B:

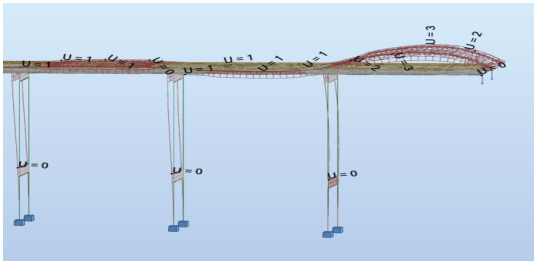

(a) Displacement, U. U_{max} = 3 mm

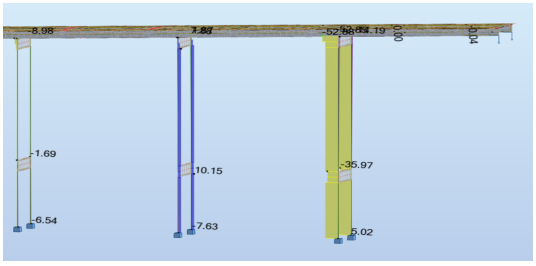

(b) Axial forces, N. N_{max} = -36 kN (tension)

Figure 10.6: ASR-load on section A, B. The support conditions between sections B and C allow for rotation of the bridge deck, resulting in an axial tension force in column 31. The displacements are low

Section C:

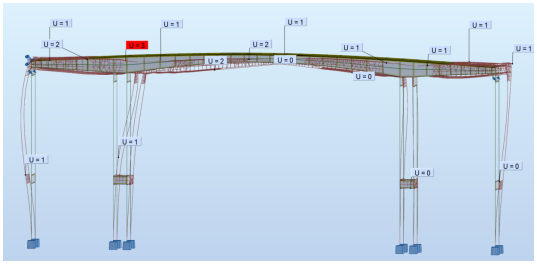

(a) Displacement, U. U_{max} = 1 mm

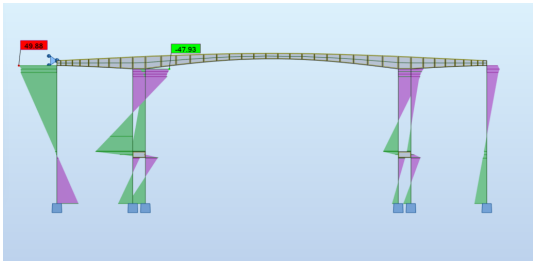

(b) Moment, M_y. $M_y.max$ = 50 kNm

Figure 10.7: ASR-load on section C. The choice of boundary conditions gives a small moment on one side of the symmetry axis. As in model A,B, the displacement and moments are low

Section D, E:

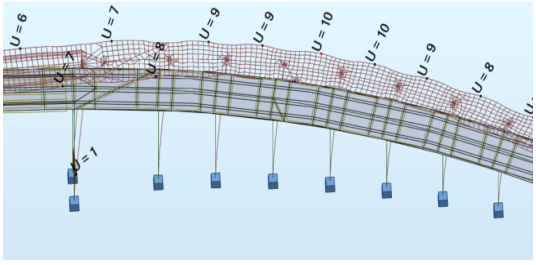

(a) Displacement, U. U_{max} = 10 mm

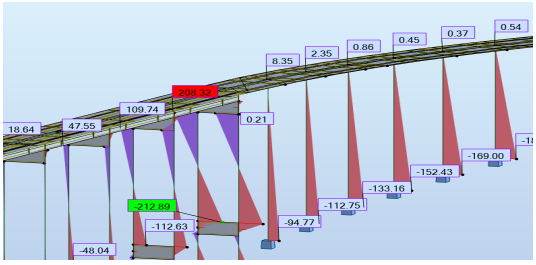

(b) Moments, M_z. $M_{z.max}$ = 213 kNm

Figure 10.8: ASR-load on section D,E. In Section E, the expansion pushes the bridge deck horizontally out of the curve. This displacement gives moments in the transversal direction

10.3.3 Temperature loads

As explained in Subchapter 6.2.3, the load case of temperatures $> 17\ ^{\circ}C$ (temperature gradient of 14 °C) are modelled where the expansion joints are closed and thus not allowing displacement in the longitudinal direction of the bridge. This is presented in Figures 10.9 to 10.11. The expansions are of the same shape as the ASR loads but of a higher magnitude when the expansion joints are closed. This is especially evident in Figure 10.11 where the displacement shown is 150% larger than in the ASR load.

Section A, B:

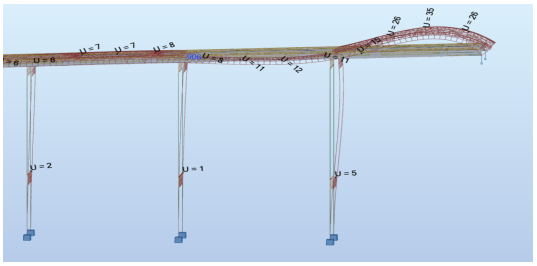

(a) Displacement, U. $U_{max} = 35$ mm

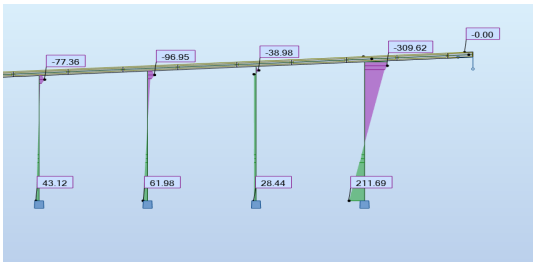

(b) Moment, M_y. $M_y.max = 310$ kNm

Figure 10.9: Temperature-load on section A, B. This load gives the same deformation as the ASR load, and the highest moment is found in column 31 due to the support conditions between sections B and C

Section C:

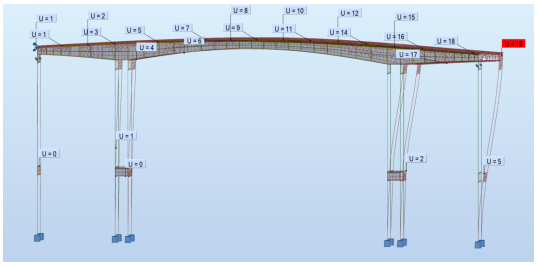

(a) Displacement, U. $U_{max} = 19$ mm

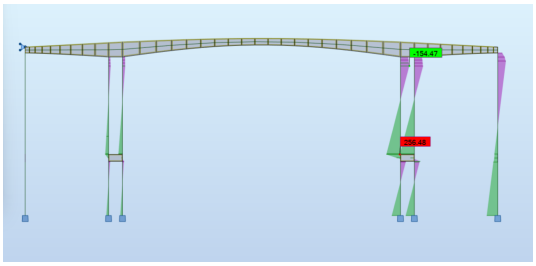

(b) Moment, M_y. $M_y.max = 256$ kNm

Figure 10.10: Temperature-load on section C. Due to the support conditions, the moment diagram and displacement are asymmetrical

Section D, E:

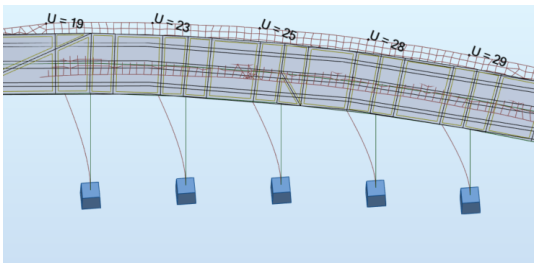

(a) Displacement, U. $U_{max} = 29$ mm

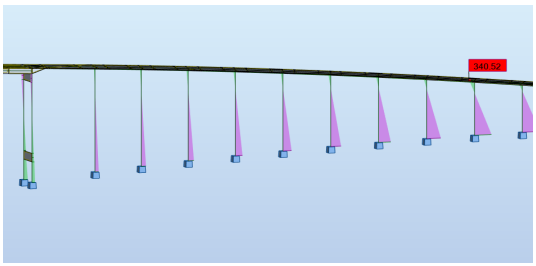

(b) Moment, M_y. $M_y.max = 341$ kNm

Figure 10.11: Temperature-load on section D, E. The displacement is in the same direction as for the ASR load but almost three times the magnitude. Consequently, the moments due to the temperature load are higher

10.3.4 Light-traffic loads

The light-traffic load includes the live load from the pedestrian and bicycle lanes. This acts over the whole bridge as presented in Subchapter 6.1.2. This load is symmetrical over the columns, thus mostly contributing to the axial forces as presented in Figures 10.12 to 10.14.

Section A, B:

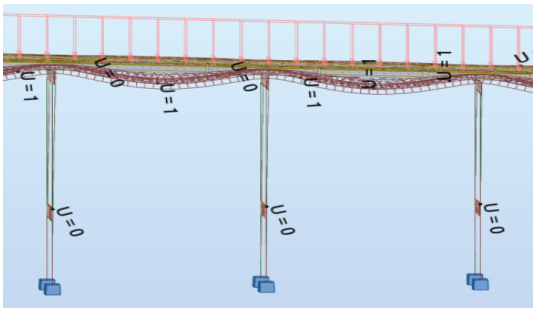

(a) Displacement, U. $U_{max} = 1$ mm

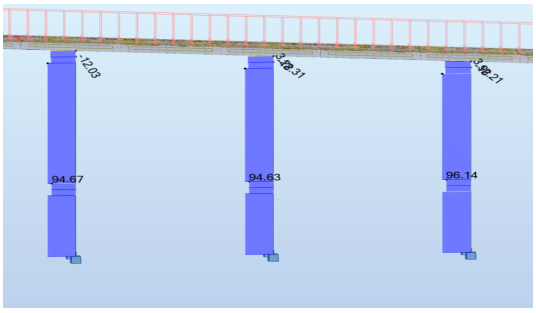

(b) Axial forces, N. $N_{max} = 96$ kN

Figure 10.12: Light traffic-load on section A, B. The load gives small displacement and axial forces

Section C:

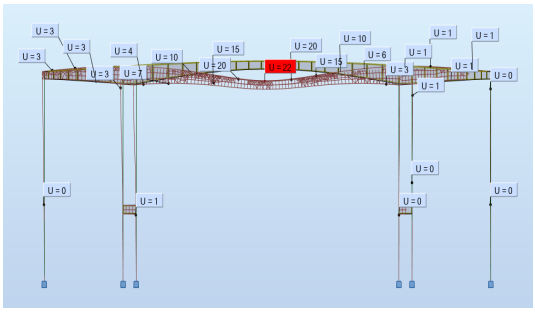

(a) Displacement, U. $U_{max} = 22$ mm

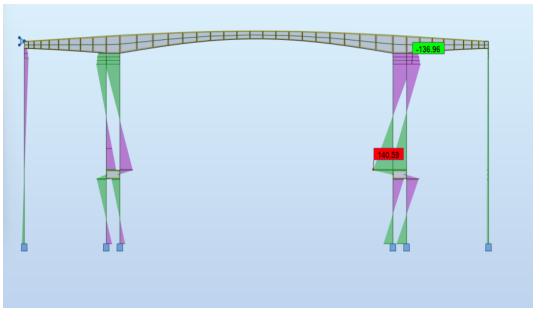

(b) Moment, M_y. $M_y.max = 141$ kNm

Figure 10.13: Light traffic-load on section C. Due to the long span of the cantilever part, this load gives high moments for axis 34 and 35 near the crossbars

Section D, E:

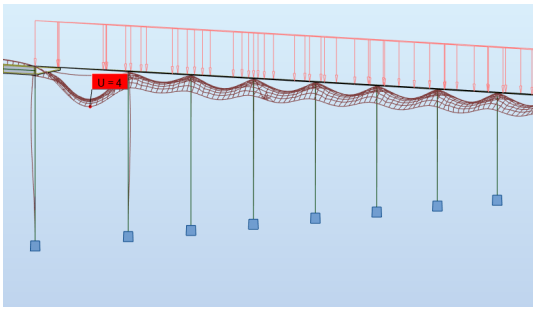

(a) Displacement, U. $U_{max} = 4$ mm

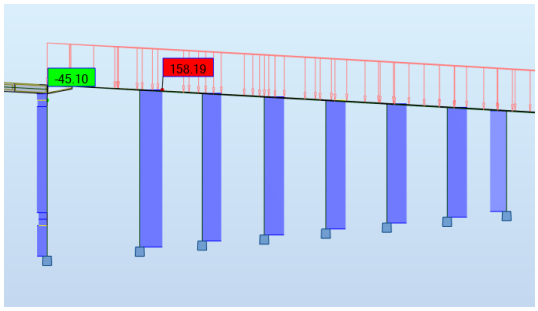

(b) Axial forces, N. $N_{max} = 158$ kN

Figure 10.14: Light traffic-load on section D,E. As with model A,B, this load contributes mostly to the axial forces. The large displacement between axis 43 and 44 is due to a longer span

10.3.5 Heavy-traffic loads

The heavy-traffic load is placed at the most decisive point to give the largest moments or axial forces in the columns. This was also the case for the different load combinations. For all sections, the largest moments in the column were found when the load was placed at mid-span. The highest axial force is found with the load placed centrally above the column top. The results are presented in Figure 10.15 to 10.17.

Section A, B:

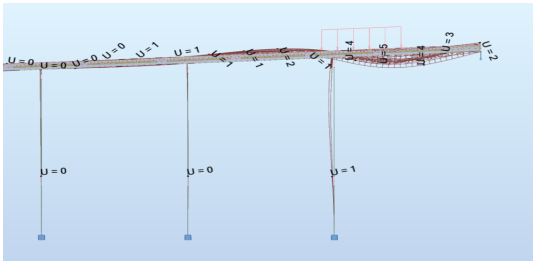

(a) Displacement, U. $U_{max} = 5$ mm

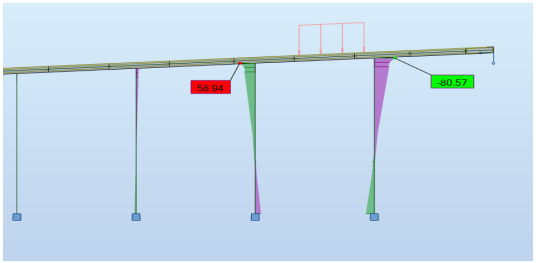

(b) Moment, M_y. $M_y.max = 81$ kNm

Figure 10.15: Heavy traffic-load on section A, B. The heavy traffic load gives the largest displacements for section A,B when placed between column 31 and section C (Figure (a). In Figure (b) the load is placed between axis 30 and 31

Section C:

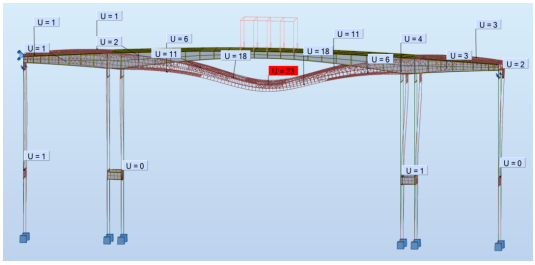

(a) Displacement, U. $U_{max} = 23$ mm

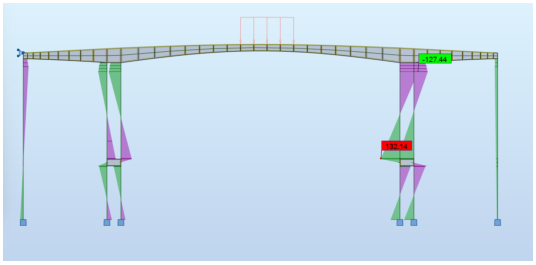

(b) Moment, M_y. $M_y.max = 132$ kNm

Figure 10.16: Heavy traffic-load on section C. One cladding with heavy-traffic load gives the equivalent displacement and moments as light load distributed over the entire model. The largest moments are found in the columns in axis 34 and 35

Section D, E:

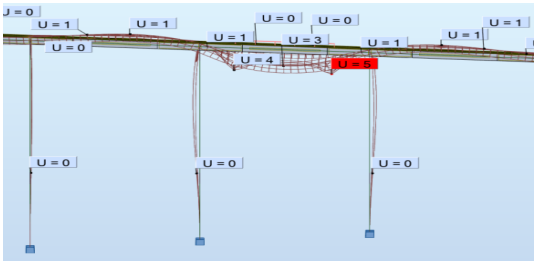

(a) Displacement, U. $U_{max} = 5$ mm

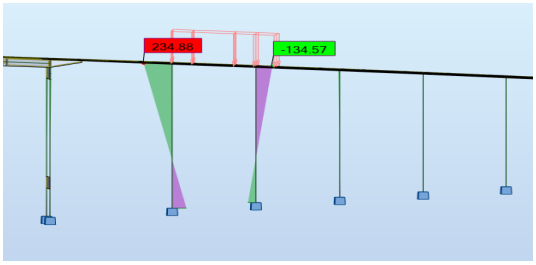

(b) Moment, M_y. $M_y.max = 235$ kNm

Figure 10.17: Heavy traffic-load on section D, E. The largest moments for the column are found when the load is placed at mid-span. Load placed between columns 44 and 45

10.3.6 Wind load in the transversal direction without traffic

The wind load in a transversal direction to the bridge without simultaneous traffic load was found to be the decisive wind load. Where the other loads primarily give displacement in the global z-direction, the wind load displaces the bridge in the y-direction (transversal direction). This leads to larger displacements and higher moments as shown in Figures 10.18 to 10.20.

Section A, B:

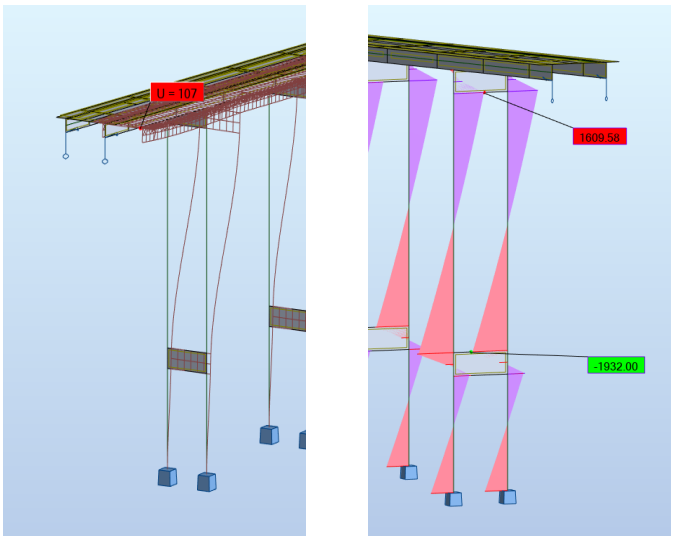

(a) Displacement, U.
$U_{max} = 107$ mm

(b) Moments, M_z.
$M_{z.max} = 1932$ kNm

Figure 10.18: Wind load on section A, B. Most loaded columns are in axis 31

Section C:

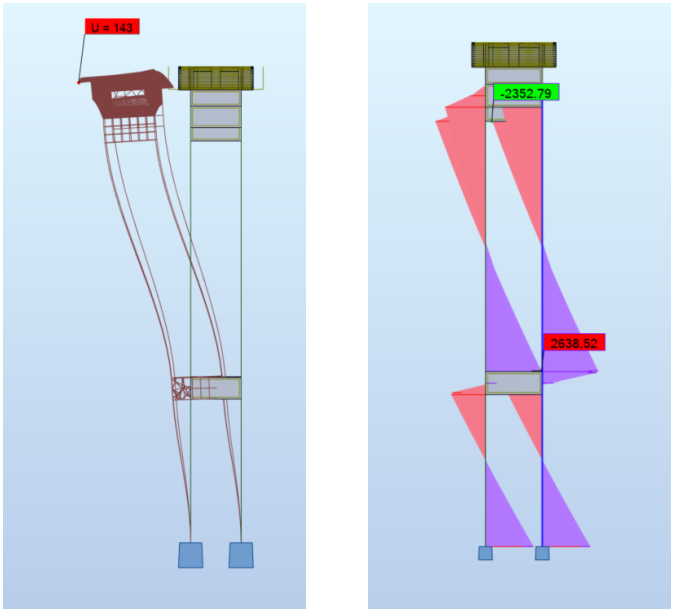

(a) Displacement, U.
$U_{max} = 143$ mm

(b) Moments, M_z.
$M_{z.max} = 2638$ kNm

Figure 10.19: Wind load on section C. Most loaded columns are in axis 34 and 35

Section D, E:

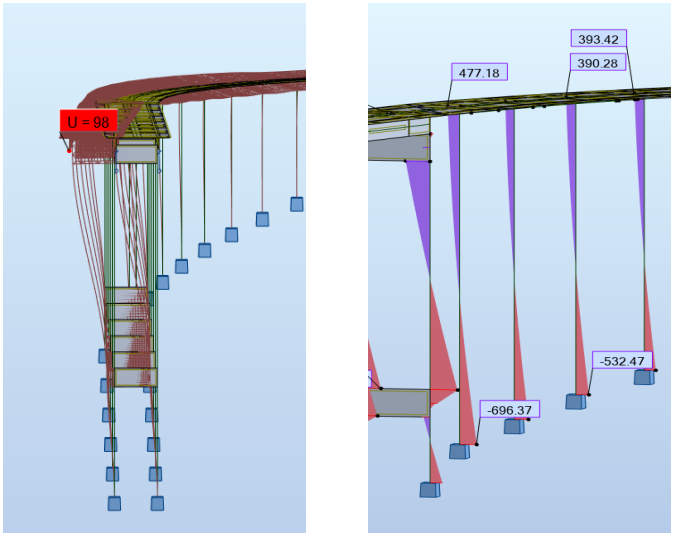

(a) Displacement, U.
$U_{max} = 98$ mm

(b) Moments, M_z.
$M_{z.max} = 696$ kNm

Figure 10.20: Wind load on section D, E. The most loaded columns relative to their capacity are in axis 38 and 44 (tallest, single column)

10.3.7 Load combinations

Five different load combinations were run for the three models to find the critical load situations for the selected columns as explained in Subchapter 6.4. Within each of these five that included heavy traffic and/or wind, the various versions of wind load or placements of the traffic loads were tested to give the largest effects. As per Table 6.9, load group "a" included only one variable load, while group "b" included two or more. The five load combinations investigated can be seen in Table 10.2

Table 10.2: Load combination

Load combination	G	D	Tr	Te	W-Tr	W
a1	1.15	1.0	1.3	-	-	-
a2	1.15	1.0	-	1.0	-	-
a3	1.15	1.0	-	-	-	1.6
b1	1.0	1.0	1.2	0.8	0.8	-
b2	1.0	1.0	0.8	0.8	1.3	-

- G - Self-weight, superimposed dead load, and railing load
- D - Deformation load (creep, shrinkage, ASR)
- Tr - Traffic load (Heavy traffic, light traffic, breaking load, and pedestrian/cyclist)
- Te - Temperature load
- W-Tr - Wind load with simultaneous traffic load with peak velocity pressure $35\frac{m}{s}$
- W - Maximum wind load

The results from the five load combinations were examined for all three models. The combination which yielded the highest axial force and moment for the columns was load case a3-wind at maximum velocity in the transversal direction. The only exception was for bending about the weak axis of column 43, being the only column with asymmetrical reinforcement. For this case, load combination b1 with wind perpendicular and heavy traffic placed at the centre point of Section C was the critical load combination. In Figures 10.22 to 10.25 the five load combinations for section C of the bridge can be seen. In Figures 10.26 and 10.27 the load combination a3-wind of models AB and DE are displayed.

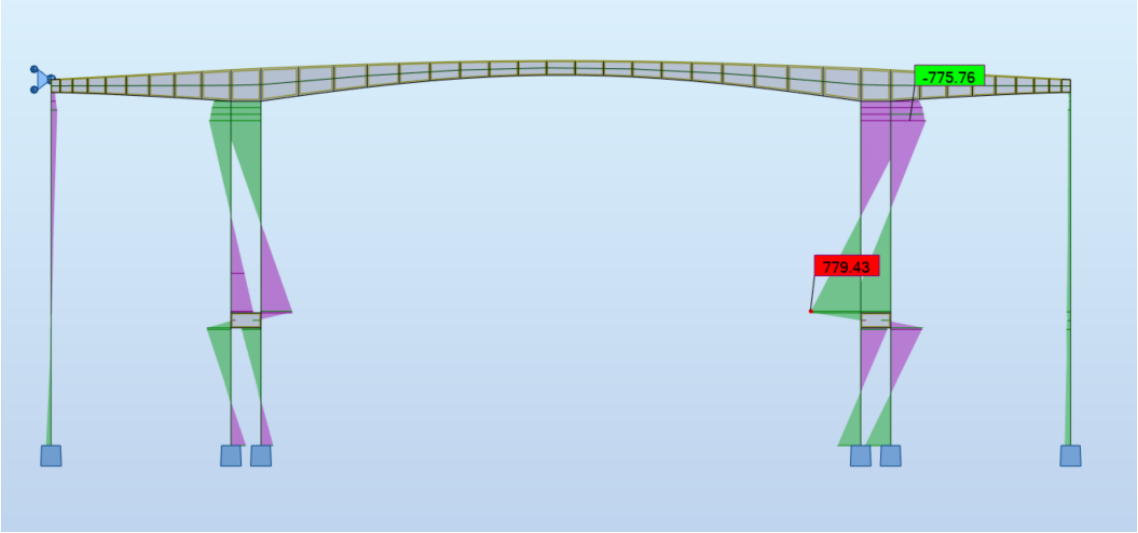

Figure 10.21: Model of section C with load combination a1-traffic. The largest moment is M_y with a maximum value of 779 kN in axis 35

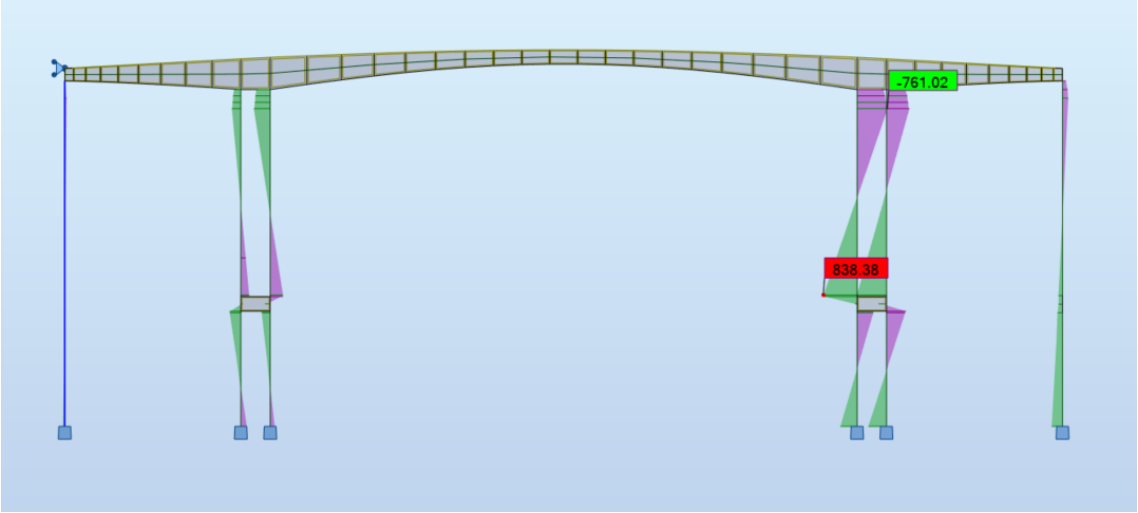

Figure 10.22: Model of section C with load combination a2-temperature. The largest moment is M_y with a maximum value of 838 kN in axis 35

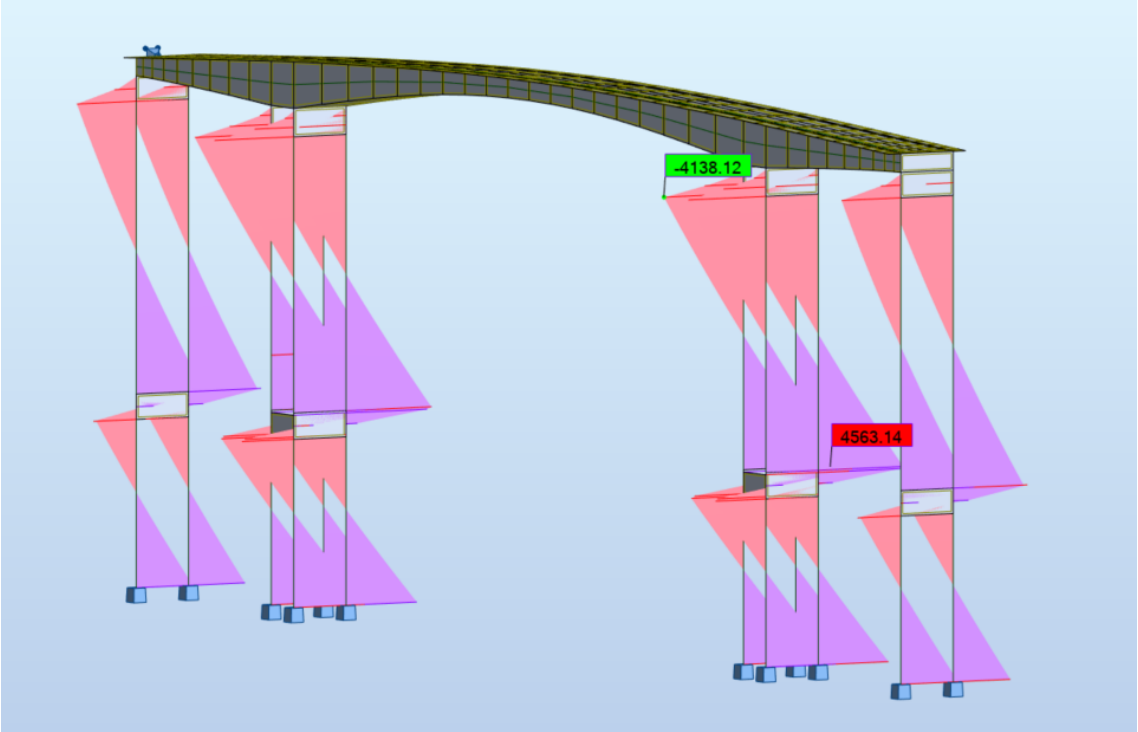

Figure 10.23: Model of section C with load combination a3-wind. The largest moment is M_x with a maximum value of 4363 kN in axis 34. This was the critical load situation for section C

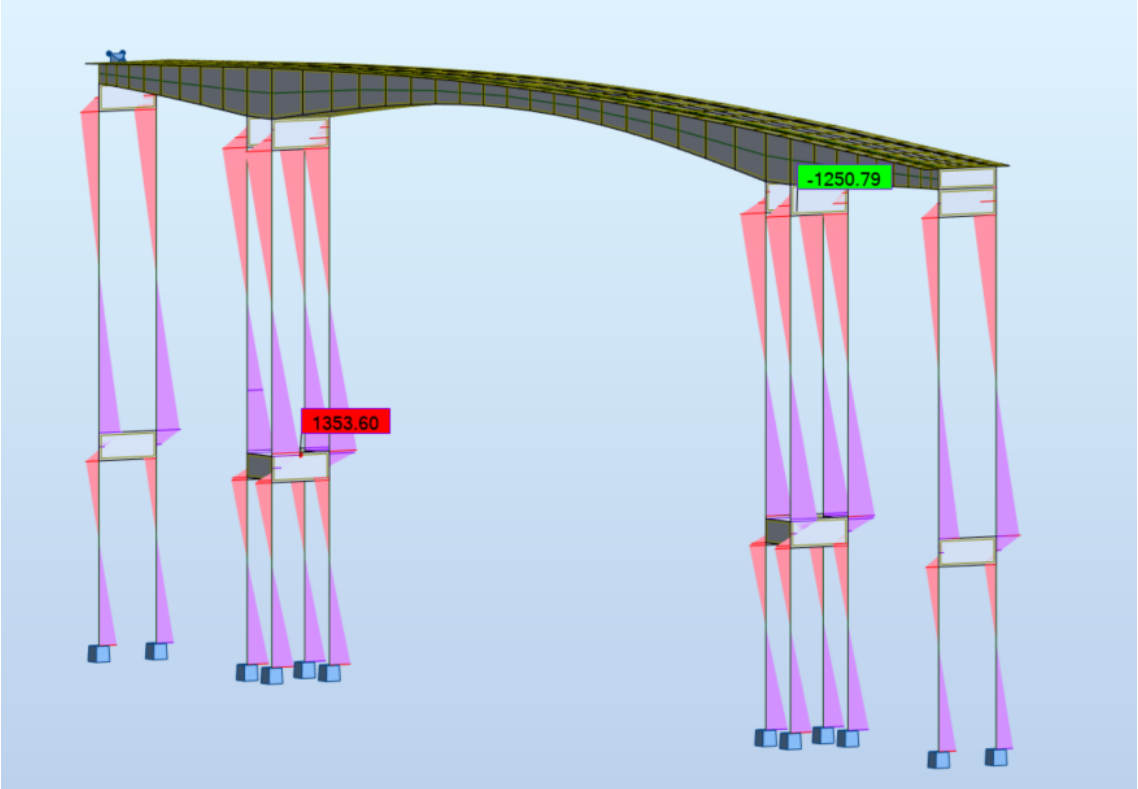

Figure 10.24: Model of section C with load combination b1-traffic. The largest moment is M_x with a maximum value of 1353 kN in axis 34

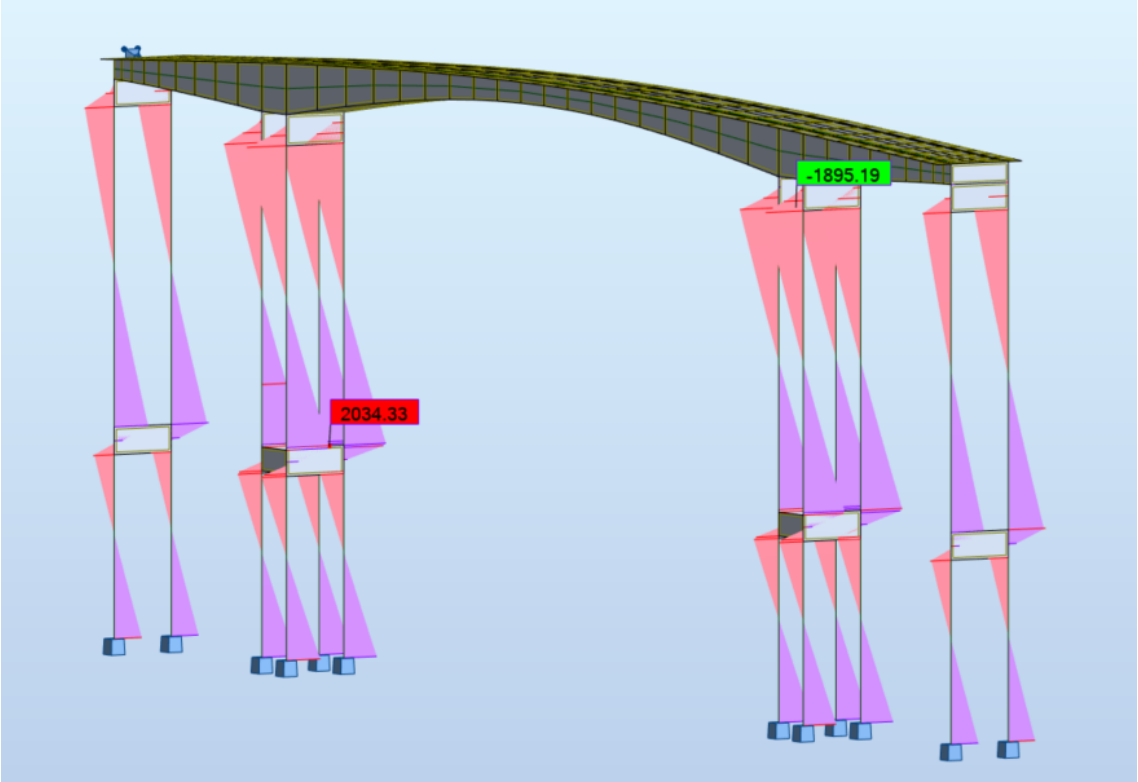

Figure 10.25: Model of section C with load combination b2-wind. The largest moment is M_x with a maximum value of 2034 kN in axis 34

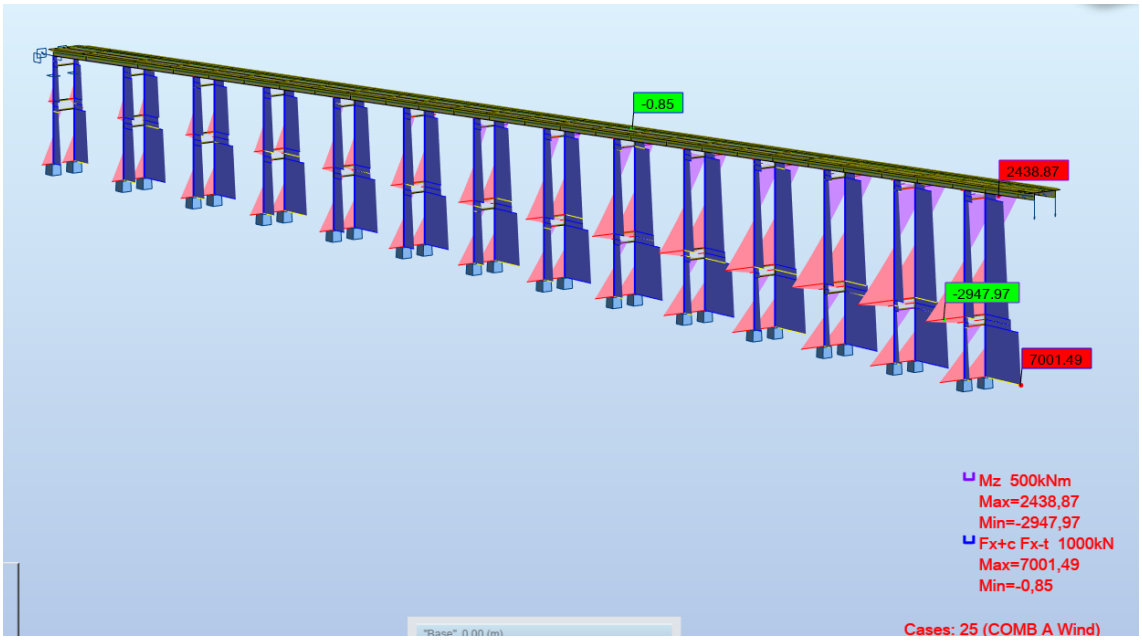

Figure 10.26: Model A, B with load combination a3-wind. The largest moment (red and purple) is M_x with a maximum value of 2947 kN in axis 31. The highest axial force (blue) has a value of 7001 kN. This was the critical load situation for section A,B

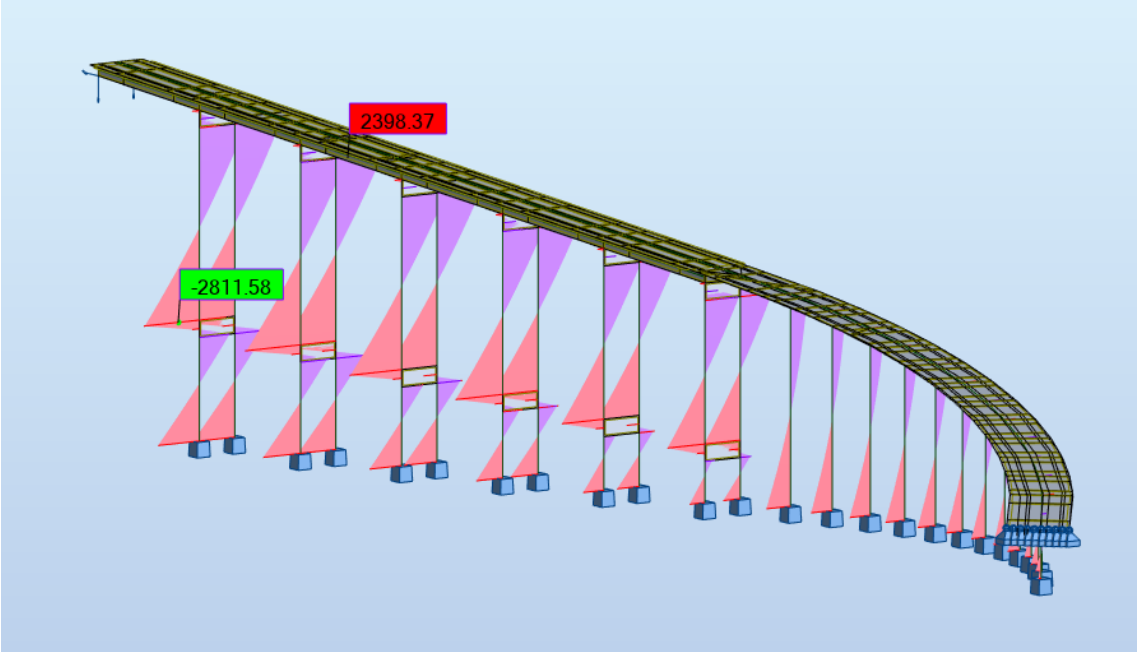

Figure 10.27: Model DE with load combination a3-wind. The largest moment is M_x with a maximum value of 2811 kN in axis 38. This was the critical load situation for section D,E

10.3.8 Transferred loads from sections A, B and D, E to section C

Since the bridge is modelled in three parts, and the last span in the highest part of the bridge deck of sections B and D is simply supported, the reaction forces in these supports need to be transferred to the cantilever model. This is explained in further detail in Chapter 7. The point loads applied to the cantilever part of the bridge from the supports in the highest part of sections B and D are listed in Table 10.3. These loads were taken from the critical load combination, a3-wind.

Table 10.3: Transferred loads. Positive loads are compression in the bridge deck and columns

Load Origin	X-direction [kN]	Z-direction [kN]
B - North	2129	800
B - South	226	650
D - North	1436	576
D - South	-1302	821

10.4 Shear capacity - columns

The shear capacity and utilization are checked based on Eurocode 2 Chapter 6.2.2 and 6.2.3 [8]. The capacity is based on the highest value of the checks in the two subchapters. The check-in Subchapter 6.2.2 is based on the concrete's capacity without shear reinforcement and will generally give higher results in columns due to the high axial force present. However, both checks are calculated. The full calculations for both subchapters can be found in Appendix E.

The capacity for members not requiring design shear reinforcement is given by the largest value of equations 10.2 and 10.3.

$$V_{Rd,c,1} = (C_{Rd,c}k(100\rho_l f_{ck})^{1/3} + k_1\sigma_{cp})b_w d \tag{10.2}$$

$$V_{Rd,c,2} = (v_{min} + k_1\sigma_{cp})b_w d \tag{10.3}$$

b_w = The smallest width of the cross-section in the tensile area [mm]. Is set to 600 mm
d = Effective depth of a cross-section
$C_{Rd,c}, k, \rho_l, k_1, \sigma_{cp}$ and v_{min} are given in Eurocode 2 Chapter 6.2.2

The shear capacity for members with shear reinforcement is the smallest of the two equations 10.4 and 10.5. The value of θ was set to 2.5.

$$V_{Rd,max} = \frac{\alpha_{cw} \cdot b_w \cdot z \cdot v_1 \cdot f_{cd}}{cot(\theta) + tan(\theta)} \tag{10.4}$$

and:

$$V_{Rd,s} = \frac{A_{sw}}{s} \cdot z \cdot f_{ywd} \cdot cot(\theta) \tag{10.5}$$

A_{sw} = Area of shear reinforcement.
s = Center distance of shear reinforcement
f_{ywd} = Design yield of shear reinforcement
α_{cw}, z and v_1 are given in Eurocode 2 Chapter 6.2.3

The maximum shear force appears at the bottom of the columns due to the critical combination a3-wind. The loads and utilization of the columns are presented in Table 10.4. All values $1 < \theta < 2.5$ gave a utilization $U < 1$.

Table 10.4: Shear capacity of the columns

Column	**Capacity,** V_{Rd}	**Shear load [kN]**	**Utilization** [%]
31	541.9	307.5	57
32	541.9	352.4	65
34	677.4	429.7	63
38	639.6	275.0	43
44	456.9	112.0	25

The shear utilization is safely within the limit. In addition, the characteristics of shear are less affected by ASR due to the internal axial compressive forces caused by the effect [44]. Hence shear capacity will not be investigated further.

10.5 Interaction diagram

Based on the load combinations, axial forces and moments for the selected columns, described in Chapter 8, were plotted in interaction diagrams. The loads are based on analysis in Robot, including second-order effects. For the columns, results for all five cross-sections were plotted, see Appendix G. The different reinforcement regions on any given twin column are shown in Figure 10.28. The reinforcement is the same for the single columns in all cross-sections.

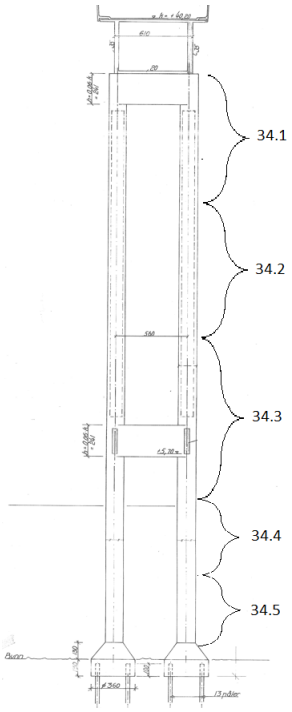

Figure 10.28: Reinforcement sections - example column 34

For all paired columns, the [xx.3]-section is the most critical, even if the reinforcement amount is higher compared to the sections [xx.2] and [xx.4]. For the single columns in Section E, the critical section is at the bottom of the column, section [xx.5]. One exception is for columns 33 and 34 at the foundation ([xx.5]). This result is also plotted in this chapter due to the high utilization. The results are plotted in Figures 10.29 to 10.33. For all results in the interaction diagrams in Chapter 10.5, the original stiffness from Chapter 3 of $E_c = 23336$ MPa is used. Utilization is not calculated for the interaction diagrams presented. This is because it can give an artificially high value due to the conservative nature of the interaction diagrams produced in SAP2000. See Chapter 9.5 for a

full explanation of the diagrams produced in SAP2000. The most critical sections will be studied in greater detail with higher accuracy through moment-curvature relationships.

Columns 30 and 31 are the most loaded columns in section B and also have similar loads and the same reinforcement as the tallest columns of section D (column 38). The load case for column 31 is (M = 2947 kN, N = 4750 kN). As the utilization is high, shown in Figure 10.29, this column will need further investigation with regards to moment-curvature and will be considered in the parametric study.

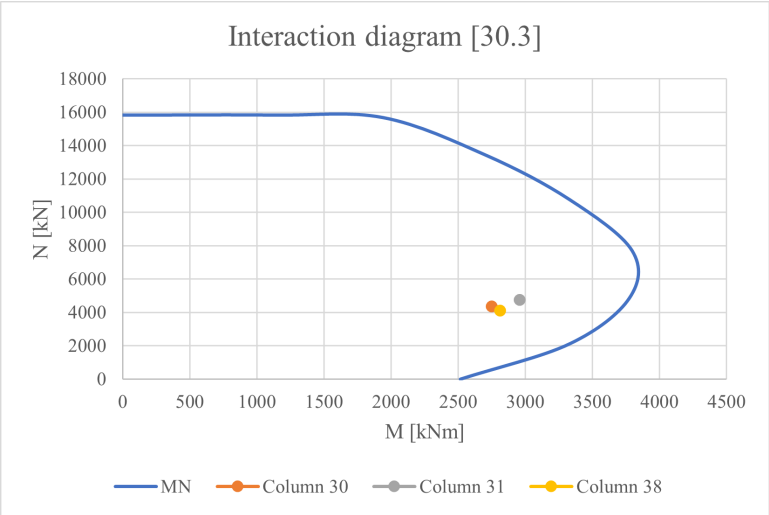

Figure 10.29: Interaction diagram, column [30.3], [31.3] and [38.3]

Column 32, in Figure 10.30, is the outermost column of section C. The load case for column 32 is (M = 1750 kN, N =3733 kN). This column will not be investigated further as the capacity is well within the limits of the interaction diagram.

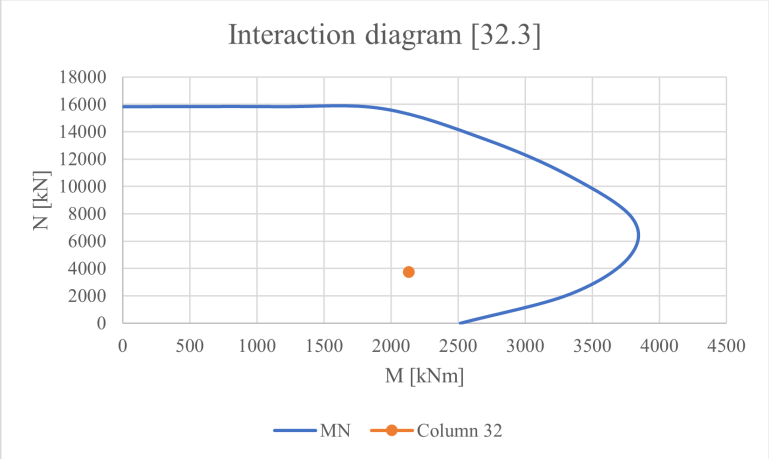

Figure 10.30: Interaction diagram, column [32.3]

Columns in axis 33 and 34 are the most loaded, located closest to the cantilever part of the bridge. The loads for columns 35 and 36 were identical due to symmetry; therefore, only columns 33 and 34 are displayed. Column 33 has slightly lower moments and substantially lower axial force. Due to this, the column in this axis will not be investigated further. The column in axis 34 has two potential critical sections in [34.3] and [34.5], Figure 10.31 and 10.32 respectively. The load-case for column [34.3] is (M = 4563 kN, N = 8630 kN).

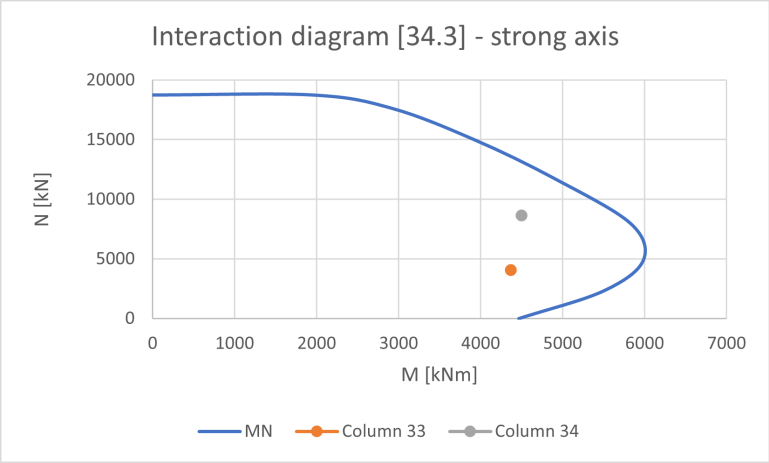

Figure 10.31: Interaction diagram column, [34.3] - strong axis

The load-case for column [34.5] is (M = 3720 kN, N = 11830 kN). Both cross-sections of column 34 will need further investigation with regards to the moment-curvature and will also be included in the parametric study.

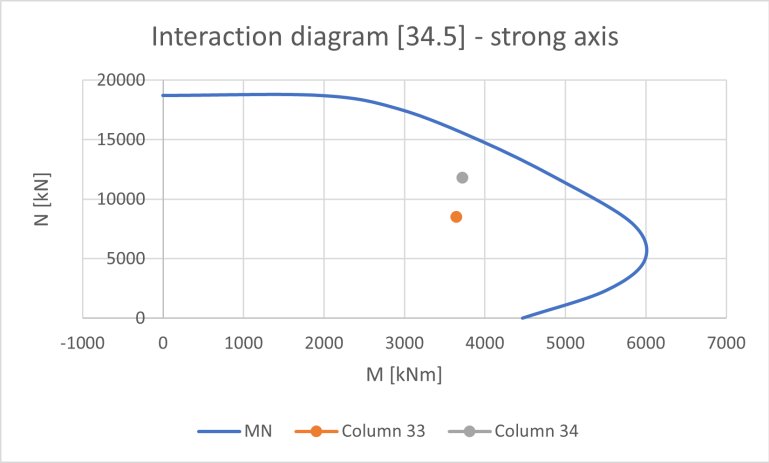

Figure 10.32: Interaction diagram, column [34.5] - strong axis

In section E, the single columns of the curved part (44-46 and 49) are most critical at the bottom. The load case for column 44 is (M = 1248 kN, N = 3003 kN). While the utilization is low, the columns will be investigated further as they are highly sensitive to displacements due to further ASR expansions.

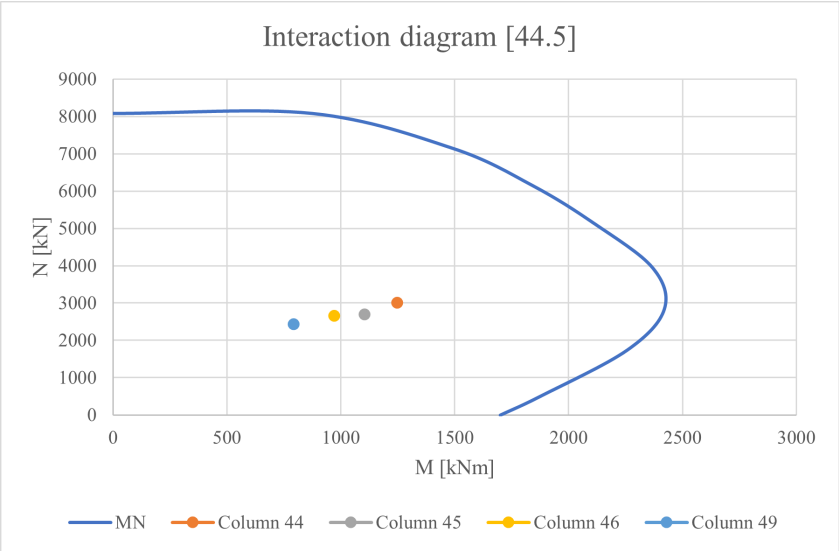

Figure 10.33: Interaction diagram, column [44.5], [45.5], [46.5] and [49.5]

All the sections of the selected columns not discussed in this subchapter are considered safe and will not be investigated further. A complete overview of all the interaction diagrams can be found in Appendix G.

10.5.1 Bi-axial moment verification

Following EC2 Chapter 5.8.9 for bi-axial moments, the Eurocode provides the following check:

$$M_{Ed} = \left(\frac{M_{Ed,y}}{M_{Rd,y}}\right)^a + \left(\frac{M_{Ed,x}}{M_{Rd,x}}\right)^a < 1 \tag{10.6}$$

$a = 2$ for circular cross-sections.

Columns 31 and 34 are checked for the bi-axial moment at the lower crossbar ([xx.3] and columns 34 and 44 to 46 are checked at the foundation ([xx.5]). All the columns are checked for load combination a3-wind. The moment capacity is chosen from the point on the interaction diagram with the same axial force as the load case. The results are given in Table 10.5.

Table 10.5: Results of Eurocode check of bi-axial moments where section [34.3] is the most utilized with a value of $U = 64.2\%$

Column and section [xx.x]	M_y **[kNm]**	M_z **[kNm]**	**Utilization** [%]
31.3	25	2950	61.9
34.3	778	4521	64.2
34.5	393	3720	60.7
44.5	317	1206	27.0
45.5	386	1053	21.8
46.5	475	918	18.5

10.6 Moment-curvature relationship

The moment-curvature relationship is found for the chosen, critical sections presented in Subchapter 10.5. The moment-curvature relationship will account for the non-linear behaviour of the reinforced concrete, providing a more accurate assessment concerning the decreased stiffness of the columns. This is explained in further detail in Subchapter 9.4. The main purpose is to acquire a more accurate determination of second-order moments. The curve indicating EI_3 is the updated stiffness for the cross-section. Compared to the interaction diagram, the updated stiffness gives a more ductile material, leading to larger displacements and eccentricities and higher moments in the columns. Evaluating the moment-curvature relationship in cross-section [xx.3] with the highest moment is conservative as this will give the lowest stiffness EI_3 of the column. The utilization is found by dividing the moment calculated by Robot with the highest value of moment from the moment-curvature iteration.

For column 31, the Young's modulus is $E_3 = 7104.4$ MPa for an axial force of $N = -4840$ kN. The difference between the last two iterations was 0.26%. The internal moment is $M_{Ed} = 3150$ kNm, giving a moment utilization of 79.0%.

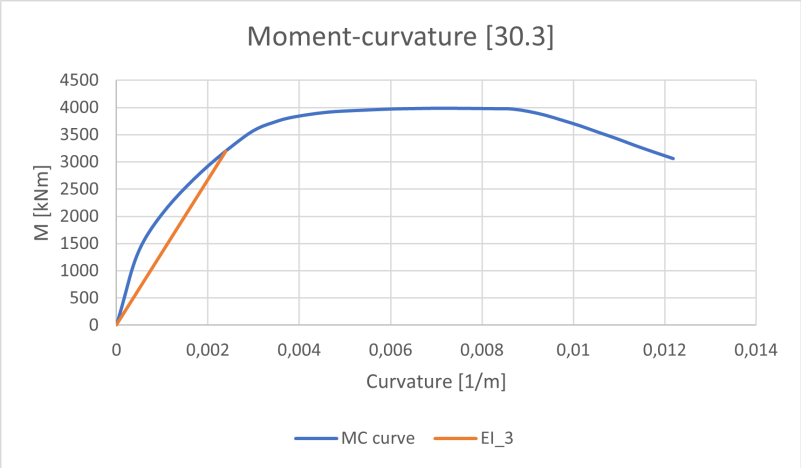

Figure 10.34: Moment-curvature diagram, column [31.3]

For column 34, the relationship is only evaluated about the strong axis as the utilization is much higher. The Young's-modulus is $E_3 = 10174$ MPa for an axial force of $N = -8630$ kN. The difference between the last two iterations is 1.03%. The moment is $M_{Ed} = 4850$ kNm, giving a utilization of 78.4%.

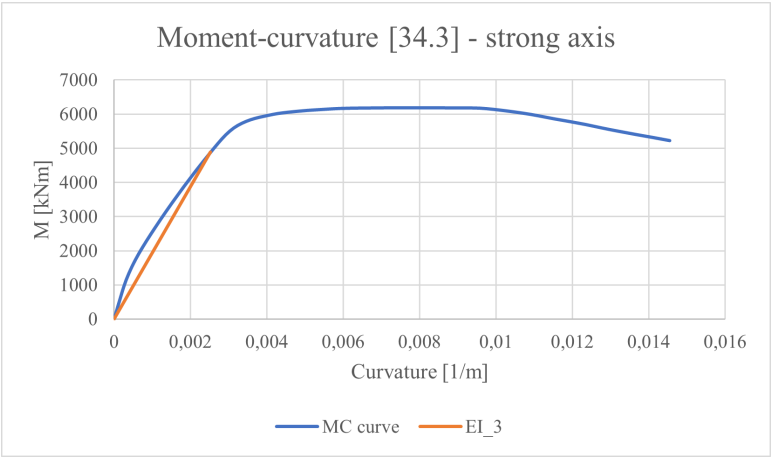

Figure 10.35: Moment-curvature diagram, column [34.3]

For column 44, the Young's-modulus is $E_3 = 14220$ MPa for an axial force of $N = -3002$ kN. The difference between the last two iterations was 2.47%. The moment is $M_{Ed} = 1127$ kNm, giving a utilization of 45.4%.

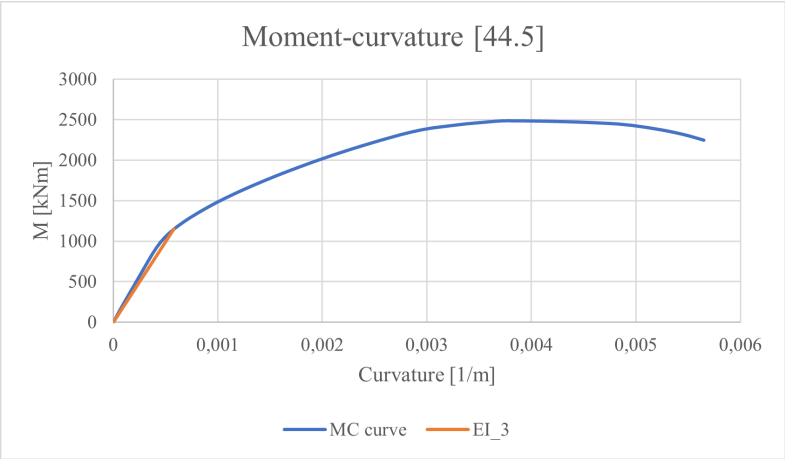

Figure 10.36: Moment-curvature diagram, column [44.5], [45.5] and [46.5]

10.7 Special ASR effects

10.7.1 Reduction of Young's Modulus

The Young's modulus is reduced for concrete affected by ASR. This subchapter will investigate the effect of this reduction on the moment-curvature diagram of a cross-section. The reduced Young's modulus is calculated as described in Subchapter 4.3.1 and presented in Equation 10.7.

$$\frac{E}{E_{ref}} = 1 - \frac{0.00055}{0.00055 + 0.0035} = 0.864 \tag{10.7}$$

An ASR expansion of 0.55‰ gives a reduction in the Young's modulus of 13.6%.

As an illustrative example, the Young's modulus is reduced by 20%. This will shift the stress-strain curve towards higher strains as shown in Figure 10.37.

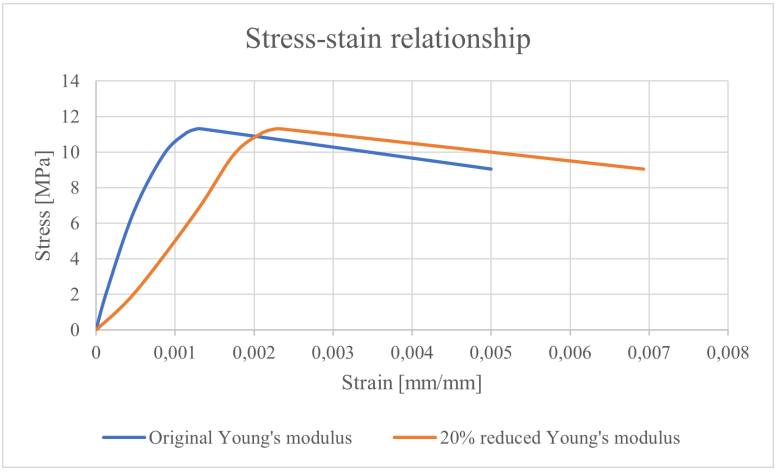

Figure 10.37: Stress - strain relationship with reduced Young's modulus

A comparison between the cross-section with the original and reduced Young's modulus is plotted in the moment-curvature relationship in Figure 10.38. For low curvatures, it is clear that the reduced Young's modulus results in a lower stiffness for any given moment. On the other hand, the cross-section is more ductile and the maximum moment is slightly higher for the reduced material.

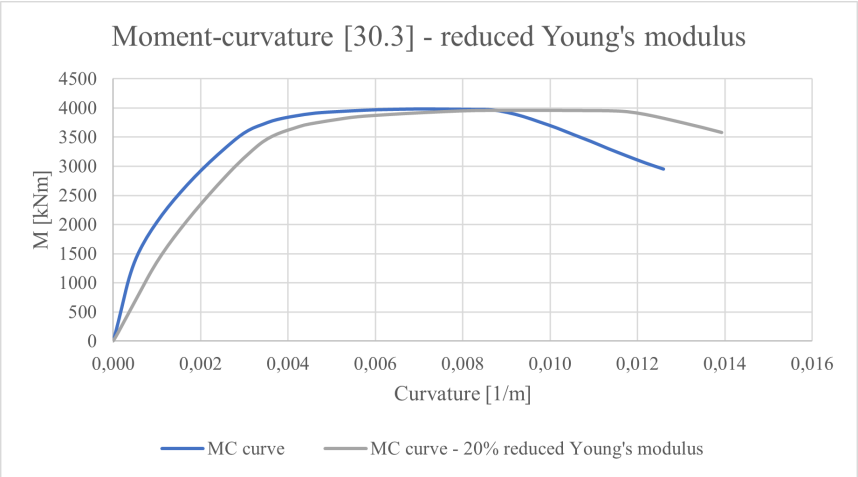

Figure 10.38: Moment-curvature relationship with reduced Young's modulus

A significant reduction of 20% in Young's modulus has a small effect on the total capacity of the columns. However, it will give larger displacements and second-order moments for the bridge as a result of the less stiff concrete in the columns.

The model and equation for calculating the reduced stiffness are based on tests conducted on samples loaded in the free expansion direction of the concrete as explained in Subchapter 4.3.1. The actual reduction in the axial direction of the columns is considered far lower and therefore, the reduction in stiffness (EI) due to ASR will not be investigated in further detail in this thesis.

10.7.2 Curvature in columns due to ASR gradient

The effects of a varying ASR expansion in the horizontal plane of the columns will be investigated in this subchapter. The effects are largest for the tallest columns. For a modelled expansion of 2.7‰ on one side and 0‰ on the other side of the cross-section for all columns in Section C, the results can be seen in Figure 10.39 (a).

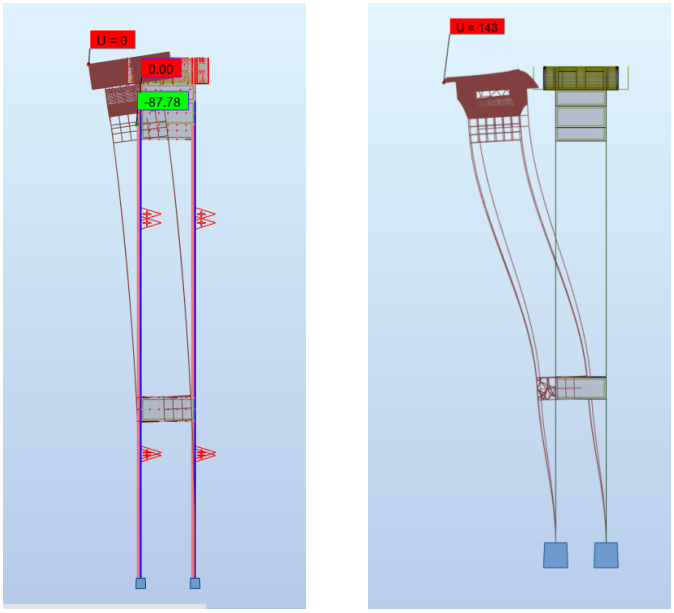

(a) Displacement < 1 mm, moment, $M_x = 88$ kNm

(b) Displacement $= 143$ mm

Figure 10.39: Displacement and moment due to ASR-gradient in the columns (a) and displacement due to wind in the transversal direction (b)

This load effect is modelled equally in all the columns in section C. This represents a situation where all the columns have a much higher degree of ASR expansion on one side due to differences in local climate (sun exposure, humidity, etc.). No effect was apparent with the load effect modelled in one column. The model has the same boundary conditions as the other loads, i.e., free to displace in all directions apart from in the longitudinal direction. Figure 10.39 (b) presents the displacement due to the wind in the transversal direction. The differences in the two results follows: Where the ASR load gives an equal curvature to all columns allowing the bridge deck to be displaced as the end of a cantilever subjected to a uniform, distributed load, the wind load is largest along the side of the bridge deck and pushes this out with little rotation in the deck, resulting in an s-shaped curved displacement in the columns. The effect gives an additional moment accounting for 1.5% of the total capacity. This effect is small and will therefore not be investigated further.

10.7.3 Additional moment due to the displacement of the column top

As explained in Chapter 5, Multiconsult performed a displacement scan of all columns from axis 1 to 34 in 2016. The measurements were taken from below the top crossbar, and roughly every 0.5 m down to 2 meters above sea level [32]. The difference in displacement in the transversal direction (eccentricity, δ) measured at the top and the lower crossbar will be multiplied by the axial force present at the top of the column and added to the internal moment, M_x, found in Robot. As presented in Subchapter 10.5.1, the moment about the y-axis contributes little to the utilization, and the displacement in the longitudinal direction will not be reviewed.

For sections B and C, the columns in axis 31 and 34 will be examined at the lower crossbar due to their high utilization. The column pair in axis 34 will also be examined at the foundation ([34.5]). In this case, the displacement variation from the foundation to the top is assumed to be the same as from the top to the sea level. For columns 44 to 46, displacement measured and presented in Subchapter 5.1.1 will be used likewise.

For sections B and C, the displacement in the transversal direction is to the north for both columns in the pairs. Therefore, only the north column will be examined for a load combination with wind from the south. For columns 44 to 46, the absolute value of the displacement in the transversal direction of the bridge will be used as they lean in opposite directions. The displacement in the transversal direction, axial force at the top of the column, and extra moment are given in Table 10.6 and interaction diagrams with the updated moments are presented in Figures 10.40 to 10.41.

Table 10.6: Effects of current displacement in selected columns due to ASR expansion

Section [xx.x]	**Displacement in the transversal direction δ [mm]**	N_{Top} **[kN]**	Δ_M **[kNm]**
31.3	5	3600	18
34.3	48	7500	360
34.5	70	7500	525
44.5	100	1747	174
45.5	85	1520	129
46.5	155	1555	241

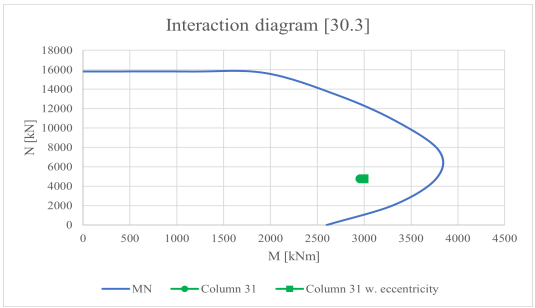

(a) [31.3] - Increase in moment by 6%

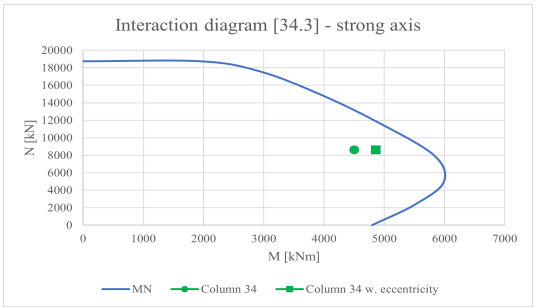

(b) [34.3] - Increase in moment by 12%

Figure 10.40: The effects of measured displacement on column sections [31.3] and [34.3] due to ASR

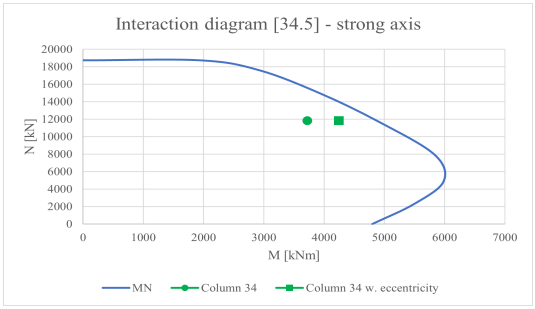

(a) [34.5] - Increase in moment by 14%

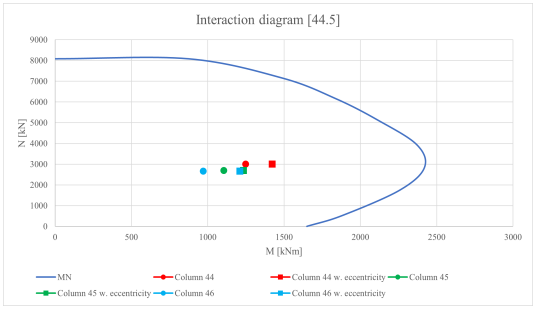

(b) [44.5], [45.5] and [46.5] - Increase in moment by 16% for column 44

Figure 10.41: The effects of measured displacement on column sections [34.5] and [44.5] to [47.5] due to ASR

11 Parametric study

The parametric study attempts to discuss and analyse potential future cases that could cause capacity problems. The cases that will be looked at separately and combined are:
- Increased expansion due to ASR, combined with high temperature.
- Limited or no strength of concrete cover due to ASR damage.
- Corrosion of reinforcement.

This chapter is intended to highlight the effects of future damage scenarios if the ASR damage is allowed to propagate without measures of mitigation. All interaction diagrams will be presented based on load combination a3 - wind, without the current displacement presented in Subchapter 10.7.3. This choice was made because some results calculated in this chapter are based on a structure not deformed by ASR. The results are showcased through interaction diagrams to best visualize the effects.

11.1 High temperature and increased ASR expansion

In the Robot model, the increase of ASR in sections B and C gave relatively low increases in moments and displacement. This is likely due to the reinforcement layout in the bridge deck, giving an equal curvature on both sides of the columns, thus not affecting them greatly. The effect giving a displacement of concern is the added effect of the closing of the expansion joints at lower temperatures than today (17 °C). Even with this, the ultimate load combination is still a3-wind, where the temperature load is not included because it is a variable load. Due to the uncertainty of the displacement resulting from higher ASR expansions combined with temperature loads for sections B, C and D, only the future displacement of section E will be discussed in this chapter. The inspection results presented in Subchapter 5.1.1 show signs that this effect causes permanent displacement of the column tops in section C and thus gives a larger second-order moment.

To investigate this effect, it is important to highlight the current displacement situation of the load cases on the columns. The current situation with a combination of high temperatures, ASR, and expansion joints closing at 17 degrees can be seen in Figure 11.1.

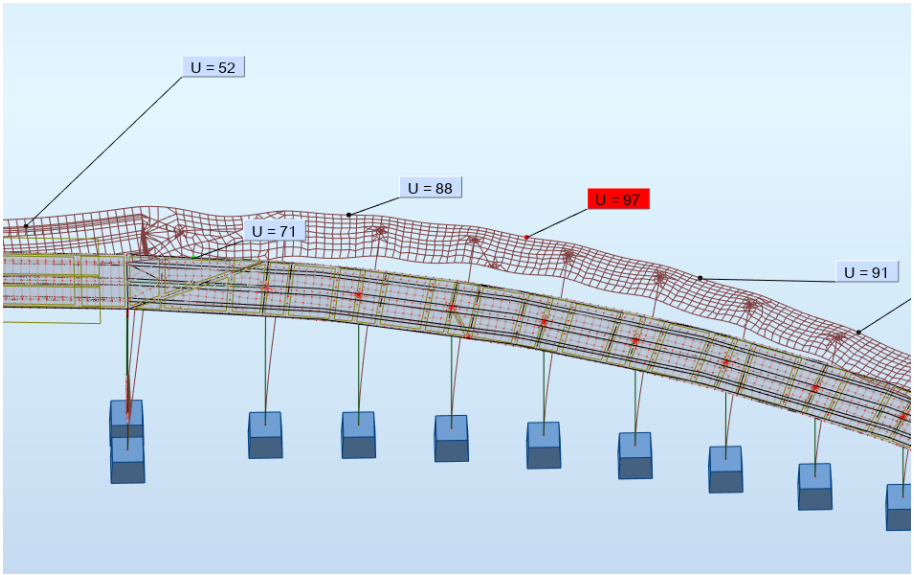

Figure 11.1: Situation today - 0.55‰ ASR, closed expansion joints and a temperature gradient of 14 °C

From Figure 11.1, the mean displacement for columns 43 to 47 is 87 mm in the transversal direction. The mean displacement for the same section was measured to 79 mm in the inspection seen in Figure 5.3. Based on these results, it can be assumed that close to 90% of the displacement due to ASR and temperature is permanent. It could be argued that the true value is closer to 100%, because column 44 leans into the curve as opposed to the others, probably due to a geometric divergence from the construction, but this is not considered to be conservative. It is also important to note that this is a mean displacement. Thus, some columns can have far larger displacements, as is displayed in Figure 5.3, where column 46 has a displacement normal to the bridge deck of 155 mm.

The extra, permanent displacement of 90% of the results from Figure 11.1 could be used to calculate an additional second-order moment in Subchapter 10.7.3. It is also interesting to study the effect of a larger expansion due to ASR that could occur in the future. From Subchapter 6.3, it is clear that the moment from ASR is quite small compared to the total moment from load combination a3-wind on column 44. Therefore, the results from this combination are used in the assessments in this chapter even though it includes ASR loads.

Two future cases are examined: ASR expansion of 1‰ and 1.5‰. It is assumed that the expansion joints were designed to close at 30 °C, by linear interpolation, they close at 5.5 °C for 1‰ ASR, and −7 °C for 1.5‰ ASR. The results are found in Figures 11.2 and 11.3.

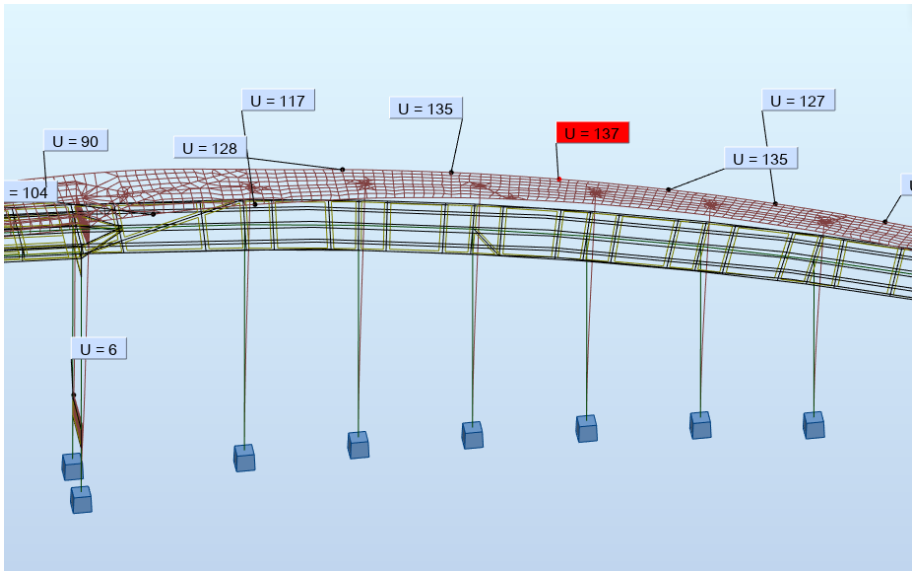

Figure 11.2: Displacement of bridge deck with combined 1‰ ASR, max temperature load and expansion joints closed at 5.5 °C

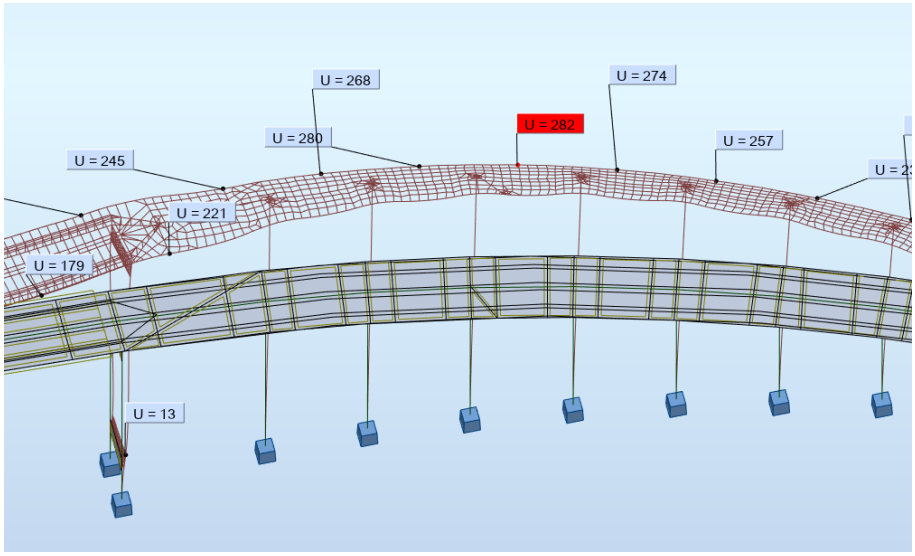

Figure 11.3: Displacement of bridge deck with combined 1.5‰ ASR and max temperature load

Based on this, the assumption can be made that the additional eccentricities of the two cases have a mean value of 116 mm for the first case and 242 mm for the second case. The effects on the capacity can be seen in Figure 11.4 where the original results from Subchapter 10.5 are plotted with the additional moment contribution from the displacement.

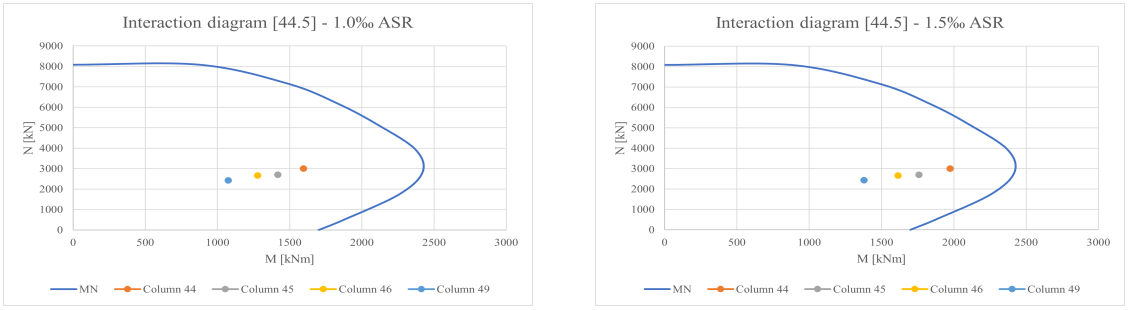

(a) (b)

Figure 11.4: Interaction diagrams for columns 44, 45, 46 and 49 with ASR expansion of 1.0‰ and 1.5‰. For column 44 the moment changes from 1250 kNm in the original interaction diagram (Figure 10.33) to 1600 kNM in figure (a) and 1950 kNm in figure (b)

11.2 Reduction of concrete cover

As presented in Chapter 4, further ASR expansion can reduce the tensile strength of the concrete to close to zero and increase cracking, which in turn can give conditions suitable for frost damage. These effects can weaken the concrete cover, thus reducing its compressive strength or, at worst, causing it to no longer contribute to the compressive capacity. This chapter will investigate the effects of reducing the effective concrete cover by 100% and the effect this has on the moment and axial capacity. Reducing or removing the concrete cover for a whole or several columns would change the entire model due to the reduced stiffness, larger displacement, and higher moments. Due to the high improbability of a situation like this, this thesis will only examine a situation where the cover is reduced locally for the investigated cross-section. Therefore it will only affect the capacity curve, and not the point indicating the loads on the interactions diagram.

The thickness of the concrete cover is different for sections above and below sea level. Figure 11.5 shows an example of column section [34.3], modelled in SAP2000, without concrete cover.

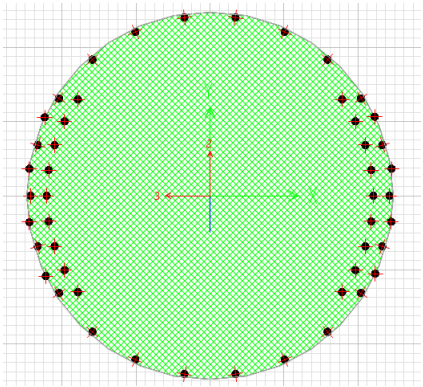

Figure 11.5: Cross-section [34.3] without cover

In Figures 11.6 and 11.7, selected column sections are modelled without concrete cover, and the axial force and moment from load combination a3-wind are displayed.

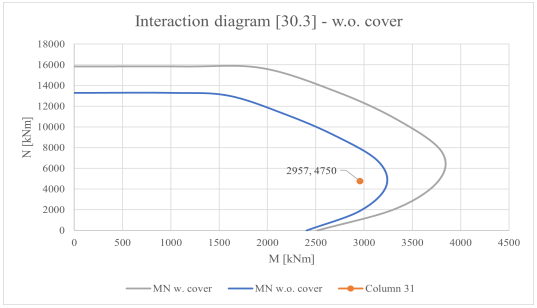

(a) Displacement

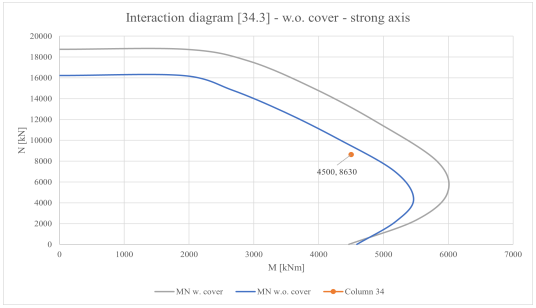

(b) Loads

Figure 11.6: Interaction diagram for column sections [30.3] and [34.3] w.o. cover

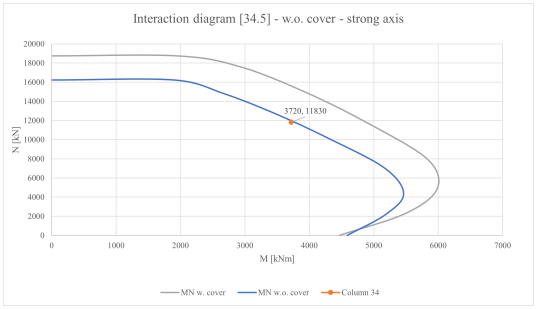

(a) Displacement

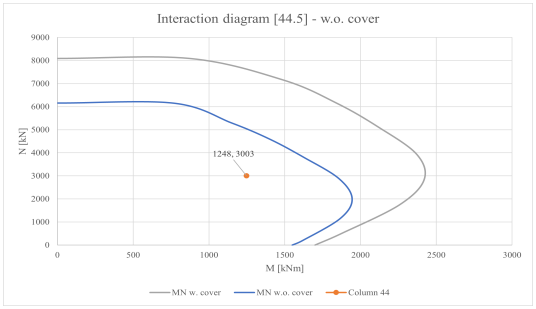

(b) Loads

Figure 11.7: Interaction diagram for column sections [34.5] and [44.5] w.o. cover

11.3 Corrosion of reinforcement

Reinforcement corrosion is expected to get worse over the coming years. The columns are especially exposed to the highly corrosive environment near the sea. As presented in Chapter 5, there are already signs of corrosive damage in the columns. The exact value of corrosive damage is unknown, but the columns are assumed to be more affected than the bridge deck [30]. The column section [44.5] is investigated as an example. The area of the reinforcement in the column is reduced to account for corrosion. By removing one and two reinforcement bars, from 16Ø25 to 15Ø25 and 14Ø25, the total reinforcement area is reduced by 6.25% and 12.5%. In Figure 11.8, the two cases are shown in comparison to the original interaction diagram and with the case of no effective concrete cover. Like the concrete cover, the reinforcement will be reduced locally for a cross-section and only affect the capacity curve, not the point indicating the loads.

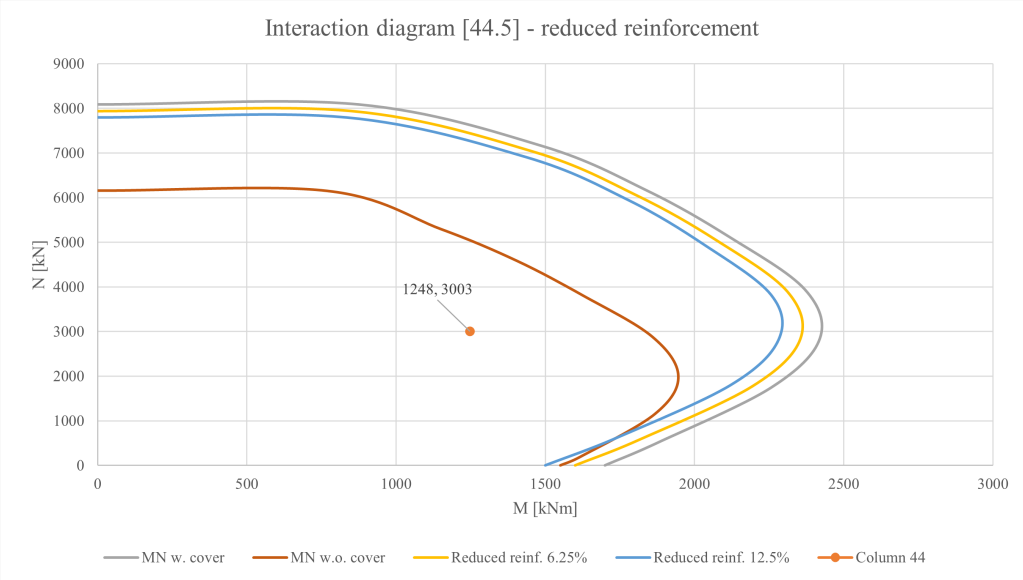

Figure 11.8: Interaction diagram column [44.5] with reduced reinforcement

From Figure 11.8 it is clear that reinforcement corrosion has a relatively small impact on the capacity compared to a reduction in concrete cover (dark blue curve).

11.4 Combined situations

Finally, to address potential future problems, the parameters are combined to illustrate the effects through some selected scenarios. Generally, the main factors that may lead to capacity problems are a significant reduction of the concrete cover and the propagation of corrosion in the reinforcement. ASR expansions will not have a critical effect on the displacement of the columns in sections A to D and are, therefore, not included in this parametric study. However, This effect will impact the curved part of section E, especially if combined with reduced concrete cover and corrosion. The cases illustrated are based on the load combination a3-wind.

As presented in Chapter 9, the interaction diagrams created by SAP2000 are conservative. Therefore, it is interesting to see the combined effects on some of the column sections, even if they are close to full capacity for one of the effects alone.

Column 31 will reach close to its capacity in a situation where the cover is neglected, and the area of reinforcement is reduced by 12.5% due to corrosion, as is shown in Figure 11.9.

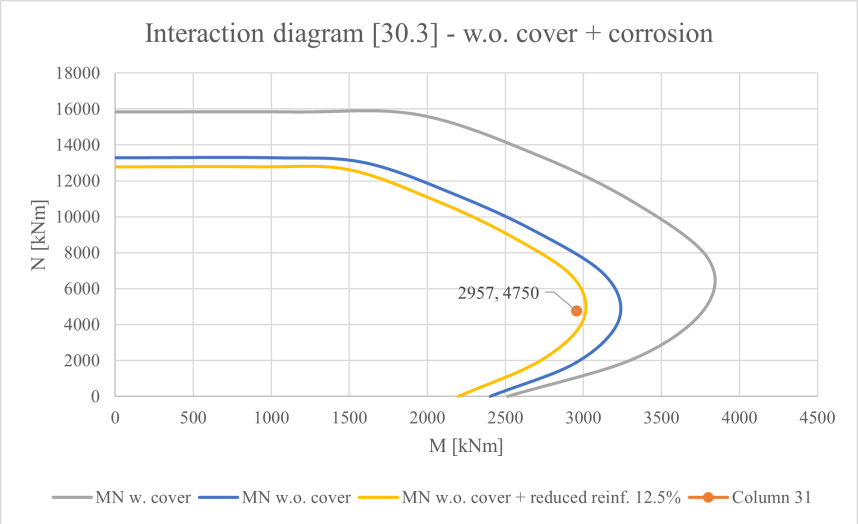

Figure 11.9: Interaction diagram column [30.3] w.o. cover and reduced reinforcement

Column 34 is already close to full capacity due to the loss of concrete cover, both at the lower crossbar and the foundation. Nevertheless, the combined effect of concrete cover loss and corrosion should be investigated and is presented in Figures 11.10 and 11.11.

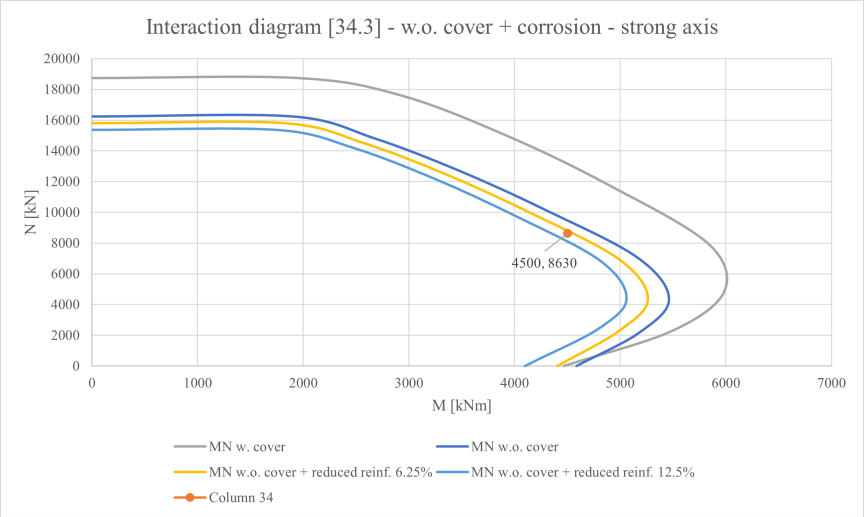

Figure 11.10: Interaction diagram column [34.3] w.o. cover and reduced reinforcement

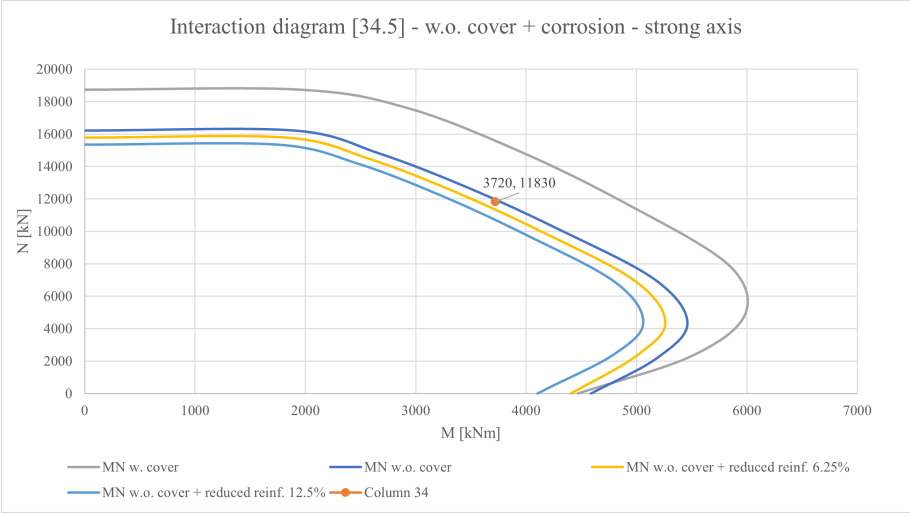

Figure 11.11: Interaction diagram column [34.5] w.o. cover and reduced reinforcement

The concrete cover is also reduced and combined with corrosion in the reinforcement for the single columns in the curved section E (44-49). In addition, ASR expansions have a significant impact on the displacement of the column top.

As shown in Figure 11.12, the capacity of column 44 is nearly reached in a situation where half of the concrete cover is neglected, in combination with a reduction of reinforcement area by 12.5% due to corrosion. This is for a situation with 1.5‰ in ASR expansion, causing an average eccentricity of 242 mm on columns 44-49.

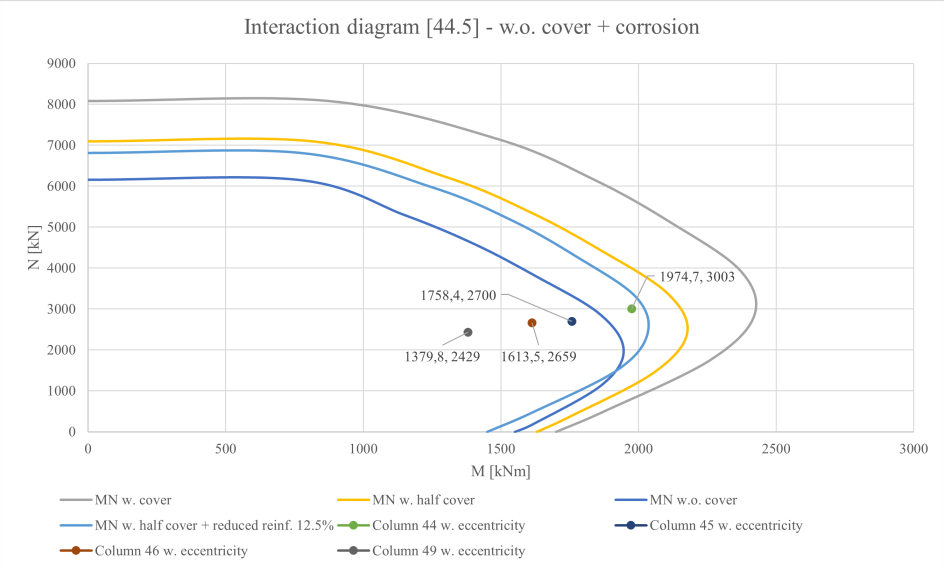

Figure 11.12: Interaction diagram column [44.5] w.o. cover and reduced reinforcement

12 Discussion

In order to verify and confirm the obtained results throughout the thesis, the work of Sandnes and Skaug, *Beregning av fritt frambyggbru med alkalireaksjoner* has been used [2]. Similar to Sandnes and Skaug, our model accurately represents the bridge and realistic loads. However, some areas of uncertainty still exist. Firstly, to account for the viaducts, the choice of support conditions on the cantilever model (section C) was complex to represent accurately. There was a slight divergence in the horizontal displacement of models C and D, E of 23 mm when subjected to load combination a3 - wind. This could have been improved by modelling the supports using springs with a defined spring constant. However, due to the relatively small divergence and complexity of implementing an accurate spring constant, this was neglected. The choice of one restraint in the longitudinal direction for the cantilever part gave some unrealistic, asymmetrical moment distributions for the ASR and temperature loads as presented in Chapter 6. Furthermore, the temperature loads are not included in the critical load combination, and the ASR moments on the columns are low. The entire bridge could also have been modelled together, but this would have resulted in a complex model with a high run time. Secondly, the technical drawings from Aas-Jacobsen were difficult to interpret accurately as the reinforcement layout and the length of the extra reinforcement areas were not described for all columns. Therefore some assumptions had to be made.

The results from the individual loads prove that the model works well and that the forces, moments, and deformations are realistic. For the load combinations, wind-load in the transversal direction with a load factor of 1.6 proved decisive for the columns. Since the bridge deck is far stiffer than the columns, only a small portion of the moment from the traffic loads is transferred to the columns. In contrast, the stiffness of the columns is the main contributor to preventing large displacements in the transversal direction. It was evident that wind in the longitudinal direction had a much smaller effect than wind in the transversal direction. The wind load in the longitudinal direction can be neglected as per *Beregningsveiledning for etteroppspente betongbruer* [33].

Slenderness was calculated for column 34. This is the tallest column of the bridge and was therefore assumed to be slender, which was proven in Subchapter 10.1. In addition, the column was proven to be stable and reach its capacity experiencing material failure. Analysis was performed accounting for second-order effects for all columns as a conservative measure.

The columns were also evaluated for shear capacity, presented in Subchapter 10.4. The utilization is safely within the limits and will not pose a critical concern for the columns. This is also true for the crossbars for all columns, being well within capacity based on compression field theory.

The interaction diagrams were made with the support of the FEM program SAP2000. As described in Chapter 9, the diagrams are conservative as the compressive capacity of the reinforcement is neglected. This has to be taken into account when studying the diagrams and assessing the remaining capacity.

Eccentricity due to geometrical deviation is not accounted for in the interaction diagram evaluation of the columns but is included later. All columns show capacity within the conservative interaction diagram. As explained in Subchapter 10.5, the utilization of the columns was not calculated for the interaction diagrams, but the columns closest to full capacity were analyzed further using moment-curvature calculations. It should be noted that the moment in column 34 is higher in the thesis of Sandnes and Skaug by approximately 12.3% [2]. This is because they included the total height of the safety barriers in the wind calculations, unlike this thesis which uses the value of 1.2 m as is given in EC1-4 Table 8.1. Both column 30 and column 38 have lower values for axial forces and moments due to the wind load compared to column 31. For column 30 this was expected since it is shorter and in between two other column axis. For column 38 the reason is assumed to be the shorter span of the double t-cross-section in section D compared to section B (lower wind forces in plate section) and the curve of the bridge in model D,E and the consequently higher resistance of displacement out of the longitudinal axis. Based on the interaction diagrams, the choice was made not to study column 32 further due to the low utilization. Column 31 is prioritized because it has higher moments and axial forces than 30 and 38.

The columns were also verified considering the bi-axial moments. For the cylindrical columns (pillars), the bi-axial moment is generally less utilized than in the critical axis due to the constant $a = 2$ in EC 2 subsection 5.8.9(4) [8]. Column [34.3] has the highest bi-axial utilization at 64.2%.

Also produced using SAP2000 were the moment-curvature relationships. The utilization for column 31 is 79.0% and for column 34 it is 78.4%. The method gives a slightly higher moment than the interaction diagrams as the sections considered have a lower stiffness (EI), giving a more ductile behaviour and, consequently higher displacement. As a result, the second-order moment is represented more accurately. The updated stiffness (EI_3) from the moment-curvature relationship is only valid for the selected cross-section [XX.3]. However, it is applied for the full length of the column, making it conservative and strengthening the conclusion that the columns are not fully utilized.

12.1 ASR effects

Alkali silica reactions have a clear impact on the material properties of concrete. This thesis mainly focuses on a lowered stiffness from a reduction in Young's modulus. Shown in Subchapter 10.7.1, a reduction of 20% in Young's modulus allows for more curvature with the higher strains permitted. The reduction did impact the moment-curvature relationship; however, Equation 10.7 for the reduced Young's modulus due to ASR is based on the expansion in the unrestrained direction of the concrete. Due to the high axial forces in the columns, the true reduction is expected to be significantly lower [1]. Furthermore, the SDI values for the two columns in axis 20 are also significantly lower than the average values, as explained in Chapter 5. Therefore, as described in the results, the true reduction of the stiffness in the columns is assumed to be of a small magnitude, not impacting the capacity significantly.

The situation with a varying degree of ASR in a column cross-section proved to have a small impact on the total moment capacity compared to the displacement of the column top as described in Subchapter 10.7.2. This was tested for the tallest columns (section C) and is thus considered to have a small effect on the capacity for the rest of the columns.

As ASR expansions can cause significant displacements of the bridge deck and the top of the columns, this must be considered carefully. The displacement scan performed by Multiconsult (2016) and the investigation of the east abutment (Chapter 5) indicate ongoing displacements, causing an eccentricity of the column tops. In section E, the curved part of the bridge deck is displaced outwards as described in Subchapter 5.1.1. This has a significant but not critical effect on the single columns even though it increases the moment by 16%. No official displacement scans have been performed on this part of the bridge and should be prioritized moving forward. For the tallest columns close to (31, 38), and within section C (32-37), the eccentricity must be monitored closely. The axial forces in the columns are of such magnitude that eccentricities can cause large additional moments. At the bottom of column 34, a displacement of 70mm in the top increases the moment by 525 kNm, an increase of 14%. As seen from the inspections, and described in Subchapter 10.7.3, the displacement of these columns is not yet critical but will have a significant effect. Simulating further displacements in the model is problematic as the boundary conditions applied to simulate the neighbouring sections (A,B and D,E) must be highly precise. If the bridge had been modelled as one global structure, analysis of further displacements for the tall columns in section C would have been possible. Since the axial forces are large, this is potentially a critical problem in the future.

12.2 Parametric study

As a final part of the thesis, the parametric study focused on highlighting the most critical problems and visualizing the effects and consequences of hypothetical combinations of these effects. The parametric study does not consider the probability of occurrence or the time frame of the potentially critical situations, as this will need further research. It does, however, indicate what should be emphasized when assessing the bridge for preventative measures and rehabilitation in the future. The parametric cases for loss of concrete cover and corrosion in the reinforcement were calculated with the same load situation and material characteristics as the original model. This was done to simulate a reduced concrete cover and corrosion at one single point in the selected column. If one or all of the columns were modelled with loss of cover and corrosion over the full length, the stiffness would be greatly reduced, the displacement higher and the resulting moments and axial forces would most likely exceed the capacity. This scenario is highly unlikely, unlike a scenario with a local reduction, which could occur with failing maintenance and further ASR propagation.

The effects of a significant increase in ASR and/or temperature have little impact on section A-D of the bridge in the model. On the curved section E, however, a high ASR expansion of 1.5‰ will have a large impact on the displacement of the single columns as the expansion joints will be permanently closed. This level of expansion is considered high and is assumed not to occur for a long time, if ever. Nevertheless, monitoring the expansion joints and evaluating if they close at decreasing temperatures in the future may be of importance.

A reduction of concrete cover is also evaluated as a potential consequence of further ASR propagation. This is proven to have a highly consequential effect as seen in the large shift of the interaction diagrams (Figures 11.6 and 11.7). The hollow column sections [30.3] and [44.5] experience an even larger effect with a loss of cover. While a loss of the full concrete cover could pose an extreme scenario, it should not be overlooked as this could occur with a lack of maintenance.

As a final factor of consideration, reinforcement corrosion is likely in a humid and chloride environment such as Tromsø. Corrosion was simulated by reducing the area of reinforcement (A_s) by 6.25% and 12.5%. While the chosen corrosion rate might be artificially high, it still has a much smaller impact compared to the loss of concrete cover. It should be noted that there are signs of corrosion initiation in large parts of the bridge as described in chapter 5. Nevertheless, it appears unlikely that this will be a decisive problem for any of the columns unless it coincides with large cracking and potential loss of concrete cover in the future.

The parameters were combined to illustrate what is required for the columns to reach a critical state. It must be noted that as seen in Figure 9.5 and described in Subchapter 9.3.3, the interaction diagrams are conservative as they neglect the compressive capacity of the reinforcement. Sections [31.3], [34.3], and [34.5] have similar characteristics and are discussed together. In a situation where the concrete cover is reduced and corrosion is present, full capacity is reached for the sections. For sections [34.3] and [34.5] full loss of concrete cover and 6.25% reduction in reinforcement area will lead to failure. For column section [31.3], full loss of concrete cover and 12.5% reduction in reinforcement area will cause failure. For these sections, eccentricity due to ASR (discussed in Subchapter 10.7.3) has not been included but could cause an even more critical situation.

For column 44, an eccentricity caused by 1.5‰ ASR and a combination of reduced concrete cover and corrosion is necessary to provoke capacity problems (see Figure 11.12). Hence, the eccentricity of the columns in section E should be monitored closely to uncover potential capacity problems early.

13 Conclusion

The capacity of the columns of the Tromsø Bridge is generally within the limits. There are no utilization problems for axial force, shear, or moment in the columns or crossbeams. The columns are slender however, no signs of buckling-related issues exist for any of the columns. The utilization of the most critical columns based on moment-curvature relationships is 79.0% for column 31 and 78.4% for column 34, with similar values for the columns opposite the cantilever part (35, 38). For the bi-axial moment verification, the utilization values were low, with a maximum value of 64.2%. The utilization for shear in the columns is low, with the highest value being 65% for column 32. In addition, ASR expansions have little to no effect on the shear capacity. The crossbeam with the highest stress was checked using compression field theory, where the concrete's compressive capacity and the reinforcement's tensile capacity showed no capacity problems with the highest utilization of the reinforcement of 86%.

ASR will have a small effect on the expansion of the columns as they are in compression. It will, however, affect the bridge deck to a greater extent causing a displacement of the column tops, inducing an increased eccentricity. This has been documented in inspections performed by Multiconsult (2016) and the authors (2023). It is reasonable to expect further displacement of the columns, mainly in the transversal direction, which should be monitored over the coming years. Further, the consequences of concrete cover loss and reinforcement corrosion were evaluated. For columns 31 and 34, a critical situation will arise if the cover is effectively removed, and 12.5% reduction of reinforcement area is assumed. For the single columns in section E (44-47) full capacity is reached in a situation where half the cover is neglected, and 12.5% reduction of reinforcement area is assumed in combination with an eccentricity of the columns due to ASR expansions of 1.5‰.

The evaluation of the columns in this study indicates how ASR may affect the structure. Based on the assumptions regarding ASR development, the calculations reveal changes in the structural behaviour of the structure, with an increase in forces and a decrease in material strength. However, the calculations demonstrate sufficient capacity at the current ASR level. Only for the extreme, hypothetical cases of the parametric study exceedances of capacity are present. Therefore, corrosion propagation, loss of concrete cover, and displacements due to ASR should be monitored and investigated further. In conclusion, there is no immediate risk of structural collapse of the construction, but this assessment is based on rough assumptions of the ASR situation. A more thorough investigation is encouraged to establish a better foundation for assessing the future condition of the bridge.

Further research and inspection of the bridge should be conducted. A thorough inspection of the bridge at a high temperature (25 °C) should be performed. This will give an insight into the combined effects of temperature and ASR expansions. In addition, neglected loads in this thesis should be included in a more detailed analysis. Further research on the propagation of ASR over time should be conducted. This would be highly supportive in assessing the state of the columns in future years. The serviceability limit state (SLS) should also be evaluated. As ASR causes cracking, investigating the consequences in SLS concerning crack widths and deformations is necessary and perhaps more decisive, looking at a shorter time span, due to decreased resistance against corrosion and frost action. Finally, a detailed inspection to document current levels of corrosion, the concrete cover, and complete documentation of the displacements caused by ASR is necessary.

Bibliography

[1] T. Kanstad, 'Structural Consequences of Alkali-Silica-Reactions (ASR)', *NTNU - Betong 3*, 2021.

[2] E. Sandnes and L. M. B. Skaug, 'Beregning av fritt frambyggbru med alkalireaksjoner', *NTNU - Institutt for konstruksjonsteknikk*, 2017.

[3] Standard Norge, *Eurocode 0, NS-EN 1990, Basis of structural design.*

[4] Standard Norge, *Eurocode 1, NS-EN 1991, Actions on structures.*

[5] Standard Norge, *Eurocode 1, NS-EN 1991-2, Traffic loads on bridges.*

[6] Standard Norge, *Eurocode 1, NS-EN 1991-4, Wind actions.*

[7] Standard Norge, *Eurocode 1, NS-EN 1991-5, Thermal actions.*

[8] Standard Norge, *Eurocode 2, NS-EN 1992, Design of concrete structures.*

[9] Standard Norge, *NS 3473:1998, Prosjektering av betongkonstruksjoner.*

[10] Statens Vegvesen, *N400, Bruprosjektering - Bridge design.*

[11] Statens Vegvesen, *V412, Bæreevneklassifisering av bruer, laster - Strength classification of bridges, loads.*

[12] Statens Vegvesen, *V413, Bæreevneklassifisering av bruer, materialer - Strength classification, materials.*

[13] Statens Vegvesen, *V441, Bruinspeksjon - Bridge inspection.*

[14] Lovdata. 'Forskrift om fredning av statens kulturhistoriske eiendommer)'. (2022), [Online]. Available: https://lovdata.no/dokument/SF/forskrift/2011-11-09-1088#KAPITTEL_30 (visited on 23rd May 2023).

[15] G. A. Stokke. 'Tromsøbrua en verdig jubelant'. (2014), [Online]. Available: https://digitaltmuseum.no/011085439624/tromsobrua-en-verdig-jubilant (visited on 2nd Mar. 2023).

[16] Gro Agnethe Stokke. 'Tromsøbrua, en verdig jubilant'. (2014), [Online]. Available: https://digitaltmuseum.no/011085439624/tromsobrua-en-verdig-jubilant (visited on 23rd May 2023).

[17] Dr. Ing. Aas. Jacobsen, *Technical drawings - Tromsø Bridge*, 1960.

[18] Store norske leksikon. 'Tromsøbrua'. (2020), [Online]. Available: https://snl.no/Troms%C3%B8brua (visited on 2nd Mar. 2023).

[19] Kartverket, *Norgeskart - Tromsø.*

[20] S. I. Sørensen, *Betongkonstruksjoner. Beregning og dimensjonering etter Eurocode 2.* Fagbokforlaget, 2013, vol. 2. 2013.

[21] S Jacobsen et. al, 'Concrete technology 1, tkt 4125', *NTNU*, 2016.

[22] E. Rodum, 'MESLA-seminar Tromsøbrua 14. mai 2022', 2022.

[23] A. Berg, 'MESLA-seminar Tromsøbrua 15. nov 2022', 2022.

[24] K. M. Stemland, E. Rodum and T. Kanstad, 'Stiffness damage testing of laboratory-cast alkali-silica reactive concrete and cores drilled from an existing concrete structure', *16th International Conference on Alkali Aggregate Reaction in Concrete*, 2022.

[25] H. Stemland, E. Rodum and H. Johansen, 'Alkalireaksjoner – veiledning for konstruktiv analyse', *Staten Vegvesen*, 2016.

[26] S. Kongshaug, 'Experimental investigation of asr-affected concrete – the influence of uniaxial loading on the evolution of mechanical properties, expansion and damage indices', *ScienceDirect*, 2020.

[27] J. Lindgård, Ö. Andiç-Çakır, I. Fernandes, T. Rønning and M. Thomas, 'Alkali-silica reactions (asr): Literature review on parameters influencing laboratory performance testing', 2012.

[28] E. Rodum, 'Tromsøbrua – utførte undersøkelser 2010-2021 felt- og laboratoriemetoder for bruinspeksjoner', 2022.

[29] Troms og Finnmark Fylkeskommune, *Avlesningsdata fukt og temperatur tromsøbrua (excel)*, 2022.

[30] A. Rexer, 'Spesialinspeksjon - 19 - 0511 tromsøbrua', 2022.

[31] SINTEF, 'Laboratorieundersøkelser av 20 stk. utborede betongkjerner', 2023.

[32] Multiconsult, 'Spesialinspeksjon bru nr. 19-0511 tromsøbrua', 2016.

[33] Statens Vegvesen, *SVV668, Beregningsveiledning for etteroppspente betongbruer - Calculation guidelines for PT concrete bridges.*

[34] Inc. Autodesk, *Dynamo Sandbox.*

[35] Inc. Autodesk, *Robot Structural Analysis Professional 2022.*

[36] *Google maps*, https://www.google.com/maps, 2023.

[37] K. Bell, 'An engineering approach to finite element analysis of linear structural mechanics problems', *Fagbokforlaget*, 2013.

[38] L. Aadnesen and H. Frost, 'Tromsøbroen', *Teknisk Ukeblad*, vol. Særtrykk nr. 1885, no. nr. 2, 1962, p. 12, 1962.

[39] E. Rodum, 'Befaringsnotater 18-19 juni 2014', 2014.

[40] P. K. Larsen, A. H. Clausen and A. Aalberg, *Stålkonstruksjoner - Profiler og Formler*. Fagbokforlaget, 2017.

[41] Computers and Structures, Inc., *Sap2000.*

[42] *Microsoft excel*, Computer software.

[43] J. Hellesland, *Slanke betongkonstruksjoner - forenklet og optimal dimensjonering med hensyn til sikkerhet og økonomi.* Norsk betongforening, 1998.

[44] K. Kobayashi, T. Fukushima and K. Rokugo, 'Shear strength of asr-deteriorated rc members and shear reinforcing effect of repair by adding rebar', *VIII International Conference on Fracture Mechanics of Concrete and Concrete Structures*, 2013.

Appendix

- Appendix A - Technical drawings
- Appendix B - Column reinforcement
- Appendix C - Loads
- Appendix D - Buckling and slenderness
- Appendix E - Capacity shear and crossbars
- Appendix F - ASR
- Appendix G - Interaction diagrams
- Appendix H - Scanning of columns 31 and 34

A Technical drawings

The following technical drawings from Dr. Ing. Aas. Jakobsen were used:

- Overview - bridge
- Overview - columns
- Reinforcement - columns
- Overview - bridge deck
- Overview - cantilever part
- Details - cantilever part
- Transition - section D to plate bridge

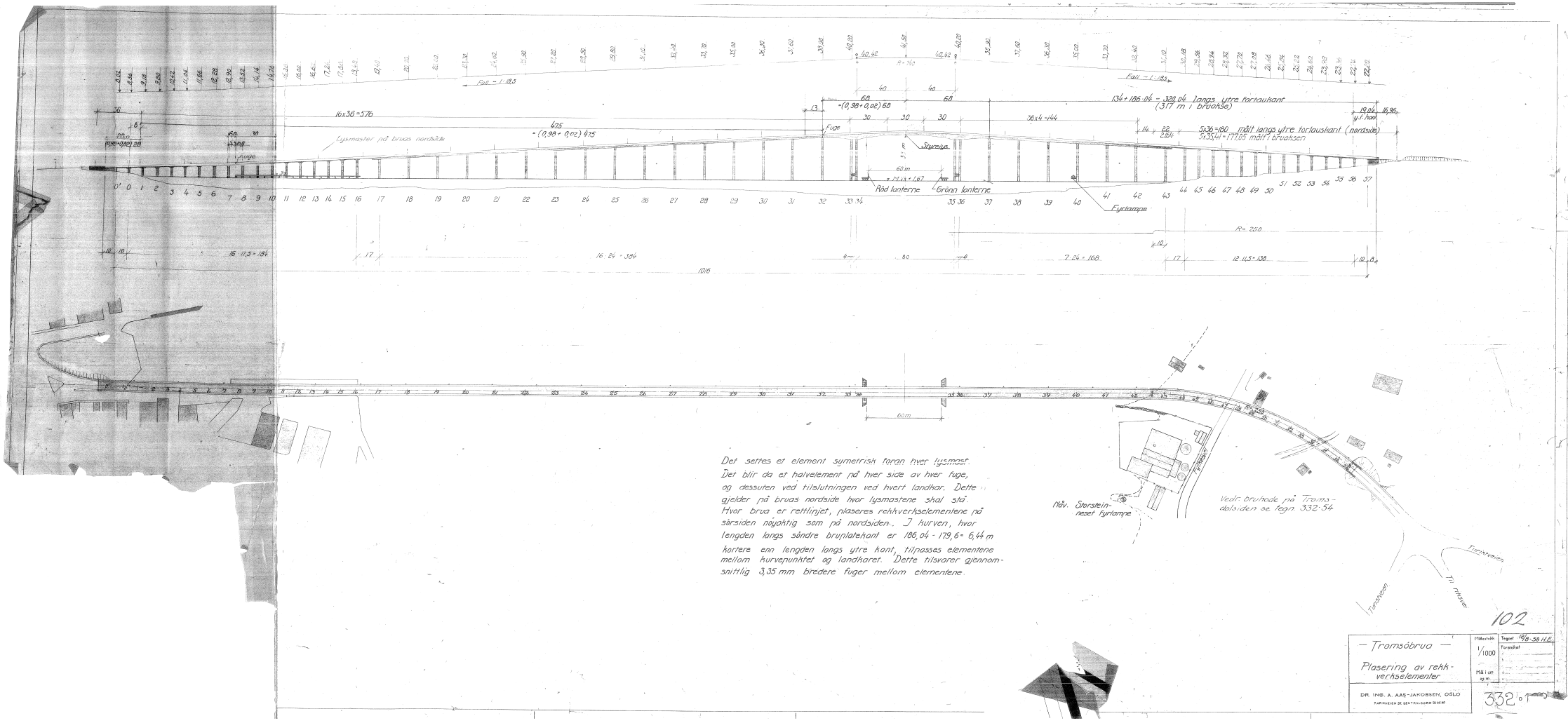
Fall = 1:183
16x36=576
Lysmaster på bruas nordside
Fuge
Styrhus
Rød lanterne
Grønn lanterne
Fyrlampe
R= 250
60m
134+186.04 = 320.04 langs ytre forlauskant (317 m i bruakse)
5x36=180 målt langs ytre forlauskant (nordside)
5x35.41 = 177.05 målt i bruaksen
1016
Det settes et element symetrisk foran hver lysmast. Det blir da et halvelement på hver side av hver fuge, og dessuten ved tilslutningen ved hvert landkar. Dette gjelder på bruas nordside hvor lysmastene skal stå. Hvor brua er rettlinjet, plaseres rekkverkselementene på sørsiden nøyaktig som på nordsiden. I kurven, hvor lengden langs søndre brunlateñant er 186,04 - 179,6 = 6,44 m kortere enn lengden langs ytre kant, tilpasses elementene mellom kurvepunktet og landkaret. Dette tilsvarer gjennomsnittlig 3,35 mm bredere fuger mellom elementene.
Nåv. Storsteinneset fyrlampe
Vedr. bruhode på Tromsdalssiden se tegn. 332:54
Tromsdalen
Tromsøysund
Tromsøya
102
— Tromsøbrua —
Plasering av rekkverkselementer
1:1000
1:50 i cm
DR. ING. A. AAS-JAKOBSEN, OSLO
FARVEIEN 2E SENTRALBORD 56 48 80
Tegnet 1960-58 H.E.
Forandret
332:01

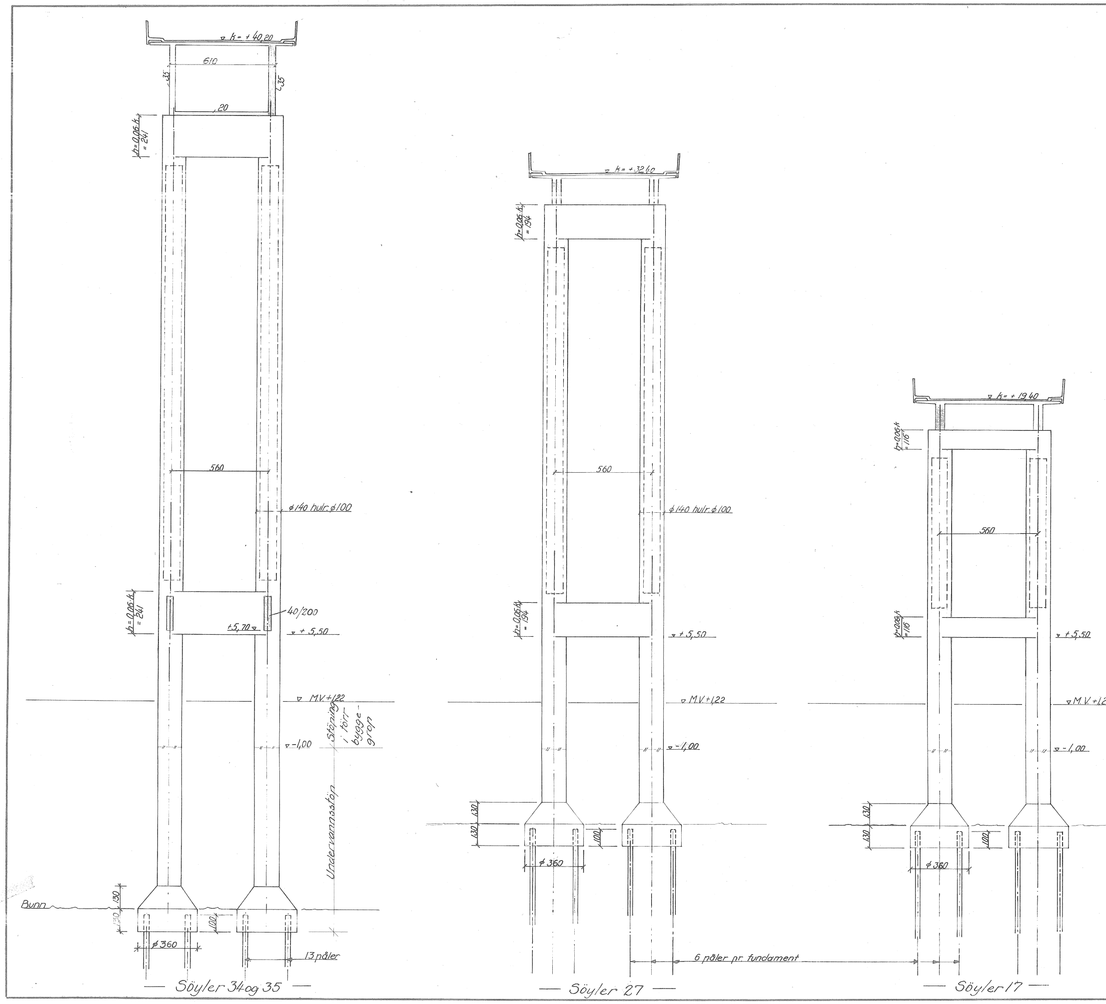

NB! Söylepar 32 og 37 skal stöpes massive.
Söylepar 33,34,35,36 og 17 til og med 20
kan stöpes massive, kfr. Kontrolling.

f 9/2-59 LA.

— Tromsöbrua — — Pillarer i sidespenn —	Målestokk 1/100 Mål i cm og m	Tegnet 24/6-57 O.O. Forandret a 18/7-57 IB b 23/7-57 IB c 6/11-57 IB d 2/1-58 E.B. e 27/8-58 H.E.
DR. ING. A. AAS-JAKOBSEN, OSLO PARKVEIEN 57 — SENTRALBORD 56 45 80		332·49f

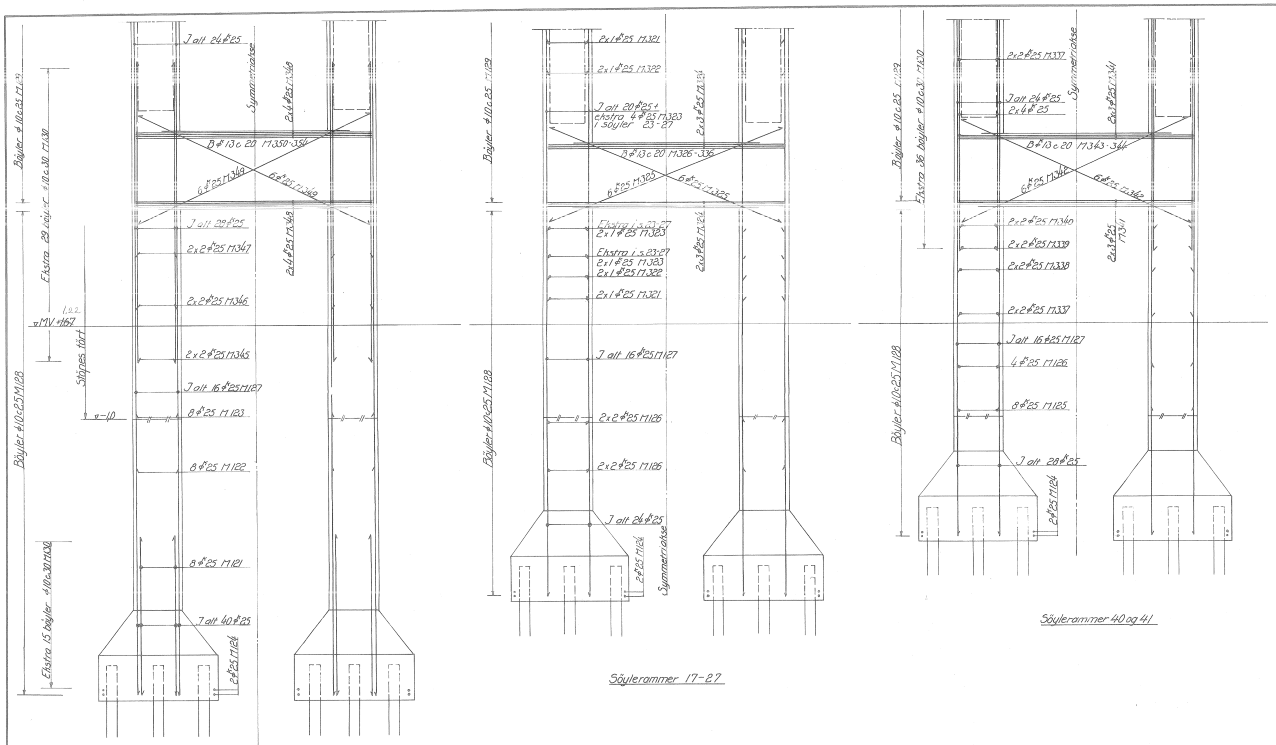

A-betong med min. 375 kg sement pr m³
Armeringens betongoverdekning
under kt. +3,30 : 7 cm
i søyler over " +3,30 : 5 cm
i travers og fund på land 4 cm
Armering ø 10 av glatt stål St 37
ø 25 gjennomgående søylearmering av CSF 405,
armering forøvrig av CSF 50

— Tromsøbrua —	Målestokk 1/50	Tegnet 4/10-57 JB
— Søylerammer 17-31 og 38-41 —		Forandret a CSF - 58 E.B. b 23/12-58 L.H. c d e
— Armering —	Mål i cm og m	
DR. ING. A. AAS-JAKOBSEN, OSLO WERGELANDSVEIEN 17 — SENTRALBORD 56 46 80		332.65 b

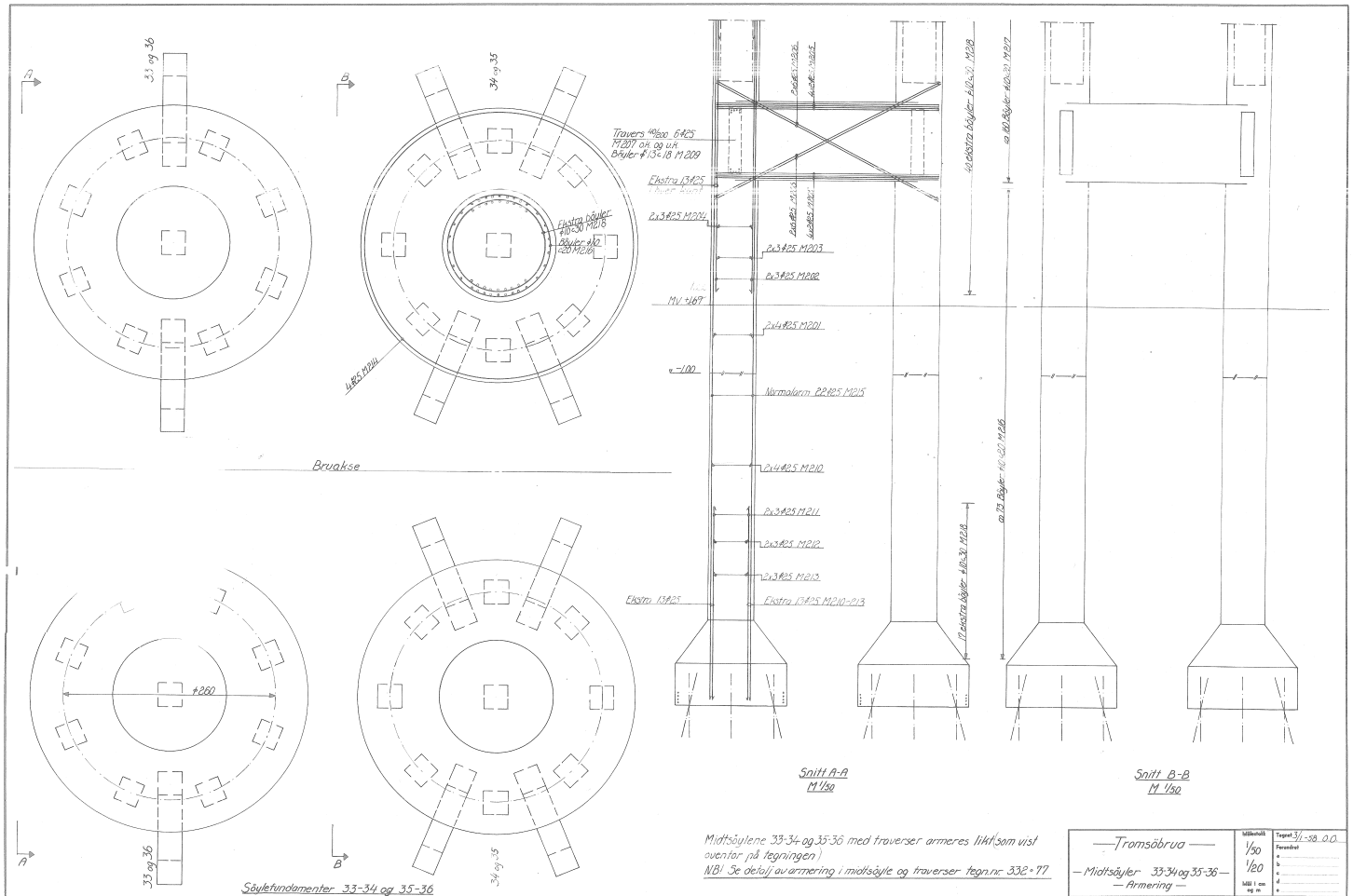

Snitt A-A
M 1/50

Snitt B-B
M 1/50

Søylefundamenter 33-34 og 35-36
M 1/20

Midtsøylene 33-34 og 35-36 med traverser armeres likt som vist ovenfor på tegningen.
NB! Se detalj av armering i midtsøyle og traverser tegn.nr. 332-77

Tromsöbrua Midtsøyler 33-34 og 35-36 Armering	Målestokk 1/50 1/20 Mål i cm og m	Tegnet 31-38 O.O. Forandret a. b. c. d. e.
DR. ING. A. AAS-JAKOBSEN, OSLO RÅDGIVENDE IV – SENTRALBORD 56 48 00		332-66

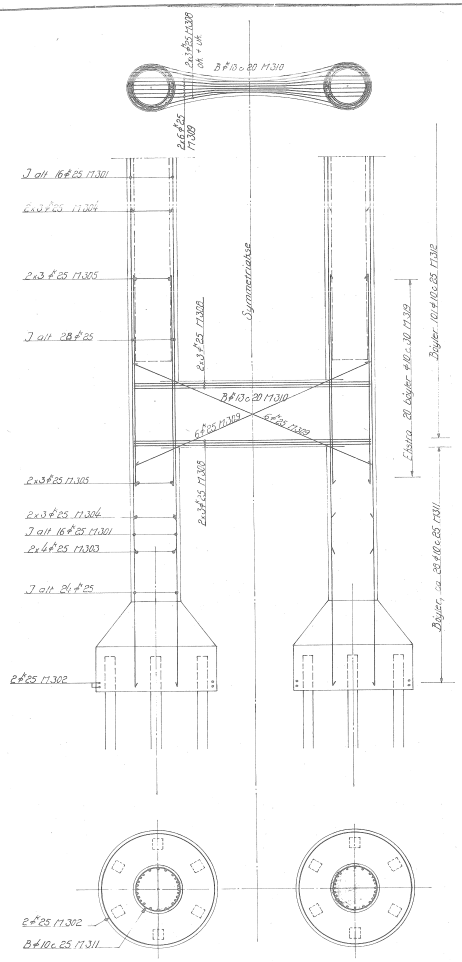

— Søyler nr. 42 —

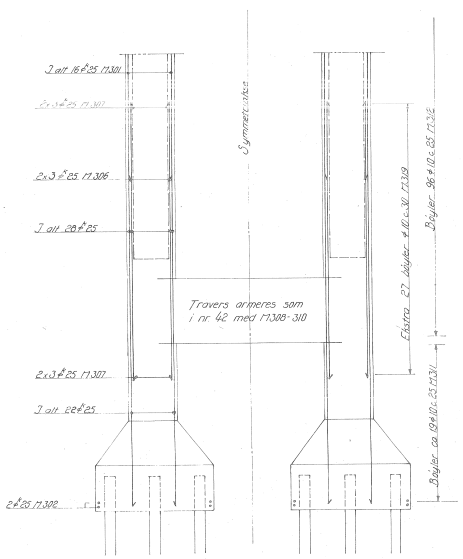

— Søyler nr. 43 —

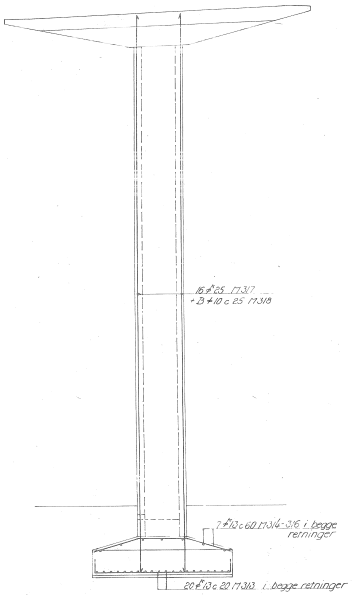

— Søyler 44 - 56 —

A-betong med min 375 kg sement pr m³
Armeringens betongoverdekning
under ht +3,50: 7 cm
i søyler over " +3,50: 5 cm
i travers og fund på land 4 cm

Armering Φ10 av glatt stål St 37,
Φ25 gjennomgående søylearmering av CSF 405,
armering forøvrig av CSF 50

Fikssumkontrakt

— Tromsøbrua —	Målestokk 1/50	Tegnet 17/1-58 E.B.
Armering fundamenter og søyler 42-56	Mål i cm og m	Forandret a b c d e
DR. ING. A. AAS-JAKOBSEN, OSLO PARKVEIEN 87 — SENTRALBORD 56 45 80		332 - 81

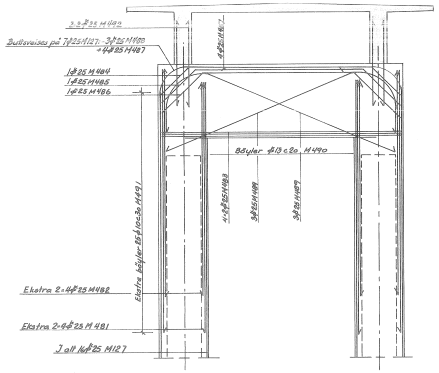

Armering øvre travers, Søyler 41-38
M 1:50

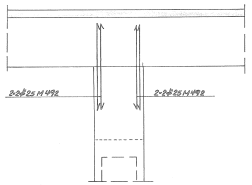

Armering travers-bjelke
Søyler 41-38
M 1:50

Armering:
Ø10 av St 37
Ø25 bultsveiset gjennomgående søyle-armering av C5F 405
All armering forøvrig C5F 50

Se også tegn nr. 332.107 og -65a

Tromsøbrua	Målestokk	Tegnet Ø.A. 10.38 L.H.
		Kontr.
Armering av øvre travers, Søyler 41-38	1:50	Forandret a. b. c. d.
	Mål i cm og m	
DR. ING. A. AAS-JAKOBSEN, OSLO		332.118

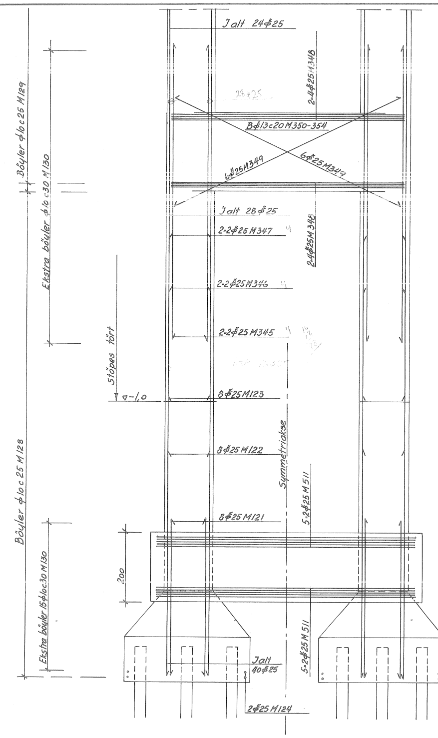

— Söylerammer 32 og 37 —

M 1/50

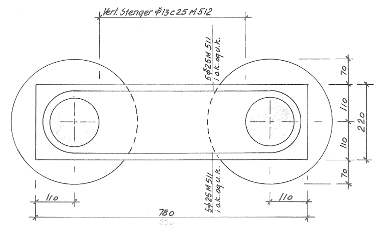

— Armering av nederste travers —

M 1/50

For söylerammer og nedre travers:- Se anm. på tegn.nr. 332.65b.

Nederste travers:- Armering av CST 50, min. betongoverdekning 15cm.

—Tromsöbrua—	Målestokk 1/50	Tegnet 23/12-58 LH. Kontr. Forandret a b c d
—Armering av Söylerammer 32 og 37—	Mål i cm og m	
DR. ING. A. AAS-JAKOBSEN, OSLO PARKVEIEN 57 — SENTRALBORD 56 45 80		332.120

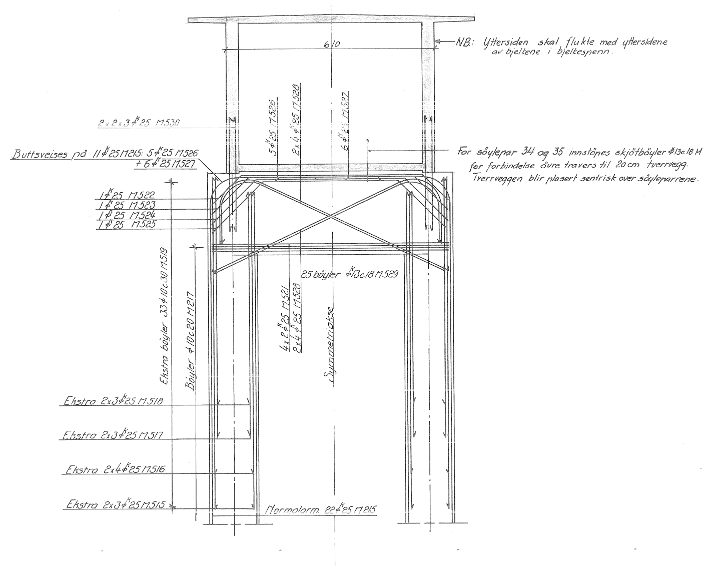

— Armering søyletopp og øvre travers —
Søylepar 33, 34, 35 og 36
M 1/50

Armering
ϕ10 - St. 37
ϕ25 buttsveiset gjennomgående søyle-armering CSF 40S
All armering forøvrig CSF 50

Se også tegn.nr. 332·49^f og ·66

— Tromsøbrua —	Målestokk 1/50	Tegnet 12/2-59 L.A. Kontr.
— Søylepar 33, 34, 35 og 36 — Arm. søyletopp og øvre travers	Mål i cm og m	Forandret a 12/3-59 L.A. b c d
DR. ING. A. AAS-JAKOBSEN, OSLO PARKVEIEN 57 — SENTRALBORD 56 45 80	332·122^a	

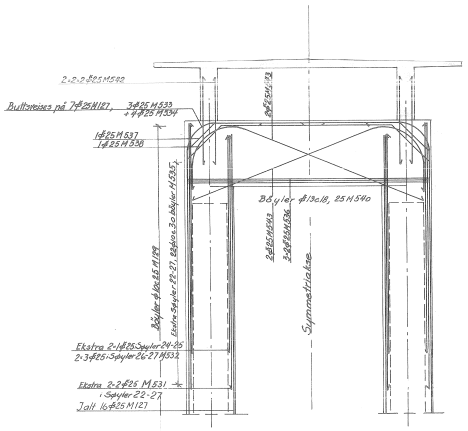

— Armering øvre travers, Søyler 17 – 27 —

M 1/50

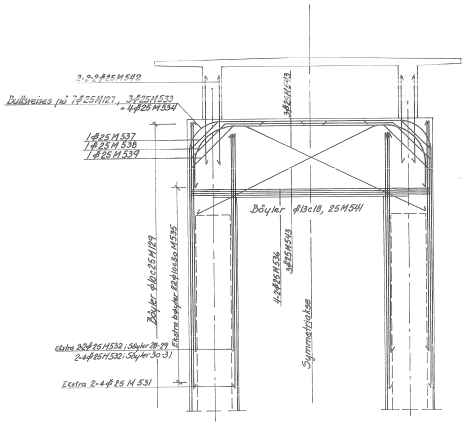

— Armering øvre travers, Søyler 28-31 —

M 1/50

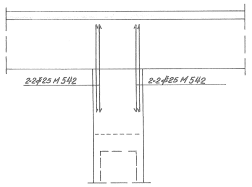

Armering travers - bjelke, Søyler 17-31

M 1/50

Armering: -

Ø10 av St 37.

Ø25 bultsveisel, gjennomgående søylearmering av CSF 40 S

All armering forøvrig CSF 50

Se også tegn. 332.49[f] og 65[b]

— Tromsøbrua —	Målestokk 1/50	Tegnet 12/2-59 LA. Kontr.
Armering Øvre Travers, Søyler 17-31	Mål i cm og m	Forandret a. b. c. d.
DR. ING. A. AAS-JAKOBSEN, OSLO PARKVEIEN 57 — SENTRALBORD 46 45 80		332.123

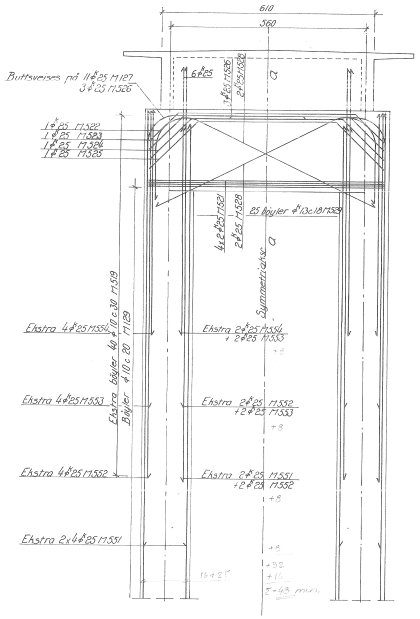

— Armering søyletopp og øvre travers —
Søyler 32 og 37

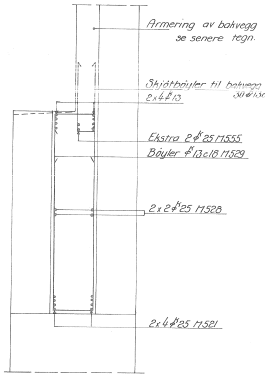

— Snitt a-a —
M 1:20

Bare armering fra halve travers er vist

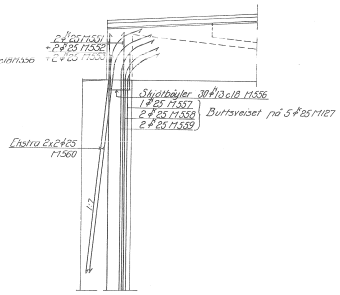

Detalj armering for forankring av endefeltdrager til søyle
M 1:50

Armering:
ϕ 10 : St 37
ϕ 25 : buttsveiset gjennomgående søylearmering CSF 405
All armering forøvrig CSF 50

Se også tegn. nr. 332.120 og 127

— Tromsøbrua —	Målestokk 1/50 1/20	Tegnet 13/3-59 LA. Kontr.
Armering søyletopp og øvre travers søyler 32 og 37	Mål i cm og m	Forandret a. d. c. b.
DR. ING. A. AAS-JAKOBSEN, OSLO PARKVEIEN 87 — SENTRALBORD 56 45 00		332.128

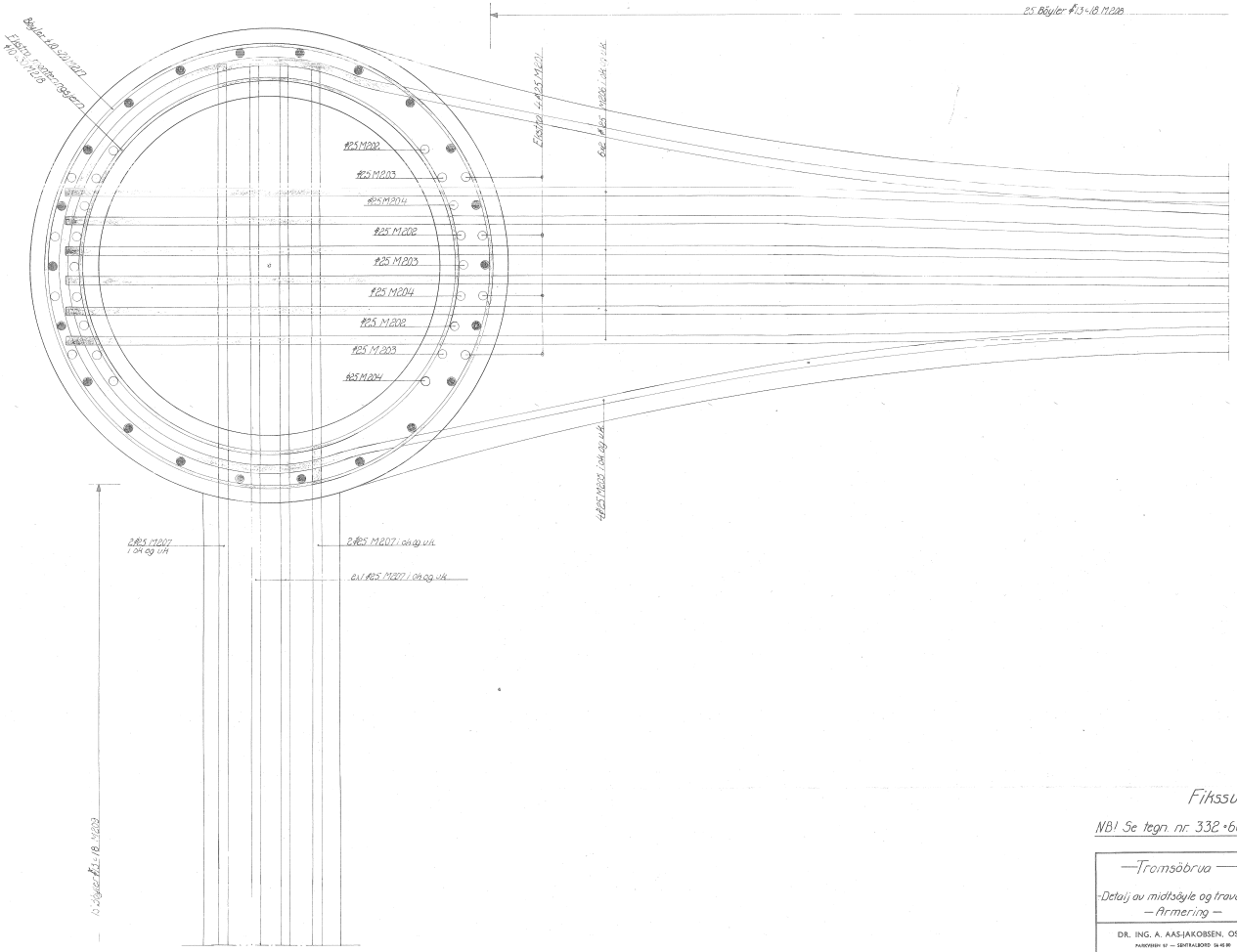

Fikssumkontrakt

NB! Se tegn. nr. 332-66

—Tromsöbrua—	Målestokk 1/5	Tegnet 3/11-58 O.O.
-Detalj av midtsøyle og traverser- —Armering—	Mål i cm og m	Forandret a b c d e
DR. ING. A. AAS-JAKOBSEN, OSLO PARKVEIEN 57 — SENTRALBORD 56 45 80		332-77

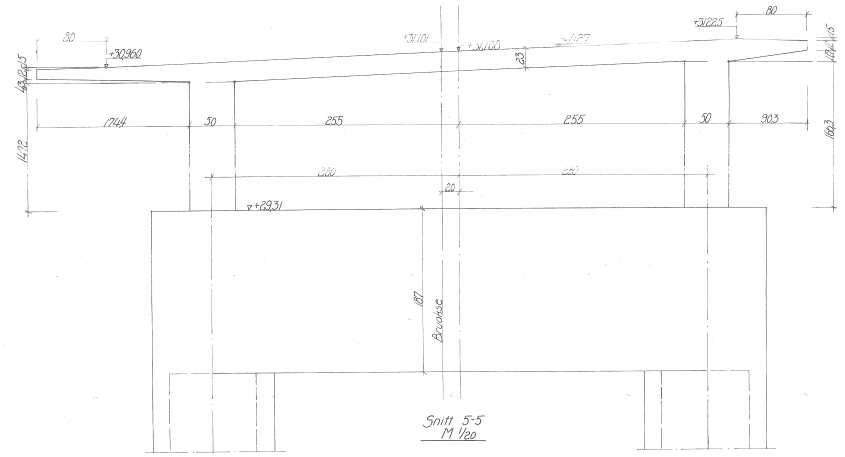

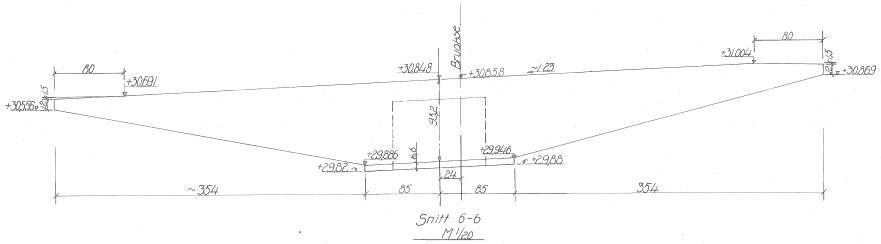

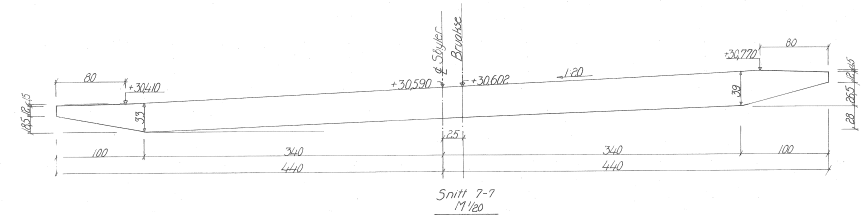

Fiksumkontrakt

A-betong med min. 375 kg sement pr. m³

Snittenes beliggenhet se tegning nr. 332•76 og 80

—Tromsøbrua—	Målestokk 1/20	Tegnet 15/1-58 IB Kontr. Reviderat a b c d
Tverrsnitt 5,6 og 7 i feltet 43-44	Mål i cm og m	
DR. ING. A. AAS-JAKOBSEN, OSLO PARKVEIEN 27 — SENTRALBORD 56 45 80		332•79

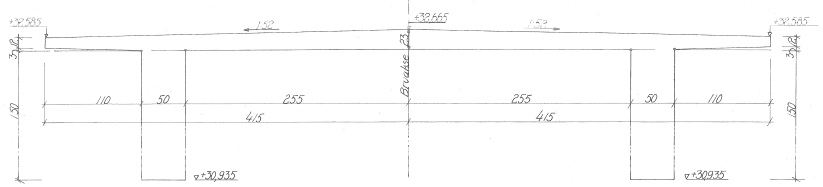

Snitt 1-1
M 1/20

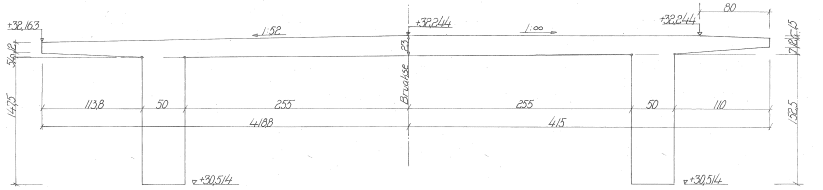

Snitt 2-2
M 1/20

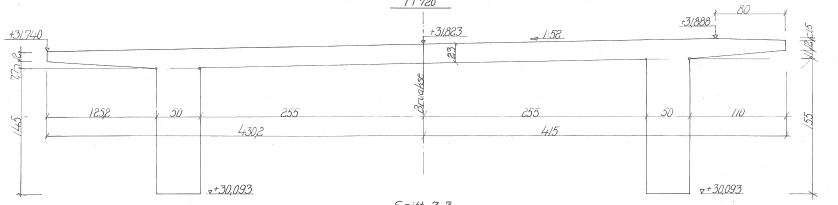

Snitt 3-3
M 1/20

Snitt 4-4
M 1/20

Fikssumkontrakt

A-betong med min. 375 kg. sement pr. m³

Snittenes beliggenhet, se tegning nr. 332-76 og 80

—— Tromsöbrua ——	Målestokk 1/20	Tegnet 13/1-58 JB Kontr.
Tverrsnitt 1, 2, 3 og 4 i tellene 41-42-43	Mål i cm og m	Forandret a b c d
DR. ING. A. AAS-JAKOBSEN, OSLO PARKVEIEN 37 — SENTRALBORD 56 45 80		332 - 82

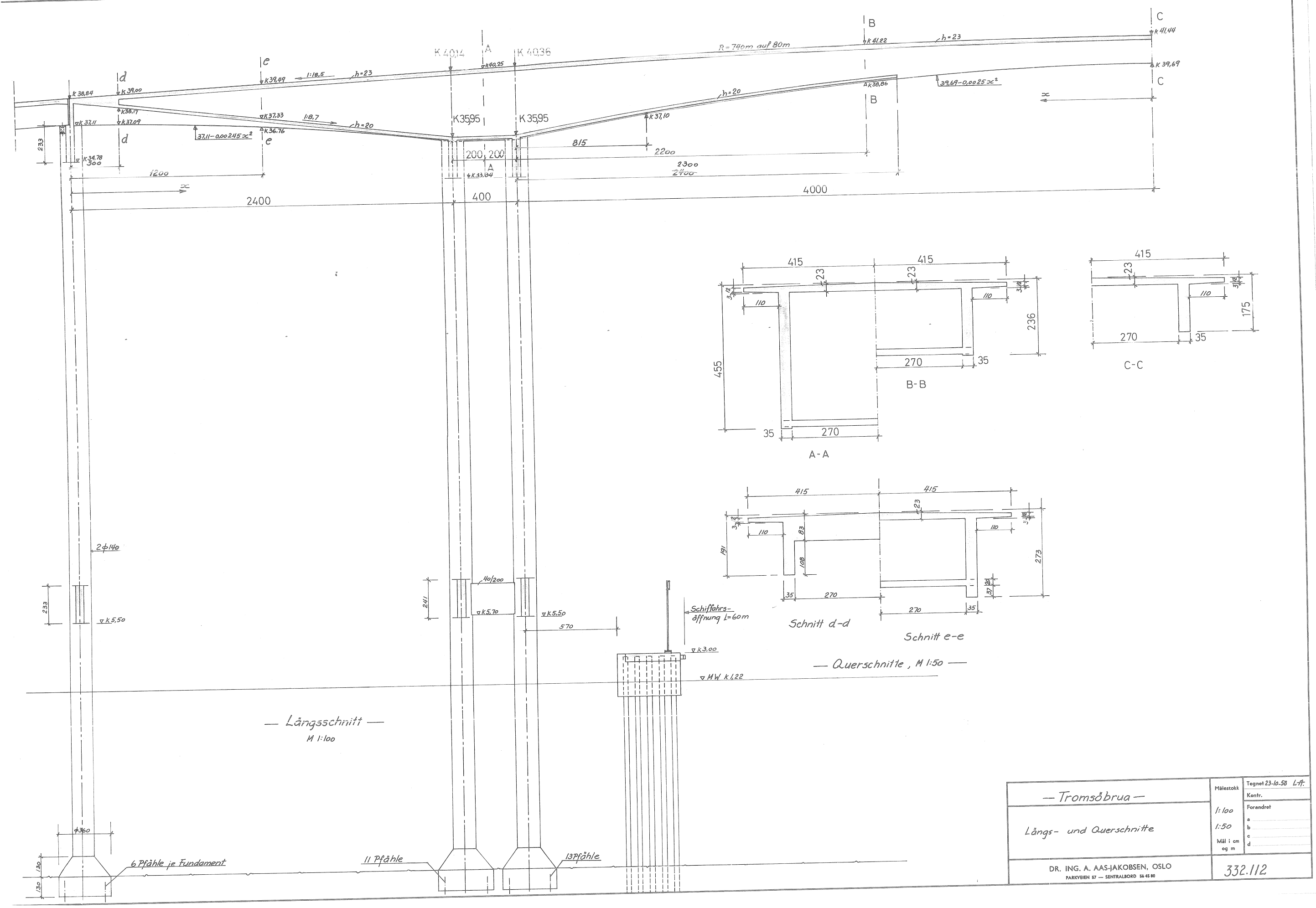

— Tromsøbrua —	Målestokk	Tegnet 23-10-58 L.N.
Längs- und Querschnitte	1:100 / 1:50	Kontr. / Forandret a b c d
DR. ING. A. AAS-JAKOBSEN, OSLO / PARKVEIEN 57 — SENTRALBORD 56 45 80	332.112	

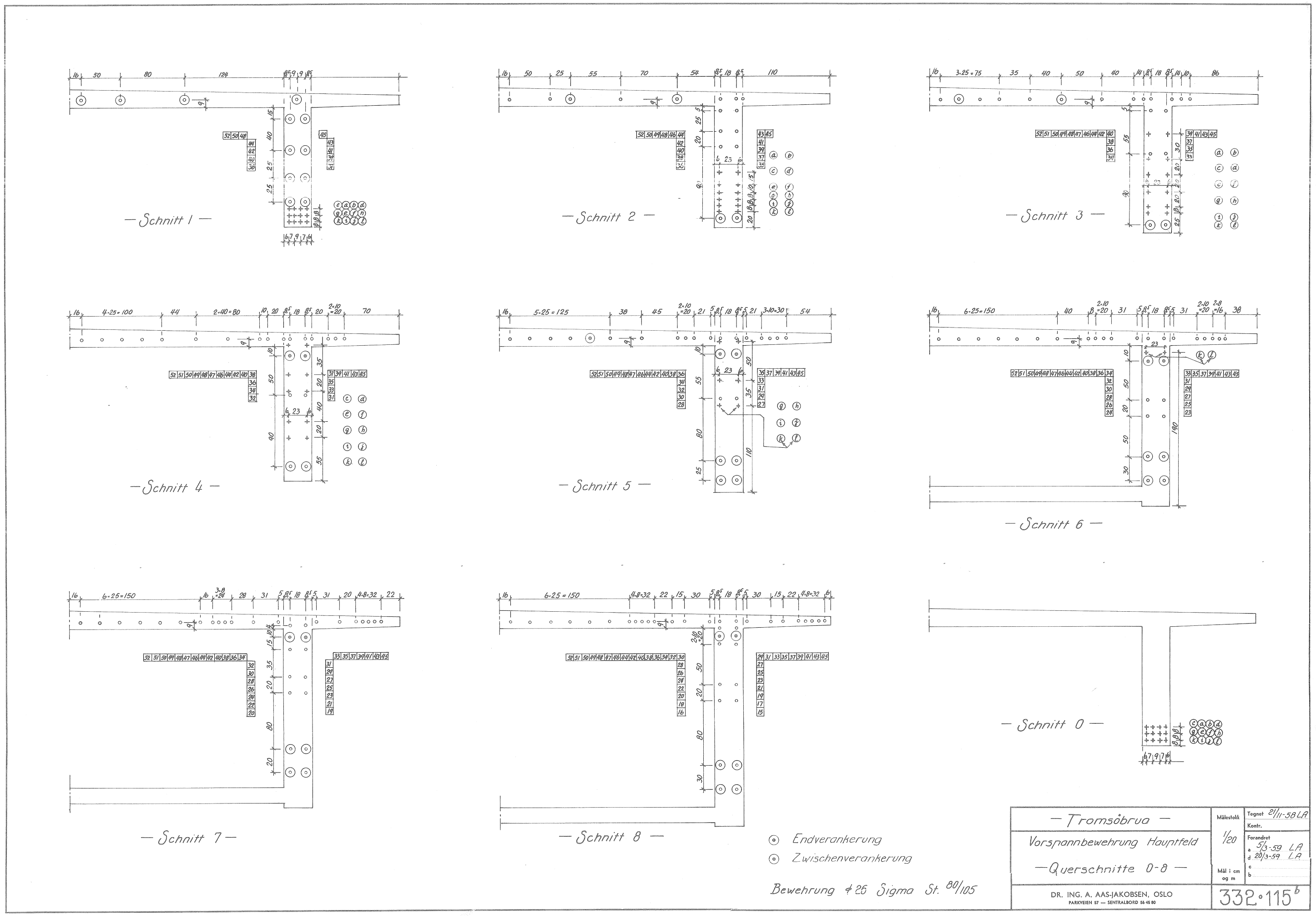

— Schnitt 1 —
— Schnitt 2 —
— Schnitt 3 —
— Schnitt 4 —
— Schnitt 5 —
— Schnitt 6 —
— Schnitt 7 —
— Schnitt 8 —
— Schnitt 0 —
Endverankerung
Zwischenverankerung
Bewehrung ϕ 25 Sigma St. 80/105
— Tromsöbrua —
Vorspannbewehrung Hauptfeld
— Querschnitte 0-8 —
Målestokk 1/20
Tegnet 21/11-58 LA
Kontr.
Forandret
a 5/3-59 LA
b 20/3-59 LA
Mål i cm og m
DR. ING. A. AAS-JAKOBSEN, OSLO
PARKVEIEN 57 — SENTRALBORD 56 45 80
332·115 b

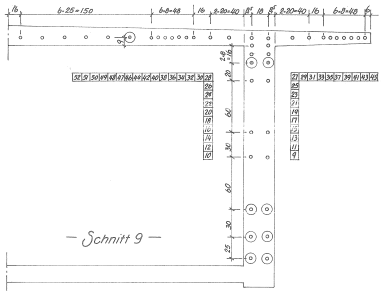

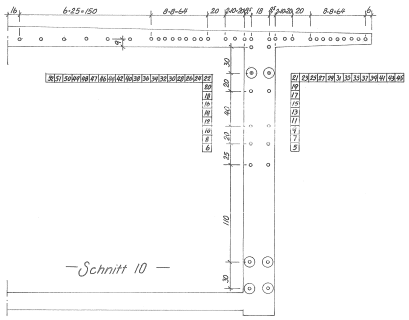

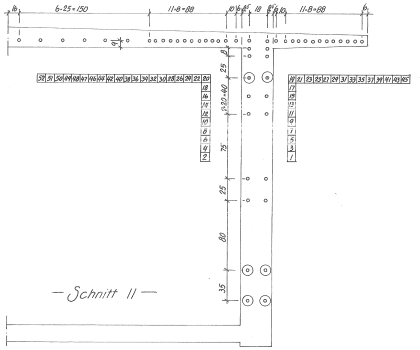

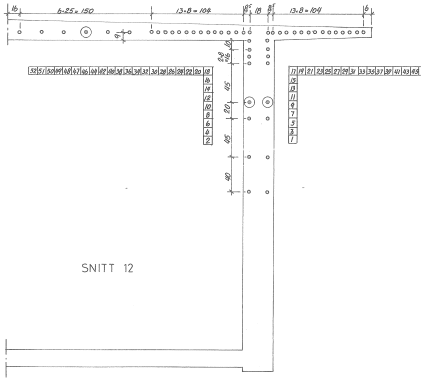

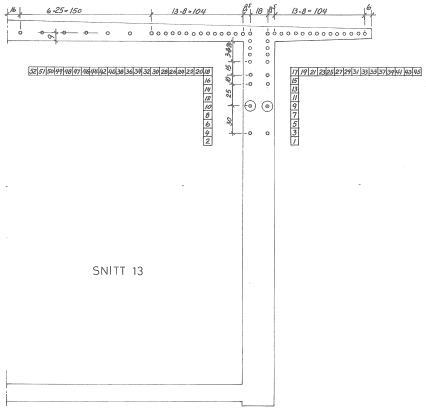

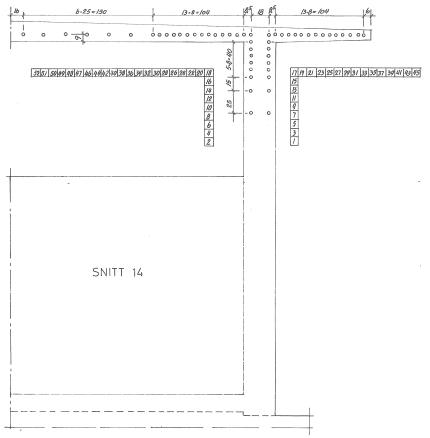

Bewehrung: ϕ 26 Sigma St. 80/105

⊙ Endverankerung

⊙ Zwischenverankerung

— Tromsöbrua —	Målestokk 1/20	Tegnet 21/11-58 LA Kontr.
Vorspannbewehrung Hauptfeld		Forandret ϕ 26/3-59 LA ϕ 20/3-59 LA
— Querschnitte 9-14 —	Mål i cm eg m	a b
DR. ING. A. AAS-JAKOBSEN, OSLO FABRIKKER OG — SENTRALBORD 36 40 80		332.116 b

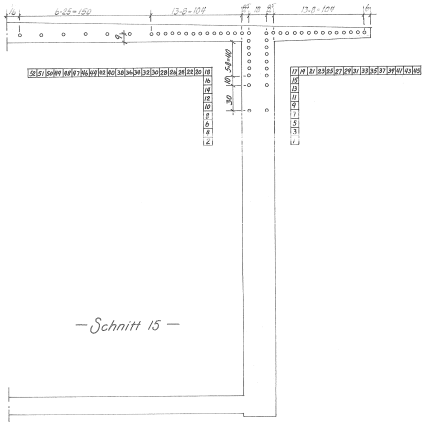

— Schnitt 15 —

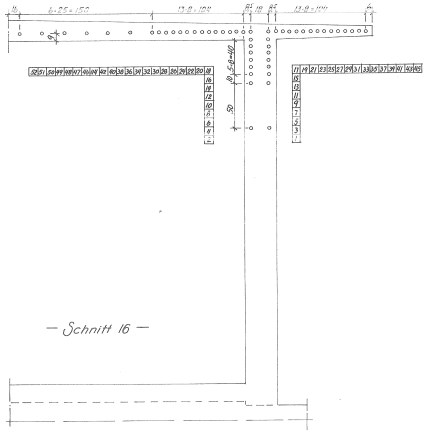

— Schnitt 16 —

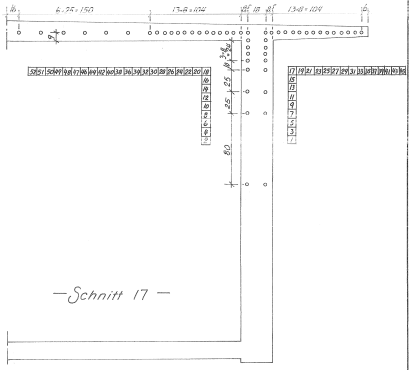

— Schnitt 17 —

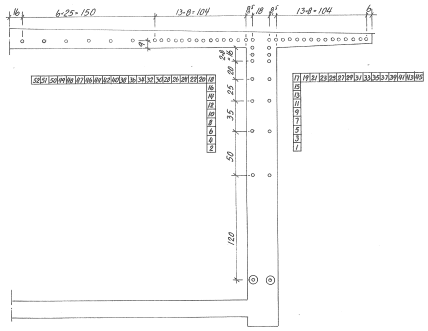

— Schnitt 18 —

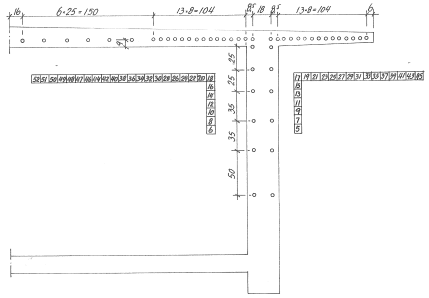

— Schnitt 19 —

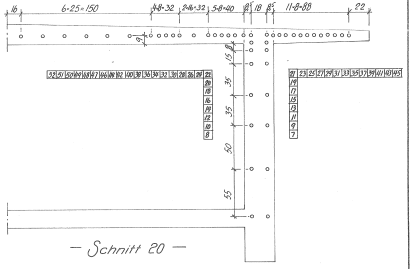

— Schnitt 20 —

◎ Endverankrung

Bewehrung 426 Sigma St 80/105

— Tromsöbrua —	Målestokk 1/20	Tegnet 23-59 LA	
Vorspannbewehrung Nebenfelder		Kontr.	
— Querschnitte 15-20 —		Forandret 20/3-59 LA 16-9-59 LA	
	Mål i cm og m	a	
DR. ING. A. AAS-JAKOBSEN, OSLO PARKVEIEN 37 — SENTRALBORD 55 45 80		b	332.124 b

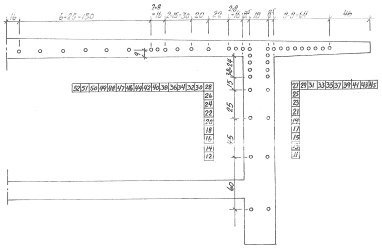

— Schnitt 21 —

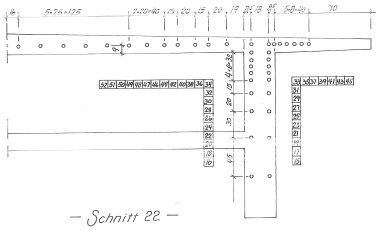

— Schnitt 22 —

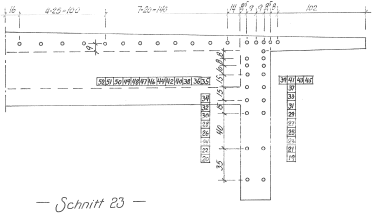

— Schnitt 23 —

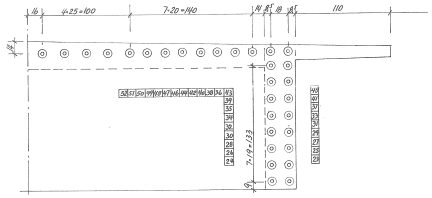

— Schnitt 24 —

⊙ Endverankerung

Bewehrung – ϕ 26 Sigma St. 80/105

— Tromsøbrua —	Målestokk	Tegnet 23-59 LA.
Vorspannbewehrung Nebenfelder	1/100	Kontr.
— Querschnitte 21-24 —	Mål i cm og m	Forandret a 20/3-59 LA a 26-59 LA c b
DR. ING. A. AAS-JAKOBSEN, OSLO PARKVEIEN 57 — SENTRALBORD 56 45 00		332.125 b

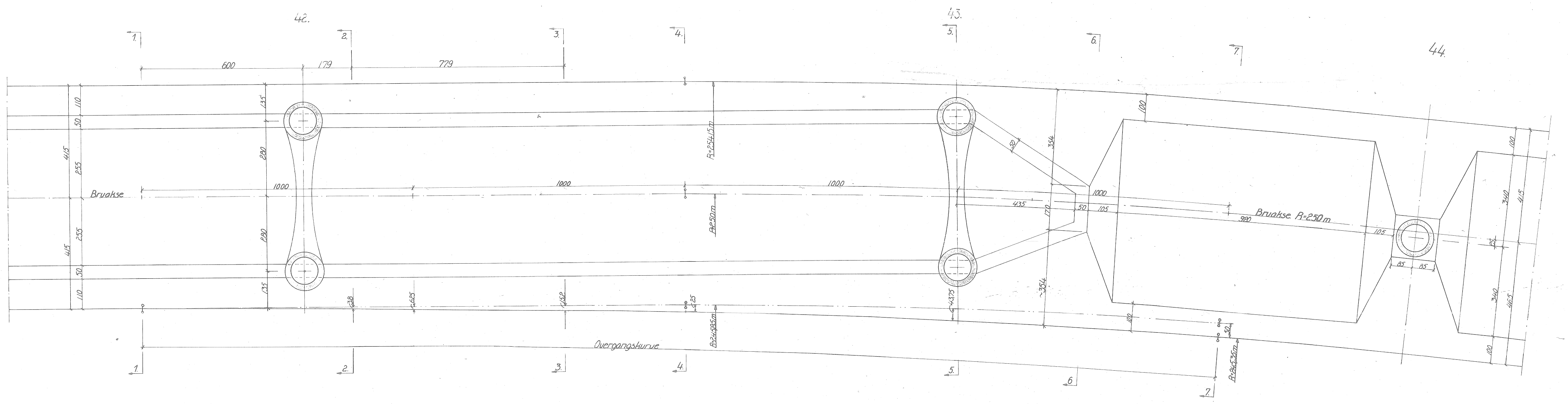

A-betong med min. 375 kg sement pr. m³

Fikssumkontrakt

—Tromsöbrua—	Målestokk 1/50	9/1-58 IB
Plan av feltene 42-43-44		9/1-58 IB
DR. ING. A. AAS-JAKOBSEN, OSLO		332·76a

B Column reinforcement

Column reinforcement

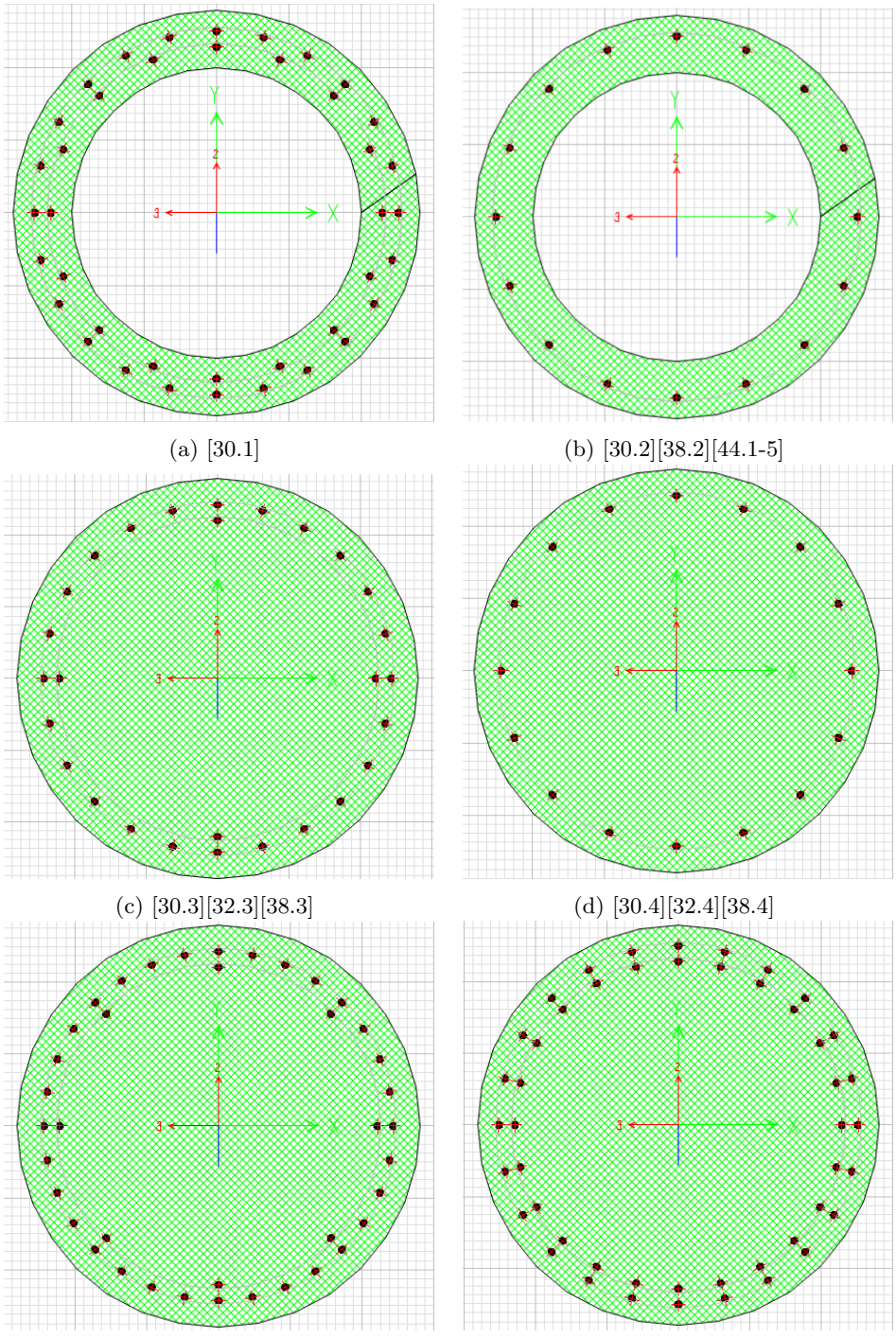

(a) [30.1]

(b) [30.2][38.2][44.1-5]

(c) [30.3][32.3][38.3]

(d) [30.4][32.4][38.4]

(e) [30.5][32.5][38.5]

(f) [32.1]

Figure B.1: Cross-sections columns 30,32,38,44

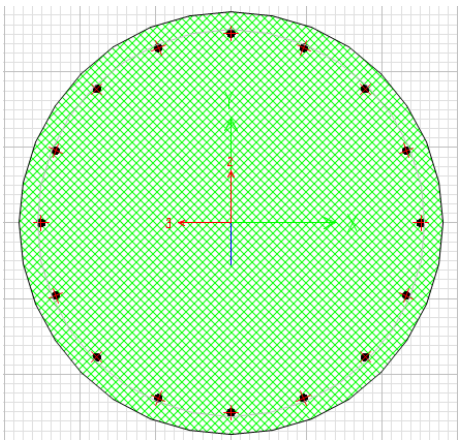

(a) [32.2]

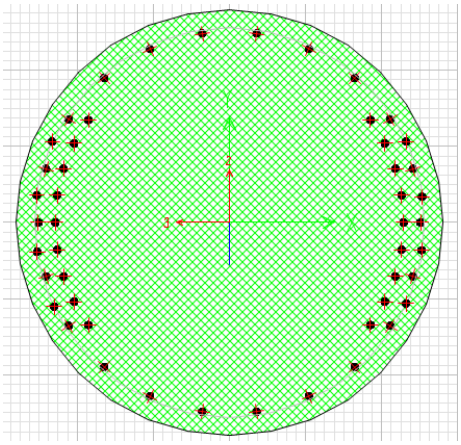

(b) [34.1]

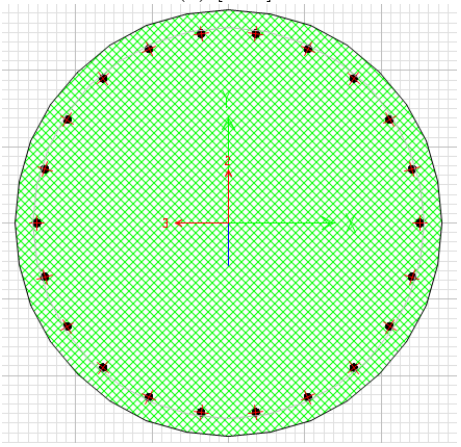

(c) [34.2]

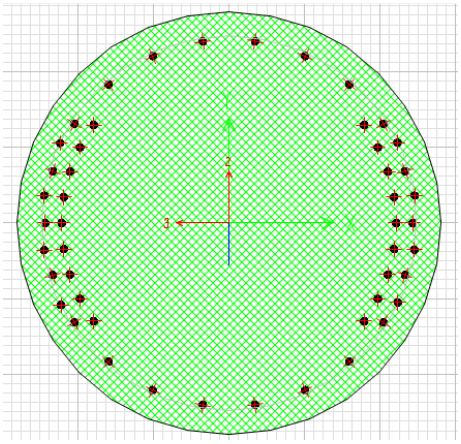

(d) [34.3][34.5]

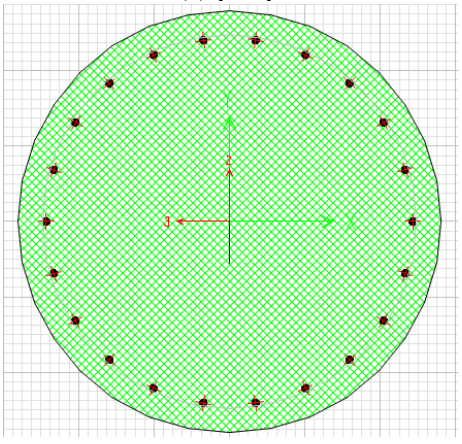

(e) [34.4]

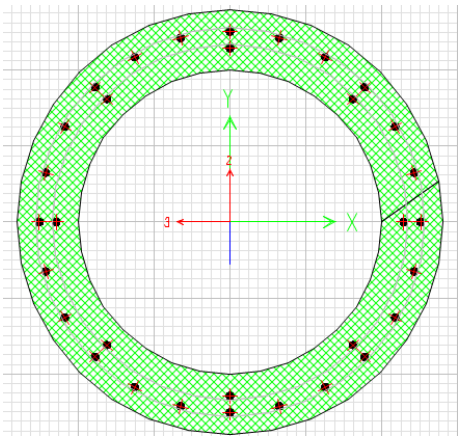

(f) [38.1]

Figure B.2: Cross-sections columns 32,34,38

C Loads

- C1 - Wind load calculations
- C2 - Shrinkage calculations
- C3 - Creep calculations

C1 Wind load calculation

All calculations are based on Eurocode 1-4 and Handbook N400 - Bruprosjektering

C1.1 Basis for calculations

C1.1.1 Z-values

$h_{forskjell} := 1.7\ m$

$h_{forskjell.E} := 0.93\ m$

$h_{bd.FFB} := \frac{41.5\ m + 38.9\ m}{2} = 40.2\ m$

$h_{col.FFB} := \left(38.9\ m - h_{forskjell}\right) = 37.2\ m$

$h_{bd.D.Be} := \frac{38.9\ m + 31.1\ m}{2} = 35\ m$

$h_{col.D.Be} := \left(37.6\ m - h_{forskjell}\right) = 35.9\ m$

$h_{bd.E.Bw} := \frac{31.1\ m + 22.22\ m}{2} = 26.66\ m$

$h_{col.E.Bw} := \left(30.18\ m - h_{forskjell.E}\right) = 29.25\ m$

$z_b := h_{bd.D.Be} = 35\ m$

$z_{b.c} := h_{col.D.Be} = 35.9\ m$

$z_{ffb} := h_{bd.FFB} = 40.2\ m$

$z_{ffb.c} := h_{col.FFB} = 37.2\ m$

$z_e := h_{bd.E.Bw} = 26.66\ m$

$z_{e.c} := h_{col.E.Bw} = 29.25\ m$

C1.1.2 Roughness factor

$C_{r.b} := 0.17 \cdot \ln\left(\frac{z_b}{0.01\ m}\right) = 1.387$

$C_{r.b.c} := 0.17 \cdot \ln\left(\frac{z_{b.c}}{0.01\ m}\right) = 1.392$

$C_{r.ffb} := 0.17 \cdot \ln\left(\frac{z_{ffb}}{0.01\ m}\right) = 1.411$

$C_{r.ffb.c} := 0.17 \cdot \ln\left(\frac{z_{ffb.c}}{0.01\ m}\right) = 1.398$

$C_{r.e} := 0.17 \cdot \ln\left(\frac{z_e}{0.01\ m}\right) = 1.341$

$C_{r.e.c} := 0.17 \cdot \ln\left(\frac{z_{e.c}}{0.01\ m}\right) = 1.357$

C1.1.3 Mean wind velocity

$v_{m.b} := \left(C_{r.b} \cdot 27\right) = 37.457$

$v_{m.b.c} := \left(C_{r.b.c} \cdot 27\right) = 37.573$

$v_{m.ffb} := \left(C_{r.ffb} \cdot 27\right) = 38.093$

$v_{m.ffb.c} := \left(C_{r.ffb.c} \cdot 27\right) = 37.737$

$v_{m.e} := \left(C_{r.e} \cdot 27\right) = 36.207$

$v_{m.e.c} := \left(C_{r.e.c} \cdot 27\right) = 36.633$

C1.1.4 Turbulence intensity

$$I_{v.b} := \frac{1}{1 \cdot \ln\left(\frac{z_b}{0.01\ m}\right)} = 0.123$$

$$I_{v.b.c} := \frac{1}{1 \cdot \ln\left(\frac{z_{b.c}}{0.01\ m}\right)} = 0.122$$

$$I_{v.ffb} := \frac{1}{1 \cdot \ln\left(\frac{z_{ffb}}{0.01\ m}\right)} = 0.12$$

$$I_{v.ffb.c} := \frac{1}{1 \cdot \ln\left(\frac{z_{ffb.c}}{0.01\ m}\right)} = 0.122$$

$$I_{v.e} := \frac{1}{1 \cdot \ln\left(\frac{z_e}{0.01\ m}\right)} = 0.127$$

$$I_{v.e.c} := \frac{1}{1 \cdot \ln\left(\frac{z_{e.c}}{0.01\ m}\right)} = 0.125$$

C1.1.5 Wind gust velocity

$$v_{p.b} := \left(1 + 2 \cdot 3.5 \cdot I_{v.b}\right)^{0.5} \cdot v_{m.b} = 51.054$$

$$v_{p.b.c} := \left(1 + 2 \cdot 3.5 \cdot I_{v.b.c}\right)^{0.5} \cdot v_{m.b.c} = 51.176$$

$$v_{p.ffb} := \left(1 + 2 \cdot 3.5 \cdot I_{v.ffb}\right)^{0.5} \cdot v_{m.ffb} = 51.72$$

$$v_{p.ffb.c} := \left(1 + 2 \cdot 3.5 \cdot I_{v.ffb.c}\right)^{0.5} \cdot v_{m.ffb.c} = 51.347$$

$$v_{p.e} := \left(1 + 2 \cdot 3.5 \cdot I_{v.e}\right)^{0.5} \cdot v_{m.e} = 49.743$$

$$v_{p.e.c} := \left(1 + 2 \cdot 3.5 \cdot I_{v.e.c}\right)^{0.5} \cdot v_{m.e.c} = 50.19$$

C1.1.6 Peak velocity pressure

$$q_{p.b} := 0.5 \cdot 1.25 \cdot {v_{p.b}}^2 \cdot \frac{N}{m^2} = 1.629\ \frac{kN}{m^2}$$

$$q_{p.b.c} := 0.5 \cdot 1.25 \cdot {v_{p.b.c}}^2 \cdot \frac{N}{m^2} = \left(1.637 \cdot 10^3\right)\ Pa$$

$$q_{p.ffb} := 0.5 \cdot 1.25 \cdot {v_{p.ffb}}^2 \cdot \frac{N}{m^2} = \left(1.672 \cdot 10^3\right)\ Pa$$

$$q_{p.ffb.c} := 0.5 \cdot 1.25 \cdot {v_{p.ffb.c}}^2 \cdot \frac{N}{m^2} = \left(1.648 \cdot 10^3\right)\ Pa$$

$$q_{p.e} := 0.5 \cdot 1.25 \cdot {v_{p.e}}^2 \cdot \frac{N}{m^2} = \left(1.546 \cdot 10^3\right)\ Pa$$

$$q_{p.e.c} := 0.5 \cdot 1.25 \cdot {v_{p.e.c}}^2 \cdot \frac{N}{m^2} = \left(1.574 \cdot 10^3\right)\ Pa$$

C1.1.7 Peak velocity pressure with traffic load

$$q'_p := 0.5 \cdot 1.25 \cdot 35^2\ \frac{N}{m^2} = 765.625\ Pa$$

C1.2 Loads on bridge deck

C1.2.1 Values for width and depth of bridge deck

As per table 8.1 in EC1-4, d is increased with 1.2 m with open parapets and safetybarriers on each side

$d_{b.ut} := 1.5\ \boldsymbol{m} + 0.23\ \boldsymbol{m} + 1.2\ \boldsymbol{m} = 2.93\ \boldsymbol{m}$

$a := \left(\frac{1.73 + 4.19}{2} \cdot \frac{2.4}{6.8} + \frac{4.41 + 4.19}{2} \cdot \frac{0.4}{6.8} + \frac{4.41 + 1.75}{2} \cdot \frac{4}{6.8}\right) \cdot \boldsymbol{m} = 3.109\ \boldsymbol{m}$ Middelhøyde ffb-del

$d_{ffb.ut} := a + 1.2\ \boldsymbol{m} = 4.31\ \boldsymbol{m}$

$d_{e.ut} := 0.93\ \boldsymbol{m} + 1.2\ \boldsymbol{m} = 2.13\ \boldsymbol{m}$

$b := 1.8\ \boldsymbol{m} \cdot 2 + 6.5\ \boldsymbol{m} = 10.1\ \boldsymbol{m}$

$d_{b.mt} := 1.73\ \boldsymbol{m} + 2\ \boldsymbol{m} = 3.73\ \boldsymbol{m}$

$d_{ffb.mt} := 3.1\ \boldsymbol{m} + 2\ \boldsymbol{m} = 5.1\ \boldsymbol{m}$

$d_{e.mt} := 0.93\ \boldsymbol{m} + 2\ \boldsymbol{m} = 2.93\ \boldsymbol{m}$

C1.2.2 Loads without traffic

$\frac{b}{d_{b.ut}} = 3.447$ $\frac{b}{d_{ffb.ut}} = 2.344$ $\frac{b}{d_{e.ut}} = 4.742$

$y(x) := -0.3\ x + 2.5$

$c_{fx.tr.bjelke} := y\left(\frac{b}{d_{b.ut}}\right) = 1.466$ $c_{fx.tr.plate} := y\left(\frac{b}{d_{e.ut}}\right) = 1.077$ $c_{fz} := 0.9$

$c_{fx.tr.ffb} := y\left(\frac{b}{d_{ffb.ut}}\right) = 1.797$ EC1-4 NA.8.3.3

EC1-4 figure 8.3

$q_b := \left(27 \cdot \frac{\boldsymbol{m}}{\boldsymbol{s}}\right)^2 \cdot 1.25 \cdot \frac{\boldsymbol{kg}}{\boldsymbol{m}^3} \cdot 0.5 = 455.625\ \frac{\boldsymbol{N}}{\boldsymbol{m}^2}$

$c_{e.b} := \frac{q_{p.b}}{q_b} = 3.575$ $c_{e.ffb} := \frac{q_{p.ffb}}{q_b} = 3.669$ $c_{e.e} := \frac{q_{p.e}}{q_b} = 3.394$

$\rho := 1.25 \cdot \frac{\boldsymbol{kg}}{\boldsymbol{m}^3}$

Horisontal load in transversal direction

$$f_{wt.B.wesr} := c_{fx.tr.bjelke} \cdot d_{b.ut} \cdot q_{p.e} = 6.642 \ \frac{kN}{m}$$

$$f_{wt.B.east.D} := c_{fx.tr.bjelke} \cdot d_{b.ut} \cdot q_{p.b} = 6.997 \ \frac{kN}{m}$$

$$f_{wt.ffb} := c_{fx.tr.ffb} \cdot d_{ffb.ut} \cdot q_{p.ffb} = 12.946 \ \frac{kN}{m}$$

$$f_{wt.E} := c_{fx.tr.plate} \cdot d_{e.ut} \cdot q_{p.e} = 3.549 \ \frac{kN}{m}$$

Vertical load

$$f_{wz.B.west} := b \cdot c_{fz} \cdot q_{p.e} = 14.057 \ \frac{kN}{m}$$

$$f_{wz.B.east.D} := c_{fz} \cdot b \cdot q_{p.b} = 14.808 \ \frac{kN}{m}$$

$$f_{wz.ffb} := c_{fz} \cdot b \cdot q_{p.ffb} = 15.197 \ \frac{kN}{m}$$

$$f_{wz.e} := c_{fz} \cdot b \cdot q_{p.e} = 14.057 \ \frac{kN}{m}$$

Horizontal load in longitudinal direction

$$f_{wl.B.west} := c_{fx.tr.bjelke} \cdot d_{b.ut} \cdot q_{p.e} \cdot 0.25 = 1.661 \ \frac{kN}{m}$$

$$f_{wl.B.east.D} := c_{fx.tr.bjelke} \cdot d_{b.ut} \cdot q_{p.b} \cdot 0.25 = 1.749 \ \frac{kN}{m}$$

$$f_{wl.ffb} := c_{fx.tr.ffb} \cdot d_{ffb.ut} \cdot q_{p.ffb} \cdot 0.25 = 3.237 \ \frac{kN}{m}$$

$$f_{wl.E} := c_{fx.tr.plate} \cdot d_{e.ut} \cdot q_{p.e} \cdot 0.25 = 0.887 \ \frac{kN}{m}$$

Moment in bridge deck

$$M_{B.west} := f_{wz.B.west} \cdot \frac{b}{4} = 35.495 \ \frac{kN \cdot m}{m}$$

$$M_{B.east.D} := f_{wz.B.east.D} \cdot \frac{b}{4} = 37.391 \ \frac{kN \cdot m}{m}$$

$$M_{ffb} := f_{wz.ffb} \cdot \frac{b}{4} = 38.373 \ \frac{kN \cdot m}{m}$$

$$M_{E} := f_{wz.e} \cdot \frac{b}{4} = 35.495 \ \frac{kN \cdot m}{m}$$

C1.2.3 Loads with traffic

$\frac{b}{d_{b.mt}} = 2.708$ $\frac{b}{d_{ffb.mt}} = 1.98$ $\frac{b}{d_{e.mt}} = 3.447$

$c_{fx.b} := y\left(\frac{b}{d_{b.mt}}\right) = 1.688$ $c_{fx.e} := y\left(\frac{b}{d_{e.mt}}\right) = 1.466$ $c_{fz} := 0.9$ EC1-4 NA.8.3.3

EC1-4 Figure 8.3

$c_{fx.ffb} := y\left(\frac{b}{d_{ffb.mt}}\right) = 1.906$ $c_{e.wotr} := \frac{q'_p}{q_b} = 1.68$

Horizontal load in transversal direction

$f_{wot.B.west} := c_{fx.b} \cdot d_{b.mt} \cdot q'_p = 4.82 \ \frac{kN}{m}$

$f_{wot.B.east.D} := c_{fx.b} \cdot d_{b.mt} \cdot q'_p = 4.82 \ \frac{kN}{m}$

$f_{wot.ffb} := c_{fx.ffb} \cdot d_{ffb.mt} \cdot q'_p = 7.442 \ \frac{kN}{m}$

$f_{wot.e} := c_{fx.e} \cdot d_{e.mt} \cdot q'_p = 3.288 \ \frac{kN}{m}$

Vertical load

$f_{woz.B.west} := c_{fz} \cdot b \cdot q'_p = 6.96 \ \frac{kN}{m}$

$f_{woz.B.east.D} := c_{fz} \cdot b \cdot q'_p = 6.96 \ \frac{kN}{m}$

$f_{woz.ffb} := c_{fz} \cdot b \cdot q'_p = 6.96 \ \frac{kN}{m}$

$f_{woz.e} := c_{fz} \cdot b \cdot q'_p = 6.96 \ \frac{kN}{m}$

Horizontal load in longitudinal direction

$f_{wot.p.B.east} := c_{fx.b} \cdot d_{b.mt} \cdot q'_p \cdot \frac{0.25}{b} = 0.119 \ \frac{1}{m} \cdot \frac{kN}{m}$

$f_{wot.p.B.west.D} := c_{fx.b} \cdot d_{b.mt} \cdot q'_p \cdot \frac{0.25}{b} = 0.119 \ \frac{1}{m} \cdot \frac{kN}{m}$

$f_{wot.p.ffb} := c_{fx.ffb} \cdot d_{ffb.mt} \cdot q'_p \cdot \frac{0.25}{b} = 0.184 \ \frac{1}{m} \cdot \frac{kN}{m}$

$f_{wot.p.e} := c_{fx.e} \cdot d_{e.mt} \cdot q'_p \cdot \frac{0.25}{b} = 0.081 \ \frac{1}{m} \cdot \frac{kN}{m}$

Moment in bridge deck

$M_{with.tr} := f_{woz.B.west} \cdot \frac{b}{4} = 17.573 \ \frac{kN \cdot m}{m}$

C1.3 Loads on columns

C1.3.1 Basis for calculations

$b_s := 1.4\ \boldsymbol{m}$ $c_s c_d := 1$ 8.2 NOTE 2

Table 7.16 - Slenderness - linear interpolation

$\lambda_{15} := \max\left(\frac{15}{1.4}, 70\right) = 70$ $\lambda_{50} := \max\left(0.7 \cdot \frac{50}{1.4}, 70\right) = 70$ $\lambda := 70$

$\varphi := 1$ (7.28) $\psi_\lambda := 0.925$ Figure 7.36

$D := 1.4 \cdot \frac{\boldsymbol{m}^2}{\boldsymbol{m}}$ $v_{luft} := 15 \cdot 10^{\langle -6 \rangle} \cdot \frac{\boldsymbol{m}^2}{\boldsymbol{s}}$

$v_{m.b} := v_{m.b.c} \cdot \frac{\boldsymbol{m}}{\boldsymbol{s}} = 37.573\ \frac{\boldsymbol{m}}{\boldsymbol{s}}$ $v_{m.ffb} := v_{m.ffb.c} \cdot \frac{\boldsymbol{m}}{\boldsymbol{s}} = 37.737\ \frac{\boldsymbol{m}}{\boldsymbol{s}}$ $v_{m.e} := v_{m.e.c} \cdot \frac{\boldsymbol{m}}{\boldsymbol{s}} = 36.633\ \frac{\boldsymbol{m}}{\boldsymbol{s}}$

$q_{p.b.c} = \langle 1.637 \cdot 10^3 \rangle\ \boldsymbol{Pa}$ $q_{p.ffb.c} = \langle 1.648 \cdot 10^3 \rangle\ \boldsymbol{Pa}$ $q_{p.e.c} = \langle 1.574 \cdot 10^3 \rangle\ \boldsymbol{Pa}$

C1.3.2 Reynolds number for circular cylinders.

$Re_b := \frac{D \cdot v_{m.b}}{v_{luft}} = 3.507 \cdot 10^6$ $Re_{ffb} := \frac{D \cdot v_{m.ffb}}{v_{luft}} = 3.522 \cdot 10^6$ $Re_e := \frac{D \cdot v_{m.e}}{v_{luft}} = 3.419 \cdot 10^6$

$k_{ru} := 1\ \boldsymbol{mm}$ Equivavelent roughness for rough concrete

$\frac{k_{ru}}{D} = 7.143 \cdot 10^{-4}$

C1.3.3 Cicular cylinders on a row

$$c_{f.s.0.b} := 1.2 + \frac{0.18 \cdot \log\left(10 \cdot \frac{k_{ru}}{D}\right)}{1 + 0.4 \cdot \log\left(\frac{Re_b}{10^6}\right)} = 0.88283$$

$$c_{f.s.0.ffb} := 1.2 + \frac{0.18 \cdot \log\left(10 \cdot \frac{k_{ru}}{D}\right)}{1 + 0.4 \cdot \log\left(\frac{Re_{ffb}}{10^6}\right)} = 0.883026$$

$$c_{f.s.0.e} := 1.2 + \frac{0.18 \cdot \log\left(10 \cdot \frac{k_{ru}}{D}\right)}{1 + 0.4 \cdot \log\left(\frac{Re_e}{10^6}\right)} = 0.881679$$

$d := 1.4\ \boldsymbol{m}$

Tabell 7.14: *Faktor for vertikale sylindere ordnet i rekke:*

Tabell 7.14 – Faktor *k* for vertikale sylindere ordnet i rekke

a/b	κ
$a/b < 3{,}5$	1,15
$3{,}5 < a/b < 30$	$\kappa = \frac{210 - \frac{a}{b}}{180}$
$a/b > 30$	1,00

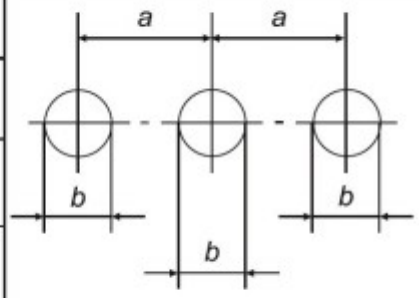

a: avstand
b: diameter

$a_{spenn} := 24\ \boldsymbol{m}$ $a_{33.34} := 4\ \boldsymbol{m}$ $a_{tvers} := 5.6\ \boldsymbol{m}$ $a_{hovedspenn} := 60\ \boldsymbol{m}$

$\frac{a_{spenn}}{d} = 17.143$ $\frac{a_{33.34}}{d} = 2.857$ $\frac{a_{tvers}}{d} = 4$ $\frac{a_{hovedspenn}}{d} = 42.857$

$$\kappa_{spenn} := \frac{210 - \frac{a_{spenn}}{d}}{180} = 1.071$$

$\kappa_{33.34} := 1.15$ $\kappa_{hovedspenn} := 1$

$$\kappa_{tvers} := \frac{210 - \frac{a_{tvers}}{d}}{180} = 1.144$$

C1.3.4 Loads without traffic

$c_{f.c.b.west.paralell} := c_{f.s.0.e} \cdot \psi_{\lambda} \cdot \kappa_{tvers} = 0.933$

$c_{f.c.b.west.tvers} := c_{f.s.0.e} \cdot \psi_{\lambda} \cdot \kappa_{spenn} = 0.874$

B-west

$c_{f.c.b.d.paralell} := c_{f.s.0.b} \cdot \psi_{\lambda} \cdot \kappa_{tvers} = 0.935$

$c_{f.c.b.d.tvers} := c_{f.s.0.b} \cdot \psi_{\lambda} \cdot \kappa_{spenn} = 0.875$

B-east, D and axis 32/37

$c_{f.c.ffb.paralell} := c_{f.s.0.ffb} \cdot \psi_{\lambda} \cdot \kappa_{tvers} = 0.935$

$c_{f.c.ffb.tvers} := c_{f.s.0.ffb} \cdot \psi_{\lambda} \cdot \kappa_{spenn} = 0.875$

$c_{f.c.ffb.tvers.33.34} := c_{f.s.0.ffb} \cdot \psi_{\lambda} \cdot \kappa_{33.34} = 0.939$

C - FFB axis 33 - 36

$c_{f.c.e.paralell} := c_{f.s.0.e} \cdot \psi_{\lambda} = 0.816$

$c_{f.c.e.tvers} := c_{f.s.0.e} \cdot \psi_{\lambda} = 0.816$

E - in a curve and therefore not in a row

$f_{c.b.west.paralell} := c_s c_d \cdot c_{f.c.b.west.paralell} \cdot q_{p.e} \cdot d = 2.021 \ \frac{kN}{m}$

$f_{c.b.west.tvers} := c_s c_d \cdot c_{f.c.b.west.tvers} \cdot q_{p.e} \cdot d = 1.892 \ \frac{kN}{m}$

Sections B-west and E

$f_{c.b.paralell} := c_s c_d \cdot c_{f.c.b.d.paralell} \cdot q_{p.b} \cdot d = 2.131 \ \frac{kN}{m}$

$f_{c.b.tvers} := c_s c_d \cdot c_{f.c.b.d.tvers} \cdot q_{p.b} \cdot d = 1.995 \ \frac{kN}{m}$

Sections B-east, D and 32/37

$f_{c.ffb.paralell} := c_s c_d \cdot c_{f.c.ffb.paralell} \cdot q_{p.b} \cdot d = 2.132 \ \frac{kN}{m}$

$f_{c.ffb.tvers} := c_s c_d \cdot c_{f.c.ffb.tvers} \cdot q_{p.b} \cdot d = 1.996 \ \frac{kN}{m}$

$f_{c.ffb.tvers.33.34} := c_s c_d \cdot c_{f.c.ffb.tvers.33.34} \cdot q_{p.b} \cdot d = 2.142 \ \frac{kN}{m}$

Columns 33-36

$f_{c.e.paralell} := c_s c_d \cdot c_{f.c.e.paralell} \cdot q_{p.b} \cdot d = 1.86 \ \frac{kN}{m}$

$f_{c.e.tvers} := c_s c_d \cdot c_{f.c.e.tvers} \cdot q_{p.b} \cdot d = 1.86 \ \frac{kN}{m}$

Section E

C1.3.5 Loads with traffic

$f_{c.tra.b.west.paralell} := c_s c_d \cdot c_{f.c.b.west.paralell} \cdot q'_p \cdot d = 1.0004 \ \frac{kN}{m}$

$f_{c.tra.b.west.tvers} := c_s c_d \cdot c_{f.c.b.west.tvers} \cdot q'_p \cdot d = 0.937 \ \frac{kN}{m}$

Sections B-west and E

$f_{c.tra.b.paralell} := c_s c_d \cdot c_{f.c.b.d.paralell} \cdot q'_p \cdot d = 1.002 \ \frac{kN}{m}$

$f_{c.tra.b.tvers} := c_s c_d \cdot c_{f.c.b.d.tvers} \cdot q'_p \cdot d = 0.938 \ \frac{kN}{m}$

Sections B-east, D and 32/37

$f_{c.tra.ffb.paralell} := c_s c_d \cdot c_{f.c.ffb.paralell} \cdot q'_p \cdot d = 1.002 \ \frac{kN}{m}$

$f_{c.tra.ffb.tvers} := c_s c_d \cdot c_{f.c.ffb.tvers} \cdot q'_p \cdot d = 0.938 \ \frac{kN}{m}$

$f_{c.tra.ffb.tvers.33.34} := c_s c_d \cdot c_{f.c.ffb.tvers.33.34} \cdot q'_p \cdot d = 1.007 \ \frac{kN}{m}$

Columns 33-36

$f_{c.tra.e.paralell} := c_s c_d \cdot c_{f.c.e.paralell} \cdot q'_p \cdot d = 0.874 \ \frac{kN}{m}$

$f_{c.tra.e.tvers} := c_s c_d \cdot c_{f.c.e.tvers} \cdot q'_p \cdot d = 0.874 \ \frac{kN}{m}$

Section E

C2 Shrinkage calculations

All calculations are based on EC1-4 B.1 and EC1-4 3.1.4

C2.1 Calculation of shrinkage - Section C

$A_c := 3.890 \cdot 10^6 \ \boldsymbol{mm}^2$ Area

$b := 8300 \ \boldsymbol{mm}$ Width of top plate

$b_f := 1100 \ \boldsymbol{mm}$ Width of cantilever plate on top

$t_t := 230 \ \boldsymbol{mm}$ Thickness of top plate

$t_b := 200 \ \boldsymbol{mm}$ Thickness of bottom plate

$h := 2390 \ \boldsymbol{mm}$ Height of cross section

$a := 2 \cdot 2700 \ \boldsymbol{mm}$ Distance between web

$b_b := 6100 \ \boldsymbol{mm}$ Width plate bottom

$U := b + 2 \cdot b_f + 2 \cdot t_t + 2 \cdot a + 2 \cdot \left(h - t_t - t_b\right) + b_b = 31780 \ \boldsymbol{mm}$

$RH := 80$

$\alpha_{ds1} := 4$ $\alpha_{ds2} := 0.12$ Cement class N

$f_{ck.ffb} := 32 \ \boldsymbol{MPa}$ $f_{cm.ffb} := f_{ck.ffb} + 8 \ \boldsymbol{MPa} = 40 \ \boldsymbol{MPa}$ $f_{cmo} := 10 \ \boldsymbol{MPa}$

$\beta_{RH} := 1.55 \cdot \left(1 - \left(\frac{RH}{100}\right)^3\right) = 0.756$

$\varepsilon_{cd.0} := 0.85 \cdot \left(\left(220 + 110 \cdot \alpha_{ds1}\right) \cdot e^{\left(-\alpha_{ds2} \cdot \frac{f_{cm.ffb}}{f_{cmo}}\right)}\right) \cdot 10^{-6} \cdot \beta_{RH} = 2.626 \cdot 10^{-4}$

$h_0 := 2 \cdot \frac{A_c}{U} = 244.808 \ \boldsymbol{mm}$

$k_h := 0.80$ $t := 365 \cdot 63 = 2.3 \cdot 10^4$ $t_s := 4$

$$\beta_{ds} := \frac{\left(t - t_s\right)}{\left(t - t_s\right) + 0.04 \cdot \sqrt{\left(\frac{h_0}{mm}\right)^3}} = 0.993$$

$$\varepsilon_{cd} := \beta_{ds} \cdot k_h \cdot \varepsilon_{cd.0} = 2.087 \cdot 10^{-4}$$

$$\beta_{as} := 1 - e^{\left(-0.2 \cdot t^{0.5}\right)} = 1$$

$$\varepsilon_{ca.inf} := 2.5 \cdot \left(\frac{f_{ck.ffb}}{MPa} - 10\right) \cdot 10^{-6} = 5.5 \cdot 10^{-5}$$

$$\varepsilon_{ca} := \beta_{as} \cdot \varepsilon_{ca.inf} = 5.5 \cdot 10^{-5}$$

$$\varepsilon_{cs} := \left(\varepsilon_{ca} + \varepsilon_{cd}\right) \cdot 1000 = 0.264$$ Final shrinkage

C2.2 Calculation of shrinkage - Section B and D

$A_c := 3043800\ mm^2$ Area

$b := 8300\ mm$ Width of top plate

$h_b := 1500\ mm$ Height of beam

$t_s := 186\ mm$ Thickness of deck

$t_b := 500\ mm$ Thickness of beam

$a := 5100\ mm$ Arm between beams inside

$b_f := \frac{b - a - 2 \cdot t_b}{2} = 1100\ mm$ Width of flange outside beam

$U := b + 2 \cdot t_s + 2 \cdot b_f + 2 \cdot h_b + 2 \cdot t_b + 2 \cdot h_b + a = 22972\ mm$

$RH := 80$

$\alpha_{ds1} := 4$ $\alpha_{ds2} := 0.12$ Cement class N

$f_{ck.ffb} := 20\ MPa$ $f_{cm.ffb} := f_{ck.ffb} + 8\ MPa = 28\ MPa$ $f_{cmo} := 10\ MPa$

$\beta_{RH} := 1.55 \cdot \left(1 - \left(\frac{RH}{100}\right)^3\right) = 0.756$

$\varepsilon_{cd.0} := 0.85 \cdot \left(\left(220 + 110 \cdot \alpha_{ds1}\right) \cdot e^{\left(-\alpha_{ds2} \cdot \frac{f_{cm.ffb}}{f_{cmo}}\right)}\right) \cdot 10^{-6} \cdot \beta_{RH} = 3.032 \cdot 10^{-4}$

$h_0 := 2 \cdot \frac{A_c}{U} = 265.001\ mm$

$k_h := 0.80$ $t := 365 \cdot 63 = 2.3 \cdot 10^4$ $t_s := 4$

$\beta_{ds} := \frac{\left(t - t_s\right)}{\left(t - t_s\right) + 0.04 \cdot \sqrt{\left(\frac{h_0}{mm}\right)^3}} = 0.993$

$\varepsilon_{cd} := \beta_{ds} \cdot k_h \cdot \varepsilon_{cd.0} = 2.408 \cdot 10^{-4}$

$\beta_{as} := 1 - e^{\left(-0.2 \cdot t^{0.5}\right)} = 1$

$\varepsilon_{ca.inf} := 2.5 \cdot \left(\frac{f_{ck.ffb}}{MPa} - 10\right) \cdot 10^{-6} = 2.5 \cdot 10^{-5}$

$\varepsilon_{ca} := \beta_{as} \cdot \varepsilon_{ca.inf} = 2.5 \cdot 10^{-5}$

$\varepsilon_{cs} := \left(\varepsilon_{ca} + \varepsilon_{cd}\right) \cdot 1000 = 0.266$ Final shrinkage

C2.3 Calculation of shrinkage - Section A and E

$A_c := 2788000\ mm^2$ Area

$b := 8300\ mm$ Width of top plate

$t_s := 336\ mm$ Thickness of deck

$U := 2 \cdot b + 2 \cdot t_s = 17272\ mm$

$RH := 80$

$\alpha_{ds1} := 4$ $\alpha_{ds2} := 0.12$ Cement class N

$f_{ck.ffb} := 20\ MPa$ $f_{cm.ffb} := f_{ck.ffb} + 8\ MPa = 28\ MPa$ $f_{cmo} := 10\ MPa$

$\beta_{RH} := 1.55 \cdot \left(1 - \left(\frac{RH}{100}\right)^3\right) = 0.756$

$\varepsilon_{cd.0} := 0.85 \cdot \left(\left(220 + 110 \cdot \alpha_{ds1}\right) \cdot e^{\left(-\alpha_{ds2} \cdot \frac{f_{cm.ffb}}{f_{cmo}}\right)}\right) \cdot 10^{-6} \cdot \beta_{RH} = 3.032 \cdot 10^{-4}$

$h_0 := 2 \cdot \frac{A_c}{U} = 322.835\ mm$

$k_h := 0.74$ $t := 365 \cdot 63 = 2.3 \cdot 10^4$ $t_s := 4$

$\beta_{ds} := \frac{\left(t - t_s\right)}{\left(t - t_s\right) + 0.04 \cdot \sqrt{\left(\frac{h_0}{mm}\right)^3}} = 0.99$

$\varepsilon_{cd} := \beta_{ds} \cdot k_h \cdot \varepsilon_{cd.0} = 2.222 \cdot 10^{-4}$

$\beta_{as} := 1 - e^{\left(-0.2 \cdot t^{0.5}\right)} = 1$

$\varepsilon_{ca.inf} := 2.5 \cdot \left(\frac{f_{ck.ffb}}{MPa} - 10\right) \cdot 10^{-6} = 2.5 \cdot 10^{-5}$

$\varepsilon_{ca} := \beta_{as} \cdot \varepsilon_{ca.inf} = 2.5 \cdot 10^{-5}$

$\varepsilon_{cs} := \left(\varepsilon_{ca} + \varepsilon_{cd}\right) \cdot 1000 = 0.247$ Final shrinkage

C2.4 Calculation of shrinkage - massive columns above water

$A_c := (700\ mm)^2 \cdot \pi = 1539380.4\ mm^2$ Area

$U := 2 \cdot \pi \cdot 700\ (mm) = 4398.23\ mm$

$RH := 80$

$\alpha_{ds1} := 4$ $\alpha_{ds2} := 0.12$ Cement class N

$f_{ck.ffb} := 20\ MPa$ $f_{cm.ffb} := f_{ck.ffb} + 8\ MPa = 28\ MPa$ $f_{cmo} := 10\ MPa$

$\beta_{RH} := 1.55 \cdot \left(1 - \left(\frac{RH}{100}\right)^3\right) = 0.756$

$\varepsilon_{cd.0} := 0.85 \cdot \left((220 + 110 \cdot \alpha_{ds1}) \cdot e^{\left(-\alpha_{ds2} \cdot \frac{f_{cm.ffb}}{f_{cmo}}\right)}\right) \cdot 10^{-6} \cdot \beta_{RH} = 3.032 \cdot 10^{-4}$

$h_0 := 2 \cdot \frac{A_c}{U} = 700\ mm$

$k_h := 0.70$ $t := 365 \cdot 63 = 2.3 \cdot 10^4$ $t_s := 4$

$$\beta_{ds} := \frac{(t - t_s)}{(t - t_s) + 0.04 \cdot \sqrt{\left(\frac{h_0}{mm}\right)^3}} = 0.969$$

$\varepsilon_{cd} := \beta_{ds} \cdot k_h \cdot \varepsilon_{cd.0} = 2.056 \cdot 10^{-4}$

$\beta_{as} := 1 - e^{(-0.2 \cdot t^{0.5})} = 1$

$\varepsilon_{ca.inf} := 2.5 \cdot \left(\frac{f_{ck.ffb}}{MPa} - 10\right) \cdot 10^{-6} = 2.5 \cdot 10^{-5}$

$\varepsilon_{ca} := \beta_{as} \cdot \varepsilon_{ca.inf} = 2.5 \cdot 10^{-5}$

$\varepsilon_{cs} := (\varepsilon_{ca} + \varepsilon_{cd}) \cdot 1000 = 0.231$ Final shrinkage

C2.5 Calculation of shrinkage - hollow columns above water

$A_c := (700\ mm)^2 \cdot \pi = 1539380.4\ mm^2$ Area

$U := 2 \cdot \pi \cdot 700\ mm + 2 \cdot \pi \cdot 500\ mm = 7539.822\ mm$

$RH := 80$

$\alpha_{ds1} := 4$ $\alpha_{ds2} := 0.12$ Cement class N

$f_{ck.ffb} := 20\ MPa$ $f_{cm.ffb} := f_{ck.ffb} + 8\ MPa = 28\ MPa$ $f_{cmo} := 10\ MPa$

$$\beta_{RH} := 1.55 \cdot \left(1 - \left(\frac{RH}{100}\right)^3\right) = 0.756$$

$$\varepsilon_{cd.0} := 0.85 \cdot \left(\left(220 + 110 \cdot \alpha_{ds1}\right) \cdot e^{\left(-\alpha_{ds2} \cdot \frac{f_{cm.ffb}}{f_{cmo}}\right)}\right) \cdot 10^{-6} \cdot \beta_{RH} = 3.032 \cdot 10^{-4}$$

$$h_0 := 2 \cdot \frac{A_c}{U} = 408.333\ mm$$

$k_h := 0.72$ $t := 365 \cdot 63 = 2.3 \cdot 10^4$ $t_s := 4$

$$\beta_{ds} := \frac{\left(t - t_s\right)}{\left(t - t_s\right) + 0.04 \cdot \sqrt{\left(\frac{h_0}{mm}\right)^3}} = 0.986$$

$$\varepsilon_{cd} := \beta_{ds} \cdot k_h \cdot \varepsilon_{cd.0} = 2.152 \cdot 10^{-4}$$

$$\beta_{as} := 1 - e^{\left(-0.2 \cdot t^{0.5}\right)} = 1$$

$$\varepsilon_{ca.inf} := 2.5 \cdot \left(\frac{f_{ck.ffb}}{MPa} - 10\right) \cdot 10^{-6} = 2.5 \cdot 10^{-5}$$

$$\varepsilon_{ca} := \beta_{as} \cdot \varepsilon_{ca.inf} = 2.5 \cdot 10^{-5}$$

$\varepsilon_{cs} := \left(\varepsilon_{ca} + \varepsilon_{cd}\right) \cdot 1000 = 0.24$ Final shrinkage

C2.6 Calculation of shrinkage - massive columns below water

$A_c := (700\ mm)^2 \cdot \pi = 1539380.4\ mm^2$ Area

$U := 2 \cdot \pi \cdot 700\ (mm) = 4398.23\ mm$

$RH := 100$

$\alpha_{ds1} := 4$ $\alpha_{ds2} := 0.12$ Cement class N

$f_{ck.ffb} := 20\ MPa$ $f_{cm.ffb} := f_{ck.ffb} + 8\ MPa = 28\ MPa$ $f_{cmo} := 10\ MPa$

$\beta_{RH} := 1.55 \cdot \left(1 - \left(\frac{RH}{100}\right)^3\right) = 0$

$\varepsilon_{cd.0} := 0.85 \cdot \left((220 + 110 \cdot \alpha_{ds1}) \cdot e^{\left(-\alpha_{ds2} \cdot \frac{f_{cm.ffb}}{f_{cmo}}\right)}\right) \cdot 10^{-6} \cdot \beta_{RH} = 0$

$h_0 := 2 \cdot \frac{A_c}{U} = 700\ mm$

$k_h := 0.70$ $t := 365 \cdot 63 = 2.3 \cdot 10^4$ $t_s := 4$

$\beta_{ds} := \frac{(t - t_s)}{(t - t_s) + 0.04 \cdot \sqrt{\left(\frac{h_0}{mm}\right)^3}} = 0.969$

$\varepsilon_{cd} := \beta_{ds} \cdot k_h \cdot \varepsilon_{cd.0} = 0$

$\beta_{as} := 1 - e^{(-0.2 \cdot t^{0.5})} = 1$

$\varepsilon_{ca.inf} := 2.5 \cdot \left(\frac{f_{ck.ffb}}{MPa} - 10\right) \cdot 10^{-6} = 2.5 \cdot 10^{-5}$

$\varepsilon_{ca} := \beta_{as} \cdot \varepsilon_{ca.inf} = 2.5 \cdot 10^{-5}$

$\varepsilon_{cs} := (\varepsilon_{ca} + \varepsilon_{cd}) \cdot 1000 = 0.025$ Final shrinkage

C2.7 Calculation of shrinkage - Hollow columns below water

$A_c := (700\ mm)^2 \cdot \pi = 1539380.4\ mm^2$ Area

$U := 2 \cdot \pi \cdot 700\ mm + 2 \cdot \pi \cdot 500\ mm = 7539.822\ mm$

$RH := 100$

$\alpha_{ds1} := 4$ $\alpha_{ds2} := 0.12$ Cement class N

$f_{ck.ffb} := 20\ MPa$ $f_{cm.ffb} := f_{ck.ffb} + 8\ MPa = 28\ MPa$ $f_{cmo} := 10\ MPa$

$\beta_{RH} := 1.55 \cdot \left(1 - \left(\frac{RH}{100}\right)^3\right) = 0$

$\varepsilon_{cd.0} := 0.85 \cdot \left(\left(220 + 110 \cdot \alpha_{ds1}\right) \cdot e^{\left(-\alpha_{ds2} \cdot \frac{f_{cm.ffb}}{f_{cmo}}\right)}\right) \cdot 10^{-6} \cdot \beta_{RH} = 0$

$h_0 := 2 \cdot \frac{A_c}{U} = 408.333\ mm$

$k_h := 0.72$ $t := 365 \cdot 63 = 2.3 \cdot 10^4$ $t_s := 4$

$$\beta_{ds} := \frac{\left(t - t_s\right)}{\left(t - t_s\right) + 0.04 \cdot \sqrt{\left(\frac{h_0}{mm}\right)^3}} = 0.986$$

$\varepsilon_{cd} := \beta_{ds} \cdot k_h \cdot \varepsilon_{cd.0} = 0$

$\beta_{as} := 1 - e^{\left(-0.2 \cdot t^{0.5}\right)} = 1$

$\varepsilon_{ca.inf} := 2.5 \cdot \left(\frac{f_{ck.ffb}}{MPa} - 10\right) \cdot 10^{-6} = 2.5 \cdot 10^{-5}$

$\varepsilon_{ca} := \beta_{as} \cdot \varepsilon_{ca.inf} = 2.5 \cdot 10^{-5}$

$\varepsilon_{cs} := \left(\varepsilon_{ca} + \varepsilon_{cd}\right) \cdot 1000 = 0.025$ Final shrinkage

C3 Creep calculations

Calculations for determining the creep number follow the procedure given in NS-EN 1992-1-1, B.1.

C3.1 Creep section C

$f_{ck} := 32\ \boldsymbol{MPa}$ $f_{cm} := f_{ck} + 8\ \boldsymbol{MPa} = 40\ \boldsymbol{MPa}$

$f_{cmo} := 10\ \boldsymbol{MPa}$ $RH_0 := 100\%$ $RH := 80\%$

Factors to take into account the importance of concrete strength:

$$\alpha_1 := \left(\frac{35}{\frac{f_{cm}}{\boldsymbol{MPa}}}\right)^{0.7} = 0.911 \qquad \alpha_2 := \left(\frac{35}{\frac{f_{cm}}{\boldsymbol{MPa}}}\right)^{0.2} = 0.974 \qquad \alpha_3 := \left(\frac{35}{\frac{f_{cm}}{\boldsymbol{MPa}}}\right)^{0.5} = 0.935$$

Effective cross-section thickness for cross sections XX:

$h_{xx} := 244.8\ \boldsymbol{mm}$ From shrinkage calculation

Factor that depends on RH and h0 for cross-sections:

$$\beta_H := 1.5 \cdot \left\langle 1 + \left(0.0012 \cdot RH \cdot 100\right)^{18} \right\rangle \cdot \frac{h_{xx}}{\boldsymbol{mm}} + 250 \cdot \alpha_3 = 601.054$$

$$test_{xx} := \mathbf{if}\left(\beta_H \leq 1500 \cdot \alpha_3, \text{“TRUE”}, \text{“FALSE”}\right) = \text{“TRUE”}$$

The FFB part is cast in stages and the load is applied at different times. The age of the concrete is assumed at 28 days at time of load:

$t_0 := 28\ \boldsymbol{day}$

Age of concrete:

$t := 2023\ \boldsymbol{yr} - 1960\ \boldsymbol{yr} = 23010\ \boldsymbol{day}$

Factor that describes the creep development in terms of time after loading.

$$\beta_c := \left(\frac{\frac{\langle t - t_0 \rangle}{\boldsymbol{day}}}{\beta_H + \frac{\langle t - t_0 \rangle}{\boldsymbol{day}}}\right)^{0.3} = 0.992$$

Factor that takes into account the effect of the standard creep rate at the age of the concrete when loaded:

$$\beta_{t.0} := \frac{1}{0.1 + \left(\frac{t_0}{\mathbf{day}}\right)^{0.2}} = 0.488$$

Factor that takes into account the effect of the concrete strength on the normed creep rate:

$$\beta_{f.cm} := \frac{16.8}{\sqrt{\frac{f_{cm}}{\mathbf{MPa}}}} = 2.656$$

Factor that takes into account the effect of relative humidity on the normalized creep rate.

$$\varphi_{RH} := \left(1 + \alpha_1 \cdot \frac{1 - \frac{RH}{100\%}}{0.1 \cdot \left(\frac{h_{xx}}{\mathbf{mm}}\right)^{\frac{1}{3}}}\right) \cdot \alpha_2 = 1.257$$

Normal creep:

$$\varphi := \varphi_{RH} \cdot \beta_{f.cm} \cdot \beta_{t.0} = 1.631$$

Final creep number:

$$\varphi_{t.t0} := \varphi \cdot \beta_c = 1.619$$

Long time E-modulus:

$$E_{cm} := 26870\ \mathbf{MPa}$$

$$E_{cL} := \frac{E_{cm}}{1 + \varphi_{t.t0}} = 10261\ \mathbf{MPa}$$

C3.2 Creep section B and D

$f_{ck} := 20\ \boldsymbol{MPa}$ $f_{cm} := f_{ck} + 8\ \boldsymbol{MPa} = 28\ \boldsymbol{MPa}$

$f_{cmo} := 10\ \boldsymbol{MPa}$ $RH_0 := 100\%$ $RH := 80\%$

Factors to take into account the importance of concrete strength:

$\alpha_1 := \left(\frac{35}{\frac{f_{cm}}{\boldsymbol{MPa}}}\right)^{0.7} = 1.169$ $\alpha_2 := \left(\frac{35}{\frac{f_{cm}}{\boldsymbol{MPa}}}\right)^{0.2} = 1.046$ $\alpha_3 := \left(\frac{35}{\frac{f_{cm}}{\boldsymbol{MPa}}}\right)^{0.5} = 1.118$

Effective cross-section thickness

$h_{xx} := 265\ \boldsymbol{mm}$ From shrinkage calculation

Factor that depends on RH and h0 for cross-sections

$\beta_H := 1.5 \cdot \left(1 + \left(0.0012 \cdot RH \cdot 100\right)^{18}\right) \cdot \frac{h_{xx}}{\boldsymbol{mm}} + 250 = 647.5$

$test_{xx} := \mathbf{if}\left(\beta_H \leq 1500\ ,\ \text{“TRUE”}\ ,\ \text{“FALSE”}\right) = \text{“TRUE”}$

The part is cast in stages and the load is applied at different times. The age of the concrete is assumed at 28 days at time of load:

$t_0 := 28\ \boldsymbol{day}$

Age of concrete:

$t := 2023\ \boldsymbol{yr} - 1960\ \boldsymbol{yr} = 23010\ \boldsymbol{day}$

Factor that describes the creep development in terms of time after loading.

$\beta_c := \left(\frac{\frac{\left(t - t_0\right)}{\boldsymbol{day}}}{\beta_H + \frac{\left(t - t_0\right)}{\boldsymbol{day}}}\right)^{0.3} = 0.992$

Factor that takes into account the effect of the standard creep rate at the age of the concrete when loaded:

$\beta_{t.0} := \frac{1}{0.1 + \left(\frac{t_0}{\boldsymbol{day}}\right)^{0.2}} = 0.488$

Factor that takes into account the effect of the concrete strength on the normed creep rate:

$$\beta_{f.cm} := \frac{16.8}{\sqrt{\frac{f_{cm}}{\mathbf{MPa}}}} = 3.175$$

Factor that takes into account the effect of relative humidity on the normalized creep rate.

$$\varphi_{RH} := \left(1 + \frac{1 - \frac{RH}{100\%}}{0.1 \cdot \left(\frac{h_{xx}}{\mathbf{mm}} \right)^{\frac{1}{3}}} \right) = 1.311$$

Normal creep:

$$\varphi := \varphi_{RH} \cdot \beta_{f.cm} \cdot \beta_{t.0} = 2.034$$

Final creep number:

$$\varphi_{t.t0} := \varphi \cdot \beta_c = 2.017$$

Long time E-modulus:

$$E_{cm} := 23336\ \mathbf{MPa}$$

$$E_{cL} := \frac{E_{cm}}{1 + \varphi_{t.t0}} = 7735\ \mathbf{MPa}$$

C3.3 Creep section A and E

$f_{ck} := 20\ \boldsymbol{MPa}$ $f_{cm} := f_{ck} + 8\ \boldsymbol{MPa} = 28\ \boldsymbol{MPa}$

$f_{cmo} := 10\ \boldsymbol{MPa}$ $RH_0 := 100\%$ $RH := 80\%$

Factors to take into account the importance of concrete strength:

$\alpha_1 := \left(\frac{35}{\frac{f_{cm}}{\boldsymbol{MPa}}}\right)^{0.7} = 1.169$ $\alpha_2 := \left(\frac{35}{\frac{f_{cm}}{\boldsymbol{MPa}}}\right)^{0.2} = 1.046$ $\alpha_3 := \left(\frac{35}{\frac{f_{cm}}{\boldsymbol{MPa}}}\right)^{0.5} = 1.118$

Effective cross-section thickness for cross sections XX:

$h_{xx} := 322.8\ \boldsymbol{mm}$ From shrinkage calculation

Factor that depends on RH and h0 for cross-sections

$\beta_H := 1.5 \cdot \left(1 + \left(0.0012 \cdot RH \cdot 100\right)^{18}\right) \cdot \frac{h_{xx}}{\boldsymbol{mm}} + 250 = 734.2$

$test_{xx} := \mathbf{if}\left(\beta_H \leq 1500\ , \text{“TRUE”}\ , \text{“FALSE”}\right) = \text{“TRUE”}$

The part is cast in stages and the load is applied at different times. The age of the concrete is assumed at 28 days at time of load:

$t_0 := 28\ \boldsymbol{day}$

Age of concrete:

$t := 2023\ \boldsymbol{yr} - 1960\ \boldsymbol{yr} = 23010\ \boldsymbol{day}$

Factor that describes the creep development in terms of time after loading.

$\beta_c := \left(\frac{\frac{\left(t - t_0\right)}{\boldsymbol{day}}}{\beta_H + \frac{\left(t - t_0\right)}{\boldsymbol{day}}}\right)^{0.3} = 0.991$

Factor that takes into account the effect of the standard creep rate at the age of the concrete when loaded:

$\beta_{t.0} := \frac{1}{0.1 + \left(\frac{t_0}{\boldsymbol{day}}\right)^{0.2}} = 0.488$

Factor that takes into account the effect of the concrete strength on the normed creep rate:

$$\beta_{f.cm} := \frac{16.8}{\sqrt{\frac{f_{cm}}{\mathbf{MPa}}}} = 3.175$$

Factor that takes into account the effect of relative humidity on the normalized creep rate.

$$\varphi_{RH} := \left(1 + \frac{1 - \frac{RH}{100\%}}{0.1 \cdot \left(\frac{h_{xx}}{\mathbf{mm}} \right)^{\frac{1}{3}}} \right) = 1.292$$

Normal creep:

$$\varphi := \varphi_{RH} \cdot \beta_{f.cm} \cdot \beta_{t.0} = 2.003$$

Final creep number:

$$\varphi_{t.t0} := \varphi \cdot \beta_c = 1.984$$

Long time E-modulus:

$$E_{cm} := 23336\ \mathbf{MPa}$$

$$E_{cL} := \frac{E_{cm}}{1 + \varphi_{t.t0}} = 7820\ \mathbf{MPa}$$

C3.4 Creep massive columns above water

$f_{ck} := 20\ \boldsymbol{MPa}$ $f_{cm} := f_{ck} + 8\ \boldsymbol{MPa} = 28\ \boldsymbol{MPa}$

$f_{cmo} := 10\ \boldsymbol{MPa}$ $RH_0 := 100\%$ $RH := 80\%$

Factors to take into account the importance of concrete strength:

$$\alpha_1 := \left(\frac{35}{\frac{f_{cm}}{\boldsymbol{MPa}}}\right)^{0.7} = 1.169 \qquad \alpha_2 := \left(\frac{35}{\frac{f_{cm}}{\boldsymbol{MPa}}}\right)^{0.2} = 1.046 \qquad \alpha_3 := \left(\frac{35}{\frac{f_{cm}}{\boldsymbol{MPa}}}\right)^{0.5} = 1.118$$

Effective cross-section thickness for cross sections XX:

$h_{xx} := 700\ \boldsymbol{mm}$ From shrinkage calculation

Factor that depends on RH and h0 for cross-sections

$$\beta_H := 1.5 \cdot \left(1 + \left(0.0012 \cdot RH \cdot 100\right)^{18}\right) \cdot \frac{h_{xx}}{\boldsymbol{mm}} + 250 = 1.3 \cdot 10^3$$

$test_{xx} := \mathbf{if}\left(\beta_H \le 1500, \text{“TRUE”}, \text{“FALSE”}\right) = \text{“TRUE”}$

The part is cast in stages and the load is applied at different times. The age of the concrete is assumed at 28 days at time of load:

$t_0 := 28\ \boldsymbol{day}$

Age of concrete:

$t := 2023\ \boldsymbol{yr} - 1960\ \boldsymbol{yr} = 23010\ \boldsymbol{day}$

Factor that describes the creep development in terms of time after loading.

$$\beta_c := \left(\frac{\frac{\left(t - t_0\right)}{\boldsymbol{day}}}{\beta_H + \frac{\left(t - t_0\right)}{\boldsymbol{day}}}\right)^{0.3} = 0.984$$

Factor that takes into account the effect of the standard creep rate at the age of the concrete when loaded:

$$\beta_{t.0} := \frac{1}{0.1 + \left(\frac{t_0}{\boldsymbol{day}}\right)^{0.2}} = 0.488$$

Factor that takes into account the effect of the concrete strength on the normed creep rate:

$$\beta_{f.cm} := \frac{16.8}{\sqrt{\frac{f_{cm}}{MPa}}} = 3.175$$

Factor that takes into account the effect of relative humidity on the normalized creep rate.

$$\varphi_{RH} := \left(1 + \frac{1 - \frac{RH}{100\%}}{0.1 \cdot \left(\frac{h_{xx}}{mm} \right)^{\frac{1}{3}}} \right) = 1.225$$

Normal creep:

$$\varphi := \varphi_{RH} \cdot \beta_{f.cm} \cdot \beta_{t.0} = 1.9$$

Final creep number:

$$\varphi_{t.t0} := \varphi \cdot \beta_c = 1.869$$

Long time E-modulus:

$$E_{cm} := 23336\ MPa$$

$$E_{cL} := \frac{E_{cm}}{1 + \varphi_{t.t0}} = 8134\ MPa$$

C3.5 Creep hollow columns above water

$f_{ck} := 20\ \boldsymbol{MPa}$ $f_{cm} := f_{ck} + 8\ \boldsymbol{MPa} = 28\ \boldsymbol{MPa}$

$f_{cmo} := 10\ \boldsymbol{MPa}$ $RH_0 := 100\%$ $RH := 80\%$

Factors to take into account the importance of concrete strength:

$\alpha_1 := \left(\frac{35}{\frac{f_{cm}}{\boldsymbol{MPa}}}\right)^{0.7} = 1.169$ $\alpha_2 := \left(\frac{35}{\frac{f_{cm}}{\boldsymbol{MPa}}}\right)^{0.2} = 1.046$ $\alpha_3 := \left(\frac{35}{\frac{f_{cm}}{\boldsymbol{MPa}}}\right)^{0.5} = 1.118$

Effective cross-section thickness for cross sections XX:

$h_{xx} := 408\ \boldsymbol{mm}$ From shrinkage calculation

Factor that depends on RH and h0 for cross-sections

$\beta_H := 1.5 \cdot \left(1 + \left(0.0012 \cdot RH \cdot 100\right)^{18}\right) \cdot \frac{h_{xx}}{\boldsymbol{mm}} + 250 = 862$

$test_{xx} := \mathbf{if}\left(\beta_H \leq 1500, \text{“TRUE”}, \text{“FALSE”}\right) = \text{“TRUE”}$

The part is cast in stages and the load is applied at different times. The age of the concrete is assumed at 28 days at time of load:

$t_0 := 28\ \boldsymbol{day}$

Age of concrete:

$t := 2023\ \boldsymbol{yr} - 1960\ \boldsymbol{yr} = 23010\ \boldsymbol{day}$

Factor that describes the creep development in terms of time after loading.

$\beta_c := \left(\frac{\frac{\langle t - t_0 \rangle}{\boldsymbol{day}}}{\beta_H + \frac{\langle t - t_0 \rangle}{\boldsymbol{day}}}\right)^{0.3} = 0.989$

Factor that takes into account the effect of the standard creep rate at the age of the concrete when loaded:

$\beta_{t.0} := \frac{1}{0.1 + \left(\frac{t_0}{\boldsymbol{day}}\right)^{0.2}} = 0.488$

Factor that takes into account the effect of the concrete strength on the normed creep rate:

$$\beta_{f.cm} := \frac{16.8}{\sqrt{\frac{f_{cm}}{\mathit{MPa}}}} = 3.175$$

Factor that takes into account the effect of relative humidity on the normalized creep rate.

$$\varphi_{RH} := \left(1 + \frac{1 - \frac{RH}{100\%}}{0.1 \cdot \left(\frac{h_{xx}}{\mathit{mm}} \right)^{\frac{1}{3}}} \right) = 1.27$$

Normal creep:

$$\varphi := \varphi_{RH} \cdot \beta_{f.cm} \cdot \beta_{t.0} = 1.969$$

Final creep number:

$$\varphi_{t.t0} := \varphi \cdot \beta_c = 1.947$$

Long time E-modulus:

$$E_{cm} := 23336 \ \mathit{MPa}$$

$$E_{cL} := \frac{E_{cm}}{1 + \varphi_{t.t0}} = 7918 \ \mathit{MPa}$$

C3.6 Creep massive columns under water

$f_{ck} := 20\ \boldsymbol{MPa}$ $f_{cm} := f_{ck} + 8\ \boldsymbol{MPa} = 28\ \boldsymbol{MPa}$

$f_{cmo} := 10\ \boldsymbol{MPa}$ $RH_0 := 100\%$ $RH := 100\%$

Factors to take into account the importance of concrete strength:

$\alpha_1 := \left(\frac{35}{\frac{f_{cm}}{\boldsymbol{MPa}}}\right)^{0.7} = 1.169$ $\alpha_2 := \left(\frac{35}{\frac{f_{cm}}{\boldsymbol{MPa}}}\right)^{0.2} = 1.046$ $\alpha_3 := \left(\frac{35}{\frac{f_{cm}}{\boldsymbol{MPa}}}\right)^{0.5} = 1.118$

Effective cross-section thickness for cross sections XX:

$h_{xx} := 700\ \boldsymbol{mm}$ From shrinkage calculation

Factor that depends on RH and h0 for cross-sections

$\beta_H := 1.5 \cdot \left(1 + \left(0.0012 \cdot RH \cdot 100\right)^{18}\right) \cdot \frac{h_{xx}}{\boldsymbol{mm}} + 250 = 1.3 \cdot 10^3$

$test_{xx} := \mathbf{if}\left(\beta_H \leq 1500, \text{“TRUE”}, \text{“FALSE”}\right) = \text{“TRUE”}$

The part is cast in stages and the load is applied at different times. The age of the concrete is assumed at 28 days at time of load:

$t_0 := 28\ \boldsymbol{day}$

Age of concrete:

$t := 2023\ \boldsymbol{yr} - 1960\ \boldsymbol{yr} = 23010\ \boldsymbol{day}$

Factor that describes the creep development in terms of time after loading.

$\beta_c := \left(\frac{\frac{\left(t - t_0\right)}{\boldsymbol{day}}}{\beta_H + \frac{\left(t - t_0\right)}{\boldsymbol{day}}}\right)^{0.3} = 0.984$

Factor that takes into account the effect of the standard creep rate at the age of the concrete when loaded:

$\beta_{t.0} := \frac{1}{0.1 + \left(\frac{t_0}{\boldsymbol{day}}\right)^{0.2}} = 0.488$

Factor that takes into account the effect of the concrete strength on the normed creep rate:

$$\beta_{f.cm} := \frac{16.8}{\sqrt{\frac{f_{cm}}{MPa}}} = 3.175$$

Factor that takes into account the effect of relative humidity on the normalized creep rate.

$$\varphi_{RH} := \left(1 + \frac{1 - \frac{RH}{100\%}}{0.1 \cdot \left(\frac{h_{xx}}{mm} \right)^{\frac{1}{3}}} \right) = 1$$

Normal creep:

$$\varphi := \varphi_{RH} \cdot \beta_{f.cm} \cdot \beta_{t.0} = 1.551$$

Final creep number:

$$\varphi_{t.t0} := \varphi \cdot \beta_c = 1.525$$

Long time E-modulus:

$$E_{cm} := 23336\ MPa$$

$$E_{cL} := \frac{E_{cm}}{1 + \varphi_{t.t0}} = 9241\ MPa$$

C3.7 Creep hollow columns under water

$f_{ck} := 20\ \mathit{MPa}$ $f_{cm} := f_{ck} + 8\ \mathit{MPa} = 28\ \mathit{MPa}$

$f_{cmo} := 10\ \mathit{MPa}$ $RH_0 := 100\%$ $RH := 100\%$

Factors to take into account the importance of concrete strength:

$$\alpha_1 := \left(\frac{35}{\frac{f_{cm}}{\mathit{MPa}}}\right)^{0.7} = 1.169 \qquad \alpha_2 := \left(\frac{35}{\frac{f_{cm}}{\mathit{MPa}}}\right)^{0.2} = 1.046 \qquad \alpha_3 := \left(\frac{35}{\frac{f_{cm}}{\mathit{MPa}}}\right)^{0.5} = 1.118$$

Effective cross-section thickness for cross sections XX:

$h_{xx} := 408\ \mathit{mm}$ From shrinkage calculation

Factor that depends on RH and h0 for cross-sections

$$\beta_H := 1.5 \cdot \left(1 + \left(0.0012 \cdot RH \cdot 100\right)^{18}\right) \cdot \frac{h_{xx}}{\mathit{mm}} + 250 = 862$$

$test_{xx} := \mathbf{if}\left(\beta_H \leq 1500\ ,\ \text{“TRUE”}\ ,\ \text{“FALSE”}\right) = \text{“TRUE”}$

The part is cast in stages and the load is applied at different times. The age of the concrete is assumed at 28 days at time of load:

$t_0 := 28\ \mathit{day}$

Age of concrete:

$t := 2023\ \mathit{yr} - 1960\ \mathit{yr} = 23010\ \mathit{day}$

Factor that describes the creep development in terms of time after loading.

$$\beta_c := \left(\frac{\frac{\left(t - t_0\right)}{\mathit{day}}}{\beta_H + \frac{\left(t - t_0\right)}{\mathit{day}}}\right)^{0.3} = 0.989$$

Factor that takes into account the effect of the standard creep rate at the age of the concrete when loaded:

$$\beta_{t.0} := \frac{1}{0.1 + \left(\frac{t_0}{\mathit{day}}\right)^{0.2}} = 0.488$$

Factor that takes into account the effect of the concrete strength on the normed creep rate:

$$\beta_{f.cm} := \frac{16.8}{\sqrt{\frac{f_{cm}}{\mathbf{MPa}}}} = 3.175$$

Factor that takes into account the effect of relative humidity on the normalized creep rate.

$$\varphi_{RH} := \left(1 + \frac{1 - \frac{RH}{100\%}}{0.1 \cdot \left(\frac{h_{xx}}{\mathbf{mm}} \right)^{\frac{1}{3}}} \right) = 1$$

Normal creep:

$$\varphi := \varphi_{RH} \cdot \beta_{f.cm} \cdot \beta_{t.0} = 1.551$$

Final creep number:

$$\varphi_{t.t0} := \varphi \cdot \beta_c = 1.534$$

Long time E-modulus:

$$E_{cm} := 23336\ \mathbf{MPa}$$

$$E_{cL} := \frac{E_{cm}}{1 + \varphi_{t.t0}} = 9210\ \mathbf{MPa}$$

D Buckling and slenderness

- D1 - Slenderness calculations

D1 Slenderness

D1.1 Basis for calculations

$D := 1400\ \boldsymbol{mm}$ Diameter

$A_c := \frac{\pi \cdot D^2}{4} = 1539380.4\ \boldsymbol{mm}^2$ Area cross-section

$I_c := \frac{\pi}{64} \cdot D^4 = 188574099031.7\ \boldsymbol{mm}^4$ Second moment of area

$E_c := 9500\ \boldsymbol{MPa}^{0.7} \cdot 20^{0.3}\ \boldsymbol{MPa}^{0.3} = 23336.3\ \boldsymbol{MPa}$ E-modulus

$L_{33\_1} := 28.05\ \boldsymbol{m}$ Length column 33 - upper part

$L_{33\_2} := 13.10\ \boldsymbol{m}$ Length column 33 -lower part

$\gamma_c := 1.5$ Partial safety factor

$f_{ck} := 20\ \boldsymbol{MPa}$ Characteristic compressive strength

$f_{cm} := 28\ \boldsymbol{MPa}$ Mean characteristic compressive strength

$f_{cd} := 0.85\ \frac{f_{ck}}{\gamma_c} = 11.3\ \boldsymbol{MPa}$ Design compressive strength

$E_s := 210000\ \boldsymbol{MPa}$ Youngs-modulus

$\gamma_s := 1.15$ Partial safety factor

$f_{yk} := 380 \cdot \boldsymbol{MPa}$ Characteristic tensile strength

$f_{yd} := \frac{f_{yk}}{\gamma_s} = 330.4\ \boldsymbol{MPa}$ Design tensile strength

$\phi := 25\ \boldsymbol{mm}$ Diameter rebar

$n_s := 22$ Number of rebars

$A_s := n_s \cdot \frac{\pi \cdot \phi^2}{4} = 10799.2\ \boldsymbol{mm}^2$ Area reinforcement

$I_s := 2.1 \cdot 10^9\ \boldsymbol{mm}^4$ Second moment of area

$d := D - 50\ \boldsymbol{mm} - 10\ \boldsymbol{mm} - \frac{\phi}{2} = 1327.5\ \boldsymbol{mm}$ Effective depth

D1.2 Buckling factor

$k_x := \frac{3 \cdot E_c \cdot I_c}{L_{33\_2}^{\ 3}} = 5872.5 \ \frac{kN}{m}$ Sideways stiffness

$\delta := \frac{k_x \cdot L_{33\_1}^{\ 3}}{E_c \cdot I_c} = 29.5$ Dimensionless stiffness parameter

$k_\phi := \infty$ Rotational stiffness

$\gamma := \infty$ Dimensionless stiffness parameter

$\beta := 0.55$ Dimentionless buckling length factor

$l_0 := \beta \cdot L_{33\_1} = 15.4 \ m$ Buckling length

D1.3 Normalised slenderness

$N_{Ed} := -8000 \ kN$ Normal force

$i := \sqrt{\frac{I_c}{A_c}} = 350 \ mm$ Radius of gyration - concrete

$i_s := \sqrt{\frac{I_s}{A_s}} = 441 \ mm$ Radius of gyration - reinforcement

$k_a := \left(\frac{i_s}{i}\right)^2 = 1.6$

$\lambda := \frac{l_0}{i} = 44.1$ Slenderness ratio

$n := \frac{-N_{Ed}}{f_{cd} \cdot A_c} = 0.5$ Relative axial force

$\omega := \frac{f_{yd} \cdot A_s}{f_{cd} \cdot A_c} = 0.2$ Mechanical reinforcement ratio

$\lambda_n := \lambda \cdot \sqrt{\frac{n}{1 + 2 \ k_a \cdot \omega}} = 23.2$ Normalised slenderness

$\varphi_{ef} := 1.87$

$A_\varphi := min\left(\frac{1.25}{1 + 0.2 \cdot \varphi_{ef}}, 1.0\right) = 0.91$

$\lambda_{n.lim} := 13 \cdot A_\varphi = 11.8$

if $\left(\lambda_{n.lim} > \lambda_n, \text{“Not Slender”}, \text{“Slender”}\right) = \text{“Slender”}$

if $\left(45 > \lambda_n, \text{“Material Failure”}, \text{“Buckling Failure”}\right) = \text{“Material Failure”}$

E Capacity Shear and crossbars

- E1 - Capacity calculations for shear
- E2 - Capacity calculations for crossbars

E1 Capacity control of shear forces

All calculations are done according to EC2 6.2.2 and 6.2.3

E1.1 Basis for calculations

$b_w := 600\ \boldsymbol{mm}$
$d := 1250\ \boldsymbol{mm}$
$z := 0.9 \cdot d$
$A_{sw} := 2 \cdot \pi \cdot (5\ \boldsymbol{mm})^2 = 157.08\ \boldsymbol{mm^2}$

Cross section data

$f_{cd} := 12\ \boldsymbol{MPa}$
$f_{ywd} := 184\ \boldsymbol{MPa}$

Material data

$\alpha_{cw} := 1$
$v_1 := 0.6$
$\theta := 2.5$

$$k := 1 + \sqrt{\frac{200}{\frac{d}{\boldsymbol{mm}}}} = 1.4$$

$$C_{Rd.c} := \frac{0.18}{1.5} = 0.12$$

Eurocode factors

$k_1 := 0.15$
$v_{min} := 0.035 \cdot k^{\frac{3}{2}} \cdot 20^{0.5} = 0.259$

E1.2 Shear check columns 44-49

$s := 250\ \textbf{mm}$

$A_{sl} := 16 \cdot \pi \cdot (12.5\ \textbf{mm})^2 = \left(7.854 \cdot 10^3\right)\ \textbf{mm}^2$

$N := 1500\ \textbf{kN}$

$\rho_l := \frac{A_{sl}}{b_w \cdot d} = 0.01$

$\sigma_{cp} := \frac{N}{\pi \cdot (700\ \textbf{mm})^2} = 0.974\ \textbf{MPa}$

$V_{Rd.c.1} := \left(C_{Rd.c} \cdot k \cdot \left(100 \cdot \rho_l \cdot 20\right)^{\frac{1}{3}} \cdot \textbf{MPa} + k_1 \cdot \sigma_{cp}\right) \cdot b_w \cdot d = 456.937\ \textbf{kN}$

$V_{Rd.c.2} := \left(v_{min} \cdot \textbf{MPa} + k_1 \cdot \sigma_{cp}\right) \cdot b_w \cdot d = 304.085\ \textbf{kN}$

$V_{Rd.c.max} := \max\left(V_{Rd.c.1}, V_{Rd.c.2}\right) = 456.937\ \textbf{kN}$

$V_{Rd.s} := \frac{A_{sw}}{s} \cdot z \cdot f_{ywd} \cdot \theta = 325.155\ \textbf{kN}$

$V_{Rd.max} := \frac{\alpha_{cw} \cdot b_w \cdot z \cdot v_1 \cdot f_{cd}}{\left(\theta + \frac{1}{\theta}\right)} = 1675.862\ \textbf{kN}$

$V_{Rd.s.max} := min\left(V_{Rd.s}, V_{Rd.max}\right) = 325.155\ \textbf{kN}$

$V_{Rd} := \max\left(V_{Rd.c.max}, V_{Rd.s.max}\right) = 456.937\ \textbf{kN}$

$U := \frac{112.0\ \textbf{kN}}{V_{Rd}} = 0.245$ Utilization

E1.2 Shear check column 38

$s := 150\ \boldsymbol{mm}$

$A_{sl} := 16 \cdot \pi \cdot (12.5\ \boldsymbol{mm})^2 = \left(7.854 \cdot 10^3\right)\ \boldsymbol{mm}^2$

$N := 4000\ \boldsymbol{kN}$

$\rho_l := \frac{A_{sl}}{b_w \cdot d} = 0.01$

$\sigma_{cp} := \frac{N}{\pi \cdot (700\ \boldsymbol{mm})^2} = 2.598\ \boldsymbol{MPa}$

$V_{Rd.c.1} := \left(C_{Rd.c} \cdot k \cdot \left(100 \cdot \rho_l \cdot 20\right)^{\frac{1}{3}} \cdot \boldsymbol{MPa} + k_1 \cdot \sigma_{cp}\right) \cdot b_w \cdot d = 639.64\ \boldsymbol{kN}$

$V_{Rd.c.2} := \left(v_{min} \cdot \boldsymbol{MPa} + k_1 \cdot \sigma_{cp}\right) \cdot b_w \cdot d = 486.788\ \boldsymbol{kN}$

$V_{Rd.c.max} := \max\left(V_{Rd.c.1}, V_{Rd.c.2}\right) = 639.64\ \boldsymbol{kN}$

$V_{Rd.s} := \frac{A_{sw}}{s} \cdot z \cdot f_{ywd} \cdot \theta = 541.925\ \boldsymbol{kN}$

$V_{Rd.max} := \frac{\alpha_{cw} \cdot b_w \cdot z \cdot v_1 \cdot f_{cd}}{\left(\theta + \frac{1}{\theta}\right)} = 1675.862\ \boldsymbol{kN}$

$V_{Rd.s.max} := min\left(V_{Rd.s}, V_{Rd.max}\right) = 541.925\ \boldsymbol{kN}$

$V_{Rd} := \max\left(V_{Rd.c.max}, V_{Rd.s.max}\right) = 639.64\ \boldsymbol{kN}$

$U := \frac{275\ \boldsymbol{kN}}{V_{Rd}} = 0.43$

E1.2 Shear check column 31

$s := 150\ \boldsymbol{mm}$

$A_{sl} := 16 \cdot \pi \cdot (12.5\ \boldsymbol{mm})^2 = \left(7.854 \cdot 10^3\right)\ \boldsymbol{mm}^2$

$N := 1500\ \boldsymbol{kN}$

$\rho_l := \frac{A_{sl}}{b_w \cdot d} = 0.01$

$\sigma_{cp} := \frac{N}{\pi \cdot (700\ \boldsymbol{mm})^2} = 0.974\ \boldsymbol{MPa}$

$V_{Rd.c.1} := \left(C_{Rd.c} \cdot k \cdot \left(100 \cdot \rho_l \cdot 20\right)^{\frac{1}{3}} \cdot \boldsymbol{MPa} + k_1 \cdot \sigma_{cp}\right) \cdot b_w \cdot d = 456.937\ \boldsymbol{kN}$

$V_{Rd.c.2} := \left(v_{min} \cdot \boldsymbol{MPa} + k_1 \cdot \sigma_{cp}\right) \cdot b_w \cdot d = 304.085\ \boldsymbol{kN}$

$V_{Rd.c.max} := \max\left(V_{Rd.c.1}, V_{Rd.c.2}\right) = 456.937\ \boldsymbol{kN}$

$V_{Rd.s} := \frac{A_{sw}}{s} \cdot z \cdot f_{ywd} \cdot \theta = 541.925\ \boldsymbol{kN}$

$V_{Rd.max} := \frac{\alpha_{cw} \cdot b_w \cdot z \cdot \nu_1 \cdot f_{cd}}{\left(\theta + \frac{1}{\theta}\right)} = 1675.862\ \boldsymbol{kN}$

$V_{Rd.s.max} := min\left(V_{Rd.s}, V_{Rd.max}\right) = 541.925\ \boldsymbol{kN}$

$V_{Rd} := \max\left(V_{Rd.c.max}, V_{Rd.s.max}\right) = 541.925\ \boldsymbol{kN}$

$U := \frac{307\ \boldsymbol{kN}}{V_{Rd}} = 0.566$

E1.3 Shear check column 32

$s := 150\ \boldsymbol{mm}$

$A_{sl} := 16 \cdot \pi \cdot (12.5\ \boldsymbol{mm})^2 = \langle 7.854 \cdot 10^3 \rangle\ \boldsymbol{mm}^2$

$N := 1500\ \boldsymbol{kN}$

$\rho_l := \frac{A_{sl}}{b_w \cdot d} = 0.01$

$\sigma_{cp} := \frac{N}{\pi \cdot (700\ \boldsymbol{mm})^2} = 0.974\ \boldsymbol{MPa}$

$V_{Rd.c.1} := \left(C_{Rd.c} \cdot k \cdot \left(100 \cdot \rho_l \cdot 20\right)^{\frac{1}{3}} \cdot \boldsymbol{MPa} + k_1 \cdot \sigma_{cp} \right) \cdot b_w \cdot d = 456.937\ \boldsymbol{kN}$

$V_{Rd.c.2} := \left(v_{min} \cdot \boldsymbol{MPa} + k_1 \cdot \sigma_{cp} \right) \cdot b_w \cdot d = 304.085\ \boldsymbol{kN}$

$V_{Rd.c.max} := \max\left(V_{Rd.c.1}, V_{Rd.c.2}\right) = 456.937\ \boldsymbol{kN}$

$V_{Rd.s} := \frac{A_{sw}}{s} \cdot z \cdot f_{ywd} \cdot \theta = 541.925\ \boldsymbol{kN}$

$V_{Rd.max} := \frac{\alpha_{cw} \cdot b_w \cdot z \cdot v_1 \cdot f_{cd}}{\left(\theta + \frac{1}{\theta}\right)} = 1675.862\ \boldsymbol{kN}$

$V_{Rd.s.max} := min\left(V_{Rd.s}, V_{Rd.max}\right) = 541.925\ \boldsymbol{kN}$

$V_{Rd} := \max\left(V_{Rd.c.max}, V_{Rd.s.max}\right) = 541.925\ \boldsymbol{kN}$

$U := \frac{352.4\ \boldsymbol{kN}}{V_{Rd}} = 0.65$

E1.4 Shear check column 34

$s := 120\ \boldsymbol{mm}$

$A_{sl} := 16 \cdot \pi \cdot (12.5\ \boldsymbol{mm})^2 = \langle 7.854 \cdot 10^3 \rangle\ \boldsymbol{mm}^2$

$N := 1500\ \boldsymbol{kN}$

$\rho_l := \frac{A_{sl}}{b_w \cdot d} = 0.01$

$\sigma_{cp} := \frac{N}{\pi \cdot (700\ \boldsymbol{mm})^2} = 0.974\ \boldsymbol{MPa}$

$V_{Rd.c.1} := \left(C_{Rd.c} \cdot k \cdot (100 \cdot \rho_l \cdot 20)^{\frac{1}{3}} \cdot \boldsymbol{MPa} + k_1 \cdot \sigma_{cp} \right) \cdot b_w \cdot d = 456.937\ \boldsymbol{kN}$

$V_{Rd.c.2} := \left(v_{min} \cdot \boldsymbol{MPa} + k_1 \cdot \sigma_{cp} \right) \cdot b_w \cdot d = 304.085\ \boldsymbol{kN}$

$V_{Rd.c.max} := \max\left(V_{Rd.c.1}, V_{Rd.c.2} \right) = 456.937\ \boldsymbol{kN}$

$V_{Rd.s} := \frac{A_{sw}}{s} \cdot z \cdot f_{ywd} \cdot \theta = 677.406\ \boldsymbol{kN}$

$V_{Rd.max} := \frac{\alpha_{cw} \cdot b_w \cdot z \cdot v_1 \cdot f_{cd}}{\left(\theta + \frac{1}{\theta} \right)} = 1675.862\ \boldsymbol{kN}$

$V_{Rd.s.max} := min\left(V_{Rd.s}, V_{Rd.max} \right) = 677.406\ \boldsymbol{kN}$

$V_{Rd} := \max\left(V_{Rd.c.max}, V_{Rd.s.max} \right) = 677.406\ \boldsymbol{kN}$

$U := \frac{429.7\ \boldsymbol{kN}}{V_{Rd}} = 0.634$

E2 Capacity control of crossbars

All calculations are done with compression field theory

E2.1 Basis for calculations

$f_{cd} := 11.3\ \mathit{MPa}$ $f_{yd} := 384\ \mathit{MPa}$

$f_{td} := 1\ \mathit{MPa}$

$A_{sx.1} := 12 \cdot \pi \cdot (12.5\ \mathit{mm})^2 = 5890.486\ \mathit{mm}^2$

$A_{sy.1} := 48 \cdot \pi \cdot (12.5\ \mathit{mm})^2 = (2.356 \cdot 10^4)\ \mathit{mm}^2$

$A_{s.f.1} := \frac{A_{sy.1}}{A_{sx.1}} = 4$

E2.2 points chosen for evaluation

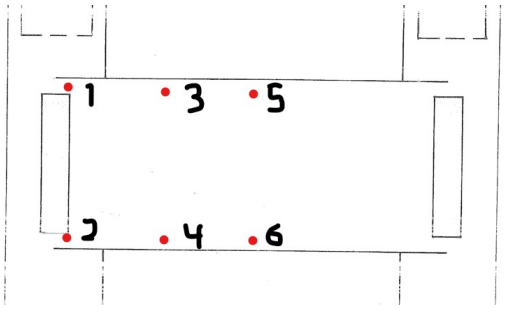

E2.2.1 Point 1

$N_x := 500 \ \frac{N}{mm}$

$N_y := -4909 \ \frac{N}{mm}$

$N_{xy} := 389 \ \frac{N}{mm}$

$\varphi := 17$

$F_c := \frac{N_{xy}}{\sin(\varphi \cdot deg) \cdot \cos(\varphi \cdot deg)} = \left(2.087 \cdot 10^9\right) \ \frac{N}{mm}$

$F_{sx.1} := N_x + N_{xy} \cdot \tan(\varphi \cdot deg) = \left(9.284 \cdot 10^8\right) \ \frac{N}{mm}$

$F_{sy.1} := N_y + N_{xy} \cdot \cot(\varphi \cdot deg) = -5.455 \cdot 10^9 \ \frac{N}{mm}$

$\sigma_{sx} := \frac{F_{sx.1} \cdot 1000 \ mm}{A_{sx.1}} = 157609035.501 \ MPa$

$\sigma_{sy} := \frac{F_{sy.1} \cdot 1000 \ mm}{A_{sy.1}} = -231515586.673 \ MPa$

$\sigma_c := \frac{F_c}{1000 \ mm} = 2086936.356 \ MPa$

$\eta_c := \frac{\sigma_{sx}}{f_{yd}} = 4.104 \cdot 10^5 \qquad \eta_c := \frac{\mathrm{abs}(\sigma_{sy})}{f_{yd}} = 6.029 \cdot 10^5 \qquad \eta_c := \frac{\sigma_c}{f_{cd}} = 1.847 \cdot 10^5$

E2.2.2 Point 2

$N_x := -1156 \ \frac{N}{mm}$

$N_y := -3700 \ \frac{N}{mm}$

$N_{xy} := -500 \ \frac{N}{mm}$

$\varphi := -28$

$F_c := \frac{N_{xy}}{\sin(\varphi \cdot deg) \cdot \cos(\varphi \cdot deg)} = \langle 1.809 \cdot 10^9 \rangle \ \frac{N}{mm}$

$F_{sx.1} := N_x + N_{xy} \cdot \tan(\varphi \cdot deg) = -1.335 \cdot 10^9 \ \frac{N}{mm}$

$F_{sy.1} := N_y + N_{xy} \cdot \cot(\varphi \cdot deg) = -4.139 \cdot 10^9 \ \frac{N}{mm}$

$\sigma_{sx} := \frac{F_{sx.1} \cdot 1000 \ mm}{A_{sx.1}} = -226673635.273 \ MPa$

$\sigma_{sy} := \frac{F_{sy.1} \cdot 1000 \ mm}{A_{sy.1}} = -175683933.063 \ MPa$

$\sigma_c := \frac{F_c}{1000 \ mm} = 1809326.923 \ MPa$

$\eta_c := \frac{\text{abs}(\sigma_{sx})}{f_{yd}} = 5.903 \cdot 10^5 \qquad \eta_c := \frac{\text{abs}(\sigma_{sy})}{f_{yd}} = 4.575 \cdot 10^5 \qquad \eta_c := \frac{\sigma_c}{f_{cd}} = 1.601 \cdot 10^5$

E2.2.3 Point 3

$N_x := 888 \ \frac{N}{mm}$

$N_y := 128 \ \frac{N}{mm}$

$N_{xy} := -890 \ \frac{N}{mm}$

$\varphi := -50$

$F_c := \frac{N_{xy}}{\sin(\varphi \cdot deg) \cdot \cos(\varphi \cdot deg)} = 2711189053.735 \ \frac{N}{mm}$

$F_{sx.1} := N_x + N_{xy} \cdot \tan(\varphi \cdot deg) = 2922991046.113 \ \frac{N}{mm}$

$F_{sy.1} := N_y + N_{xy} \cdot \cot(\varphi \cdot deg) = \langle 1.312 \cdot 10^9 \rangle \ \frac{N}{mm}$

$\sigma_{sx} := \frac{F_{sx.1} \cdot 1000 \ mm}{A_{sx.1}} = 496222371.842 \ MPa$

$\sigma_{sy} := \frac{F_{sy.1} \cdot 1000 \ mm}{A_{sy.1}} = 55691413.128 \ MPa$

$\sigma_c := \frac{F_c}{1000 \ mm} = 2711189.054 \ MPa$

$\eta_c := \frac{\text{abs}(\sigma_{sx})}{f_{yd}} = 1.292 \cdot 10^6$ $\eta_c := \frac{\sigma_{sy}}{f_{yd}} = 1.45 \cdot 10^5$ $\eta_c := \frac{\sigma_c}{f_{cd}} = 2.399 \cdot 10^5$

E2.2.4 Point 4

$$A_{sx.1} := 12 \cdot \pi \cdot (12.5\ mm)^2 = 5890.486\ mm^2$$

$$A_{sy.1} := 6 \cdot \pi \cdot (12.5\ mm)^2 = (2.945 \cdot 10^3)\ mm^2$$

$$A_{s.f.1} := \frac{A_{sx.1}}{A_{sy.1}} = 2$$

$$N_x := -1000\ \frac{N}{mm}$$

$$N_y := 115\ \frac{N}{mm}$$

$$N_{xy} := -170\ \frac{N}{mm}$$

$$\varphi := -28$$

$$F_c := \frac{N_{xy}}{\sin(\varphi \cdot deg) \cdot \cos(\varphi \cdot deg)} = 615171153.737\ \frac{N}{mm}$$

$$F_{sx.1} := N_x + N_{xy} \cdot \tan(\varphi \cdot deg) = -1364414094.926\ \frac{N}{mm}$$

$$F_{sy.1} := N_y + N_{xy} \cdot \cot(\varphi \cdot deg) = (6.521 \cdot 10^8)\ \frac{N}{mm}$$

$$\sigma_{sx} := \frac{F_{sx.1} \cdot 1000\ mm}{A_{sx.1}} = -231630130.807\ MPa$$

$$\sigma_{sy} := \frac{F_{sy.1} \cdot 1000\ mm}{A_{sy.1}} = 221402860.036\ MPa$$

$$\sigma_c := \frac{F_c}{1000\ mm} = 615171.154\ MPa$$

$$\eta_c := \frac{\mathrm{abs}(\sigma_{sx})}{f_{yd}} = 6.032 \cdot 10^5 \qquad \eta_c := \frac{\sigma_{sy}}{f_{yd}} = 5.766 \cdot 10^5 \qquad \eta_c := \frac{\sigma_c}{f_{cd}} = 5.444 \cdot 10^4$$

E2.2.4 Point 5

$N_x := -300 \ \frac{N}{mm}$

$N_y := -110 \ \frac{N}{mm}$

$N_{xy} := -176 \ \frac{N}{mm}$

$\varphi := -50$

$F_c := \frac{N_{xy}}{\sin(\varphi \cdot deg) \cdot \cos(\varphi \cdot deg)} = 536145251.076 \ \frac{N}{mm}$

$F_{sx.1} := N_x + N_{xy} \cdot \tan(\varphi \cdot deg) = -135377051.555 \ \frac{N}{mm}$

$F_{sy.1} := N_y + N_{xy} \cdot \cot(\varphi \cdot deg) = (5.652 \cdot 10^7) \ \frac{N}{mm}$

$\sigma_{sx} := \frac{F_{sx.1} \cdot 1000 \ mm}{A_{sx.1}} = -22982322.065 \ MPa$

$\sigma_{sy} := \frac{F_{sy.1} \cdot 1000 \ mm}{A_{sy.1}} = 19191048.232 \ MPa$

$\sigma_c := \frac{F_c}{1000 \ mm} = 536145.251 \ MPa$

$\eta_c := \frac{\text{abs}(\sigma_{sx})}{f_{yd}} = 5.985 \cdot 10^4 \quad \eta_c := \frac{\sigma_{sy}}{f_{yd}} = 4.998 \cdot 10^4 \quad \eta_c := \frac{\sigma_c}{f_{cd}} = 4.745 \cdot 10^4$

E2.2.6 Point 6

$$A_{sx.1} := 12 \cdot \pi \cdot (12.5\ mm)^2 = 5890.486\ mm^2$$

$$A_{sy.1} := 6 \cdot \pi \cdot (12.5\ mm)^2 = (2.945 \cdot 10^3)\ mm^2$$

$$A_{s.f.1} := \frac{A_{sx.1}}{A_{sy.1}} = 2$$

$$N_x := 980\ \frac{N}{mm}$$

$$N_y := 1.5\ \frac{N}{mm}$$

$$N_{xy} := -413\ \frac{N}{mm}$$

$$\varphi := -40$$

$$F_c := \frac{N_{xy}}{\sin(\varphi \cdot deg) \cdot \cos(\varphi \cdot deg)} = 1258113572.126\ \frac{N}{mm}$$

$$F_{sx.1} := N_x + N_{xy} \cdot \tan(\varphi \cdot deg) = 1989822221.514\ \frac{N}{mm}$$

$$F_{sy.1} := N_y + N_{xy} \cdot \cot(\varphi \cdot deg) = (7.405 \cdot 10^8)\ \frac{N}{mm}$$

$$\sigma_{sx} := \frac{F_{sx.1} \cdot 1000\ mm}{A_{sx.1}} = 337802711.923\ MPa$$

$$\sigma_{sy} := \frac{F_{sy.1} \cdot 1000\ mm}{A_{sy.1}} = 251436408.563\ MPa$$

$$\sigma_c := \frac{F_c}{1000\ mm} = 1258113.572\ MPa$$

$$\eta_c := \frac{\sigma_{sx}}{f_{yd}} = 8.797 \cdot 10^5 \qquad \eta_c := \frac{\sigma_{sy}}{f_{yd}} = 6.548 \cdot 10^5 \qquad \eta_c := \frac{\sigma_c}{f_{cd}} = 1.113 \cdot 10^5$$

F ASR

- F1 - Calculations of ASR loads

F1 ASR calculation

F1.1 Section B/D - 17 to 32 and 38 to 43 - Field

Cross section data:

$A_c := 3043800\ \boldsymbol{mm}^2$

$h_{tot} := 1686\ \boldsymbol{mm}$

$I_c := 82.64 \cdot 10^{10}\ \boldsymbol{mm}^4$

$e_z := 1178\ \boldsymbol{mm}$

Reinforcement

$A_{su} := 7854\ \boldsymbol{mm}^2$

$y_{su} := 165\ \boldsymbol{mm}$

E-modulus

$E_{cL} := 7174\ \boldsymbol{MPa}$ Long time Youngs module due to creep

$E_s := 200000\ \boldsymbol{MPa}$

Transformed cross-section (EC2)

$$\eta := \frac{E_s}{E_{cL}} = 27.878$$

$A_t := A_c + (\eta - 1) \cdot A_{su} = \left(3.255 \cdot 10^6\right)\ \boldsymbol{mm}^2$

$$e_{zt} := \frac{A_c \cdot e_z + (\eta - 1) \cdot A_{su} \cdot y_{su}}{A_t} = \left(1.112 \cdot 10^3\right)\ \boldsymbol{mm}$$

$y_t := e_z - e_{zt} = 65.7\ \boldsymbol{mm}$

$e_s := e_{zt} - y_{su} = 947.3\ \boldsymbol{mm}$

$$I_t := I_c + A_c \cdot y_t^{\,2} + (\eta - 1)\, A_{su} \cdot e_s^{\,2} = (1.029 \cdot 10^{12})\ \boldsymbol{mm}^4$$

$$‰ := \frac{1}{1000}$$

Total strain from ASR:

$$\varepsilon_{asr} := 0.55 \cdot ‰ = 5.5 \cdot 10^{-4} \qquad \varepsilon_{Shrinkage} := 0.266 \cdot ‰$$

$$\varepsilon_{ASR} := \varepsilon_{asr} - \varepsilon_{Shrinkage} = 0.284\ ‰$$

$$N_{ASR} := \varepsilon_{ASR} \cdot E_s \cdot A_{su} = 446.107\ \boldsymbol{kN}$$

$$M_{ASR} := N_{ASR} \cdot e_s = 422.597\ \boldsymbol{kN} \cdot \boldsymbol{m}$$

Curvature due to ASR

$$\kappa_{ASR} := \frac{M_{ASR}}{E_{cL} \cdot I_t} = (5.725 \cdot 10^{-5})\ \frac{1}{\boldsymbol{m}}$$

Curvature due to temperature:

$$\alpha_T := 9.8 \cdot 10^{-6} \cdot \boldsymbol{K}^{-1}$$

$$\Delta_T := \kappa_{ASR} \cdot \frac{h_{tot}}{\alpha_T} = 9.849\ \boldsymbol{K}$$

F1.2 Section A/E- 1 to 16 and 43 to 55- Field

Cross section data:

$A_c := 2788000\ \boldsymbol{mm}^2$

$h_{tot} := 336\ \boldsymbol{mm}$

$I_c := 2.624 \cdot 10^{10}\ \boldsymbol{mm}^4$

$e_z := 168\ \boldsymbol{mm}$

Reinforcement

$A_{su} := 11437\ \boldsymbol{mm}^2$

$y_{su} := 29.5\ \boldsymbol{mm}$

E-modulus

$E_{cL} := 7174\ \boldsymbol{MPa}$ Long time Youngs module due to creep

$E_s := 200000\ \boldsymbol{MPa}$

Transformed cross-section (EC2)

$\eta := \frac{E_s}{E_{cL}} = 27.878$

$A_t := A_c + (\eta - 1) \cdot A_{su} = \langle 3.095 \cdot 10^6 \rangle\ \boldsymbol{mm}^2$

$e_{zt} := \frac{A_c \cdot e_z + (\eta - 1) \cdot A_{su} \cdot y_{su}}{A_t} = 154.245\ \boldsymbol{mm}$

$y_t := e_z - e_{zt} = 13.755\ \boldsymbol{mm}$

$e_s := e_{zt} - y_{su} = 124.745\ \boldsymbol{mm}$

$I_t := I_c + A_c \cdot y_t^2 + (\eta - 1)\ A_{su} \cdot e_s^2 = \langle 3.155 \cdot 10^{10} \rangle\ \boldsymbol{mm}^4$

$‰ := \frac{1}{1000}$ $\varepsilon_{Shrinkage} := 0.247 \cdot ‰$

$\varepsilon_{ASR} := \varepsilon_{asr} - \varepsilon_{Shrinkage} = 0.303\ ‰$

$N_{ASR} := \varepsilon_{ASR} \cdot E_s \cdot A_{su} = 693.082\ \boldsymbol{kN}$

$M_{ASR} := N_{ASR} \cdot e_s = 86.459\ \boldsymbol{kN \cdot m}$

Curvature due to ASR

$\kappa_{ASR} := \frac{M_{ASR}}{E_{cL} \cdot I_t} = \langle 3.82 \cdot 10^{-4} \rangle\ \frac{1}{\boldsymbol{m}}$

Curvature due to temperature:

$\alpha_T := 9.8 \cdot 10^{-6} \cdot \boldsymbol{K}^{-1}$

$\Delta_T := \kappa_{ASR} \cdot \frac{h_{tot}}{\alpha_T} = 13.096\ \boldsymbol{K}$

F1.3 Section B/D - 31 to 32 and 37 to 38 - Field

Cross section data:

$A_c := 3043800\ \boldsymbol{mm}^2$

$h_{tot} := 1686\ \boldsymbol{mm}$

$I_c := 82.64 \cdot 10^{10}\ \boldsymbol{mm}^4$

$e_z := 1178\ \boldsymbol{mm}$

Reinforcement

$A_{su} := 11290\ \boldsymbol{mm}^2$

$y_{su} := 190\ \boldsymbol{mm}$

E-modulus

$E_{cL} := 7174\ \boldsymbol{MPa}$ Long time Youngs module due to creep

$E_s := 200000\ \boldsymbol{MPa}$

Transformed cross-section (EC2)

$\eta := \frac{E_s}{E_{cL}} = 27.878$

$A_t := A_c + (\eta - 1) \cdot A_{su} = \left(3.347 \cdot 10^6\right)\ \boldsymbol{mm}^2$

$e_{zt} := \frac{A_c \cdot e_z + (\eta - 1) \cdot A_{su} \cdot y_{su}}{A_t} = \left(1.088 \cdot 10^3\right)\ \boldsymbol{mm}$

$y_t := e_z - e_{zt} = 89.571\ \boldsymbol{mm}$

$e_s := e_{zt} - y_{su} = 898.429\ \boldsymbol{mm}$

$I_t := I_c + A_c \cdot y_t^2 + (\eta - 1)\ A_{su} \cdot e_s^2 = \left(1.096 \cdot 10^{12}\right)\ \boldsymbol{mm}^4$

$‰ := \frac{1}{1000}$ $\varepsilon_{Shrinkage} := 0.266 \cdot ‰$

$\varepsilon_{ASR} := \varepsilon_{asr} - \varepsilon_{Shrinkage} = 0.284\ ‰$

$N_{ASR} := \varepsilon_{ASR} \cdot E_s \cdot A_{su} = 641.272\ \boldsymbol{kN}$

$M_{ASR} := N_{ASR} \cdot e_s = 576.138\ \boldsymbol{kN \cdot m}$

Curvature due to ASR

$\kappa_{ASR} := \frac{M_{ASR}}{E_{cL} \cdot I_t} = \left\langle 7.329 \cdot 10^{-5} \right\rangle\ \frac{1}{\boldsymbol{m}}$

Curvature due to temperature:

$\alpha_T := 9.8 \cdot 10^{-6} \cdot \boldsymbol{K}^{-1}$

$\Delta_T := \kappa_{ASR} \cdot \frac{h_{tot}}{\alpha_T} = 12.609\ \boldsymbol{K}$

F1.4 Section B/D - 17 to 32 and 38 to 43 - Support

Cross section data:

$A_c := 3043800\ \boldsymbol{mm}^2$

$h_{tot} := 1686\ \boldsymbol{mm}$

$I_c := 82.64 \cdot 10^{10}\ \boldsymbol{mm}^4$

$e_z := 1178\ \boldsymbol{mm}$

Reinforcement

$A_{su} := 7829\ \boldsymbol{mm}^2$

$y_{su} := 1567\ \boldsymbol{mm}$

E-modulus

$E_{cL} := 7174\ \boldsymbol{MPa}$ Long time Youngs module due to creep

$E_s := 200000\ \boldsymbol{MPa}$

Transformed cross-section (EC2)

$\eta := \frac{E_s}{E_{cL}} = 27.878$

$A_t := A_c + (\eta - 1) \cdot A_{su} = \langle 3.254 \cdot 10^6 \rangle\ \boldsymbol{mm}^2$

$e_{zt} := \frac{A_c \cdot e_z + (\eta - 1) \cdot A_{su} \cdot y_{su}}{A_t} = \langle 1.203 \cdot 10^3 \rangle\ \boldsymbol{mm}$

$y_t := e_z - e_{zt} = -25.154\ \boldsymbol{mm}$

$e_s := e_{zt} - y_{su} = -363.846\ \boldsymbol{mm}$

$I_t := I_c + A_c \cdot y_t^2 + (\eta - 1)\ A_{su} \cdot e_s^2 = \langle 8.562 \cdot 10^{11} \rangle\ \boldsymbol{mm}^4$

$‰ := \frac{1}{1000}$ $\varepsilon_{Shrinkage} := 0.266 \cdot ‰$

$\varepsilon_{ASR} := \varepsilon_{asr} - \varepsilon_{Shrinkage} = 0.284\ ‰$

$N_{ASR} := \varepsilon_{ASR} \cdot E_s \cdot A_{su} = 444.687\ \boldsymbol{kN}$

$M_{ASR} := N_{ASR} \cdot e_s = -161.798\ \boldsymbol{kN \cdot m}$

Curvature due to ASR

$\kappa_{ASR} := \frac{M_{ASR}}{E_{cL} \cdot I_t} = -2.634 \cdot 10^{-5}\ \frac{1}{\boldsymbol{m}}$

Curvature due to temperature:

$\alpha_T := 9.8 \cdot 10^{-6} \cdot \boldsymbol{K}^{-1}$

$\Delta_T := \kappa_{ASR} \cdot \frac{h_{tot}}{\alpha_T} = -4.532\ \boldsymbol{K}$

F1.5 Section A/E - 1 to 16 and 43 to 55 - Support

Cross section data:

$A_c := 5356060\ \boldsymbol{mm}^2$

$h_{tot} := 932\ \boldsymbol{mm}$

$I_c := 24.06 \cdot 10^{10}\ \boldsymbol{mm}^4$

$e_z := 571\ \boldsymbol{mm}$

Reinforcement

$A_{su} := 11437.8\ \boldsymbol{mm}^2$

$y_{su} := 902.5\ \boldsymbol{mm}$

E-modulus

$E_{cL} := 7174\ \boldsymbol{MPa}$ Long time Youngs module due to creep

$E_s := 200000\ \boldsymbol{MPa}$

Transformed cross-section (EC2)

$\eta := \frac{E_s}{E_{cL}} = 27.878$

$A_t := A_c + (\eta - 1) \cdot A_{su} = \langle 5.663 \cdot 10^6 \rangle\ \boldsymbol{mm}^2$

$e_{zt} := \frac{A_c \cdot e_z + (\eta - 1) \cdot A_{su} \cdot y_{su}}{A_t} = 588.995\ \boldsymbol{mm}$

$y_t := e_z - e_{zt} = -17.995\ \boldsymbol{mm}$

$e_s := e_{zt} - y_{su} = -313.505\ \boldsymbol{mm}$

$I_t := I_c + A_c \cdot y_t^2 + (\eta - 1)\ A_{su} \cdot e_s^2 = \langle 2.726 \cdot 10^{11} \rangle\ \boldsymbol{mm}^4$

$‰ := \frac{1}{1000}$ $\varepsilon_{Shrinkage} := 0.247 \cdot ‰$

$\varepsilon_{ASR} := \varepsilon_{asr} - \varepsilon_{Shrinkage} = 0.303\ ‰$

$N_{ASR} := \varepsilon_{ASR} \cdot E_s \cdot A_{su} = 693.131\ \boldsymbol{kN}$

$M_{ASR} := N_{ASR} \cdot e_s = -217.3\ \boldsymbol{kN \cdot m}$

Curvature due to ASR

$\kappa_{ASR} := \frac{M_{ASR}}{E_{cL} \cdot I_t} = -1.111 \cdot 10^{-4}\ \frac{1}{\boldsymbol{m}}$

Curvature due to temperature:

$\alpha_T := 9.8 \cdot 10^{-6} \cdot \boldsymbol{K}^{-1}$

$\Delta_T := \kappa_{ASR} \cdot \frac{h_{tot}}{\alpha_T} = -10.569\ \boldsymbol{K}$

F1.6 Section B/D - 31 to 32 and 37 to 38 - Support

Cross section data:

$A_c := 3043800\ \boldsymbol{mm}^2$

$h_{tot} := 1686\ \boldsymbol{mm}$

$I_c := 82.64 \cdot 10^{10}\ \boldsymbol{mm}^4$

$e_z := 1178\ \boldsymbol{mm}$

Reinforcement

$A_{su} := 10589\ \boldsymbol{mm}^2$

$y_{su} := 1562\ \boldsymbol{mm}$

E-modulus

$E_{cL} := 7174\ \boldsymbol{MPa}$ Long time Youngs module due to creep

$E_s := 200000\ \boldsymbol{MPa}$

Transformed cross-section (EC2)

$\eta := \frac{E_s}{E_{cL}} = 27.878$

$A_t := A_c + (\eta - 1) \cdot A_{su} = \langle 3.328 \cdot 10^6 \rangle\ \boldsymbol{mm}^2$

$e_{zt} := \frac{A_c \cdot e_z + (\eta - 1) \cdot A_{su} \cdot y_{su}}{A_t} = \langle 1.211 \cdot 10^3 \rangle\ \boldsymbol{mm}$

$y_t := e_z - e_{zt} = -32.836\ \boldsymbol{mm}$

$e_s := e_{zt} - y_{su} = -351.164\ \boldsymbol{mm}$

$I_t := I_c + A_c \cdot y_t^2 + (\eta - 1)\ A_{su} \cdot e_s^2 = \langle 8.648 \cdot 10^{11} \rangle\ \boldsymbol{mm}^4$

$‰ := \frac{1}{1000}$ $\varepsilon_{Shrinkage} := 0.266 \cdot ‰$

$\varepsilon_{ASR} := \varepsilon_{asr} - \varepsilon_{Shrinkage} = 0.284\ ‰$

$N_{ASR} := \varepsilon_{ASR} \cdot E_s \cdot A_{su} = 601.455\ \boldsymbol{kN}$

$M_{ASR} := N_{ASR} \cdot e_s = -211.209\ \boldsymbol{kN \cdot m}$

Curvature due to ASR

$\kappa_{ASR} := \frac{M_{ASR}}{E_{cL} \cdot I_t} = -3.404 \cdot 10^{-5}\ \frac{1}{\boldsymbol{m}}$

Curvature due to temperature:

$\alpha_T := 9.8 \cdot 10^{-6} \cdot \boldsymbol{K}^{-1}$

$\Delta_T := \kappa_{ASR} \cdot \frac{h_{tot}}{\alpha_T} = -5.857\ \boldsymbol{K}$

F1.7 Section C - Section 0

Cross section data:

$A_c := 2607760\ \boldsymbol{mm}^2$

$h_{tot} := 1750\ \boldsymbol{mm}$

$I_c := 67.37 \cdot 10^{10}\ \boldsymbol{mm}^4$

$e_z := 1268\ \boldsymbol{mm}$

Reinforcement

$A_{su} := 2 \cdot 1062\ \boldsymbol{mm}^2 = 2124\ \boldsymbol{mm}^2$

$y_{su} := 200\ \boldsymbol{mm}$

$Ø_p := 26\ \boldsymbol{mm}$

$n_p := 24$

$A_p := n_p \cdot \frac{\pi \cdot (26\ \boldsymbol{mm})^2}{4} = 12742.3\ \boldsymbol{mm}^2$

$y_p := 160\ \boldsymbol{mm}$

$A_{so} := 2 \cdot 4115\ \boldsymbol{mm}^2$

$y_{so} := 1520\ \boldsymbol{mm} + 69\ \boldsymbol{mm} = 1589\ \boldsymbol{mm}$

E-modulus

$E_{cL} := 10261\ \boldsymbol{MPa}$ Long time Youngs module due to creep

$E_s := 200000\ \boldsymbol{MPa}$

$E_p := 205000\ \boldsymbol{MPa}$

$y_m := \frac{E_s \cdot A_{so} \cdot y_{so} + E_p \cdot A_p \cdot y_p + E_s \cdot A_{su} \cdot y_{su}}{E_s \cdot (A_{so} + A_{su}) + E_p \cdot A_p} = 0.666\ \boldsymbol{m}$

Transformed cross-section (EC2)

$$\eta := \frac{E_p}{E_{cL}} = 19.979$$

$$A_t := A_c + (\eta - 1) \cdot A_p = \langle 2.85 \cdot 10^6 \rangle \ \boldsymbol{mm}^2$$

$$e_{zt} := \frac{A_c \cdot e_z + (\eta - 1) \cdot A_p \cdot y_p}{A_t} = \langle 1.174 \cdot 10^3 \rangle \ \boldsymbol{mm}$$

$$y_t := e_z - e_{zt} = 94.03 \ \boldsymbol{mm}$$

$$e_p := e_z - y_p = \langle 1.108 \cdot 10^3 \rangle \ \boldsymbol{mm}$$

$$I_t := I_c + A_c \cdot y_t^2 + (\eta - 1) \ A_p \cdot \langle e_p - y_t \rangle^2 = \langle 9.454 \cdot 10^{11} \rangle \ \boldsymbol{mm}^4$$

$$‰ := \frac{1}{1000} \qquad \varepsilon_{Shrinkage} := 0.264 \cdot ‰$$

$$\varepsilon_{ASR} := \varepsilon_{asr} - \varepsilon_{Shrinkage} = 0.286 \ ‰$$

$$N_{ASR} := -\varepsilon_{ASR} \cdot \langle E_p \cdot A_p + E_s \cdot \langle A_{so} + A_{su} \rangle \rangle = -1339.33 \ \boldsymbol{kN}$$

$$M_{ASR} := N_{ASR} \cdot \langle y_m - e_{zt} \rangle = 680.47 \ \boldsymbol{kN \cdot m}$$

Curvature due to ASR

$$\kappa_{ASR} := \frac{M_{ASR}}{E_{cL} \cdot I_t} = \langle 7.015 \cdot 10^{-5} \rangle \ \frac{1}{\boldsymbol{m}}$$

Curvature due to temperature:

$$\alpha_T := 9.8 \cdot 10^{-6} \cdot \boldsymbol{K}^{-1}$$

$$\Delta_T := \kappa_{ASR} \cdot \frac{h_{tot}}{\alpha_T} = 12.526 \ \boldsymbol{K}$$

F1.8 Section C - Section 4

Cross section data:

$A_c := 2762490\ \boldsymbol{mm}^2$

$h_{tot} := 1971\ \boldsymbol{mm}$

$I_c := 91.15 \cdot 10^{10}\ \boldsymbol{mm}^4$

$e_z := 1346\ \boldsymbol{mm}$

Reinforcement

$A_{su} := 0\ \boldsymbol{mm}^2$

$y_{su} := 0\ \boldsymbol{mm}$

$Ø_p := 26\ \boldsymbol{mm}$

$n_p := 32$

$A_p := n_p \cdot \frac{\pi \cdot (26\ \boldsymbol{mm})^2}{4} = 16989.733\ \boldsymbol{mm}^2$

$y_p := 1442\ \boldsymbol{mm}$

$A_{so} := 4115\ \boldsymbol{mm}^2$

$y_{so} := 1856\ \boldsymbol{mm}$

E-modulus

$E_{cL} := 10261\ \boldsymbol{MPa}$ Long time Youngs module due to creep

$E_s := 200000\ \boldsymbol{MPa}$

$E_p := 205000\ \boldsymbol{MPa}$

$y_m := \frac{E_s \cdot A_{so} \cdot y_{so} + E_p \cdot A_p \cdot y_p + E_s \cdot A_{su} \cdot y_{su}}{E_s \cdot (A_{so} + A_{su}) + E_p \cdot A_p} = 1.521\ \boldsymbol{m}$

Transformed cross-section (EC2)

$\eta_1 := \frac{E_p}{E_{cL}} = 19.979$ $\eta_2 := \frac{E_s}{E_{cL}} = 19.491$

$A_t := A_c + (\eta_1 - 1) \cdot A_p + (\eta_2 - 1) \cdot A_{so} = (3.161 \cdot 10^6)\ \boldsymbol{mm}^2$

$e_{zt} := \frac{A_c \cdot e_z + (\eta_1 - 1) \cdot A_p \cdot y_p + (\eta_2 - 1) \cdot A_{so} \cdot y_{so}}{A_t} = (1.368 \cdot 10^3)\ \boldsymbol{mm}$

$y_t := e_{zt} - e_z = 22.069\ \boldsymbol{mm}$

$e := y_m - e_{zt} = 153.06\ \boldsymbol{mm}$

$I_t := I_c + A_c \cdot y_t^2 + (\eta_1 - 1)\ A_p \cdot (y_p - e_{zt})^2 + (\eta_2 - 1) \cdot (A_{so} \cdot (y_{so} - e_{zt})^2) = (9.327 \cdot 10^{11})\ \boldsymbol{mm}^4$

$‰ := \frac{1}{1000}$ $\varepsilon_{Shrinkage} := 0.264 \cdot ‰$

$\varepsilon_{ASR} := \varepsilon_{asr} - \varepsilon_{Shrinkage} = 0.286\ ‰$

$N_{ASR} := -\varepsilon_{ASR} \cdot (E_p \cdot A_p + E_s \cdot (A_{so} + A_{su})) = -1231.486\ \boldsymbol{kN}$

$M_{ASR} := N_{ASR} \cdot (y_m - e_{zt}) = -188.491\ \boldsymbol{kN \cdot m}$

Curvature due to ASR

$\kappa_{ASR} := \frac{M_{ASR}}{E_{cL} \cdot I_t} = -1.969 \cdot 10^{-5}\ \frac{1}{\boldsymbol{m}}$

Curvature due to temperature:

$\alpha_T := 9.8 \cdot 10^{-6} \cdot \boldsymbol{K}^{-1}$

$\Delta_T := \kappa_{ASR} \cdot \frac{h_{tot}}{\alpha_T} = -3.961\ \boldsymbol{K}$

F1.9 Section C - Section 7

Cross section data:

$A_c := 2858250\ mm^2$

$h_{tot} := 2108\ mm$

$I_c := 115.44 \cdot 10^{10}\ mm^4$

$e_z := 1499\ mm$

Reinforcement

$A_{su} := 2522\ mm^2$

$y_{su} := 100\ mm$

$Ø_p := 26\ mm$

$n_p := 68$

$A_p := n_p \cdot \frac{\pi \cdot (26\ mm)^2}{4} = 36103.183\ mm^2$

$y_p := 1707\ mm$

$A_{so} := 3982\ mm^2$

$y_{so} := 1993\ mm$

E-modulus

$E_{cL} := 10261\ MPa$ Long time Youngs module due to creep

$E_s := 200000\ MPa$

$E_p := 205000\ MPa$

$y_m := \frac{E_s \cdot A_{so} \cdot y_{so} + E_p \cdot A_p \cdot y_p + E_s \cdot A_{su} \cdot y_{su}}{E_s \cdot (A_{so} + A_{su}) + E_p \cdot A_p} = 1.64\ m$

Transformed cross-section (EC2)

$\eta_1 := \frac{E_p}{E_{cL}} = 19.979$ $\eta_2 := \frac{E_s}{E_{cL}} = 19.491$

$A_t := A_c + (\eta_1 - 1) \cdot A_p = (3.543 \cdot 10^6)\ \boldsymbol{mm}^2$

$e_{zt} := \frac{A_c \cdot e_z + (\eta_1 - 1) \cdot A_p \cdot y_p + (\eta_2 - 1) \cdot (A_{so} \cdot y_{so} + A_{su} \cdot y_{su})}{A_t} = (1.582 \cdot 10^3)\ \boldsymbol{mm}$

$y_t := e_{zt} - e_z = 82.951\ \boldsymbol{mm}$

$e := y_m - e_{zt} = 58.076\ \boldsymbol{mm}$

$I_t := I_c + A_c \cdot y_t^2 + (\eta_1 - 1)\ A_p \cdot (e - y_t)^2 + (\eta_2 - 1) \cdot (A_{so} \cdot (e_{zt} - y_{so})^2) + (\eta_2 - 1) \cdot (A_{su} \cdot (e_{zt} - y_{su})^2) = (1.289 \cdot 10^{12})\ \boldsymbol{mm}^4$

$‰ := \frac{1}{1000}$ $\varepsilon_{Shrinkage} := 0.264 \cdot ‰$

$\varepsilon_{ASR} := \varepsilon_{asr} - \varepsilon_{Shrinkage} = 0.286\ ‰$

$N_{ASR} := -\varepsilon_{ASR} \cdot (E_p \cdot A_p + E_s \cdot (A_{so} + A_{su})) = -2488.758\ \boldsymbol{kN}$

$M_{ASR} := N_{ASR} \cdot (y_m - e_{zt}) = -144.536\ \boldsymbol{kN \cdot m}$

Curvature due to ASR

$\kappa_{ASR} := \frac{M_{ASR}}{E_{cL} \cdot I_t} = -1.092 \cdot 10^{-5}\ \frac{1}{\boldsymbol{m}}$

Curvature due to temperature:

$\alpha_T := 9.8 \cdot 10^{-6} \cdot \boldsymbol{K}^{-1}$

$\Delta_T := \kappa_{ASR} \cdot \frac{h_{tot}}{\alpha_T} = -2.35\ \boldsymbol{K}$

F1.10 Section C - Section 10

Cross section data:

$A_c := 4761730\ \boldsymbol{mm}^2$

$h_{tot} := 3284\ \boldsymbol{mm}$

$I_c := 757.6 \cdot 10^{10}\ \boldsymbol{mm}^4$

$e_z := 1742\ \boldsymbol{mm}$

Reinforcement

$A_{su} := 5575\ \boldsymbol{mm}^2$

$y_{su} := 100\ \boldsymbol{mm}$

$Ø_p := 26\ \boldsymbol{mm}$

$n_p := 96$

$A_p := n_p \cdot \frac{\pi \cdot (26\ \boldsymbol{mm})^2}{4} = 50969.199\ \boldsymbol{mm}^2$

$y_p := 2710\ \boldsymbol{mm}$

$A_{so} := 4115\ \boldsymbol{mm}^2$

$y_{so} := 3169\ \boldsymbol{mm}$

E-modulus

$E_{cL} := 10261\ \boldsymbol{MPa}$ Long time Youngs module due to creep

$E_s := 200000\ \boldsymbol{MPa}$

$E_p := 205000\ \boldsymbol{MPa}$

$y_m := \frac{E_s \cdot A_{so} \cdot y_{so} + E_p \cdot A_p \cdot y_p + E_s \cdot A_{su} \cdot y_{su}}{E_s \cdot (A_{so} + A_{su}) + E_p \cdot A_p} = 2.506\ \boldsymbol{m}$

Transformed cross-section (EC2)

$\eta_1 := \frac{E_p}{E_{cL}} = 19.979$ $\eta_2 := \frac{E_s}{E_{cL}} = 19.491$

$A_t := A_c + (\eta_1 - 1) \cdot A_p + (\eta_2 - 1) \cdot (A_{su} + A_{so}) = (5.908 \cdot 10^6)\ \boldsymbol{mm^2}$

$e_{zt} := \frac{A_c \cdot e_z + (\eta_1 - 1) \cdot A_p \cdot y_p + (\eta_2 - 1) \cdot (A_{so} \cdot y_{so} + A_{su} \cdot y_{su})}{A_t} = (1.89 \cdot 10^3)\ \boldsymbol{mm}$

$y_t := e_{zt} - e_z = 148.213\ \boldsymbol{mm}$

$e := y_m - e_{zt} = 615.342\ \boldsymbol{mm}$

$I_t := I_c + A_c \cdot y_t^2 + (\eta_1 - 1)\ A_p \cdot (y_p - e_{zt})^2 + (\eta_2 - 1) \cdot (A_{so} \cdot (y_{so} - e_{zt})^2) + (\eta_2 - 1) \cdot (A_{su} \cdot (e_{zt} - y_{su})^2) = (8.786 \cdot 10^{12})\ \boldsymbol{mm^4}$

$‰ := \frac{1}{1000}$ $\varepsilon_{Shrinkage} := 0.264 \cdot ‰$

$\varepsilon_{ASR} := \varepsilon_{asr} - \varepsilon_{Shrinkage} = 0.286\ ‰$

$N_{ASR} := -\varepsilon_{ASR} \cdot (E_p \cdot A_p + E_s \cdot (A_{so} + A_{su})) = -3542.592\ \boldsymbol{kN}$

$M_{ASR} := N_{ASR} \cdot (e_{zt} - y_m) = 2179.906\ \boldsymbol{kN \cdot m}$

Curvature due to ASR

$\kappa_{ASR} := \frac{M_{ASR}}{E_{cL} \cdot I_t} = (2.418 \cdot 10^{-5})\ \frac{1}{\boldsymbol{m}}$

Curvature due to temperature:

$\alpha_T := 9.8 \cdot 10^{-6} \cdot \boldsymbol{K}^{-1}$

$\Delta_T := \kappa_{ASR} \cdot \frac{h_{tot}}{\alpha_T} = 8.103\ \boldsymbol{K}$

F1.11 Section C - Section 14

Cross section data:

$A_c := 5730460\ mm^2$

$h_{tot} := 4668\ mm$

$I_c := 1.77 \cdot 10^{13}\ mm^4$

$e_z := 2453\ mm$

Reinforcement

$A_{su} := 2655\ mm^2$

$y_{su} := 150\ mm$

$\emptyset_p := 26\ mm$

$n_p := 104$

$A_p := n_p \cdot \frac{\pi \cdot (26\ mm)^2}{4} = 55216.632\ mm^2$

$y_p := 4410\ mm$

$A_{so} := 4115\ mm^2$

$y_{so} := 4507\ mm$

E-modulus

$E_{cL} := 10261\ MPa$ Long time Youngs module due to creep

$E_s := 200000\ MPa$

$E_p := 205000\ MPa$

$y_m := \frac{E_s \cdot A_{so} \cdot y_{so} + E_p \cdot A_p \cdot y_p + E_s \cdot A_{su} \cdot y_{su}}{E_s \cdot (A_{so} + A_{su}) + E_p \cdot A_p} = 4.238\ m$

Transformed cross-section (EC2)

$$\eta_1 := \frac{E_p}{E_{cL}} = 19.979$$

$$A_t := A_c + (\eta_1 - 1) \cdot A_p = (6.778 \cdot 10^6)\ \boldsymbol{mm}^2$$

$$e_{zt} := \frac{A_c \cdot e_z + (\eta_1 - 1) \cdot A_p \cdot y_p}{A_t} = (2.756 \cdot 10^3)\ \boldsymbol{mm}$$

$$y_t := e_{zt} - e_z = 302.55\ \boldsymbol{mm}$$

$$e := y_p - e_z = (1.957 \cdot 10^3)\ \boldsymbol{mm}$$

$$I_t := I_c + A_c \cdot y_t^2 + (\eta_1 - 1)\ A_p \cdot (y_p - e_{zt})^2 = (2.109 \cdot 10^{13})\ \boldsymbol{mm}^4$$

$$‰ := \frac{1}{1000} \qquad \varepsilon_{Shrinkage} := 0.264 \cdot ‰$$

$$\varepsilon_{ASR} := \varepsilon_{asr} - \varepsilon_{Shrinkage} = 0.286\ ‰$$

$$N_{ASR} := -\varepsilon_{ASR} \cdot (E_p \cdot A_p + E_s \cdot (A_{so} + A_{su})) = -3624.595\ \boldsymbol{kN}$$

$$M_{ASR} := -N_{ASR} \cdot (e_{zt} - y_m) = -5372.594\ \boldsymbol{kN \cdot m}$$

Curvature due to ASR

$$\kappa_{ASR} := \frac{M_{ASR}}{E_{cL} \cdot I_t} = -2.482 \cdot 10^{-5}\ \frac{1}{\boldsymbol{m}}$$

Curvature due to temperature:

$$\alpha_T := 9.8 \cdot 10^{-6} \cdot \boldsymbol{K}^{-1}$$

$$\Delta_T := \kappa_{ASR} \cdot \frac{h_{tot}}{\alpha_T} = -11.824\ \boldsymbol{K}$$

F1.12 Section C - Section 20

Cross section data:

$A_c := 4380440\ \boldsymbol{mm}^2$

$h_{tot} := 2739\ \boldsymbol{mm}$

$I_c := 406.57 \cdot 10^{10}\ \boldsymbol{mm}^4$

$e_z := 1687\ \boldsymbol{mm}$

Reinforcement

$A_{su} := 3053\ \boldsymbol{mm}^2$

$y_{su} := 325\ \boldsymbol{mm}$

$Ø_p := 26\ \boldsymbol{mm}$

$n_p := 92$

$A_p := n_p \cdot \frac{\pi \cdot (26\ \boldsymbol{mm})^2}{4} = 48845.483\ \boldsymbol{mm}^2$

$y_p := 2337\ \boldsymbol{mm}$

$A_{so} := 4247\ \boldsymbol{mm}^2$

$y_{so} := 2624\ \boldsymbol{mm}$

E-modulus

$E_{cL} := 10261\ \boldsymbol{MPa}$ Long time Youngs module due to creep

$E_s := 200000\ \boldsymbol{MPa}$

$E_p := 205000\ \boldsymbol{MPa}$

$y_m := \frac{E_s \cdot A_{so} \cdot y_{so} + E_p \cdot A_p \cdot y_p + E_s \cdot A_{su} \cdot y_{su}}{E_s \cdot (A_{so} + A_{su}) + E_p \cdot A_p} = 2.251\ \boldsymbol{m}$

Transformed cross-section (EC2)

$\eta_1 := \frac{E_p}{E_{cL}} = 19.979$ $\eta_2 := \frac{E_s}{E_{cL}} = 19.491$

$A_t := A_c + (\eta_1 - 1) \cdot A_p + (\eta_2 - 1) \cdot (A_{su} + A_{so}) = (5.442 \cdot 10^6)\ \boldsymbol{mm^2}$

$e_{zt} := \frac{A_c \cdot e_z + (\eta_1 - 1) \cdot A_p \cdot y_p + (\eta_2 - 1) \cdot (A_{so} \cdot y_{so} + A_{su} \cdot y_{su})}{A_t} = (1.797 \cdot 10^3)\ \boldsymbol{mm}$

$y_t := e_{zt} - e_z = 110.108\ \boldsymbol{mm}$

$e := y_m - e_{zt} = 454.063\ \boldsymbol{mm}$

$I_t := I_c + A_c \cdot y_t^2 + (\eta_1 - 1)\ A_p \cdot (y_p - e_{zt})^2 + (\eta_2 - 1) \cdot (A_{so} \cdot (y_{so} - e_{zt})^2) + (\eta_2 - 1) \cdot (A_{su} \cdot (e_{zt} - y_{su})^2) = (4.565 \cdot 10^{12})\ \boldsymbol{mm^4}$

$‰ := \frac{1}{1000}$ $\varepsilon_{Shrinkage} := 0.264 \cdot ‰$

$\varepsilon_{ASR} := \varepsilon_{asr} - \varepsilon_{Shrinkage} = 0.286\ ‰$

$N_{ASR} := -\varepsilon_{ASR} \cdot (E_p \cdot A_p + E_s \cdot (A_{so} + A_{su})) = -3281.371\ \boldsymbol{kN}$

$M_{ASR} := N_{ASR} \cdot e = -1489.948\ \boldsymbol{kN \cdot m}$

Curvature due to ASR

$\kappa_{ASR} := \frac{M_{ASR}}{E_{cL} \cdot I_t} = -3.181 \cdot 10^{-5}\ \frac{1}{\boldsymbol{m}}$

Curvature due to temperature:

$\alpha_T := 9.8 \cdot 10^{-6} \cdot \boldsymbol{K^{-1}}$

$\Delta_T := \kappa_{ASR} \cdot \frac{h_{tot}}{\alpha_T} = -8.89\ \boldsymbol{K}$

G Interaction diagrams

Column 30, 31:

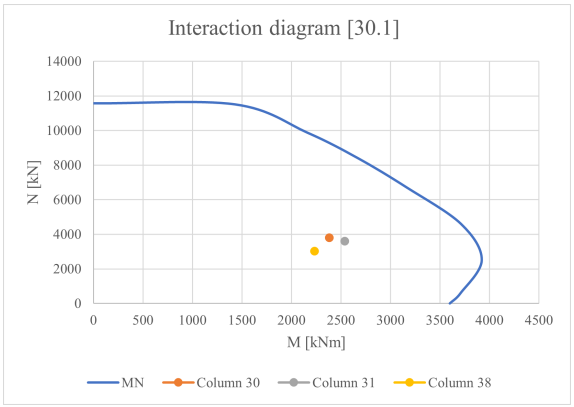

(a) Crossbar top

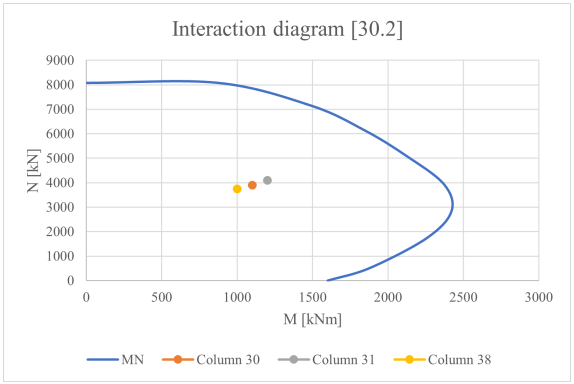

(b) Middle upper part

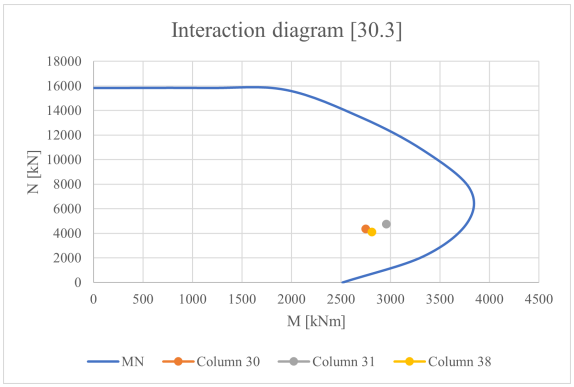

(c) Crossbar bottom

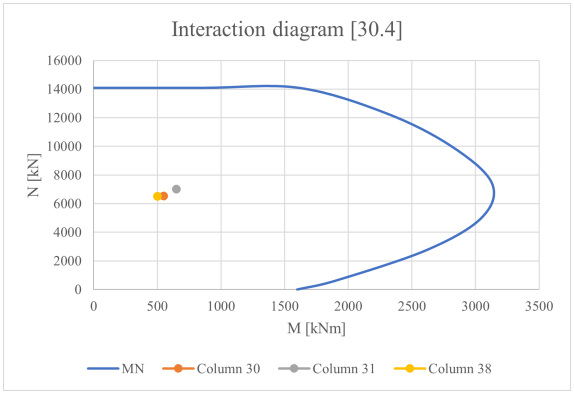

(d) Middle bottom part

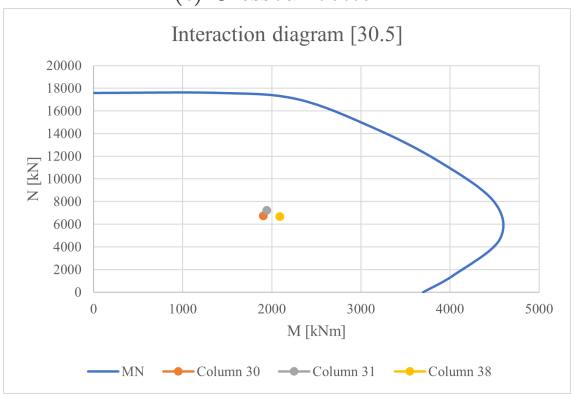

(e) Bottom

Figure G.1: Interaction diagrams column 30, 31

Column 32:

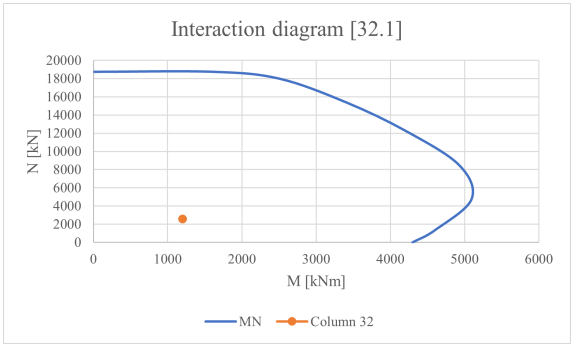

(a) Crossbar top

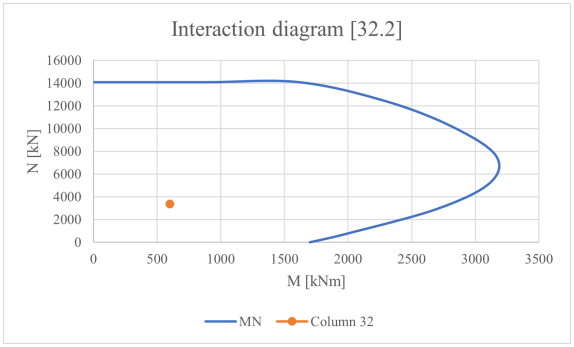

(b) Middle upper part

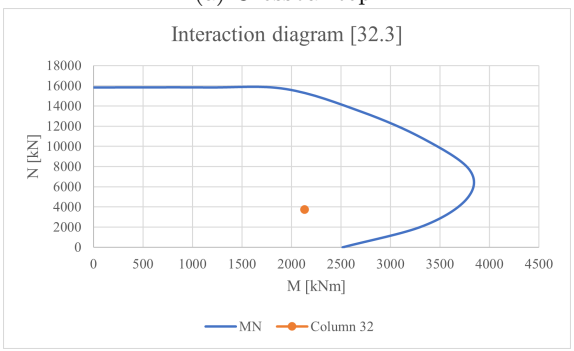

(c) Crossbar bottom

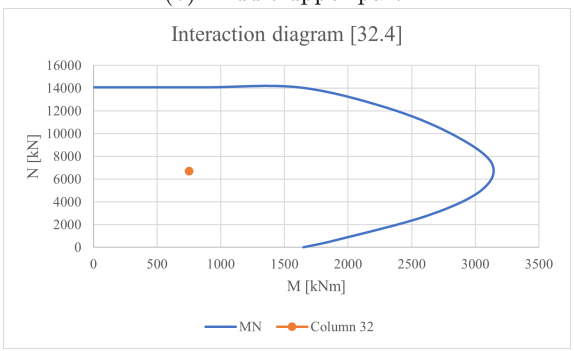

(d) Middle bottom part

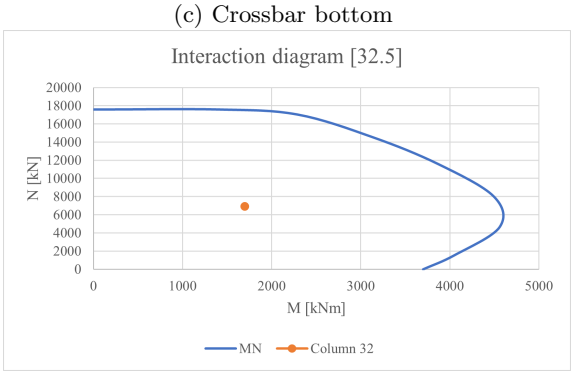

(e) Bottom

Figure G.2: Interaction diagrams column 32

Column 33, 34:

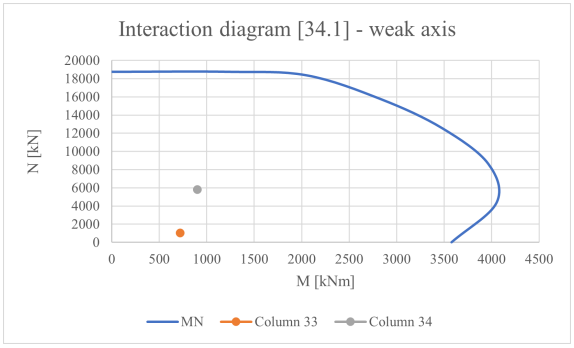

(a) Crossbar top - weak axis

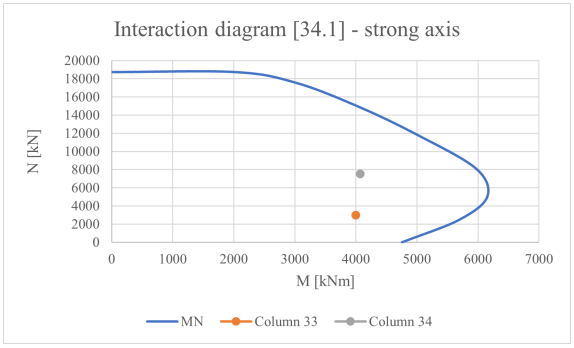

(b) Crossbar top - strong axis

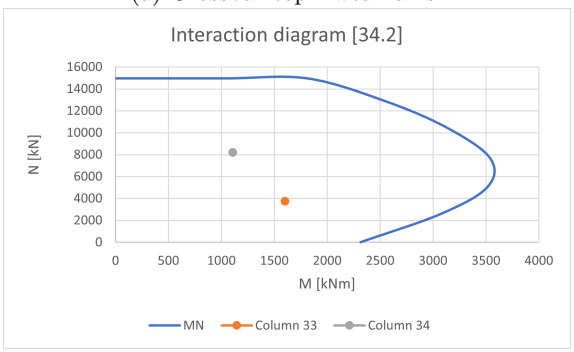

(c) Middle upper part

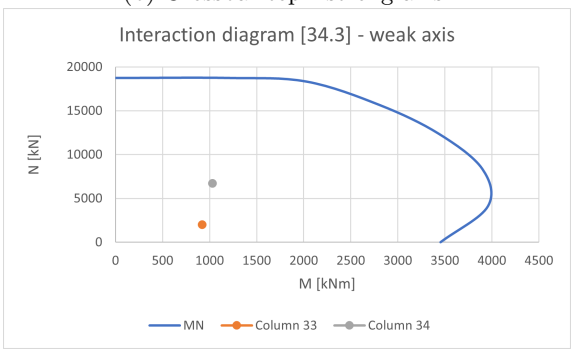

(d) Crossbar bottom - weak axis

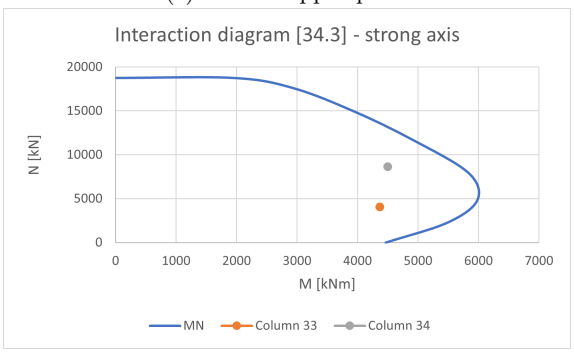

(e) Crossbar bottom - strong axis

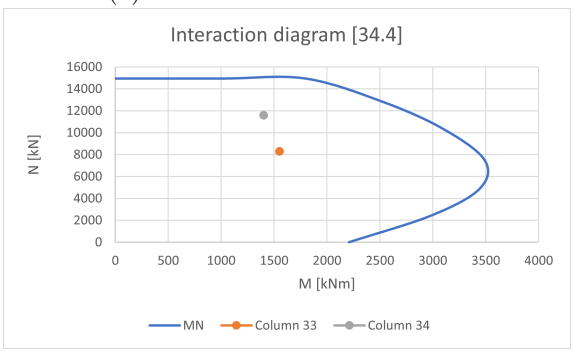

(f) Middle bottom part

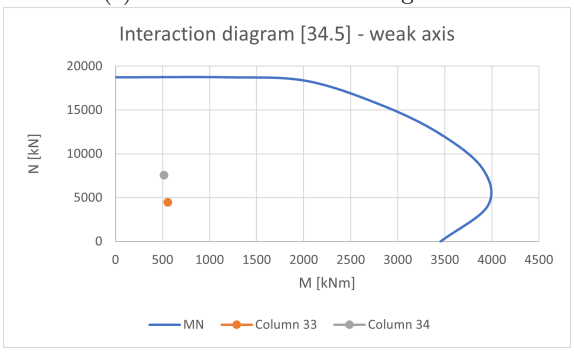

(g) Bottom - weak axis

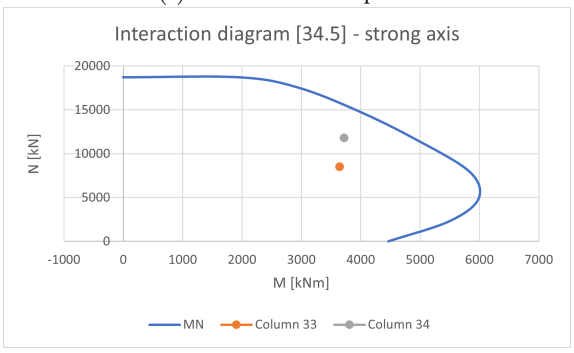

(h) Bottom - strong axis

Figure G.3: Interaction diagrams column 33, 34

Column 38, 42, 43:

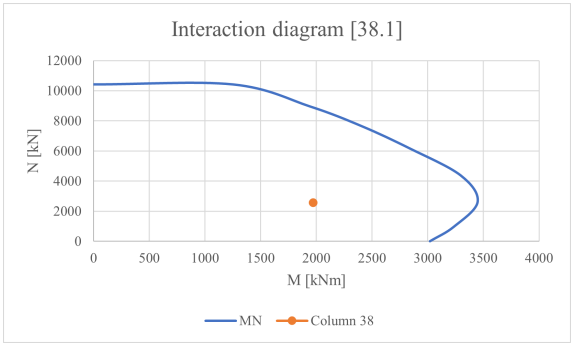

(a) Crossbar top

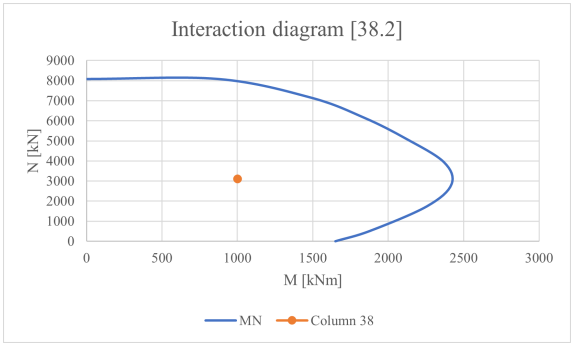

(b) Middle upper part

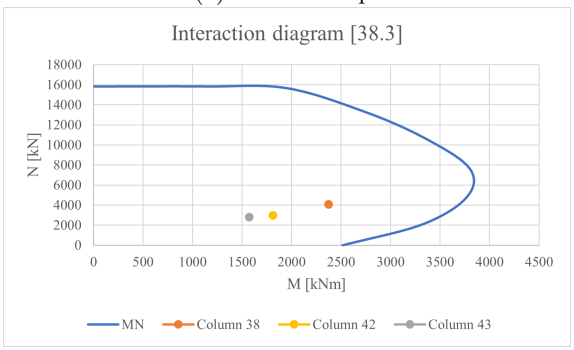

(c) Crossbar bottom

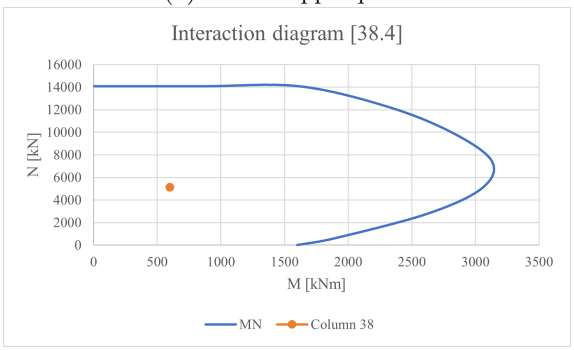

(d) Middle bottom part

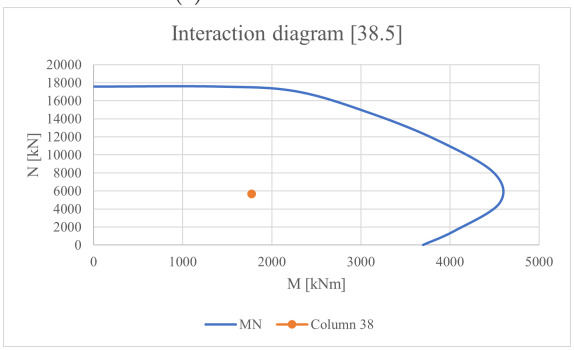

(e) Bottom

Figure G.4: Interaction diagrams column 38, 42, 43

Column 44, 45, 46, 47, 48, 49:

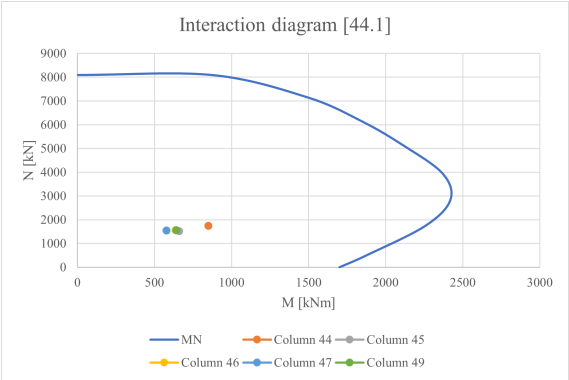

(a) Crossbar top

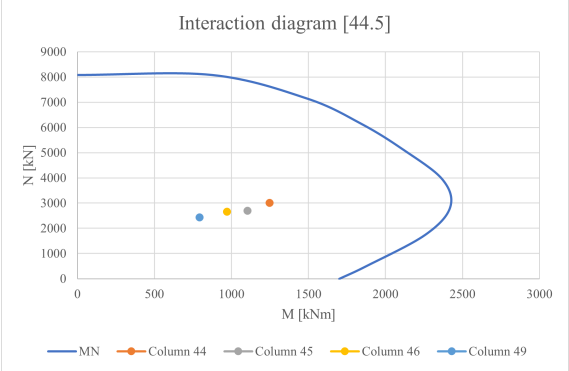

(b) Bottom

Figure G.5: Interaction diagrams column 44, 45, 46, 47, 48, 49

H Scanning of columns 31 and 34

TROMSØBRUA VEST N33.dwg

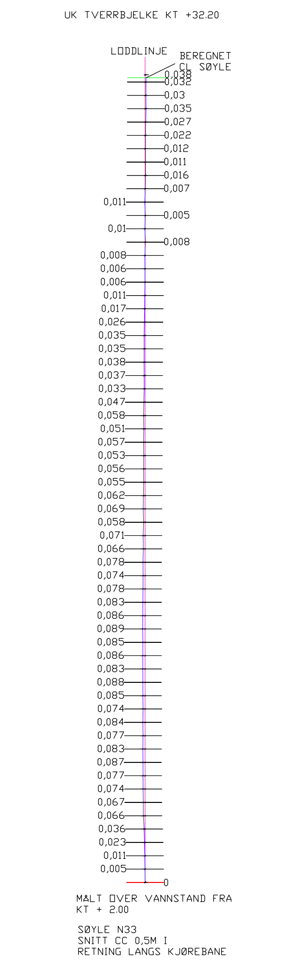

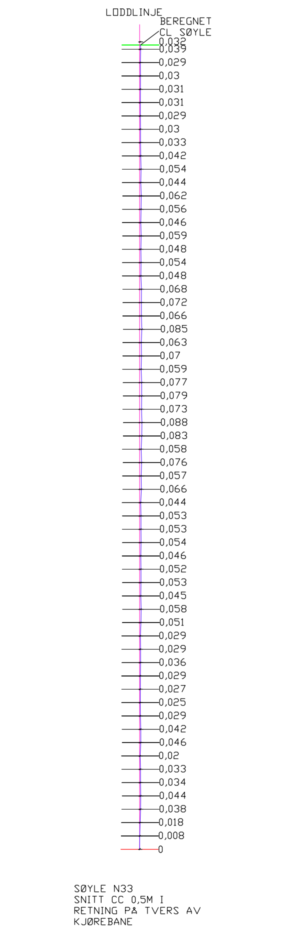

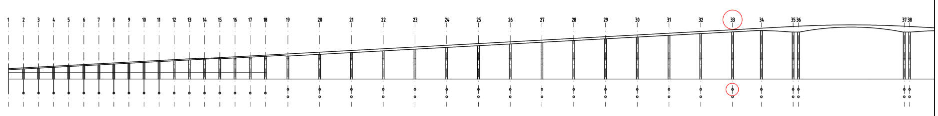

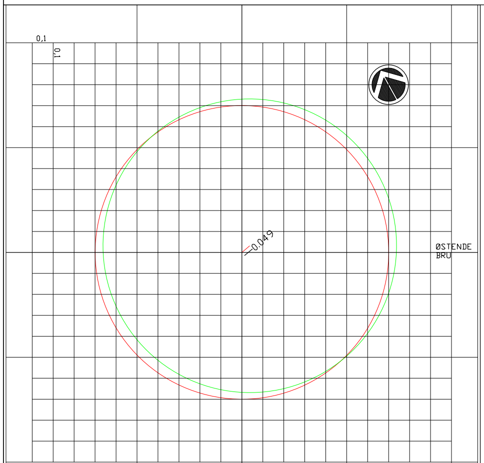

VISER HORISONTAL DIFFERANSE MELLOM NEDERSTE OG ØVERSTE SIKRE MÅLING

REV	ENDRINGEN GJELDER	DAK	KONTROLLERT	DATO

ING. GRANBERG AS

KIRKEGATA 12 * 8516 NARVIK
TELF: 900 65 321
ORG.NR: 913 580 648 MVA
post@idagas.no

MULTICONSULT ASA
SØYLER TROMSØBRUA VEST
SNITT AV SØYLE N33

MÅLESTOKK	INGEN MÅLESTOKK	FORMAT	A1
OPPDRAGSANSVARLIG: DAG ARNE GRANBERG	DAK: SVEIN-OVE RØLVÅG	DATO: 02.11.2016	KONTROLLERT: DG
FAG: B	TEGNINGSNUMMER: 1622-N33	REV	

UK TVERRBJELKE KT + 32.05

LODDLINJE

BEREGNET CL SØYLE

0,024
0,023
0,019
0,011
0,015
0,012
0,006
0,01
0,011
0,006
0,002
-0,001
0,005
0
-0,002
0,001
-0,002
-0,009
-0,005
0
0,003
0,002
-0,002
-0,002
-0,001
-0,008
-0,004
-0,002
-0,01
-0,009
-0,006
-0,013
-0,015
-0,011
-0,012
-0,014
-0,018
-0,022
-0,02
-0,014
-0,024
-0,024
-0,026
-0,02
-0,017
-0,009
-0,005
-0,007
-0,006
-0,006
-0,004
-0,005
0,004
0,001
0,001
-0,004
-0,005
-0,008
0

MÅLT OVER VANNSTAND FRA KT + 3.00

SØYLE N36
SNITT CC 0,5M I RETNING LANGS KJØREBANE

LODDLINJE

BEREGNET CL SØYLE

0,07
0,07
0,072
0,073
0,073
0,072
0,065
0,064
0,057
0,058
0,064
0,066
0,066
0,06
0,064
0,063
0,057
0,059
0,059
0,052
0,051
0,044
0,051
0,049
0,033
0,034
0,037
0,034
0,038
0,037
0,04
0,041
0,037
0,034
0,042
0,037
0,035
0,035
0,025
0,041
0,033
0,031
0,031
0,034
0,031
0,029
0,022
0,034
0,037
0,019
0,013
0,013
0,006
0,006
0,009
0,01
0,007
0,005
0

SØYLE N36
SNITT CC 0,5M I RETNING PÅ TVERS AV KJØREBANE

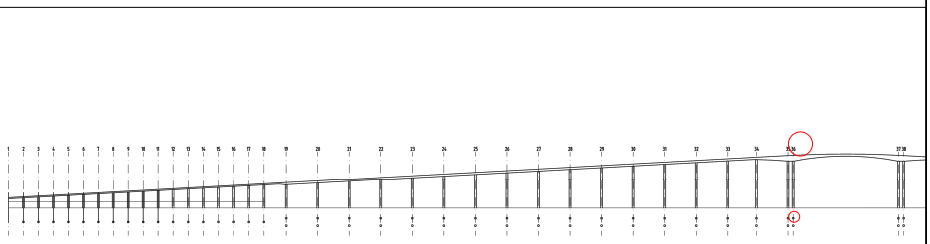

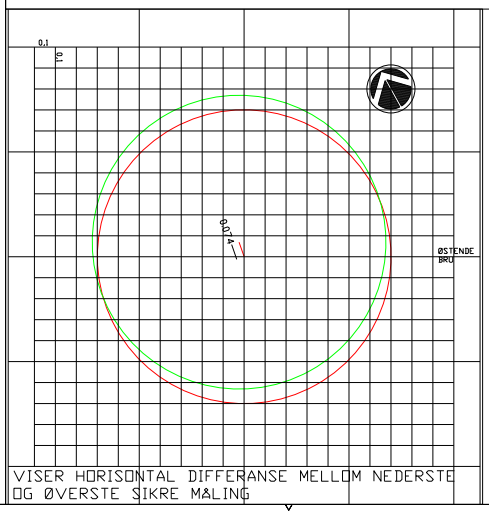

VISER HORISONTAL DIFFERANSE MELLOM NEDERSTE OG ØVERSTE SIKRE MÅLING

NO	ENDRINGSBESKRIVELSE	DAK	KONTROLLERT	DATO

ING. GRANBERG AS

KRINGSATA 12 * 8510 NARVIK
TELF: 980 85 323
ORG.NR: 913 580 840 MVA
post@dagsa.no

MULTICONSULT ASA
SØYLER TROMSØBRUA VEST
SNITT AV SØYLE S36

OPPRINNSKRIVELSE	DAK	DATO	KONTROLLERT	FAG	TEGNINGSNUMMER	REV
DAG ARNE GRANBERG	SVEIN-OVE RØLVÅG	14.11.2016	DG	B	1622-S36	

MÅLESTOKK INGEN MÅLESTOKK FORMAT A1

TROMSØBRUA VEST N36.dwg

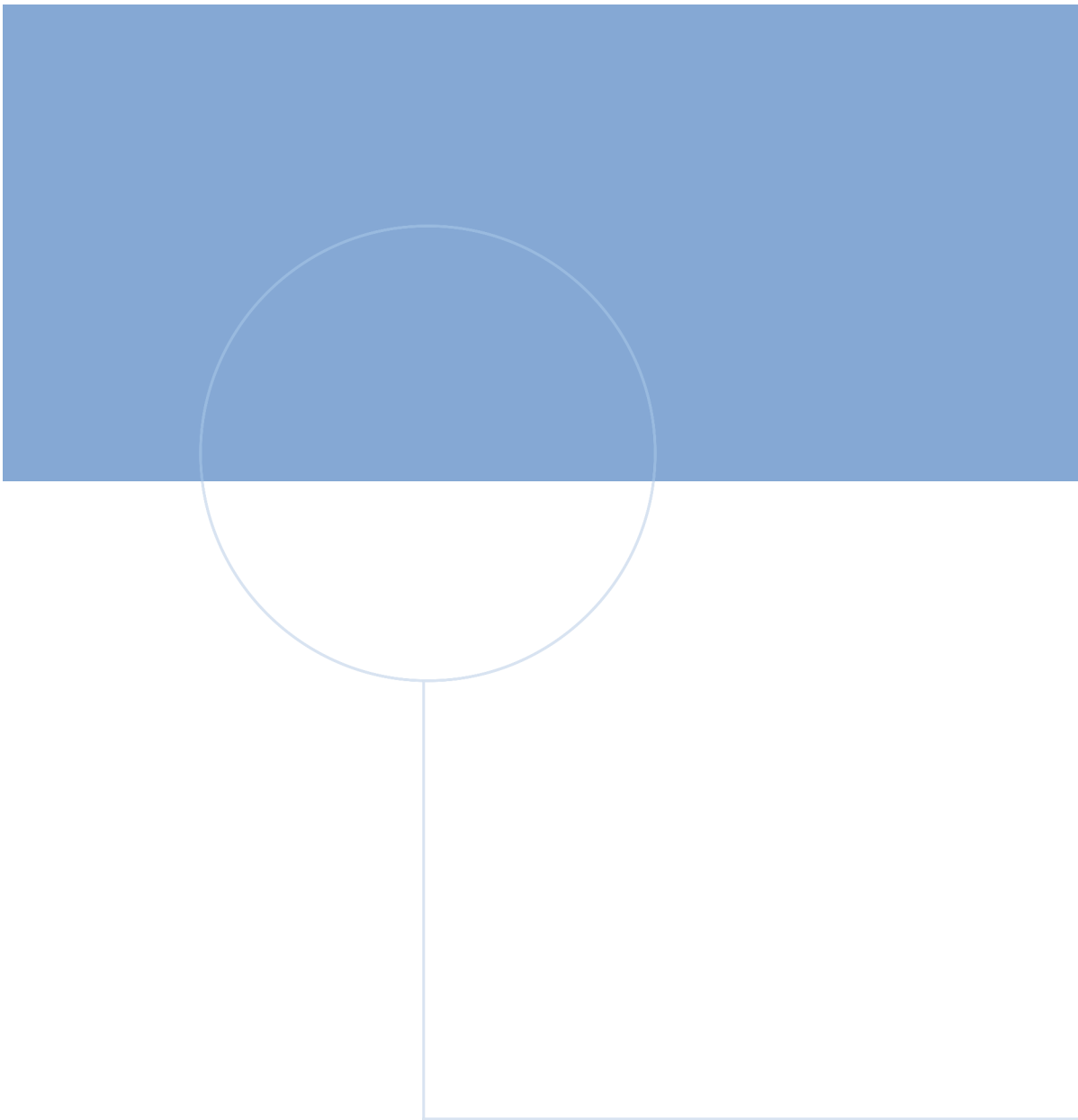

NTNU

Norwegian University of
Science and Technology